SOLUTE MIXING IN OPEN CHANNEL FLOW

by

Andrew Moores

Thesis submitted for the degree of

Doctor of Philosophy

in accordance with the requirements of

Heriot-Watt University

on completion of research in the Civil & Offshore Engineering Department

August 1996

Table of contents

List of tables

List of Figures

List of Plates

Notation

A	cross-sectional area
b	width of channel
b_0, b_1	constants used in log-law fitted to measured data
c	concentration
C	constant in velocity defect law
c_{max}	maximum concentration over the depth in constant coefficient model
c_{min}	minimum concentration over the depth in constant coefficient model
d	depth of flow
D	longitudinal dispersion coefficient
f	friction factor
k	mixing coefficient (suffix gives direction)
κ	von Karman's constant
k_a	dead zone transfer rate
k_s	equivilent sand grain roughness
L_a	length of the advective zone
L_t	transverse length scale
l, l'	mixing lengths
n	Manning's constant
P_m	degree of mixing in constant coefficient model
Q	volumetric flow rate
R	hydraulic radius
t	time, turbulent shear stress

$\bar{u}$	cross-sectional average velocity
u	local velocity
u_q	volumetric discharge velocity
u_*	bed shear velocity
u_{*_b}	sidewall corrected bed shear velocity
u'	velocity variation, rms of velocity fluctuations
v'	velocity in mixing length model of turbulence
W	width
x	co-ordinate in longitudinal direction
x^*	non-dimensional distance in constant coefficient model
y	co-ordinate in vertical direction
y_0	velocity offset in velocity profile
z	co-ordinate in transverse direction
α	non-dimensional length, bed slope
γ	dead zone fraction
ε	Eddy diffusivity
Π	wake correct term in log law velocity profile
ρ	density
ξ	longitudinal co-ordinate in Lagrangian frame of reference
τ	time in Lagrangian frame of reference
σ^2	variance (suffix gives direction)

Acknowledgements

I wish to express my gratitude to some of the people who have helped me during the course of the work that led to this thesis.

Sincere thanks are due to Dr. S. G. Wallis, who was a constant source of encouragement and support and whose tireless guidance I gratefully acknowledge.

I also wish to acknowledge the efforts of the laboratory and workshop technicians of the Department of Civil and Offshore Engineering who, apart from constructing electronic and mechanical apparatus, gave freely of their time and equipment.

I would have been unable to undertake this work without the financial support of a studentship from the SERC/EPSRC.

Finally I want to thank my wife for putting up with my preoccupation with the work and the nightly disappearances into the study.

Abstract

The work has been an experimental and numerical investigation of solute mixing in open channel flow. There were two main aims of the work. Firstly, to collect good quality data sets in a flume representative of a simplified natural open channel flow. Secondly, to develop a numerical model that would allow the relative importance of the mixing processes in the flow to be understood.

Measurements were made of the longitudinal dispersion coefficient and of the mechanisms that lead to dispersion. These were: the velocity field, the vertical and transverse mixing coefficients and the transfer rates from dead zones formed in the bed of the flume. It was found that the hydraulic characteristics of the flume were consistent with natural open channel flows. The longitudinal dispersion, transverse and vertical mixing coefficients measured in the flume scaled with the flow depth and side wall corrected bed shear velocity and were also consistent with those measured in natural open channel flows. The dead zone transfer rates were a function of flow rate and were higher than those obtained by previous workers for rivers.

A random walk model of the mixing in the flume was developed and was shown, for the first time, to be able to predict longitudinal dispersion coefficients in flows with dead zones. Traditional one-dimensional models assume that the transverse velocity shear and mixing in a flow are the main causes of longitudinal dispersion. The modelling work showed that, for higher flow rates, the vertical velocity shear and longitudinal non-uniformity of the flow made a significant contribution to the longitudinal dispersion in the flume.

Chapter one Introduction

Rising industrial and domestic use of water, combined with greater public and Governmental interest in the environment, means that the problem of predicting solute transport in rivers and streams is of increasing importance.

Engineers may be faced with predicting the result of accidental spillages of chemicals or setting the level of discharges from a pollutant source. Whatever the specific application, there is a need for reliable models of solute transport in open channel flows. In the 1960's Hugo Fischer (1966a, 1966b, 1967) developed a one-dimensional model of solute transport known as the Advection Dispersion Equation (ADE). His analysis was for a solute some distance downstream from an instantaneous release in a uniform flow at a point where the solute had become well mixed across the cross-section. In order to use the ADE the cross-sectional average velocity and the longitudinal dispersion coefficient in the channel have to be known. The longitudinal dispersion coefficient represents all the mixing processes in the flow. Fischer argued that in natural open channel flows the transverse velocity shear and mixing were the dominant dispersion mechanisms. He gave an equation from which the longitudinal dispersion coefficient may be calculated if the velocity field and the rate of transverse mixing are known. It has been found by some workers, however, that the ADE model of solute transport can be a poor model for tracer data collected in natural open channel flows. Apart from the requirement for tracer to have become well mixed over the cross-section the most commonly quoted limitation of the ADE is that it ignores the existence in the flow of dead zones that trap solute and slowly release it. Modifications have been made to the one dimensional model to allow for the effect of dead zones. The work described in this thesis is an experimental and numeric investigation of the transport of solute in a simple open channel flow that incorporates dead zones. The longitudinal dispersion

coefficients in the flume were measured as were the other elements of the mixing process. Several new data sets have been generated during this work and a novel random walk model was developed that included the effect of dead zones. The model allowed the relative importance of the dead zones, vertical and transverse mixing and the longitudinal non-uniformity to be evaluated. Contrary to the assumptions that led to the ADE the vertical mixing and shear as well as the longitudinal non-uniformity made an important contribution to the longitudinal dispersion. The objectives of the work and an outline of the thesis are given below.

1.1 Objectives of the work

The overall objectives were: to measure and model the mixing processes in an open channel flow that contained dead zones. These objectives can be split down into several specific objectives:

- To measure the longitudinal dispersion coefficients
- To measure the longitudinal velocity field and understand the bulk hydraulics of the flow over this new bed form
- To measure the vertical and transverse mixing coefficients
- To measure the transfer rate into the dead zones from the main flow
- To develop a random walk model of the mixing processes in the flume
- To use the model to asses the relative importance of the various transport mechanisms
- To compare methods of predicting longitudinal dispersion coefficients

1.2 Outline of the thesis

The thesis has been laid out with each of the items of work listed in the previous section described in a self contained chapter. Each chapter begins with a short introduction, generally followed by a brief review of the literature; the experimental techniques come next followed by the results and discussion.

Chapter two outlines the development of one-dimensional models of solute transport in open-channel flows and briefly describes some alternatives to what might be considered the traditional models. It is important to examine the origin of the one-dimensional models so that the conditions under which they are applicable can be understood.

Chapter three describes the experimental facilities and the measurement of longitudinal dispersion. An existing laboratory flume was modified by the installation of a new bed. The slope of this bed was intended to be an average of the slopes found in UK rivers. The bed itself was covered in a pattern of impressions or dimples. These dimples were intended to simulate the effect of interstitial volumes in a gravel/cobble bed stream.

The measurement of the bulk flow characteristics and the longitudinal time averaged and instantaneous velocity field in the flume is described in chapter four. The time averaged velocity field was required as an input to the random walk model. Because flow over the bed roughness type used in the author's flume had not been previously investigated both the time averaged and the instantaneous longitudinal velocity field measurements formed a new data set. The equivalent sand grain roughness and Manning's n were calculated for the flume in order that it could be compared to other laboratory flumes and to natural open channels flows.

Chapter five is concerned with the measurement of dead zone transfer rates. The dimples formed in the bed of the flume were nominally identical. However it was realised

that local variations in the bed geometry and the flow velocity could influence the transfer rate out of the dimples and therefore a total of eight dimples in three longitudinal and four transverse locations were investigated. The dimple dead zone transfer rates were averaged to give a figure that could be used in the random walk model. Few measurements of dead zone transfer rates exist in the literature and the geometry used in the present work makes the data unique.

In chapter six the transverse and vertical mixing experiments are detailed. Compared to the dearth of dead zone transfer measurements, the rate of transverse mixing in open channel flows has been quite extensively investigated both in the laboratory and in the field. The hydraulic characteristics of the author's flume were unique, being consistent with both straight natural open channel as well as laboratory flows. The measured mixing coefficients are therefore compared to data obtained in laboratory and natural open channel flows.

Chapter seven is concerned with the development and use of a random walk model of the dispersion processes. Previous workers have begun to modify the random walk model to incorporate dead zones but the present work, is to the author's knowledge, the first to demonstrate that a modified random walk model can simulate laboratory mixing experiments in the presence of dead zones.

It was decided that each chapter in this work should be written to stand alone so that the data sets contained within them were as accessible as possible. Chapter eight is therefore needed to draw together and discuss the different parts of the work. Chapter nine gives the conclusions from the previous chapters and suggests areas where further work is required.

Chapter two Longitudinal Dispersion: an overview

2.1 Introduction

This thesis is concerned with the transport of conservative solutes in open channel flow. The concentration of a solute in a flow will, obviously, depend upon the nature of the source of the solute. The concentration of the solute as it enters the flow, the duration of the discharge of solute and how the solute enters the main flow, for example as a diffuse or a point source, will affect the concentrations measured downstream of the solute source. It is useful to split discharges of solute into two groups: continuous discharges and time varying discharges. For a continuous discharge of a solute into a flow the concentration of solute in the channel, after it has spread over the whole cross-section, can be predicted from a simple mass balance. For this case an understanding of longitudinal dispersion is not necessary. However for an instantaneous or time varying input of material to the channel an understanding of longitudinal dispersion is essential.

Consider an injection of a discrete mass of dye into the middle of a long straight channel. As the dye is transported downstream, cross-sectional mixing (caused by secondary currents, turbulence and molecular diffusion) tends to spread it over the depth and the width. As the dye spreads vertically and transversely it is exposed to the vertical and transverse velocity profiles. The difference between the streamwise velocity of two adjacent dye masses tends to spread the tracer cloud longitudinally; this effect is termed differential advection. The interaction of differential advection and cross-sectional mixing spreads the cloud transversely, vertically and longitudinally. It also determines the rate at which the peak dye concentration along the channel is reduced. An observer at a fixed position along the channel would note, for a given point in the cross section of the

channel, a rise and fall of the dye concentration; this curve of concentration against time at a fixed position is known as a temporal distribution of concentration. If instead of a single observer there are a number of observers spaced along the length of the water way, who all note the concentration at a given instant of time, we would obtain the spatial distribution.

By making certain assumptions it is possible to derive an equation for the change in cross-sectional average concentration following a discrete input of solute to a uniform flow. The equation is only valid after the solute is well mixed in the flow and predicts that eventually the spatial distribution is a Gaussian whose variance increases linearly with time as the dye is transported downstream. It was developed by Taylor (1954) and Fischer (1966a, 1967) and is known as the Advection Dispersion Equation (ADE). It is a one-dimensional equation; i.e. it models the change in cross-sectional averaged concentration. The ADE has the same form as a diffusion equation, but the dispersion coefficient in the ADE includes the effect of diffusion, turbulent mixing and differential advection. To calculate the dispersion coefficient requires information on velocity and turbulent mixing that is often not known; it is therefore more common to estimate the coefficient from empirical equations (which are considered later in chapter three) or to use tracer experiments and the method of moments. In the method of moments concentration distributions of a tracer material are measured at two (or more) points along the channel and the dispersion coefficient is calculated from the rate of change of variance of the distributions.

It was pointed out (Thackston & Schnelle 1970, Nordin & Thackson 1980) that the ADE is often unable to correctly model the tracer distributions observed in many natural waterways. Concentration profiles measured in natural open channels are often skewed whereas the ADE predicts a Gaussian distribution. One explanation for the

skewed concentration profiles is that they are commonly temporal rather than spatial measurements. This does not account for all the skewness in the measurements, however, and dead zones in the flow have often been considered to be the cause of the additional skewness. Dead zones are regions of the flow within which the tracer material can become temporarily trapped, and from which tracer is gradually released back into the main flow. Dead zones have been considered to be produced by the voids between individual stones of a gravel bed and also by recirculating eddies shed by obstacles or irregularities in the channel form. The ADE, when modified to incorporate dead zones is known as the ADE plus dead zone (ADE+DZ) model.

The following sections describe the development of the ADE and ADE+DZ models and the problems that arise when the models are solved numerically, as well as three alternatives to the ADE (the random walk, Aggregated Dead Zone and two zone models).

2.2 Derivation of Advection Dispersion Equation

There are several excellent treatments of solute transport in texts such as Fischer et al (1979), Chatwin & Allen (1985), Holly (1985) and Rutherford (1994). The following is a brief account of the development of one-dimensional models. Taylor's (1954) analysis for steady turbulent pipe flow is given in some detail below because it is necessary to have an understanding of the assumptions that underline the ADE when considering its application to natural waterways.

Taylor begins his paper with an acknowledgement to another eminent fluid mechanist (G.K. Batchelor) who had recognised that one of Taylor's earlier analyses, namely that of the spread of a tracer in a homogeneous turbulence field, could be extended to pipe flow. This previous analysis had shown that the spread of a tracer in

homogeneous turbulence could, after an initial time interval, be described by a diffusion equation. Batchelor noted that the analysis was valid for pipe flow if instead of a Eulerian frame of reference a Lagrangian one was used.

Taylor (1954) began his investigation by writing the conservation equation for solute mass in terms of the local time averaged solute concentration, c, in a pipe of radius, a. This equation is:

$$\frac{\partial}{\partial z}\left(\varepsilon z\frac{\partial c}{\partial z}\right)=z\left(u\frac{\partial c}{\partial x}+\frac{\partial c}{\partial t}\right) \tag{2.1}$$

where z is the non-dimensional radial distance, x is the longitudinal dimension, u is the time averaged local longitudinal velocity and ε is the local cross-stream turbulent diffusivity. He then applied a Lagrangian co-ordinate system, $\xi = x-\bar{u}t$ and $\tau=t$ from which the following chain rule operators derive:

$$\frac{\partial}{\partial x}=\frac{\partial}{\partial \xi}$$

$$\frac{\partial}{\partial t}=\frac{\partial}{\partial \tau}-\bar{u}\frac{\partial}{\partial \xi}$$

Here, $\bar{u}$ is the cross-sectional average flow velocity. An expression for the turbulent diffusivity was derived using Reynolds' analogy (which implies equivalence between mass and momentum transport). Using this with a linear shear stress profile and an empirical logarithmic velocity profile for the pipe, the following equation was obtained.

$$\frac{\partial}{\partial z}\left(\frac{z^2}{f'(z)}\frac{\partial c}{\partial z}\right)=z\left\{(f(z)-4.25)a\frac{\partial c}{\partial \xi}+\frac{a}{u_*}\frac{\partial c}{\partial \tau}\right\} \tag{2.2}$$

Here u_* is the bed shear velocity, $f(z)$ is the non-dimensional velocity profile and $f'(z)$ is its derivative.

Taylor sought a solution for equation (2.2) for the case when $\frac{\partial c}{\partial x}$ is independent of x and z and the longitudinal concentration profile changes so slowly that it can be

assumed that $\frac{\partial c}{\partial t} \approx 0$. The concentration is considered to consist of two additive components; one a function of ξ, the other a function of the radial position $\left(\text{i.e.} c = c_\xi + c_z\right)$

The assumption that $c_z \neq fn(\xi)$ requires a steady state radial concentration profile to have been set up which in turn implies a balance between longitudinal advection and radial diffusion.

With these simplifications Taylor was able to find an expression for the radial concentration profile. This, along with u' the deviation of the local velocity from the cross-sectional average flow velocity, allowed him to write an equation for the solute mass transfer rate, Q, across a plane that moved with the mean flow velocity, namely:

$$Q = -10.06\pi a^3 u_* \frac{dc}{d\xi} \tag{2.3}$$

A Fickian diffusion equation is one in which the mass transfer rate is given by the product of a (constant) diffusion coefficient and a (spatial) concentration gradient. The final step of Taylor's analysis was to note that equation 2.3 was synonymous with such a diffusion equation and that the diffusion coefficient, more properly here the dispersion coefficient, D, was given by:

$$D = 10.1 a u_* \tag{2.4}$$

Equation 2.4 includes a correction Taylor applied to account for the additional mass transport caused by longitudinal turbulent diffusion. In Eulerian co-ordinates the Fickian diffusion equation is:

$$\frac{\partial c}{\partial t} + u\frac{\partial c}{\partial x} = D\frac{\partial^2 c}{\partial x^2} \tag{2.5}$$

which is commonly termed the Advection Dispersion Equation.

Taylor performed experiments by injecting discrete doses of a salt solution into water flowing in a long straight pipe. The conductivity of the solution was measured at three locations along the pipe, and observed spatial concentration distributions were Gaussian which was consistent with the solution of equation 2.5 at large time scales. Taylor noted that as the flow rate in the pipe was reduced a longer length of pipe was required before Gaussian concentration profiles were measured; he believed that this was because at the lower flow rates some solute was trapped in the laminar sub-layer whose thickness was inversely proportional to flow rate.

Elder (1959) performed a similar analysis for a two-dimensional open channel flow with a logarithmic vertical profile for the longitudinal velocity; this two-dimensional flow is also known as wide open channel flow because in an infinitely wide channel the only velocity profile is in the vertical direction. The theoretical longitudinal dispersion coefficient, including longitudinal turbulent diffusion, was in Elder's case:

$$D = 5.93du_* \tag{2.6}$$

Elder performed experiments to confirm his analysis and found that the longitudinal dispersion coefficient was $D = 6.3du_*$. Elder believed that the difference between the measurements and theory was due to the assumptions that were made about the turbulent diffusivity.

For a number of years engineers noted that dispersion coefficients measured in natural waterways exceeded those predicted by Elder's analysis. Fischer (1967) demonstrated that the reason for this discrepancy was due to the difference between the dispersion processes in wide, two dimensional, open channel flow and natural, three dimensional flows. Fischer argued that in natural waterways it is the transverse velocity shear and transverse mixing which dominates longitudinal dispersion and that the role of the velocity shear and mixing in the vertical dimension is secondary. His analysis

followed a similar line of reasoning to Taylor's and Elder's and began with a three-dimensional transport equation, namely:

$$\frac{\partial c}{\partial t} + u\frac{\partial c}{\partial x} = \frac{\partial}{\partial y}\left(\varepsilon_y \frac{\partial c}{\partial y}\right) + \frac{\partial}{\partial z}\left(\varepsilon_z \frac{\partial c}{\partial z}\right) \tag{2.7}$$

where $x, y, z,$ are the longitudinal, vertical and transverse dimensions respectively. The vertical and transverse eddy diffusivities are ε_y and ε_z while the local longitudinal velocity is represented by u as before. Fischer wrote the time averaged longitudinal velocity and solute concentration as the sum of a cross-sectional mean value (indicated by an overbar) and a local deviation from the mean (indicated by a prime), i.e:

$u = \bar{u} + u'$ and $c = \bar{c} + c'$

He also introduced a co-ordinate system moving at the mean flow velocity ($\xi = x - \bar{u}t$) as in Taylor's analysis and obtained:

$$\frac{\partial}{\partial t}(\bar{c} + c') + u'\frac{\partial}{\partial \xi}(\bar{c} + c') = \frac{\partial}{\partial y}\left(\varepsilon_y \frac{\partial c'}{\partial y}\right) + \frac{\partial}{\partial z}\left(\varepsilon_z \frac{\partial c'}{\partial z}\right) \tag{2.8}$$

In order to simplify this equation Fischer assumed that $c' << \bar{c}$. Furthermore, he assumed that $\frac{\partial \bar{c}}{\partial t} << u'\frac{\partial \bar{c}}{\partial \xi}$ & $u'\frac{\partial c'}{\partial \xi} << u'\frac{\partial \bar{c}}{\partial \xi}$ (2.9)

and could be ignored. More detail of the justification of these assumptions was given by Fischer (1966b) where he shows that their adoption is consistent with Taylor's simplification of equation 2.2. Fischer's assumption that eventually $c' << \bar{c}$ has the advantage of being testable. Sayre (1968) suggests that while $c' << \bar{c}$ is a necessary condition for the simplifications of equation 2.8 to equation 2.9 to be valid, it is possible (and there is experimental evidence for it being the case) that they are valid before $c' << \bar{c}$.

Fischer then assumed that the contribution of the vertical velocity and concentration profiles to the longitudinal dispersion was negligible compared to that of

the transverse direction. This and an application of the above simplifications to equation 2.8 gives

$$\frac{\partial c'}{\partial t} + u' \frac{\partial \overline{c}}{\partial \xi} = \frac{\partial}{\partial z}\left(\varepsilon_z \frac{\partial c'}{\partial z} \right) \tag{2.10}$$

which has the following steady state solution if $\frac{\partial \overline{c}}{\partial \xi}$ is constant:

$$c' = fn(z) \frac{\partial \overline{c}}{\partial \xi} \tag{2.11}$$

By defining $q' = \int_0^{d(z)} u'(y,z)dy$ and integrating equation 2.10 over the depth Fischer obtained the following integral equation for $fn(z)$:

$$fn(z) = \int_0^z \frac{1}{\overline{\varepsilon_z} d(z)} dz \int_0^z q'(z)dz \tag{2.12}$$

in which $\overline{\varepsilon_z}$ is the depth averaged transverse diffusivity.

The mass transport rate, $\dot{Q}$, through a cross-section moving at the mean flow velocity is given by $\dot{Q} = \int_A u'c'dA$ in which A is the area of the cross-section. Substituting for c' gives:

$$\dot{Q} = \int_A u' fn(z) \frac{\partial \overline{c}}{\partial \xi} dA \tag{2.13}$$

which implies that the mass transport can be represented by a diffusion equation, i.e.:

$$\dot{Q} = -DA \frac{\partial \overline{c}}{\partial \xi} \tag{2.14}$$

Equating equations 2.13 and 2.14 and rearranging gives:

$$D = -\frac{1}{A} \int_A u' fn(z) dA$$

substituting for $fn(z)$ the dispersion coefficient is given by the following triple integral:

$$D = -\frac{1}{A}\int_0^b q'(z)dz \int_0^z \frac{1}{\overline{\varepsilon_z} d(z)} dz \int_0^z q' dz \qquad (2.15)$$

in which b is the channel width and $\overline{\varepsilon_z}$ is the depth average transverse mixing coefficient. Note that we use the term transverse mixing rather than transverse diffusivity in recognition of the fact that in natural open channel flows secondary currents, as well as turbulent diffusion play a role in the transverse mixing.

If the velocity field and transverse mixing in a river are known equation 2.15 can be used to estimate the longitudinal dispersion coefficient. Fischer also gave an equation for the length of time that would need to have passed before cross-sectional mixing had occurred and the analysis was valid.

We can consider the passage of a discrete cloud of solute along a channel from an instantaneous source as having three stages (see Figure 2.1). Initially advection dominates the transport and the longitudinal variance of the solute cloud changes non-linearly whilst the skewness rises; this is known as the advective zone. After some time, the change of variance becomes linear and the skewness falls; this stage is known as the equilibrium zone. Eventually the spatial concentration profile becomes Gaussian in the Gaussian zone. Rutherford (1994) gives various workers' estimates of the non-dimensional length, α , of the advective zone in various flows. These range from 0.3 (for a smooth laboratory channel) to greater than 10 (for an irrigation channel with a rough bed and sides and the presence of dead zones). The non-dimensional length is defined as:

$$\alpha = \frac{L_a k_z}{L_t^{\,2} u_q} \qquad (2.16)$$

In which L_a is the length of the advective zone, k_z is the transverse mixing coefficient, L_t is a transverse length scale (half the width for a symmetrical channel and central source) and u_q is the cross-sectional average velocity. Fischer's time scale for cross-

sectional mixing $\left(\frac{L_t^2}{k_z}\right)$ that was mentioned at the end of the preceding paragraph is equivalent to assuming α is unity because cross-sectional mixing is required before the rate of change of variance becomes linear (at the end of the advective zone). From Rutherford's data a good estimate of α for rough channels with no dead zones would also appear to be unity. In Table 2.1 data given by Rutherford (1994) for transverse mixing has been analysed using equation 2.16 to estimate the length of the advective zone. The rivers were straight and assumed to be symmetrical; α was taken to be unity. The estimated length of the advective zone ranges from one to hundreds of kilometres. This table shows that whilst the ADE has a theoretical basis a long length of uniform flow is required before it becomes valid. In a natural stream it is very likely that the stream cross section will change before the equilibrium zone is reached and hence the ADE may never become valid.

Fischer (1966a) compared the predictions of equation 2.15 to longitudinal dispersion measurements performed in straight uniform channels of various regular cross sections. He used an empirical equation $\left(\overline{\varepsilon}_z = 0.23du_*\right)$ that was developed by Elder (1959) for wide open channels to estimate the depth averaged transverse eddy diffusivity in his channels. Fischer considered that equation 2.15 then gave good predictions of the measured longitudinal dispersion for both the rectangular and trapezoidal section channels. Interestingly it will be seen later (chapter six) that Elder's equation implies a greater rate of depth averaged transverse mixing than later worker's measurements which imply that a better estimate for a wide open channel is: $\overline{\varepsilon}_z = 0.16du_*$. It will also be seen that greater rates of transverse mixing are obtained in three-dimensional flows. As the flow in Fischer's channels was not two-dimensional (he was after all interested in

confirming the analysis that led to equation 2.15) it is possible that the level of transverse mixing given by Elder's equation was appropriate.

Fischer (1966a,b) demonstrated how the change of variance of measured concentration profiles could be used to calculate a longitudinal dispersion coefficient. This technique, called either the method of moments or change of moments method, is valid as long as the rate of change of variance is linear.

$$D = \frac{1}{2}\frac{d\sigma_x^{\,2}}{dt}$$
$$D = \frac{1}{2}u^2\frac{d\sigma_t^{\,2}}{dt} \qquad (2.17a,b)$$

where the suffixes x and t refer to the variances of the spatial and temporal concentration profiles respectively and u is the cross-sectional flow velocity.

2.3 Modified Advection Dispersion Equation

The Advection Dispersion Equation predicts a Gaussian spatial distribution of solute downstream (in the Gaussian zone) of an instantaneous input. The predicted temporal distribution is skewed but not to the extent seen in tracer work undertaken in natural streams and rivers (Thackson, Hays & Krenkel 1967) the distributions of which, typically, have long tails.

Many workers (Thackston & Schnelle 1970, Nordin & Troutman 1980, Tjomsland 1983, Legrand-Marc & Laudelot 1985) have modified the ADE by incorporating the effect of dead zones which were believed to be the cause of the long tails. The equations for these ADE+DZ models are:

$$\frac{\partial \bar{c}}{\partial t} + \bar{u}\frac{\partial \bar{c}}{\partial x} - D\frac{\partial^2 \bar{c}}{\partial x^2} = \gamma k_a\left(c_d - \bar{c}\right)$$
$$\frac{\partial c_d}{\partial t} = k_a\left(\bar{c} - c_d\right) \qquad (2.18)$$

in which $\overline{u}$ is the volumetric flow velocity, γ is the dead zone fraction (the fraction of the total flow area occupied by dead zones), k_a is a transfer coefficient between the dead zones and the main flow zone, c_d is the concentration in the dead zone, $\overline{c}$ is the cross-sectional average concentration and D is the longitudinal dispersion coefficient. Nordin & Troutman (1980) applied both an ADE and an ADE+DZ model to field data. For the ADE the longitudinal dispersion coefficient was calculated by using the change of moments method. The coefficients of the ADE+DZ model, however, were selected so that the model gave a best fit to the measured data. Nordin & Troutman found that the longitudinal dispersion coefficient suggested by the ADE+DZ model was lower than that implied by the ADE. They considered the difference to be due to the additional longitudinal dispersion caused by the dead zones in the ADE+DZ model.

Valentine & Wood (1977), Purnama (1988) and Denton (1990) have shown that the incorporation of a dead zone term to a two-dimensional mass conservation equation increases the longitudinal dispersion. Denton's equations were:

$$\frac{\partial c}{\partial t} + u\frac{\partial c}{\partial x} = \frac{\partial}{\partial y}\left(\varepsilon_y \frac{\partial c}{\partial y}\right) + \frac{\partial}{\partial x}\left(\varepsilon_x \frac{\partial c}{\partial x}\right)$$
$$\varepsilon_y \frac{\partial c}{\partial y} = kR(c_{y0} - c_{dz}) \qquad (2.19)$$

where R is the ratio of the bed covered by bed zones, c_{y0} is the concentration at the bottom of the channel, c_{dz} is the concentration in the dead zone and k is the transfer coefficient between the dead zone and main flow. Such analyses indicate an increase in the time required before the change of variance of the concentration profiles become linear and a reduction in the rate at which the skewness of the profiles die away. Equation 2.19 differs from equation 2.18 in that equation 2.18 is a cross-sectional averaged equation whereas equation 2.19 retains the vertical variation of longitudinal velocity and diffusivity. Valentine & Wood (1977) showed that equation 2.17b can be

used to calculate the effective longitudinal dispersion coefficient from temporal concentration profiles if the cloud velocity, u_c, is used instead of the volumetric flow velocity. The cloud velocity is calculated from the time taken by the centroid of the concentration profiles to travel between the two measurement positions. Valentine & Wood (1979a) also found experimentally that the incorporation of dead zones into a flow reduced the cloud velocity below the cross-section average velocity by an amount proportional to the dead zone fraction.

Table 2.2 shows the results of a number of measurements and estimates of the transfer rate from dead zones. Valentine & Wood (1977) measured the dead zone transfer rate for a rectangular slot in a rectangular laboratory flume, and Seo & Maxwell (1992) measured the transfer rate from recirculation zones formed in a laboratory flume that was modified to simulate a series of pools and riffles. All the other data in Table 2.2 were obtained by adjusting the coefficients of an ADE+DZ model until the best fit to measured concentration profiles was obtained. The dead zone fractions and transfer rates in Table 2.2 cover a wide range of values. It should be noted that Yu & Wenzhi and Nordin & Troutman both applied an ADE+DZ model to the same Mississippi data but got very different values for the dead zone fraction and transfer rate (the longitudinal dispersion coefficient reported is the same for both papers). Yu & Wenzhi state that their parameter estimation method led to a better fit between the model and the tracer data than that obtained using the coefficients suggested by Nordin & Troutman. The difference between the results that these two workers obtained demonstrates the difficulty of parameter estimation by fitting an ADE+DZ model to tracer data. Thackson & Schnelle (1970) attempted to find empirical correlations with other hydraulic parameters for the dead zone transfer rate and dead zone fraction. They were able to

correlate the dead zone fraction to the friction factor in the streams but were unable to find a correlation for the time tracer spent in the dead zones.

2.4 Difficulties with numerical solutions of the ADE

Whilst an analytical solution exists for the ADE, in practice numerical solutions are required. This is because real rivers are not uniform, and while it could be argued that the ADE is then no longer valid, it is often applied with the cross-sectional area and dispersion coefficient varying along the channel length. There are various solution schemes available which are discussed in standard texts such as Abbott & Basco (1989). The majority of numerical solutions of the ADE use a Eulerian co-ordinate scheme, although as described below semi-Lagrangian schemes have certain advantages. Lagrangian schemes are described by McBride & Rutherford (1984) and Schoellhamer (1988).

Two types of Eulerian schemes exist: explicit and implicit. Explicit solutions require the use of small time steps to ensure a stable solution (the Courant number which is the product of the time step and flow velocity divided by the spatial grid size $\left(\frac{\Delta t \cdot u}{\Delta x}\right)$ having to be <1). Implicit solutions do not have a stability restriction on the Courant number but their accuracy reduces significantly if the Courant number becomes too large. In this regard the work of Manson & Wallis (1995) indicates that their use is a false economy of effort.

There are two other main difficulties with traditional Eulerian methods: numerical diffusion and grid-scale oscillations. The former is due to the truncation of the finite-difference or finite-element approximations to the governing equation which causes the numerical solution to display a different amount of dispersion to that prescribed by the

dispersion coefficient. The latter is caused by poor treatment of the advection term, particularly where the spatial resolution of steep concentration gradients is low, and results in non-physical effects such as 'saw-tooth' patterns (also known as 'wiggles') and negative concentrations. Numerical diffusion and grid-scale oscillations can be controlled (but not eliminated) by using small steps in time and space, although the computational costs can be high.

In recent years, significant improvements over the Eulerian schemes have been obtained by using semi-Lagrangian (sometimes Eulerian-Lagrangian) schemes. These exploit the physical nature of advection and combine ideas from the method of characteristics (commonly used with Lagrangian schemes) and the fixed grid (Eulerian) finite difference or finite element methods mentioned above. The main advantage of such schemes is that they are unconditionally stable and can achieve comparable accuracy with Eulerian schemes when used with much larger time steps. The latest versions of these schemes (Manson & Wallis 1995; Wallis & Manson 1996; Leonard et al 1995a, 1995b) also incorporate techniques for ensuring mass conservation (which is a well known problem with characteristic based, particularly fully Lagrangian, methods) and the elimination of the worst effects of 'wiggles'.

2.5 Alternatives to the ADE

Several alternatives to the ADE and ADE+DZ models exist in the literature and three of these, namely; random walk models, the Aggregated Dead Zone model and two zone models are briefly described below.

2.5.1 Random walk models

Random walk models are an alternative method of simulating dispersion (Heslop & Allen 1993, Heemink & Blockland 1995) and are discussed more fully in chapter

seven. In these models a large number of particles are tracked as they move through a numerical representation of the flow field. The particles follow the local time averaged velocity for each time step of the simulation and are given a random motion to model the turbulent mixing. The distribution of the particles can be taken as a representation of the spread that would be achieved by an injection of solute into the physical flow being simulated. Random walk models do not suffer from numerical dispersion or computational instability but they do require the velocity field and mixing coefficients to be known. Of course, in this regard, the ADE and ADE+DZ models require similar physical information if the longitudinal dispersion is to be correctly simulated.

2.5.2 The Aggregated Dead Zone (ADZ) Model

The derivation of the ADZ (Beer & Young (1983)) assumes that all the longitudinal dispersion in a river is due to the presence of dead zones that trap and delay solute. The model can be thought of as a move away from an attempt to model the detailed physical processes that cause the dispersion of a solute in a water course; it is rather a one-dimensional mass balance equation whose coefficients can be adjusted to allow it to describe concentration profiles. Whilst it may seem odd to use an equation in this way it should be remembered that the ADE+DZ model is usually fitted to tracer data by an iterative adjustment of its coefficients. Also, in both cases the coefficients are representative, in some sense, of the physical processes.

Beer & Young (1983) describe how a time series parameter estimation computer package can be used to identify the ADZ model coefficients that best describe data obtained from tracer experiments. For open channel flow the variation of the ADZ coefficients with flow rate was investigated (in the field) by Wallis, Young & Beven (1989) and (in the laboratory) by Wallis, Guymer & Bilgi (1989). The model was applied

to a pollution incident on the Rhine by Hottges, Wallis & Guymer (1992) and Wallis & Clarke (1995).

The ADZ model can be derived from a consideration of solute mass balance over a particular reach of a river (Young & Wallis (1991) and Wallis (1993)), to give:

$$\frac{dc_o(t)}{dt} = \frac{1}{\gamma \bar{t}}(c_o(t) - c_i(t-\tau))$$

where, c_i is the concentration at the input to the reach and c_o is the concentration at the reach output, $\bar{t}$ is the travel time, γ, is the fraction of the reach volume involved in dispersion, known as the dispersive fraction, and τ is the delay time. The travel time is the volume of water in the reach divided by the flow rate; it can be obtained from tracer tests as the time that the centroid of a tracer distribution takes to travel through the reach. The time delay is the time that is required before solute at the input of the reach is observed at the output. The product of the dispersive fraction and the travel time, $\gamma\bar{t}$, is known as the residence time, T. The parameters of the ADZ are related (Wallis (1993)), by $\bar{t} = T + \tau$ which states that the travel time is equal to the sum of the residence time and the advective time delay.

The ADZ model can be applied in a parallel or series mode. A series of ADZ elements could model a river with spatially varying dispersive properties, whilst a parallel application could model a bifurcated river or a river with a porous bed. (Wallis, Young & Beven (1989); Young & Wallis (1993).

Wallis, Young and Beven (1989) performed experiments in three rivers near Lancaster University as well as a canalised stream that ran through the campus. Mean values of dispersive fraction ranged between 0.29 and 0.37 for the rivers and appeared to be invariant with flow rate. The dispersive fraction recorded for the canalised stream was lower at 0.12; this was thought to have arisen because the relatively straight and uniform

flow produced less dispersion. In all cases the travel time was inversely proportional to flow rate, being consistent with conventional channel flow hydraulics. There are similarities here to the findings of Sabol & Nordin (1978) who reported results using a form of ADE+DZ model where the ratio of time spent in the transit zone to the total time of travel was found to be approximately independent of flow rate.

Laboratory data from a gravel bed flume was reported by Wallis, Guymer and Bilgi (1989). A slight reduction in dispersive fraction with flow rate was noted with values ranging between 0.215 and 0.312. Data collected by Graasvoll (1992) in a fairly straight reach of a small stream again showed the travel time to be inversely proportional to flow rate and the dispersive fraction to be weakly varying with flow rate. Further discussion appears in Wallis (1993).

2.5.3 Two zone models

Two zone models are models in which the flow in a channel is divided into two parts, a zone where the water flow is fast and a zone where the flow is slow. Smith (1987) gives an analytical solution for a two zone model of a meandering stream. The paper builds on earlier work with two zone models and gives time lag functions that model the asymptotic form of the dispersion process. The non-uniformity of the concentration across the river section is represented. Smith was aiming to produce an expression for a generalised two zone model that had a similar form to the ADZ model. The advantage of such a model was claimed to be that hydrodynamic principles could enable changes in parameters to be calculated if the discharge of the river changed.

Reichart & Wanner (1991) also suggested that a two zone model could be used to model concentrations closer to the injection point of a solute without the complexity of a full two-dimensional model of the transport processes. An analytical investigation of

a two zone model was presented by Chikwenou & Ojiakor (1985) who found that the two zone model was able to reproduce the skewed nature of experimental data.

2.6 Conclusions drawn from the literature

Several conclusions can be drawn from the literature reviewed above. It has been shown that there are three stages to the mixing of a discrete dose of a solute added to a uniform open channel flow. In the first stage, known as the advective zone, the solute is mixed over the cross-section of the channel. During the second stage known as the equilibrium zone the longitudinal variance of the cross-sectional average concentration grows linearly in comparison to the non-linear growth in the advective zone. In the final stage, or Gaussian zone, the spatial longitudinal concentration profile is Gaussian. A theoretical model, the Advection Dispersion Equation (ADE) exists that can be used to predict the longitudinal dispersion in the Gaussian zone. The model (as developed by Fischer 1967) has a dispersion coefficient that represents the mixing due to the longitudinal velocity field and cross-sectional eddy diffusivity. Fischer gave an equation that allows the dispersion coefficient to be calculated if the velocity field and transverse eddy diffusivity in a channel are known.

Although the solution to the ADE predicts a Gaussian concentration profile, which is only actually seen in the Gaussian zone, the rate of change of variance of the longitudinal concentration profile is the same in both the equilibrium and Gaussian zones. The rate of change of the variance can be related to the longitudinal dispersion coefficient in the ADE and this provides a method for measuring the longitudinal dispersion coefficients in practical cases.

It has been shown that a long length of channel may be required before the longitudinal variance of the cross-sectional average concentration profile grows linearly

and that for a given uniform flow field the addition of dead zones increases the length of channel that is required. Dead zones are considered to be zones in the channel that trap and slowly release solute and have been suggested as the reason why the ADE is often a poor model for dispersion in natural open channel flows. For a given uniform flow field the addition of dead zones increases the longitudinal dispersion above the value predicted by Fischer's equation.

Few measurements of transfer rates into and out of dead zones have been made; most of the data has come from fitting an ADE+DZ model to measured concentration profiles. No quantitative measurements of the transfer rates from the interstitial volumes of a gravel bed river have been given in the literature.

River	Width (m)	u_q (m/s)	k_z ($*10^{-4}$ m^2/s)	L_a (Km)
Atrisco	18.3	0.63	102	5.2
	18.3	0.66	102	5.4
	18.3	0.67	93	6.0
Bernado	20	1.25	130	9.6
South	18.3	0.24	140	1.4
	18.3	0.18	47	3.2
Athabasca	373	0.95	930	355.3

Table 2.1 Length of the advective zone in several US rivers (data from Rutherford 1994)

Reference	River	γ	k_a (s^{-1})
Valentine & Wood (1977)	Laboratory	0.04 to 0.25	0.02u/d
Valentine & Wood (1977)	Laboratory	0.5	0.02u/d (0.05 to 0.15)
Seo & Maxell (1992)	Lab' Pool & Riffle	0.45 to 0.59	0.008 to 0.019
Valentine & Wood (1979b)	New Zealand irrigation canal	0.40 to 0.45	0.02u/d
Legrand-Marc & (1985)	Small forest stream	0.20	0.61
Bencala, McKnight & Zellweger (1990)	U.S. mountain stream	0.21	$25e^{-6}$ to $0.5e^{-3}$
Nordin & Troutman (1980)	Wind Bighorn	0.045	$0.326e^{-3}$ to $0.754e^{-3}$
	Bear Creek	0.025	17
	Missouri	0.042	$70.16e^{-6}$
Yu & Wenzhi (1989)	Mississippi	0.28	$24.1e^{-6}$
	Missouri	0.17	14.1 e^{-6}
	Saline	0.055	56.1 e^{-6}
Tjosmsland (1983)	Lena	0.20	0.02u/d (0.007 to 0.021)

Table 2.2 Dead zone transfer rates.

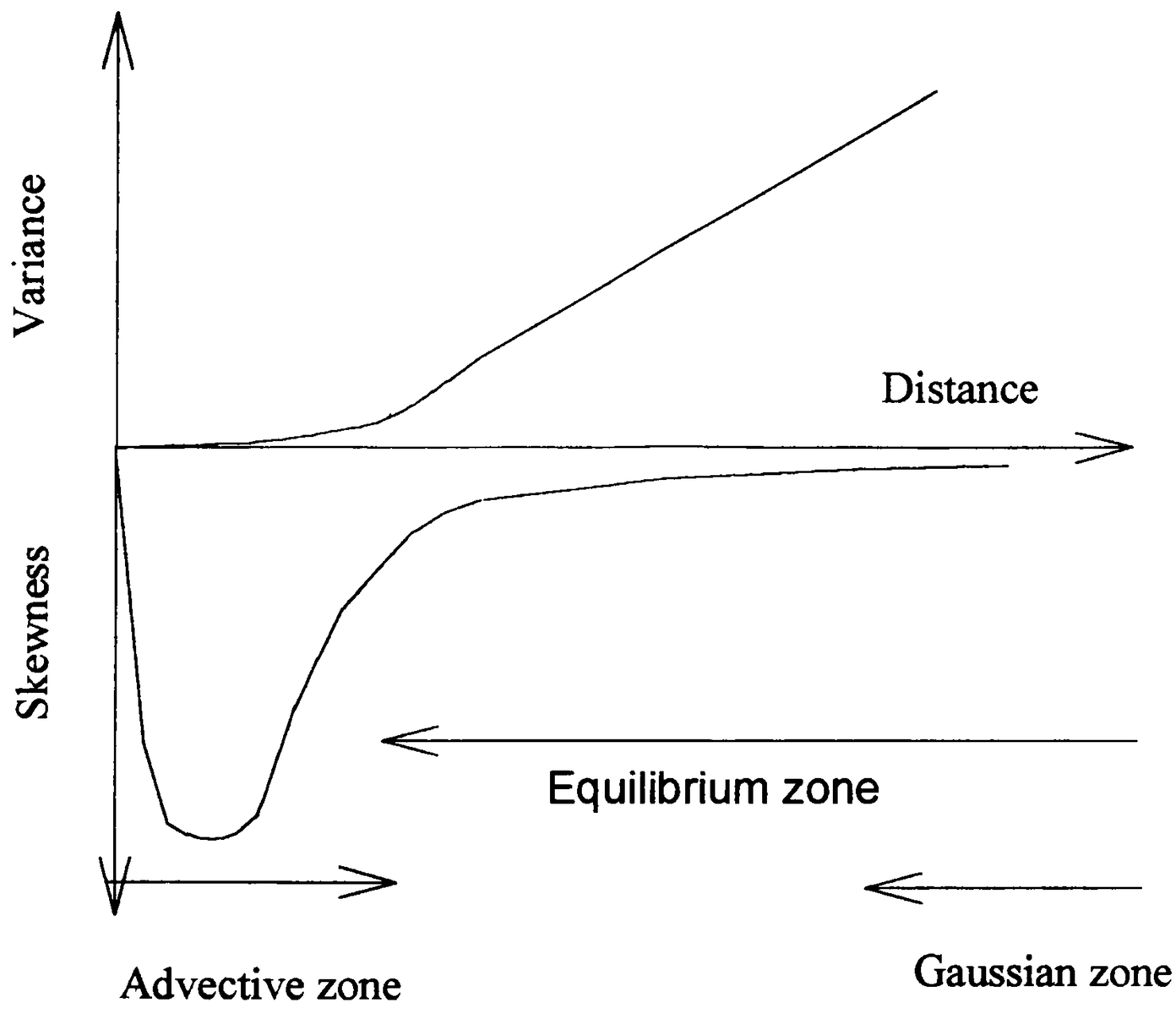

After Rutherford (1994)

Figure 2.1 Evolution of variance & skewness

Chapter Three Measurement of longitudinal dispersion

3.1 Introduction

This chapter describes the measurements of longitudinal dispersion in a laboratory flume that was intended to simulate a natural open channel flow and whose bed was covered in depressions that were intended to act as dead zones. Fluorescent dye was used as a tracer during the longitudinal dispersion experiments. The longitudinal dispersion coefficient was measured as a function of flow rate and compared to those measured by other workers in laboratory flumes and natural waterways.

3.2 Experimental Facilities

3.2.1 Laboratory flume

The recirculating flume was 28m long and 0.75m wide; it had a nominally horizontal bed and was fitted with rails for depth gauge carriages. The header tank for the flume was approximately 25m above the flume entrance to which it was connected by polythene pipe of about 154mm internal diameter. The entrance to the flume was filled with filter material (short lengths of 40mm plastic tubing) which served to break up any large eddies in the flow. Water from the main sump under the laboratory floor was pumped at a fixed rate up to the header tank and water not required by the flume overflowed from the header tank and entered a small sump at the end of the flume. The flume water exited the flume over a fixed tail gate and entered a second small sump adjacent to the first. Both sumps discharged into the main sump via weirs.

A bed of sand with a nominal slope of 1:1000 was laid in the flume, wooden spacers at 2m intervals being used to produce the slope. The slope was chosen (after referring to the data in Young & Wallis 1993) as representative of a natural open channel flow with the aspect ratios that could be obtained in the flume. A pattern (see Figure 3.1) of depressions was impressed into the sand using a number of 38mm diameter balls cut in two and glued to a board. The longitudinal spacing between the staggered rows was 27.5mm and the transverse spacing was 37mm. On average there were 450 'dimples', as the impressions were known, per square metre, with an average depth of 14mm. A general view of the flume is shown in Plate 1 while Plate 2 shows a close up of the bed. In Plate 1 the fluorometers can be seen in position for dye tracer work and in the centre of Plate 2 the intake to the fluorometer can be seen. The process of impressing the dimples led to local deviations in the sand level of ± 3mm. The dimple diameter was chosen to represent the interstitial volumes of a gravel/cobble bedded stream: the number of dimples being chosen so that their volume expressed as a ratio of the volume of water carried by the flume, was similar to the dead zone fractions found in natural open channel flows. Valentine & Wood (1979b) used a dead zone depth of 30mm in numeric simulations of the longitudinal dispersion in a straight rectangular water race. The depth was choosed after a detailed survey of the channel bed. Bray (1979) gives data on the characteristics of a number of Canadian rivers. Considering only those rivers whose bed slope and width to depth ratio is approximately the same as the laboratory flume suggests that fifty percent of the bed material had an average diameter less than 38mm and ninety percent less than 96mm. It was believed that the adoption of a semi-spherical dimple would be a better model of natural dead zones than the rectangular slots used in previous laboratory measurements of dead zone transfer rates and longitudinal dispersion.

After impressing the dimples the sand was then hardened by spraying with a solution of an adhesive (Aerolite 306) which had previously been used by Khahil (1972) to preserve sand beds formed by flowing water. Tests allowed the quantity per square metre used by Khahil to be cut by a half and a durable bed still obtained. The bed, after the adhesive dried, consisted of sand covered by a hard sand/adhesive crust. The crust was porous so the bed was painted with oil based paint and any gaps caused by shrinkage of the sand/adhesive crust filled with a silicon sealant.

3.2.2 Survey of, and stage discharge relationship for, the flume

The flume was surveyed and bed and water surface profiles along the channel were recorded. These are plotted in Figure 3.2; imperfections in the bed are evident as is the draw down as the flow approaches the horizontal tail gate. The draw down and hence the degree of longitudinal non-uniformity can be seen to increase with increasing flow rate.

The small sump supplied by the flume was surveyed and two float switches were installed to give a measurement volume of $1.573m^2$ (the uncertainty in the volume was estimated as 0.2%). The switch outputs were sampled at 10Hz by a computer controlled data logger. This sump was also fitted with submersible pumps so that steady flow could become established in the flume before the pumps were switched off, allowing the water level to increase and operate the float switches. In this way the time required to fill a known volume could be determined and hence the flume discharge calculated. A vernier depth gauge was used to measure the stage (defined as the centreline depth at a position 6m from the flume inlet) and a series of thirty eight stage and discharge measurements were taken. The flow rate in the flume was varied between 2 and 30l/s; the upper limit being set by the capacity of the submersible pumps; the lower limit by the need for a

minimum depth of flow in the flume in order to operate the fluorometers (see section 3.2). The stage discharge data is plotted as Figure 3.3; a linear regression was applied between the depth, in mm, of flow at 6m (d_{6m}) from the inlet and the flow rate, Q, in the flume in l/s. The regression gave:

$$\log_{10} Q = 1.9203 \log_{10}(d_{6m}) - 2.421 \qquad (3.1)$$

with a coefficient of determination of 0.998.

The uncertainty implied by the 0.1mm precision of the vernier gauge was insignificant. The maximum scatter of the data was 10% about the flow predicted by equation 3.1; only around a tenth of the data points showed such extreme scatter, the majority laying with 5% of the regression. Equation 3.1 was used in all subsequent experimental work to derive the flow rate in the flume.

3.2.3 Dye tracing equipment

Two Turner Designs fluorometers operating in the continuous sampling mode were used to measure the concentration of Rhodamine WT dye introduced into the flume. In the continuous sampling mode water is pumped through a glass cuvette in the fluorometer. Light from a mercury lamp is used to excite any fluorescent material in the water and the amount of fluorescent material is measured from the strength of the fluorescence. Two Jabsco Water Puppy pumps were used to draw water through the fluorometers at a fixed rate of 0.24l/s via 13mm diameter inlet tubes. The sampling, because it was not isokinetic, will have distorted the flow field around the inlet tubes but the effect was localised and would not have altered the longitudinal dispersion in the flume significantly, if at all. The more important effect of the sampling was the removal of water from the flume by the first fluorometer system. This water was not returned to the flume in order to avoid disturbances to the flow in the measurement reach. The fluorometers sampled water at 9 and 22m from the flume inlet while the stage was

measured at 6m from the inlet, so the discharge calculated for each experiment, from equation 3.1, was larger than that which actually existed between the two sampling stations by an amount equal to the quantity removed by the first fluorometer (0.24l/s). This reduction of the flow in the flume due to the extraction for the fluorometer was allowed for in the analysis of the data.

The fluorometers were calibrated by introducing five doses (each of 20μg) of a 2g/l solution of Rhodamine WT into 20l of flume water contained in a drum. The change in output voltage with concentration was plotted over the range of concentrations used (0 to 5μg/l) and the change in voltage was found to be linear. Calibrations were performed at the beginning and end of each day's work and this data for a number of days are shown in Figure 3.4 for the upstream fluorometer. The calibration applied to the fluorometer voltages recorded during a day's experiments was obtained by fitting a linear regression to the average calibration data from the morning and evening calibrations. In Figure 3.4 the morning and evening calibration data are indicated by different symbols.

3.3 Experimental technique

Each fluorometer sampled the flume water at mid span and mid depth through a 13mm internal diameter brass inlet tube. The sampling positions were 13m apart and a CED data logger sampled the output of the fluorometers at 10Hz. The first sampling position (9m from the flume inlet) was chosen to ensure that the flow was fully developed. Preliminary work (which was subsequently repeated by Downs 1994) with a sampling position closer to the flume entrance suggested that several meters of development reach were required if consistent dispersion coefficients were to be obtained.

Having set up the desired flow rate in the flume a dose of Rhodamine WT tracer was introduced into the flume's header tank. The tracer was introduced into the header tank so that it became well mixed before entering the flume, this reduced the length of flume required before the Advection Dispersion Equation became valid compared to that required if it was introduced at the flume inlet. At each flow the tracer experiment was undertaken five times. After each experiment, time was allowed for each dose of tracer to become well mixed throughout the water supply system. Although the fluorescence of Rhodamine WT is temperature dependent the difference in temperature of the water in the calibration tank and flume was less than 0.5C, as was the temperature variation over the duration of a set of runs which was considered insignificant (Smart & Laidlaw 1977).

3.3.1 Data analysis; Chatwin's method

Chatwin (1971) gave a method of plotting temporal concentration profiles that enabled their adherence to the ADE to be determined. The solution of the ADE for an instantaneous source of tracer is (Rutherford 1994):

$$c(x,t) \equiv \frac{M}{A\sqrt{4 \cdot \pi \cdot D \cdot t}} \exp\left[-\frac{(x - u_q \cdot t)^2}{4 \cdot D \cdot t}\right] \qquad (3.2)$$

where M is the mass of solute added at time t=0 (& at x=0) and A is the cross sectional area of the flow. Equation 3.2 implies a Gaussian spatial concentration profile. Chatwin plotted $\left[t \ln\left(\frac{A}{ct^{1/2}}\right)\right]^{1/2}$ against time t ; in the transformation c is the concentration and A is a constant related to the peak concentration, c_{max} which occurs at t_{max}, $A = \frac{c_{max}}{t_{max}^{-1/2}}$. Using the transformation Gaussian tracer data plots as a straight line whose slope is proportional to the longitudinal dispersion coefficient. The peak concentration occurs where the transformed data changes sign.

However, in practise, few measured data plot as a straight line (Rutherford 1994) because the ADE (and hence equation 3.2) is not valid for some distance downstream of an injection point (until the Gaussian zone; see Figure 2.1) and most data has not been collected far enough downstream. In Elder's (1959) experiments, undertaken in an essentially two-dimensional flow, the spatial concentration profiles were not Gaussian, which Elder reasoned was because tracer material became trapped in the laminar sub-layer and extended the tails of the profiles. Elder fitted a Gaussian curve to the forward part of the measured profile and used this to obtain the longitudinal dispersion coefficient. Elder's observations of skewed spatial concentration profiles were similar to those reported from flows with dead zones. In chapter two it was described how the addition of trapping, either in a sub-layer or dead zones, increases the length of channel required for a Gaussian spatial concentration to become established.

Some data from experiments at flow rates of 6.7 and 25.4l/s in the author's flume are plotted in Figure 3.5 & Figure 3.6 using Chatwin's transformation. The data did not plot as straight lines. However the slopes of the data from the forward part of the profiles were the same at the upstream and downstream sampling positions (the forward part of the tracer curve plots positive on the transformed (vertical) axis). If we follow Elder and use the forward part of the tracer plots (Figures 3.5 & 3.6) to evaluate the longitudinal dispersion coefficient, then the longitudinal dispersion coefficients evaluated at the upstream and downstream sampling locations are equal. Furthermore, it will be realised that a change in slopes of the transformed data would imply that the data in the forward part of the plots had not been collected in the equilibrium zone. The plots show a good deal of scatter on the tails which is due to noise. The longitudinal dispersion coefficients implied by the slopes of the forward part of the transformed tracer data are significantly smaller than those obtained from the rate of change of moments method.

Chatwin's transformation implies a longitudinal dispersion of $0.04m^2/s$ and $0.04m^2/s$ for the downstream and upstream traces in Figure 3.5 compared to $0.11m^2/s$ from the change of moments method. For Figure 3.6 the equivalent figures are $0.03m^2/s$, $0.03m^2/s$ and $0.22m^2/s$. The difference between the longitudinal dispersion coefficients obtained from Chatwin's transformation and the change of moments method could have a number of causes. It is known that the change of moments method can be strongly influenced by the data in the tails of the concentration profiles (Fischer 1966a), but rather than the difference in the coefficients being due to an error in the moments calculation the difference was probably due to only using the data from the forward part of the tracer curve to find a slope and hence the longitudinal dispersion coefficient. Repeating the longitudinal dispersion calculation using the slopes of the trailing part of the data gives, for Figure 3.5, $0.54m^2/s$ and $0.54m^2/s$ for the upstream and downstream data respectively. For the data shown in Figure 3.6 the longitudinal dispersion coefficients are $0.52m^2/s$ and $0.44m^2/s$ for the upstream and downstream data respectively. Although only two data sets have been analysed using Chatwin's transformation the method can be seen to have serious weaknesses. It is only valid for data collected in the Gaussian zone. For data collected in the equilibrium zone (where the method of moments allows the longitudinal dispersion coefficient to be measured) it is difficult to obtain consistent results because the slope of the transformed data and hence the dispersion coefficient depends on the portion of the data used.

The concentration data in Figure 3.5 & Figure 3.6 is plotted again in Figure 3.7 & Figure 3.8 as concentration profiles. The reduced duration of the concentration pulse seen in Figure 3.8 will be seen later (section 3.2.3) to make the task of calculating the moments of the concentration pulse more difficult.

3.3.2 Data analysis; test data sets

In order to calculate the longitudinal dispersion coefficient from an experiment using the change of moments method the variance of the concentration profiles was required.

The fluorometers gave an output voltage before tracer was added to the calibration tank or flume. This background voltage was not constant but consisted of a mean with multifrequency noise superimposed. Typical examples of the background from the upstream and downstream positions are shown in Figure 3.9 & Figure 3.12 respectively. In Figures 3.10 & 3.11 the data of Figure 3.9 is shown processed with a 1s and a 6s moving average filter. Figures 3.13 & 3.14 are the data of Figure 3.12 after processing with the same moving average filters. The plots include lines marking the mean, v, and ±2 and 3 times the standard deviation, σ, of the unfiltered data. The rise of the voltage from zero seen in the figures is a feature of the moving average filter. It will be noted that the downstream trace has noise of a greater magnitude and higher frequency than the upstream. The noise can be seen to have low frequency components of 40s or more. As would be expected the filter is able to remove the high frequency noise and gives a smoother trace with less extreme variation about the mean. The data logger recorded voltages to 4 decimal places, but it was decided to limit the precision of the data to 2 decimal places (approximately 0.25% of the full scale voltage of 5V) because this was considered to be a reasonable estimate of the precision of the fluorometer and helped to filter out noise. The fluorometer was designed to hold a steady output signal for one second between measurements of fluorescence. Any frequency higher than 1Hz in Figures 3.9 & 3.12 is therefore noise introduced by the fluorometer or the signal cables. The origins of the low frequency component of the signals in Figures 3.9 to Figure 3.4 are uncertain but were probably caused by the fluorometer. The wide

range of noise frequencies made the selection of a filtering technique a compromise between the desire to remove as much noise as possible whilst not effecting the shape of the tracer concentration profiles. The technique eventually chosen was to filter the data record with a 1s moving average filter prior to analysis. This did not appear to affect the low frequency components of the data.

In order to test the software that was written to analyse the data records two dummy data sets were created that were representative of the extreme forms of data that were expected. One was a Gaussian with a peak of 5 units and standard deviation of 33s. The other, taken to represent the type of skewed data usually obtained in the field, was derived from a Cells in Series (CIS) model (Rutherford 1994, Wallis & Clarke 1995).

The CIS model was $c = \frac{\alpha^5 t^5}{5!} 20 \exp(-\alpha t)$ in which α was taken to be $0.3892 s^{-1}$. The variance of the resulting distribution was $33 s^2$ and the centroid was 12.9s from the beginning. A lead-in and lead-out of 100s was provided and noise from the upstream fluorometer was added to both data sets. The two data sets are plotted in Figure 3.15. Experience with the dummy data sets showed that the definition of the points where the trace rose above and returned to the background was important. The accuracy with which the moments of the data could be found was much improved if the noisy lead-in and lead-out data were removed. This was because the noise on the background signal that remained after the 1s moving average filter had been applied unduly influenced the calculation of the moments.

The software developed to find the moments of the tracer data files used the following algorithm: a length of the lead-in background was examined and the mean and variance of the data calculated. The mean, V, and a number of standard deviations, $n\sigma$, was used to determine a trigger level. If a local average of the data exceeded this level the tracer concentration was considered to have risen above the background and the

concentration profile had begun. The same method was used to find the finish of the trace except that the data was examined from the end of the data file working backwards in time. The average of both the lead-in and lead-out data was calculated and the two values compared to ensure that a long enough record had been recorded to enable all the tracer profile to be measured. When the start and finish times of the concentration curve had been determined the background was removed from the trace and the calibration applied. The software gave the area, centroid and variance of the data between the start and finish times. A copy of the software is included in Appendix C.

Tests with the dummy data files showed that a local average over 2s and a trigger level of three times the standard deviation of the background data gave good results. Using these the variance of the Gaussian curve was found to within 2.2% of the actual value and for the CIS data it was found to within 3.0%. The centroid of the data was found to within 1.9% for the CIS and 0.2% of the actual value for the Gaussian data set. Uncertainty in the calibration only effected the area reported by the software, the percentage change in reported area being equal to the percentage change in the calibration. This was consistent with the calibrations of the fluorometers being linear.

The effect of using a poor estimate of the background voltage was investigated. The true background voltage of the dummy data was 0.60V with a standard deviation of 0.006V so the trigger level was 0.62V. Using a lead-in trigger voltage of 0.61V and the correct lead-out trigger voltage resulted in the variance reported for the Gaussian data being in error by 3.8% and the centroid error being 0.4%. For the CIS the same lead-in trigger voltage resulted in a 6% error in the reported variance and a 1.7% error in the centroid. If both lead-in and lead-out trigger levels for the Gaussian data set were 0.01V lower than the true background voltage the effect was a 4.2% error in the value of variance and value for the centroid 0.4% too low. The CIS data was extremely sensitive

to the value used for the mean background voltage; if the lead-out trigger level was 0.61V the software gave a variance 51 times the true value, while the centroid was in error by 6%. If the lead-out trigger was 0.83V the program reported a variance 25% and a centroid 1.3% lower than the true value. The reason for the sensitivity of the CIS data to the choice of background was because, if the mean of the lead-out data was set too low, the software found the trace to be longer than it should have and then subtracted less background voltage than necessary. The effect on the data was to leave a small voltage in the tail. These tail voltages, being far from the centroid, had a large contribution to the moment calculation. The calculation of the centroids of both data sets was less sensitive to the estimate of the background voltage than the variance was.

Using the dummy data files allowed the software to be tested and gave an insight into the possible uncertainty that might be expected when analysing experimental data sets. It was found that the definition of the lead-out background voltages was important and that it was better to overestimate the background voltage rather than underestimate. It was also found that skewed data (CIS data set) was more difficult to analyse than symmetrical data (Gaussian data set).

3.4 Results of the tracer experiments

Tracer experiments were performed five times at each of eleven flows between 2 and 26l/s. The data was analysed using the software and techniques described in the previous section and the results are given in Table 3.1. Work with the dummy data sets demonstrated the sensitivity of the variance calculation to the definition of the background. Several data sets gave negative longitudinal dispersion coefficients; these were generally those where the lead-out voltage was 0.01 to 0.02V greater than the lead-in voltage. For flow 16 several sets are marked "Poor" in the table; for these the lead-out

voltages were 0.02V greater than the lead-in; although the analysis gave positive longitudinal dispersion coefficients these were considered to be doubtful.

The cloud velocity (see section 2.3), u_c, was found to within 10% of the cross-sectional averaged velocity, u_q, for all the experiments. The cloud velocities were greater than the cross-sectional averaged velocity for 23 of the 55 experiments and equal for 20 for the experiments. As the flow approached the tail gate it accelerated and this longitudinal non-uniformity was the reason for the difference between the cloud velocity and the cross-sectional average velocity (which was evaluated at 6m from the flume inlet).

The longitudinal dispersion coefficients calculated, for a given flow rate, appeared to be more scattered at the higher flow rates. A comparison of the data for F8T4 and F12T3 plotted as Figures 3.7 & 3.8 respectively shows that the profiles recorded at the higher flow rate were shorter and more highly skewed than those at the lower flow rate. It is therefore possible that the difficulty in analysing skewed data sets that was seen with the dummy data sets was the cause of the increased uncertainty with flow rate.

The average of the reliable measurements of the longitudinal dispersion coefficient taken at the same flow rate are given in Table 3.2. Figure 3.16 shows this data plotted against the product of the depth and side wall corrected bed shear velocity (evaluated at 14m from the flume inlet). The plot shows error bars equal to one standard deviation of the data used to calculate the average, one standard deviation being about 50% of the average. A linear regression fitted to the data gave the following relationship: $D = 0.02 + 65.39du_{*_b}$ with a coefficient of determination of 0.84. The regression implied that longitudinal dispersion could occur in the flume with no flow; this is clearly ridiculous and results from the limited range of experiments that were

performed. An alternative estimate of the uncertainty in an individual calculation of a longitudinal dispersion coefficient can be obtained if we assume that the uncertainty in calculating the variance of a measured concentration profile was the same as the accuracy with which the variance of the dummy data sets could be found; namely 25% which implies an overall uncertainty in the longitudinal dispersion coefficients of 50% of the true value. This value for the uncertainty is similar to that actually found in the measured data.

There was no evidence of the non-dimensional longitudinal dispersion coefficient $\left(D/du_{*_b}\right)$ being a function of the flow rate.

3.5 Comparison to previous data

Table 3.3 gives the results of previous measurements of longitudinal dispersion coefficients for straight rectangular laboratory flumes. Fischer's experiments were performed in a smooth sided flume whose bed was roughened with 5/8 inch (15.3mm) gravel. Fischer analysed using the change of moment method the average concentration data from four runs. Miller & Richardson performed experiments in a flume whose bed was roughened with rectangular blocks. The flow was notably three-dimensional; Miller & Richardson also mentioned the possibility that the tracer may have been trapped in the wakes of the roughness elements which extended the tails of the solute traces and led to a large value of longitudinal dispersion coefficient being measured. Valentine & Wood's data was measured in a flume whose bed had rectangular slots that formed dead zones.

The tabulated data is plotted in Figure 3.17 along with the averaged data measured by the author. All the data show an increase in longitudinal dispersion coefficient with increasing du_* but that is the limit of agreement between the data sets. The longitudinal dispersion coefficients measured during the present work were larger

for a given value of du_* which was probably due to the particular nature of the flow in the flume. It will be shown, in chapter four, that the longitudinal velocity field in the author's flume was three-dimensional and longitudinally non-uniform. Furthermore in chapter seven it will be shown that the longitudinal non-uniformity led to increased longitudinal dispersion compared to that which would exist if the flow was three-dimensional but longitudinally uniform.

An idea of the nature of the flows used for the experiments in Table 3.3 can be obtained by considering their aspect ratios. For Valentine & Wood the width to depth ratio varied between 8.7 and 58.4, for Fischer it was 5.9 to 11.6, for Miller & Richardson 4.5 to 4.8. Webel & Schatztmann (1984) found that a width to depth ratio greater than five was necessary to avoid secondary flows increasing the rate of transverse mixing. Miller & Richardson measured rates of transverse mixing greater than those found in wide (two-dimensional) open channel flows probably because their flow was three-dimensional. In general, for a uniform flow, an increase in the rate of transverse mixing would lead to a reduction in longitudinal dispersion (see equation 2.15), an increase in the transverse velocity shear in a three-dimensional flow would lead to increased longitudinal dispersion. Dead zones are also known to increase the longitudinal dispersion in a channel. Unless the transverse mixing coefficients, the degree of transverse velocity shear, longitudinal non-uniformity and magnitude of any dead zone effects are known it is difficult to compare longitudinal dispersion coefficients between experiments.

In view of the differences in values of longitudinal dispersion coefficient measured in straight rectangular laboratory flumes that are plotted in Figure 3.17 the wide range of coefficients reported in natural and man made waterways is not surprising. Rutherford (1994) tabulates data from a number of sources, for canals the ratio

D/du_* has values between 3 and 469; for rivers the range is even wider 47 to 1060; the dispersion coefficients measured in the present work fall within both these bands. The reason why the longitudinal dispersion in the author's flume was greater than that previously measured in a straight rectangular laboratory flume will be discussed in detail in chapter seven.

Rutherford (1994) gives three empirical equations, due to McQuivey & Keefer (1974), Jain (1976) and Liu (1977), that allow an estimate of the longitudinal dispersion coefficients in a river to be made.

McQuivey & Keefer (1974) have:

$$D = 0.058\frac{Q}{sb}$$

where Q is the flow, s the channel slope and b the channel width.

Jain (1976) gave:

$$D = a\frac{u_q b^2}{k_z}$$

Where u_q is the discharge velocity, k_z the transverse dispersion coefficient and $0.001<\alpha>0.016$

and Liu (1977) had:

$$D = b\frac{Q^2}{u_* R^3}$$

where R is the hydraulic radius and $b = 0.18\left(\frac{u_*}{u_q}\right)$

Rutherford stated that these formulae will predict the longitudinal dispersion coefficient in a flow to within a factor of 10; they were applied to the laboratory flume with the results given in Table 3.4. None of the equations were particularly accurate. McQuivey & Keefer's equation over predicted the dispersion by a factor of 6 to 7. The

measured data fall within the range of predictions given by the equation due to Jain but then the range for each flow rate varied by more than a factor of ten. The equation due to Liu predicted a fall in dispersion with increasing flow rate which was opposite to the measured trend. Although it will be seen in chapter four that the bulk hydraulics of the flume had some similarities to a natural channel it will be appreciated that the correlations were developed using field data and that they might not be expected tp predict dispersion in a laboratory flume. Whether the uncertainty in dispersion coefficient that the use of an empirical equation implies was acceptable would, of course, depend on the application.

3.6 Conclusions

The non-dimensionalised longitudinal dispersion coefficients measured in the laboratory flume are larger than those measured in previous dispersion experiments in straight rectangular flumes and at the lower end of values measured in natural open channel flows. The coefficients were regressed against the product of the flow depth and the side wall corrected bed shear velocity to give: $D = 0.02 + 65.39du_{*_b}$. There was a good deal of scatter to the data which increased with increasing flow rate.

The longitudinal dispersion coefficients were evaluated using the method of moments. It was found that the calculation of the variance of a concentration profile was very sensitive to the definition of the background concentration, a skewed profile being more sensitive than a Guassian. The increased skewness of the concentration profiles at the higher flow rates probably led to the greater degree of scatter in the dispersion coefficients at higher flow rates. The calculation of the centroid of the distributions was insensitive to the definition of the background concentration.

Existing empirical equations gave poor predictions of the longitudinal dispersion coefficient in the author's flume.

Exp.	Q (l/s)	u_q (m/s)	u_c (m/s)	Upstream Variance (s^2)	Downstream Variance (s^2)	D (m^2/s)
F6T1	2.55	0.12	0.10	15206.3	7878.67	-ve
F6T2	2.44	0.11	0.11	16544.8	16892.5	0.0199
F6T3	2.36	0.11	0.11	17634.1	17961.6	0.017
F6T4	2.64	0.12	0.11	16130.2	16738.1	0.034
F6T5	2.46	0.11	0.14	22915.0	21052.6	-ve
F7T1	4.37	0.15	0.15	8437.6	9053.6	0.086
F7T2	4.42	0.15	0.15	8044.6	8406.9	0.046
F7T3	4.46	0.15	0.14	7301.1	8053.9	0.087
F7T4	4.39	0.15	0.16	8929.0	7448.9	-ve
F7T5	4.42	0.15	0.11	7692.2	7877.5	0.006
F8T1	6.78	0.18	0.18	4789.4	5150.1	0.085
F8T2	6.68	0.18	0.19	4195.7	4419.3	0.055
F8T3	6.71	0.18	0.18	3692.2	4366.5	0.148
F8T4	6.76	0.18	0.18	3466.3	4063.8	0.131
F8T5	6.73	0.18	0.18	3533.7	4201.1	0.149
F9T1	10.14	0.22	0.23	2567.7	2609.3	0.020
F9T2	10.14	0.22	0.22	2286.7	2556.4	0.116
F9T3	10.11	0.22	0.22	2459.3	2062.7	0.039
F9T4	9.89	0.22	0.22	2234.9	2818.6	0.227
F9T5	10.11	0.22	0.22	2461.2	2557.9	0.056
F10T1	13.25	0.25	0.27	1580.7	906.3	-ve
F10T2	13.00	0.25	0.25	1082.7	1335.1	0.158
F10T3	13.07	0.25	0.25	1025.8	1240.0	0.137
F10T4	13.03	0.25	0.24	1061.8	1643.9	0.327
F10T5	13.03	0.25	0.25	1055.2	1324.1	0.168
F11T1	16.47	0.28	0.30	794.5	929.4	Poor
F11T2	16.51	0.28	0.30	861.3	895.8	Poor
F11T3	16.51	0.28	0.30	812.4	782.1	-ve
F11T4	16.51	0.28	0.30	829.2	853.5	Poor
F11T5	16.47	0.28	0.30	849.7	892.6	Poor
F12T1	19.50	0.30	0.31	564.7	715.1	0.176
F12T2	25.33	0.34	0.37	361.6	450.4	0.170
F12T3	25.33	0.34	0.36	419.4	541.1	0.222
F12T4	25.38	0.35	0.36	383.1	588.5	0.366
F12T5	25.43	0.35	0.37	382.1	458.2	0.144
F12T6	25.48	0.35	0.35	439.5	728.9	0.489
F13T1	19.50	0.30	0.32	627.7	717.8	0.117
F13T2	19.50	0.30	0.32	626.8	729.6	0.128
F13T3	19.45	0.30	0.32	576.8	692.8	0.143
F13T4	19.45	0.30	0.31	562.0	884.0	0.361
F14T1	10.62	0.23	0.21	1810.2	2356.0	0.195
F14T2	10.62	0.23	0.22	2026.2	2130.4	0.045
F14T3	10.59	0.23	0.21	1617.0	1766.3	0.073
F14T4	10.62	0.23	0.23	1703.9	1944.9	0.189

F14T5	10.59	0.23	0.25	2166.5	1644.8	-ve
F15T1	9.54	0.22	0.21	1810.2	2356.0	0.195
F15T2	9.48	0.22	0.22	2026.2	2130.4	0.041
F15T3	9.51	0.22	0.21	1878.7	2329.5	0.159
F15T4	9.51	0.22	0.26	2015.1	2329.5	0.203
F15T5	9.45	0.22	0.21	1962.0	2326.9	0.129
F16T1	8.51	0.20	0.20	2591.6	2644.9	Poor
F16T2	8.45	0.20	0.20	2498.9	2463.8	Poor
F16T3	8.46	0.20	0.21	3406.5	2977.8	Poor
F16T4	8.43	0.20	0.19	2567.5	3660.3	0.290
F16T5	8.43	0.20	0.20	2383.1	2419.6	Poor

Table 3.1 Longitudinal dispersion coefficients.

Q (l/s)	D (m^2/s)	du_* (m^2/s)	unc' in D
2.48	0.024	5.23e-4	9.00e-3
4.42	0.073	8.36e-4	0.023
6.73	0.120	1.191e-3	0.050
9.50	0.172	1.62e-3	0.082
10.08	0.115	1.68e-3	0.082
10.61	0.111	1.76e-3	0.065
13.04	0.198	2.12e-3	0.087
25.39	0.261	3.88e-3	0.146
19.49	0.185	3.05e-3	0.101

Table 3.2 Averaged longitudinal dispersion data.

Author	du_* (m^2/s)	D (m^2/s)
Fischer (1966)	0.00377	0.058
	0.00291	0.043
	0.00449	0.0785
Miller & Richardson (1974)	0.00381	0.052
	0.00670	0.262
	0.00675	0.067
	0.01027	0.633
	0.00821	1.263
	0.01464	0.148
	0.01461	1.080
	0.02138	6.128
Valentine & Wood (1979a)	0.00205	0.0101
	0.00340	0.0113
	0.00496	0.0125
	0.00764	0.0147
	0.00912	0.0160
	0.01231	0.0186
	0.02506	0.0268
	0.05968	0.0349

Table 3.3 Previously measured values of longitudinal dispersion coefficients.

Q (l/s)	McQuivey & Keefer (m^2/s)	Jain (m^2/s)	Liu (m^2/s)	Measured (m^2/s)
7	0.42	0.05 to 0.75	0.23	0.07
13	0.78	0.04 to 0.60	0.24	0.17
26	1.55	0.05 to 0.85	0.13	0.23

Table 3.4 Predicted longitudinal dispersion coefficients.

Plate 1 **View of the laboratory flume**

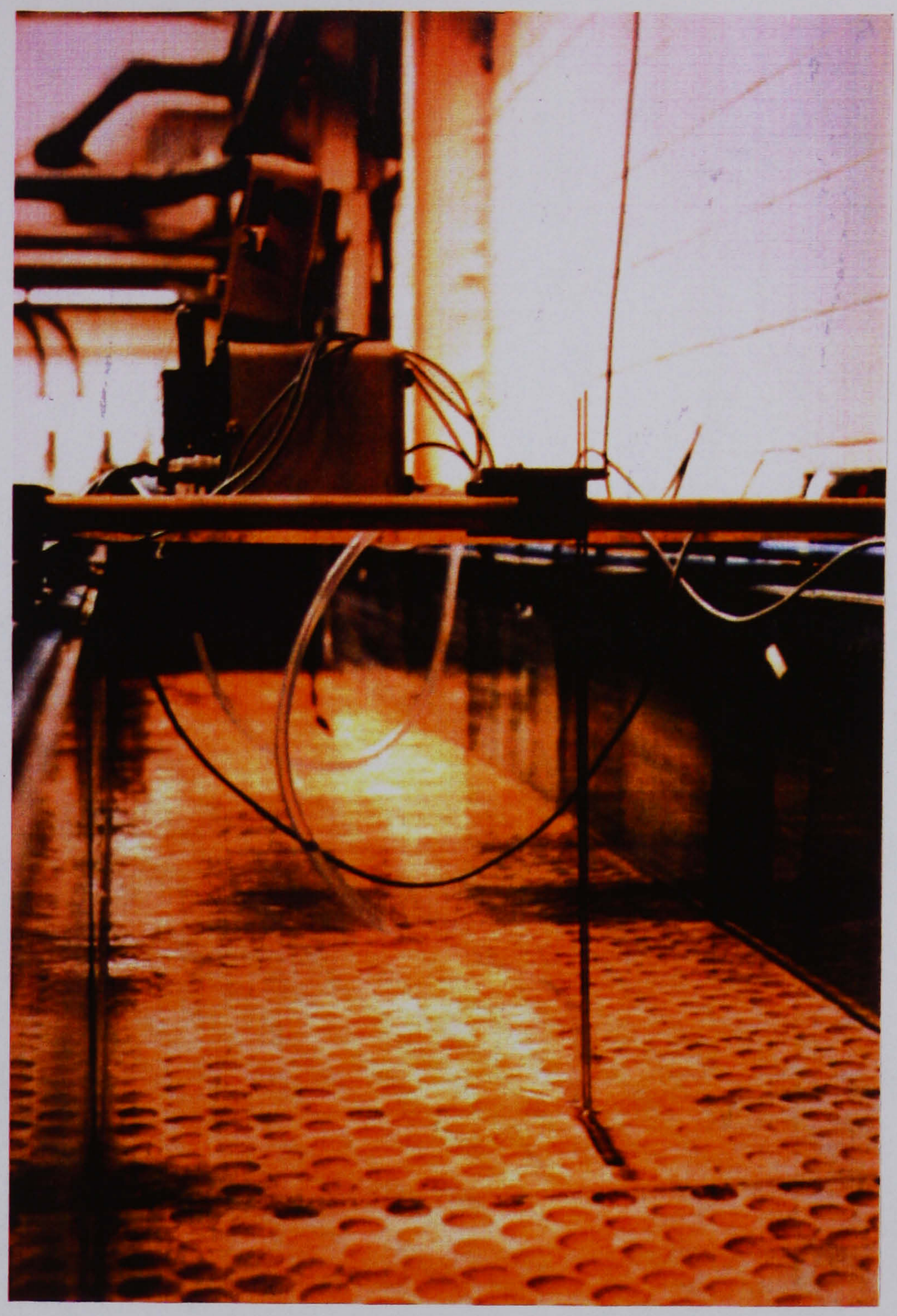

Plate 2 **Close up of the flume bed**

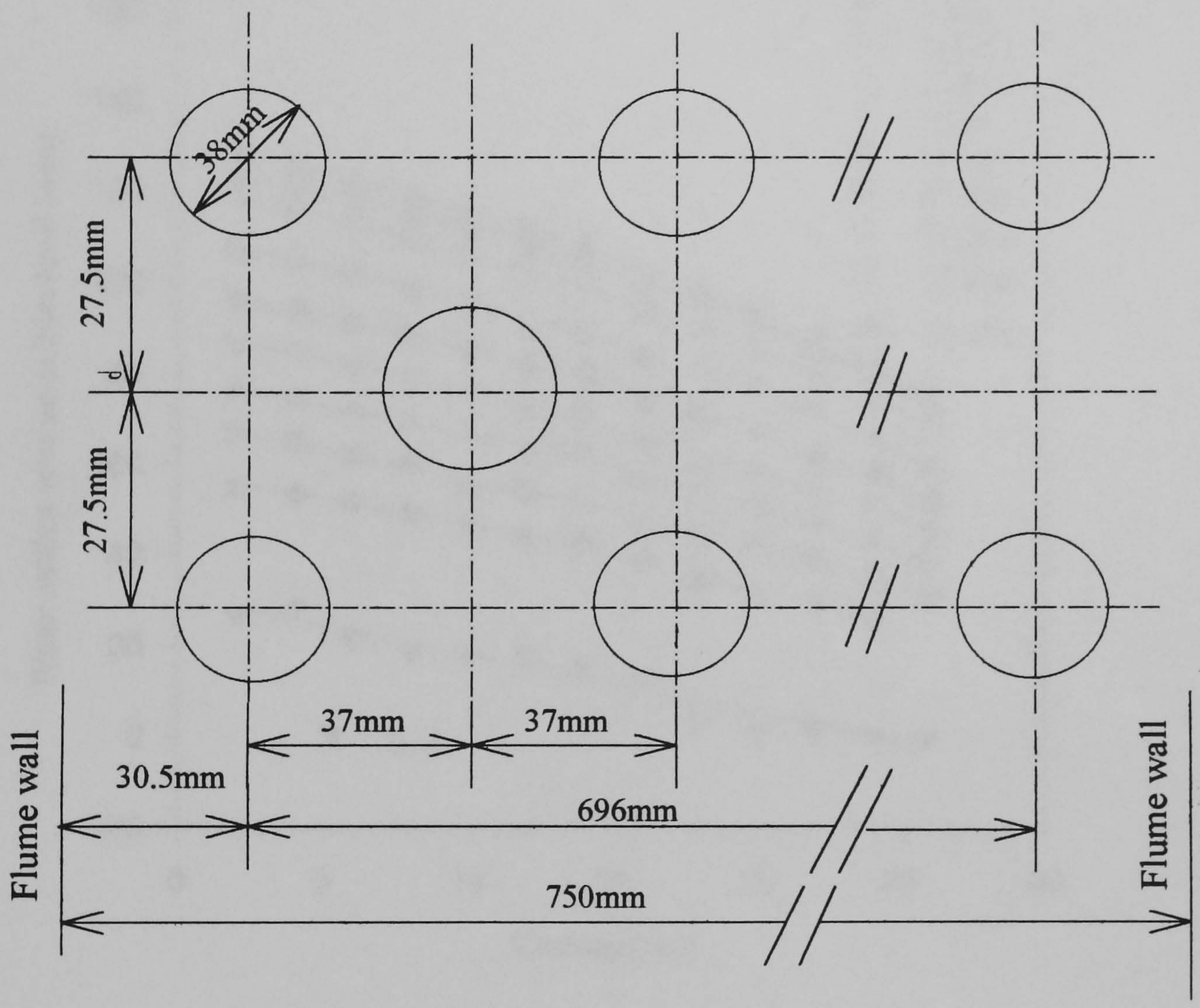

Figure 3.1 Plan of the pattern used to form the dimples

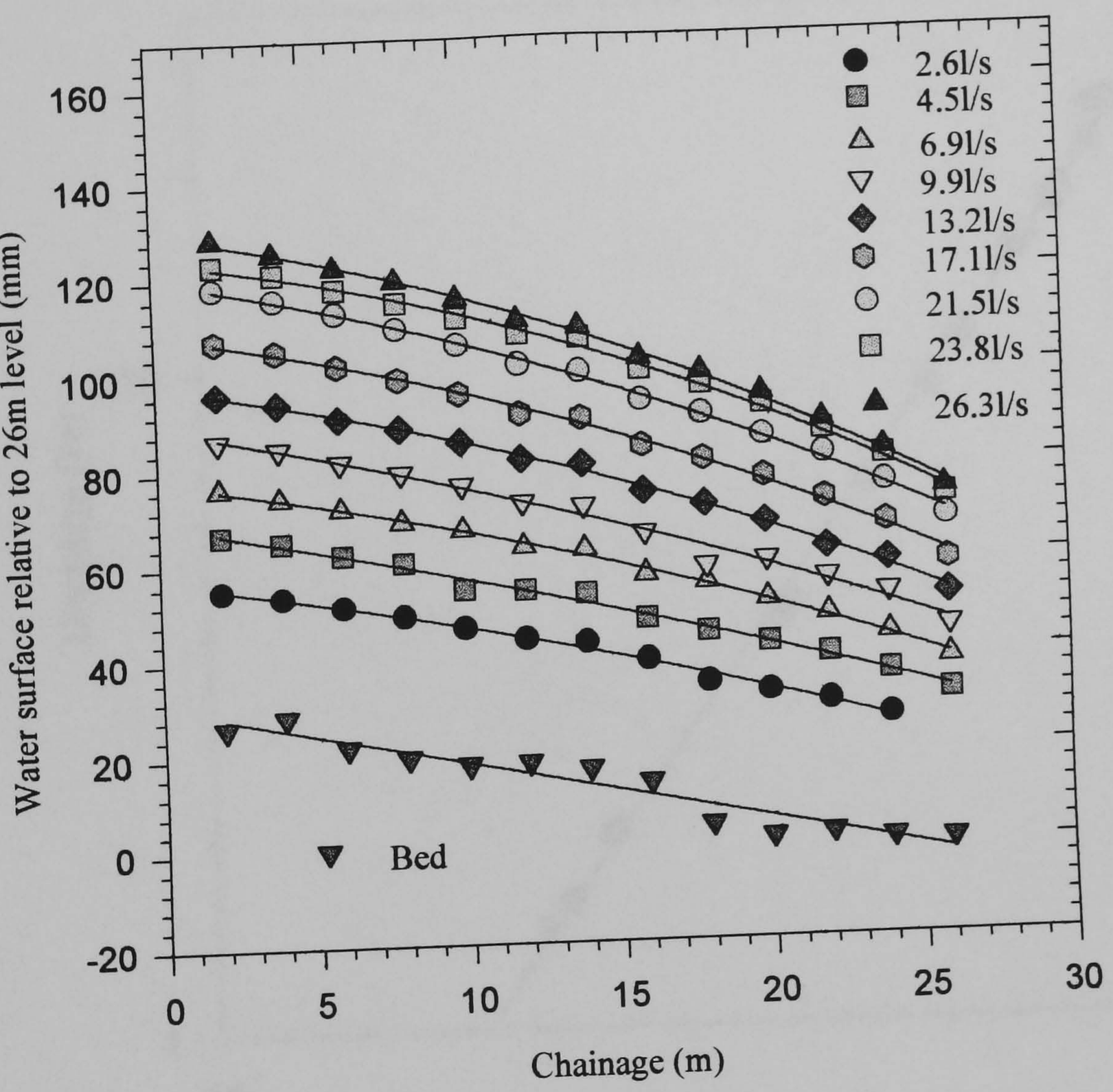

Figure 3.2 Water surface and bed profiles

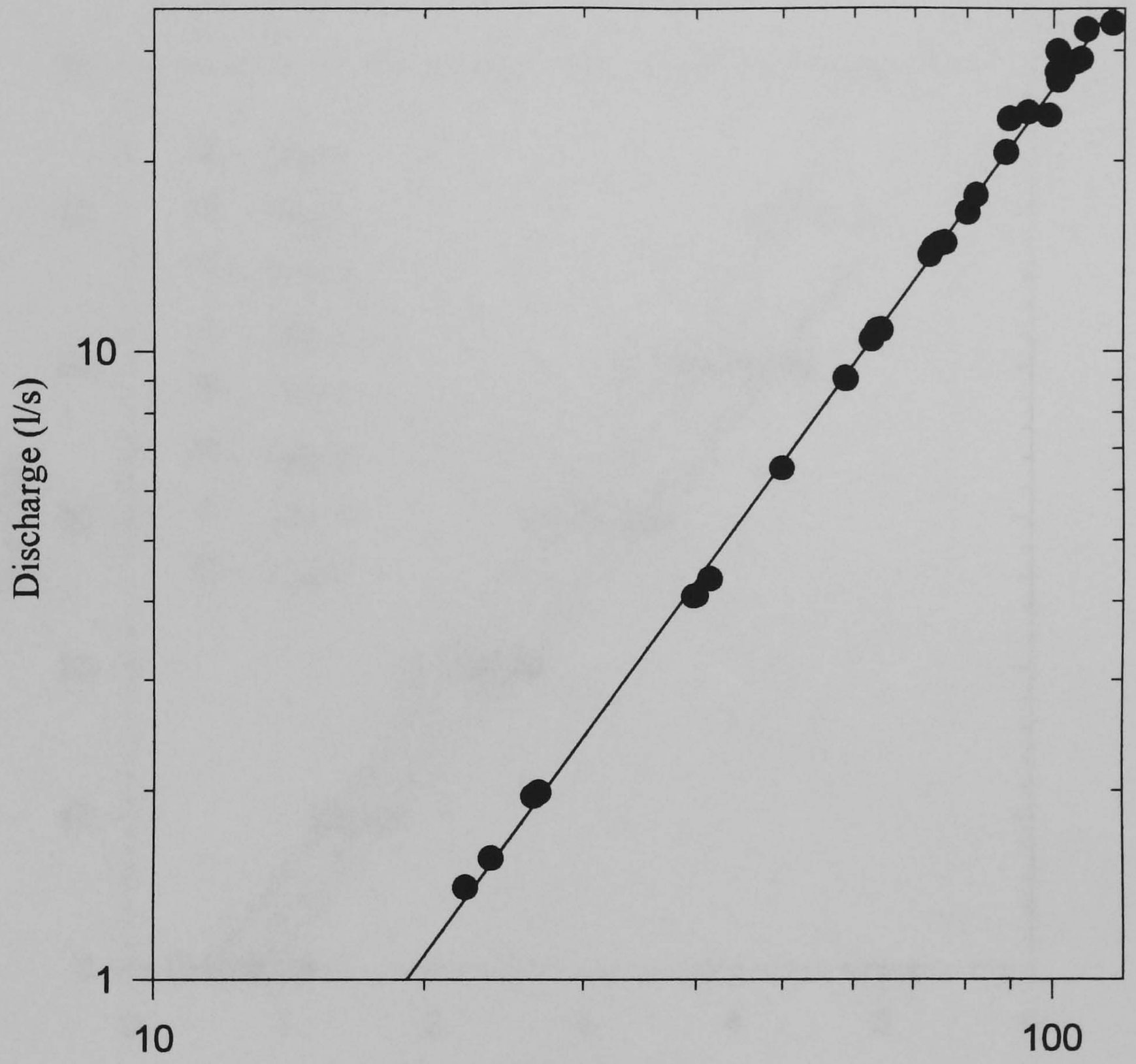

Figure 3.3 Stage discharge curve for the flume

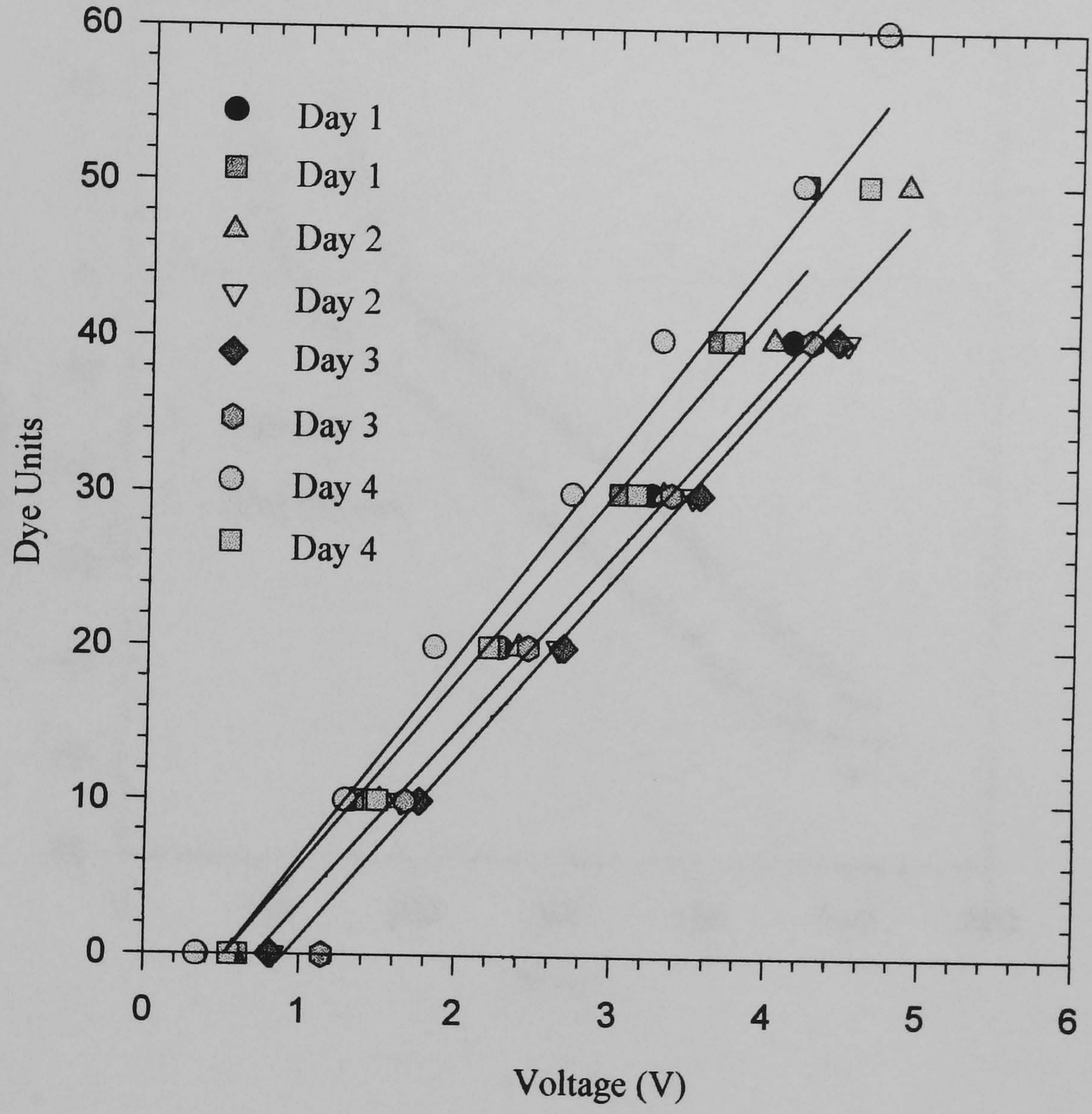

Figure 3.4 Typical fluorometer calibration curves

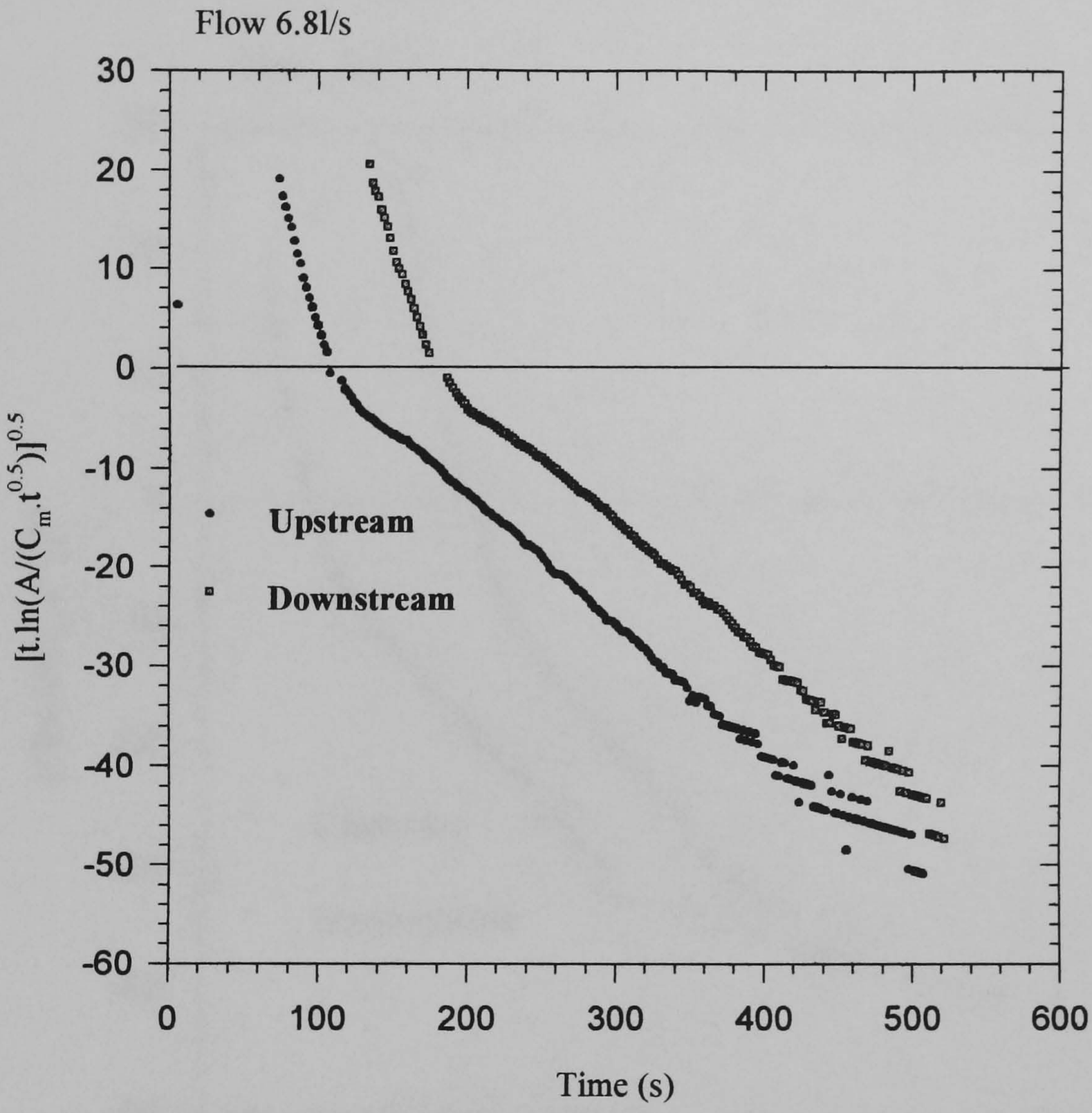

Figure 3.5 Data plotted using Chatwin's transformation for a flow of 6.8l/s

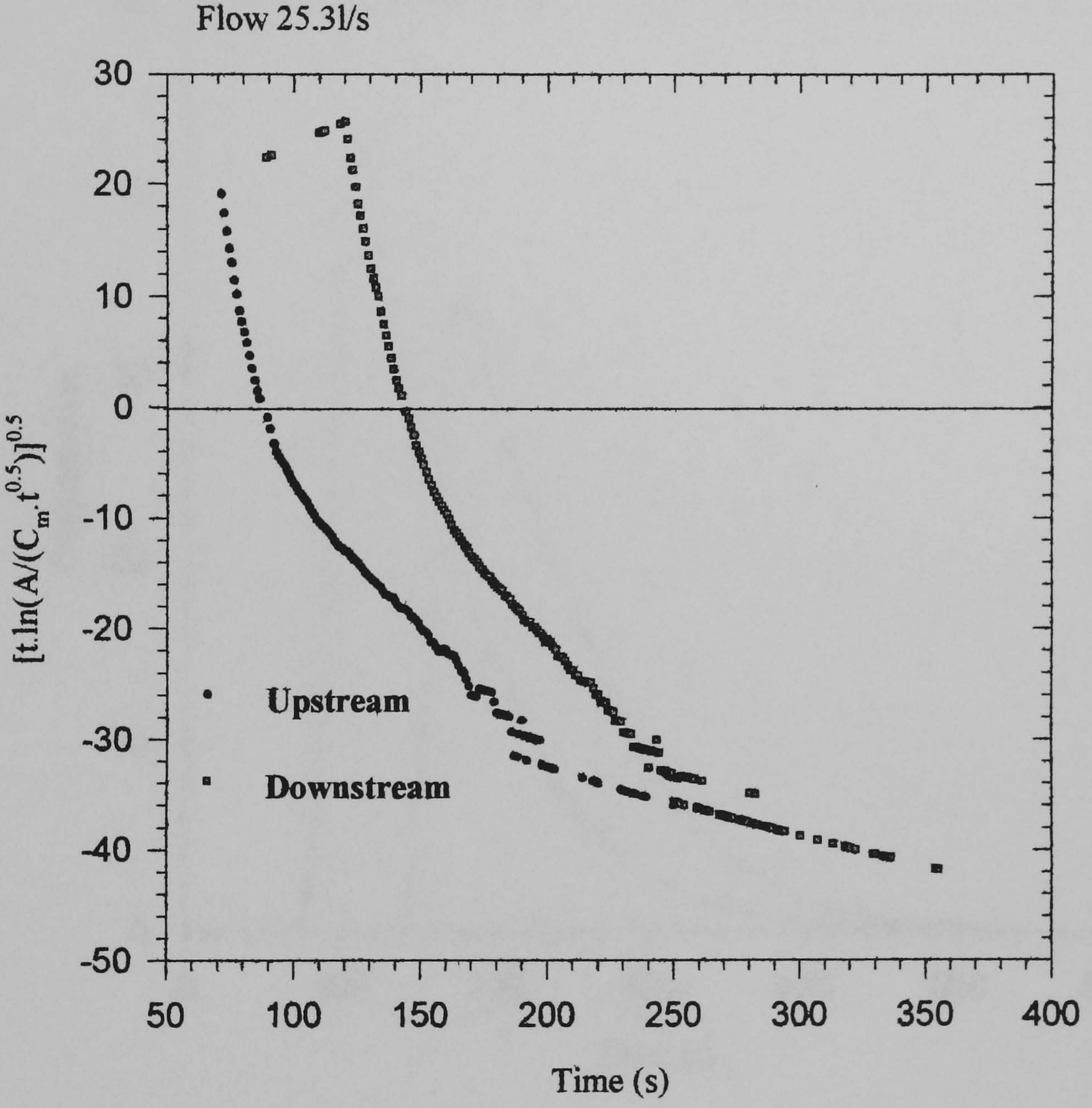

Figure 3.6 Data plotted using Chatwin's transformation for a flow of 25.3l/s

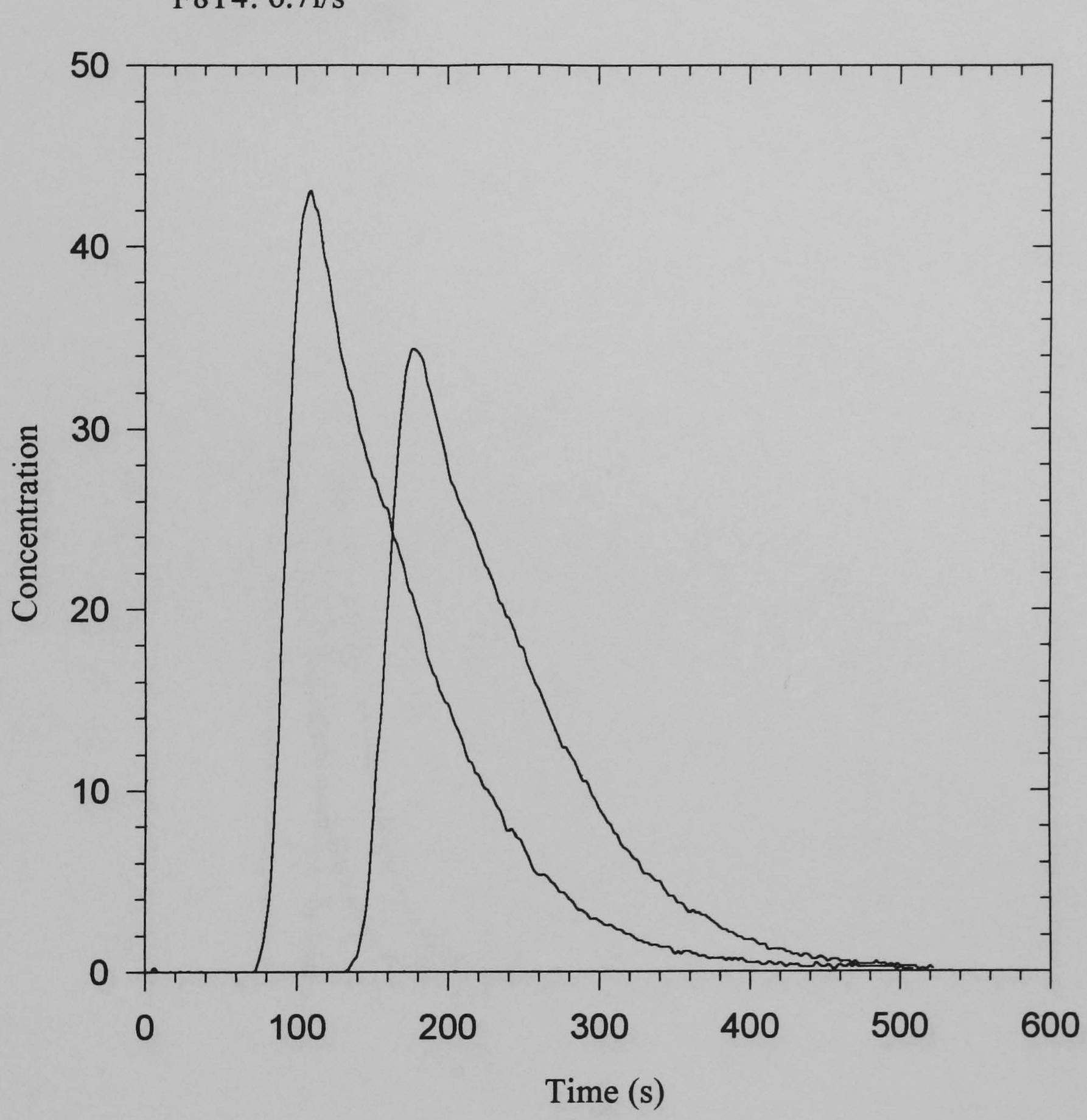

Figure 3.7 Concentration profiles from a flow of 6.7l/s

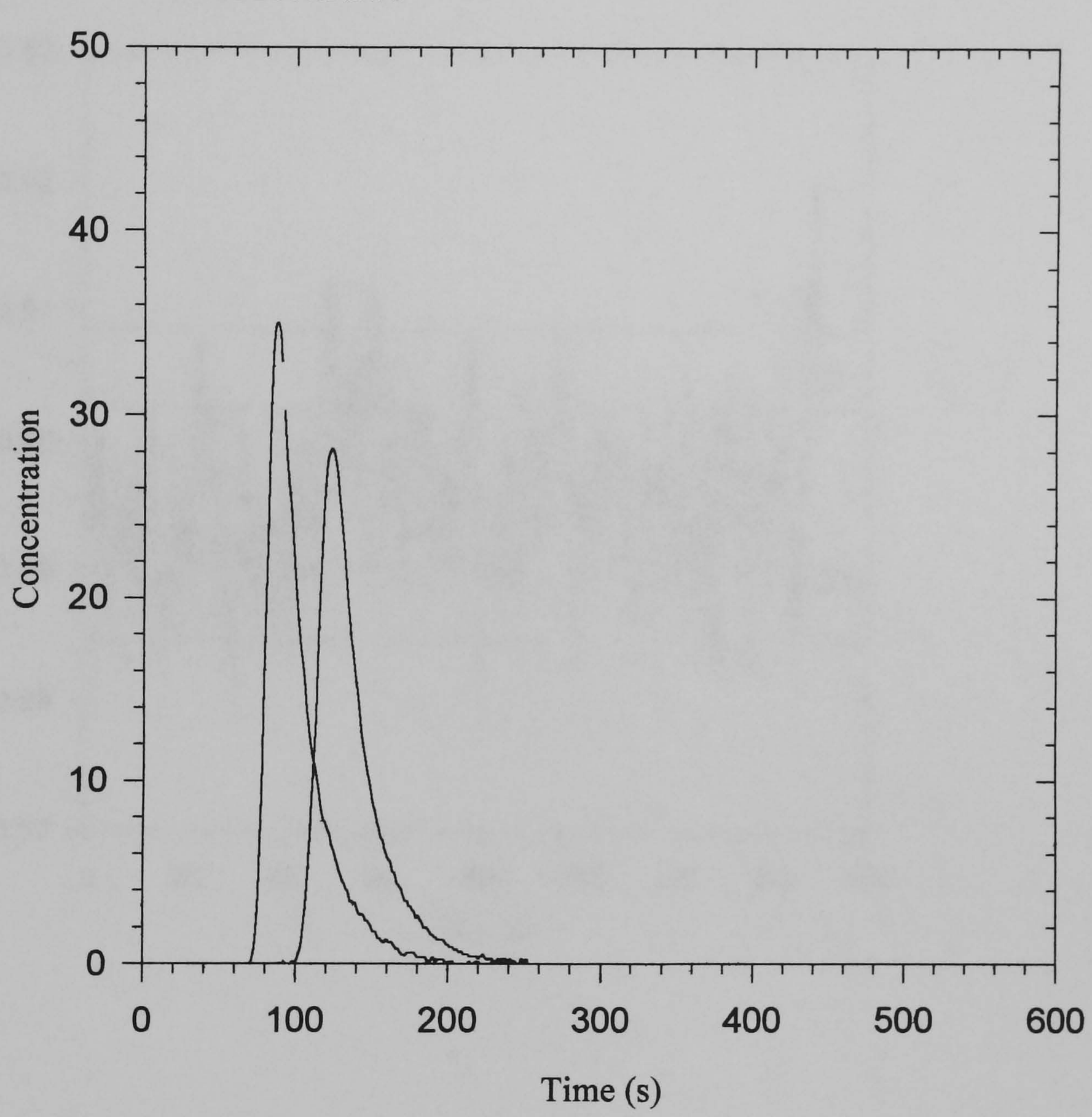

Figure 3.8 Concentration profiles from a flow of 25.3l/s

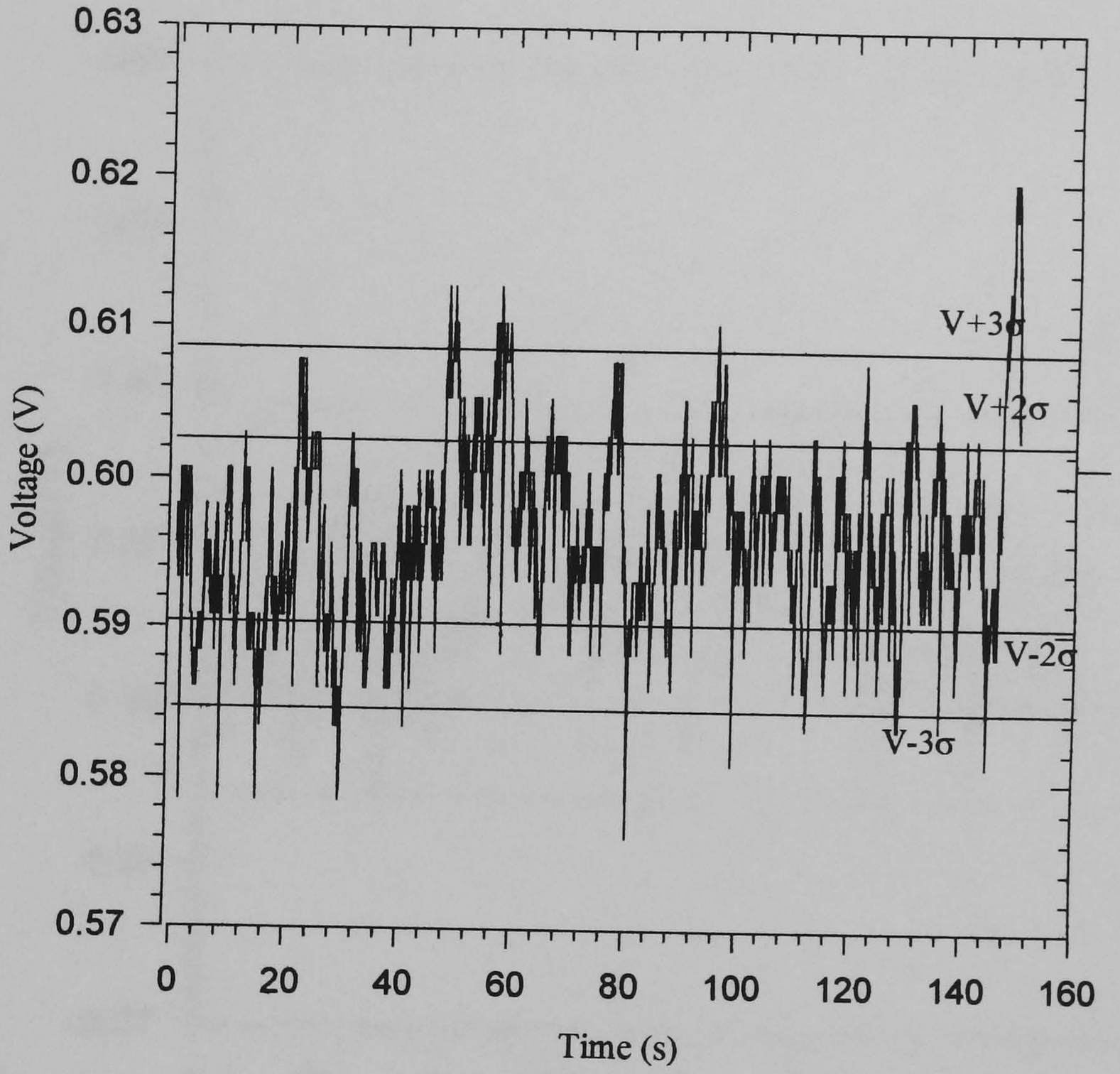

Figure 3.9 Background signal from upstream fluorometer

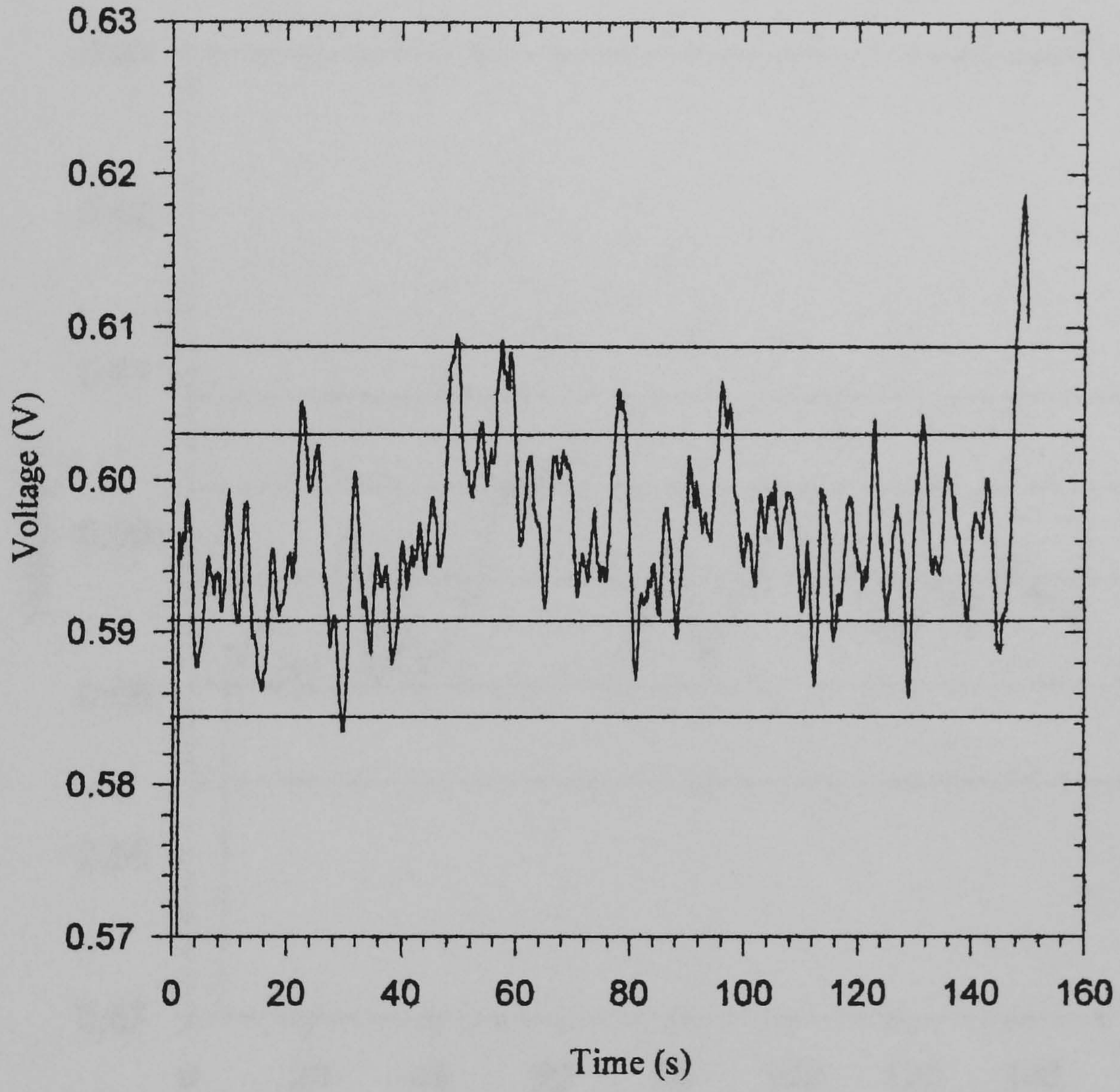

Figure 3.10 Upstream data: 1s moving average filter

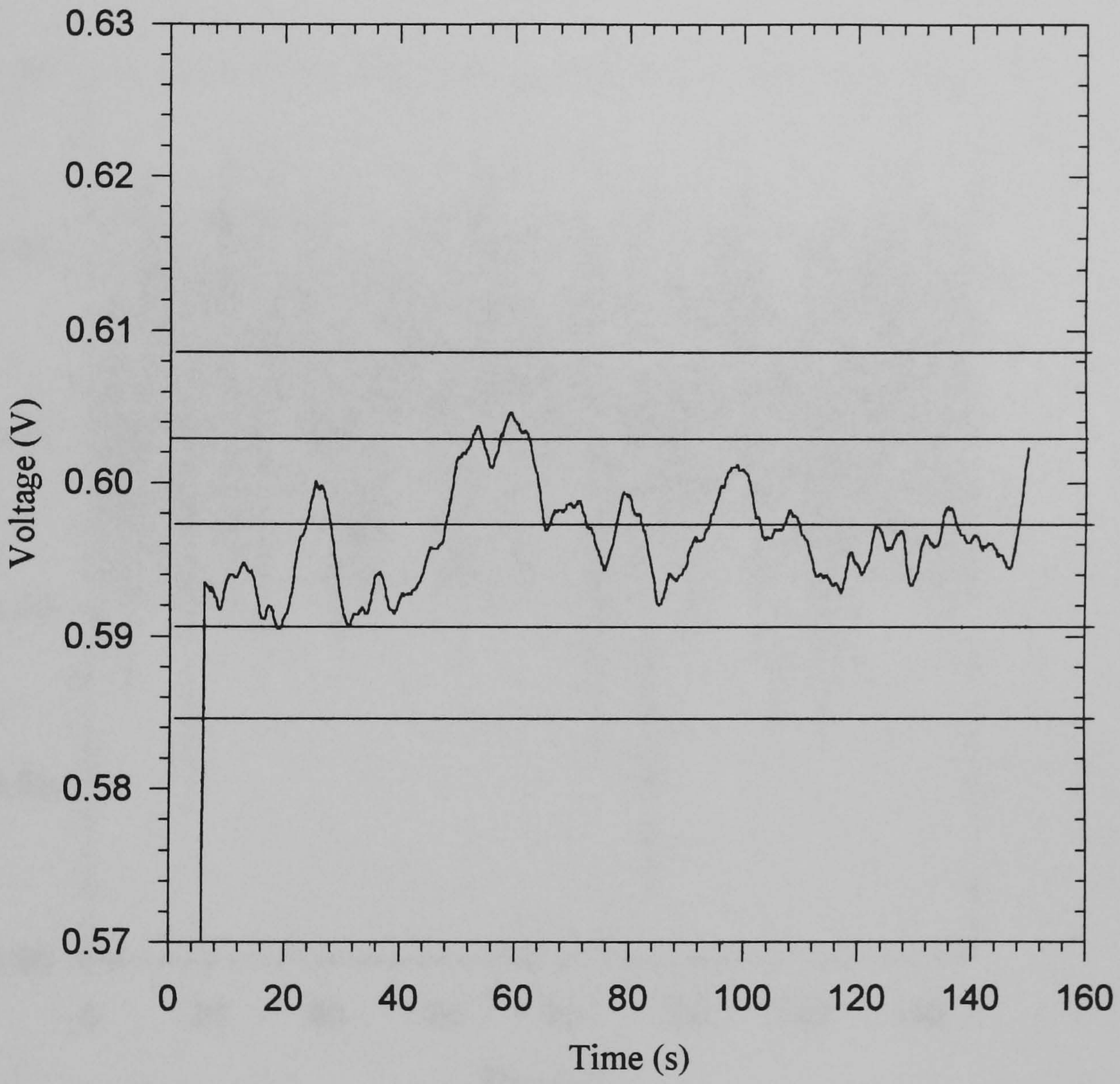

Figure 3.11 Upstream data: 6s moving average filter

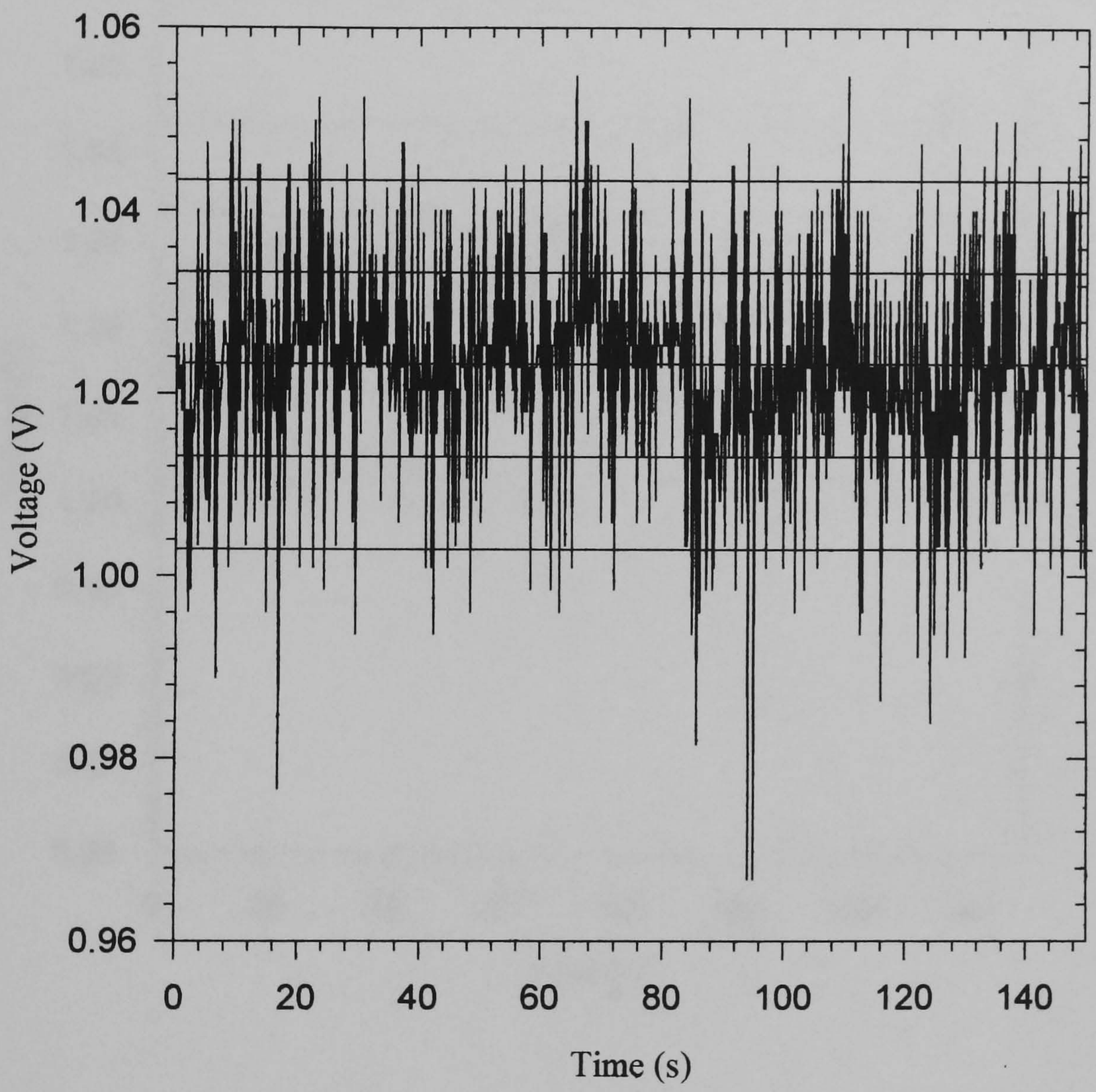

Figure 3.12 Background signal from downstream fluorometer

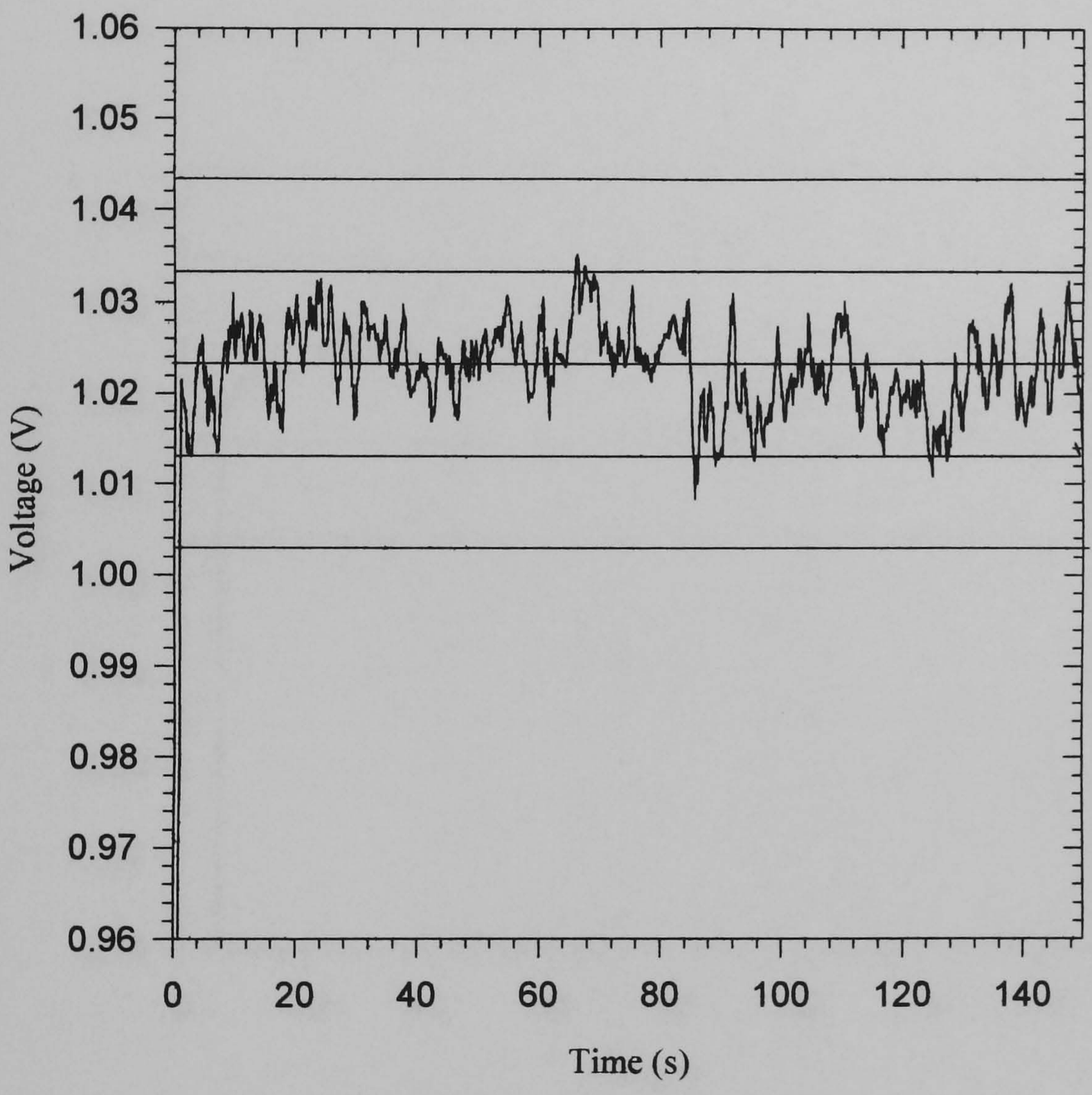

Figure 3.13 Downstream data: 1s moving average filter

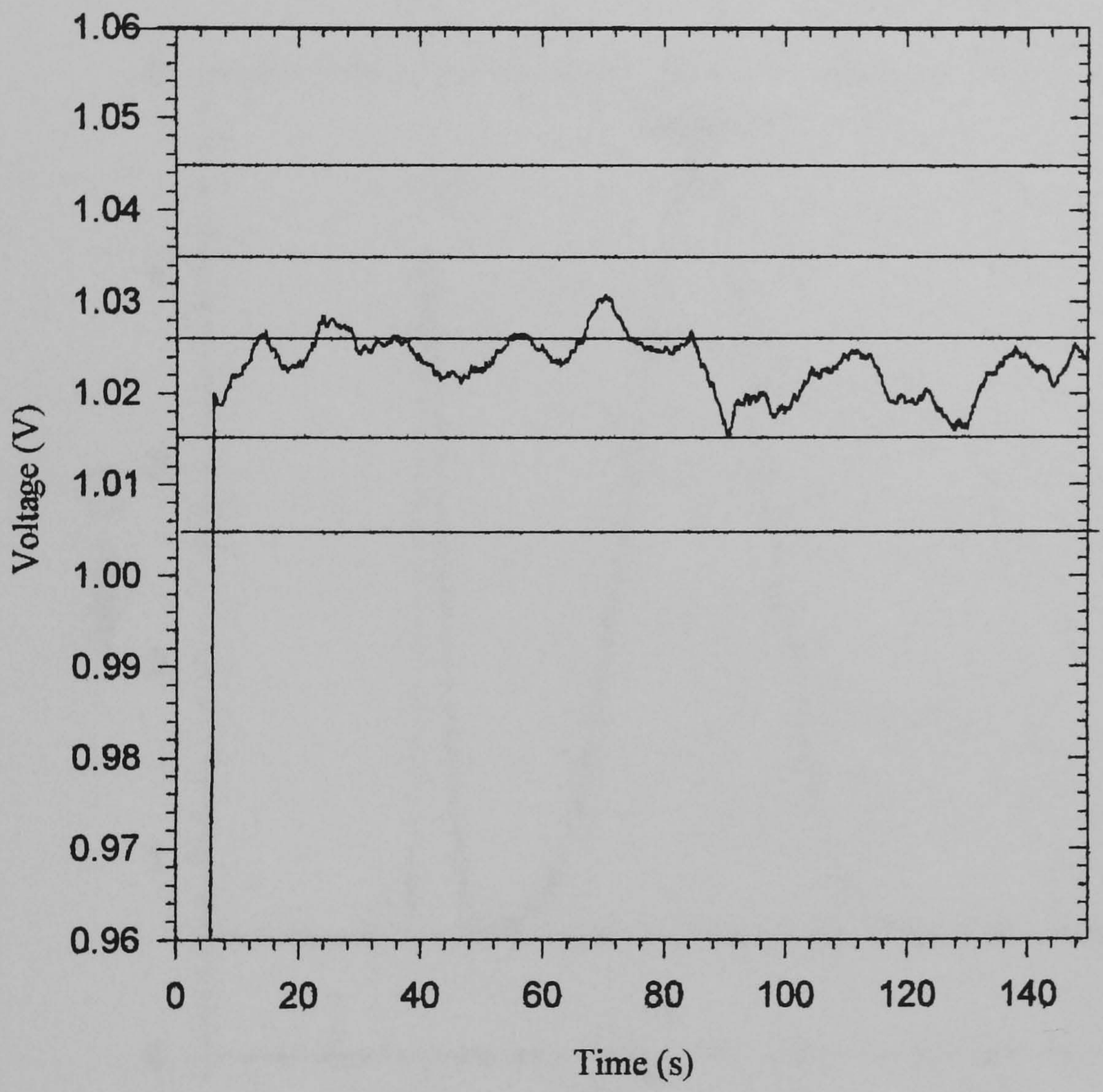

Figure 3.14 Downstream data: 6s moving average filter

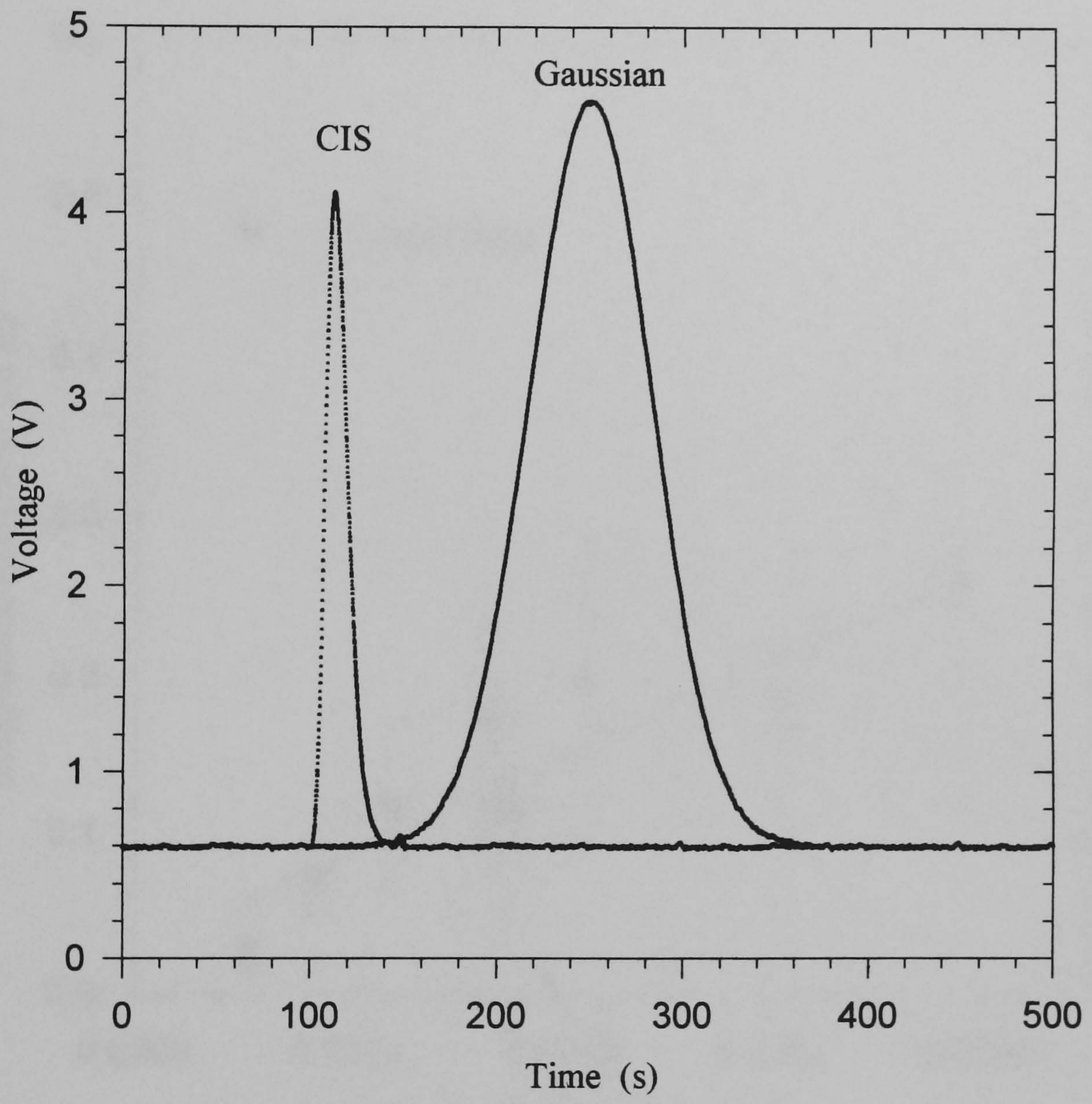

Figure 3.15 Test data sets

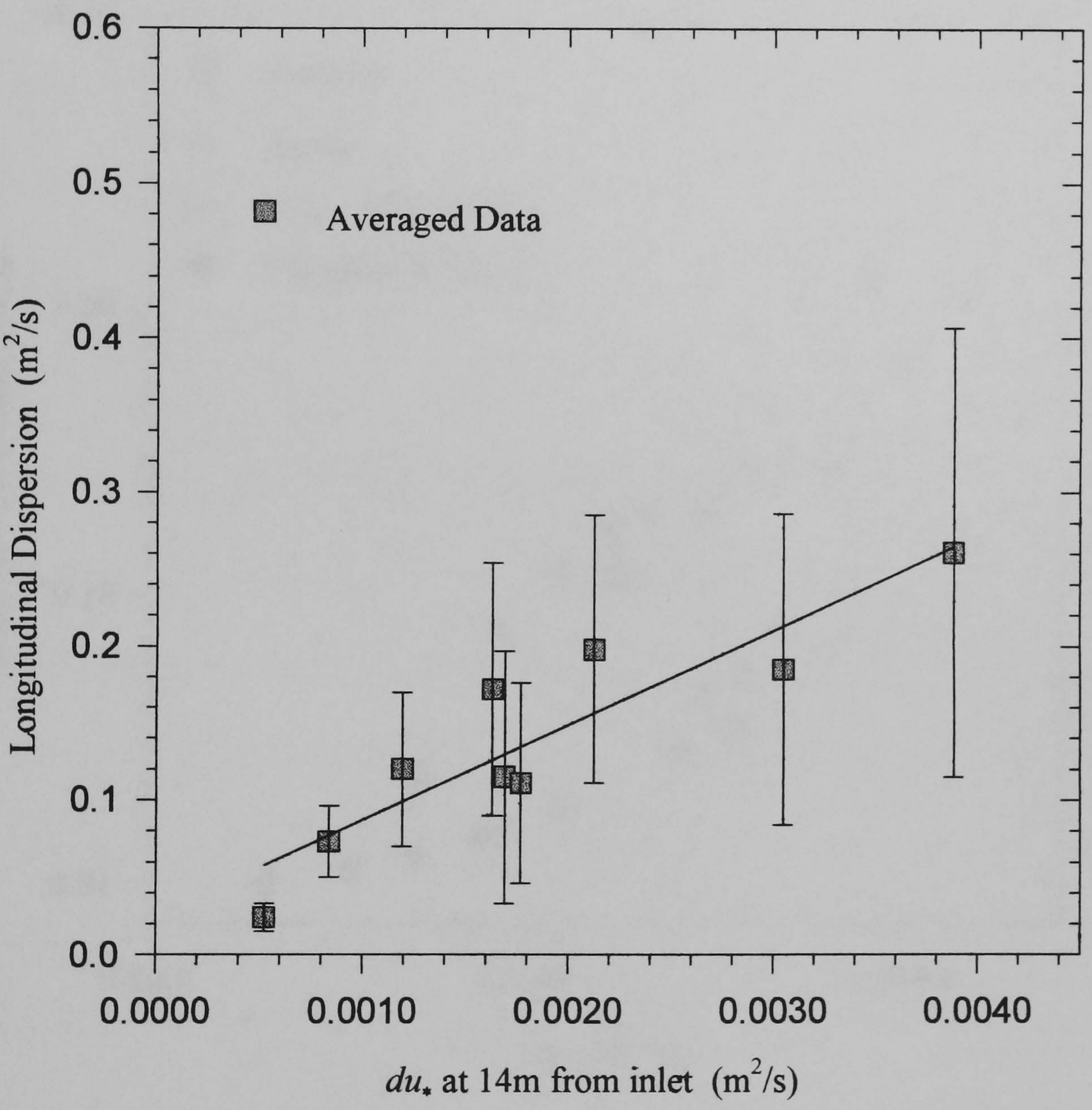

Figure 3.16 Longitudinal dispersion in the laboratory flume

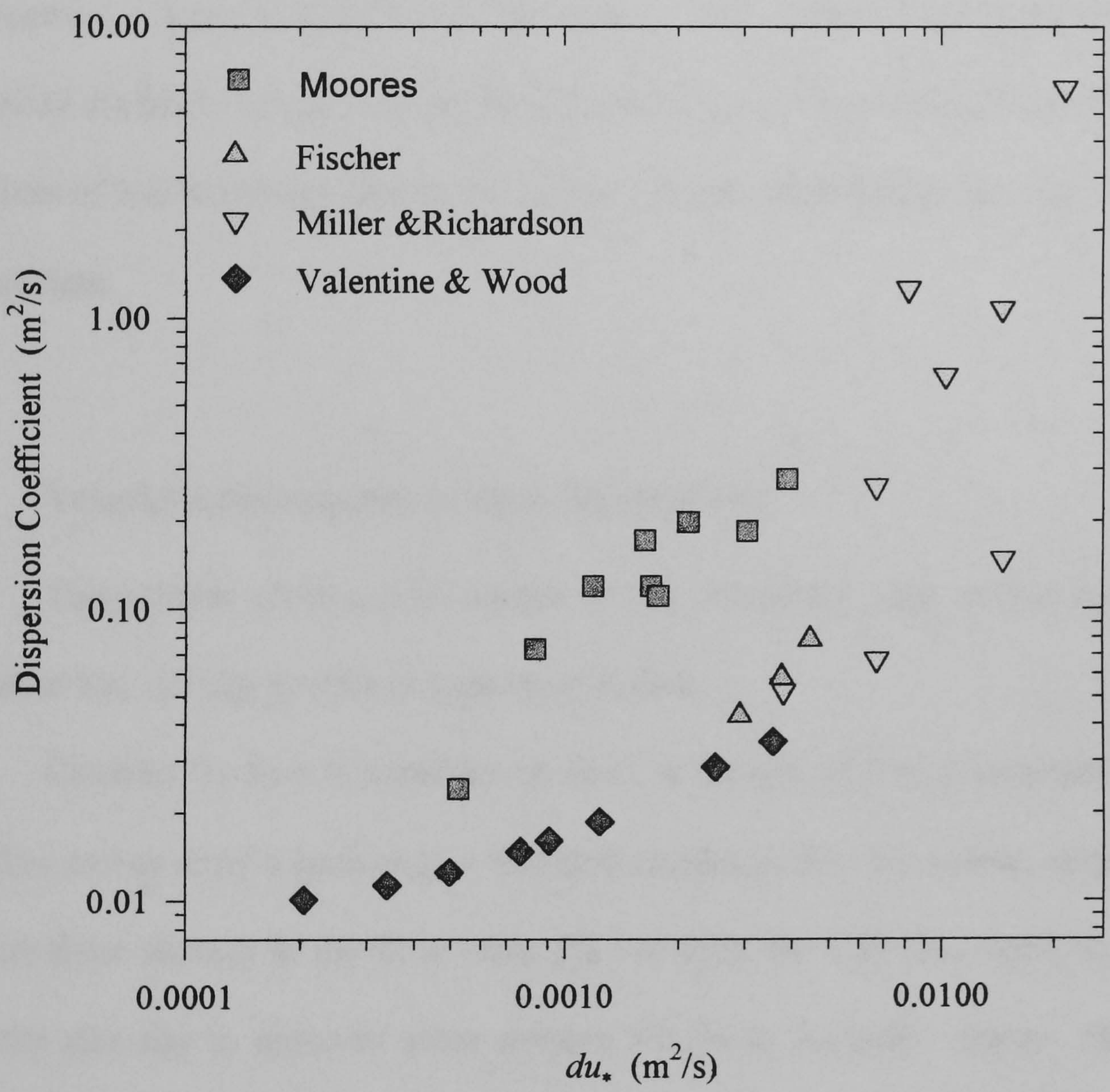

Figure 3.17 Comparison of dispersion coefficients measured in rect' lab' flumes

Chapter Four Measurement of the velocity field

4.1 Introduction

This chapter describes the results of velocity measurements undertaken in the laboratory flume used for the longitudinal dispersion experiments. Both the time averaged and instantaneous velocity fields were investigated. The time averaged longitudinal velocity is required for the random walk model of the dispersion process described in chapter seven. Velocity measurements have not previously been reported for the form of bed roughness used in the author's flume and therefore the work resulted in unique data.

4.2 Velocity measurements in open channel flows

This section gives a brief outline of the commonly used terminology of, and literature for, velocity profiles in open channel flow.

Consider the flow in a uniform channel; as the rate of flow is increased from zero the flow moves from a laminar to a turbulent condition. For the former, viscosity gives rise to shear stresses in the flow while for the latter the turbulent fluctuations of the velocity give rise to apparent shear stresses known as Reynolds stresses. In turbulent flow over a smooth wall there exists a thin layer close to the wall, where viscosity is of importance, known as the laminar sub-layer. Further away from the wall the turbulent fluctuations are of a magnitude such that the apparent Reynolds stress is of greater significance: this is the turbulent part of the flow. The thickness of the laminar sub-layer reduces as the flow rate increases. If all the roughness elements on the wall are submerged by the laminar sub-layer then the flow is considered to be hydraulically

smooth; if on the other hand the roughness elements extend beyond the sub-layer the flow is considered to be hydraulically rough.

The turbulent part of a flow can also be considered to be split into two main zones, the inner region and the outer region. The inner region is that closest to the bed and within which the flow is influenced by the bed, it extends for approximately 20% of the depth, *d*. The remainder of the flow can be considered as the outer region. Now obviously the influence of the bed does not suddenly cease at $y/d > 0.2$ (y being the distance measured from the bed) but gradually becomes less important; the free surface also has an influence. For this reason the outer region can be subdivided into an intermediate ($0.2<y/d<0.6$) and a free surface region ($y/d>0.6$). The velocity is found to vary in a logarithmic fashion over the both the inner and outer regions.

The theoretical development of the logarithmic velocity profile is given in many textbooks e.g. Goldstein (1938), Hinze (1975), Nezu & Nakagawa (1993) and only an outline is given here. Goldstein shows how the logarithmic velocity profile can be derived using three different approaches, one of which is the momentum transfer (or mixing length) theory. A mixing length is a conceptual length over which elements of fluid are considered to be exchanged by turbulent fluctuations. In a high Reynolds number flow the viscous sub-layer is very thin and the velocity gradients within it are very large. This suggests an approximation in which the viscous sub-layer is ignored and an infinite velocity gradient at the wall is used as the boundary condition. Using the momentum transfer theory, which allows us to model the Reynolds stresses in turbulent flow, and assuming that the mixing length is proportional to the distance from the wall gives a logarithmic velocity profile. This profile is sometimes known as the log-law:

$$\frac{u}{u_*} = \frac{1}{k} \ln y + const'$$

This equation is more often written as:

$$u/u_* \equiv \frac{1}{\kappa}\ln(yu_*/\nu) + B \tag{4.1}$$

to highlight the important length and velocity scales. In equation 4.1 ν is the kinematic viscosity, y is vertical distance from the (smooth) bed, κ is von Karman's constant and u_* is the bed shear velocity.

Fitting this equation to the pipe flow data of Nikuradse measured close to the wall (Goldstein 1938) gives $\kappa = 0.417; B = 5.8$ and if the equation is fitted to the velocity profile measured to the pipe centreline $\kappa = 0.4; B = 5.5$ The difference in the constants, depending upon which portion of the velocity profile the log law is fitted to, reflects the fact that the assumed mixing length distribution is valid only close to the wall.

In the outer region of open channel flow it is found that measured velocity profiles in a boundary layer deviate from the logarithmic profile (Nezu & Nakagawa 1993). This deviation can be accounted for by use of Coles' wake function which is an empirical correction to the log-law. This corrected profile is sometimes known as the log-wake law.

For rough channels the height above the bed is often scaled using the equivalent sand grain roughness, k_s, which gives the following form of the log law;

$$u/u_* = 1/\kappa \ln(y/k_s) + B' \tag{4.2}$$

This equation was originally developed for pipe flow and fitted to the experimental data of Nikuradse (Goldstein 1938). In Nikuradse's experiments sand grains were glued to the inside of the pipes and it was found that for high roughness Reynolds numbers ($u_* k_s/\nu \geq 100$) the friction factor was a function only of the sand grain size.

The flow in the outer region is often fitted to a velocity defect law. This equation is obtained by assuming a log law describes the velocity profile in the outer region as well as the inner. In a two-dimensional flow the maximum velocity occurs at the free

surface, and the equation is written as the difference between the maximum velocity in the flow and that at a given depth. It can also be developed using a log wake law as shown below; the second term on the right hand side of the equation contains the wake correction (Nezu & Nakagawa 1993):

$$\frac{u_{max} - u}{u_*} = -\frac{1}{\kappa}\ln\left(\frac{(y - y_0)}{d}\right) + \frac{2\Pi}{\kappa}\cos^2\left(\frac{(y - y_0)\pi}{2d}\right) \tag{4.3}$$

In the above equation it will be noted that the scaling factor for y has been changed from k_s to the flow depth d. This change can be achieved by rewriting the log law and incorporating the length scale into the constant, which then cancels. It has however more significance than this and shows that the flow in the outer region does not directly depend upon the inner region. This independence of the outer region is known as Reynolds number similarity (Raupach et al 1991, Krogstad et al 1992). The wall roughness is held to influence the turbulent motions within a roughness sub-layer which extends vertically to a height of about five times the roughness height. The turbulence intensities, normalised with the bed shear stress, should be independent of the roughness outside the roughness sub-layer according to the similarity hypothesis.

The wall or bed roughness controls the bed shear stress and the velocity offset, y_0, in the flow. The velocity offset expresses the difference between the geometric datum taken (often for rough open channels the top of a roughness element) and the origin of the velocity profile. Raupach et al (1991) state that, for flow over a plane surface with isolated roughness elements, the velocity profile is shifted upwards from the wall by a distance equal to the mean height of momentum absorption of the roughness elements. Whilst they give data for the velocity shift encountered in boundary layer flow over sand grain, wire mesh and natural vegetation roughness the bed roughness studied in this work is not represented. Kironoto & Graf (1994) working with open channels whose

beds were roughened with sand or gravel took the velocity profile offset to be 20% of the equivalent sand grain roughness below the top of the roughness elements. The same offset was used successfully by Dong et al (1995) for closely packed marble roughness.

Whilst the log laws are good models of the time averaged velocity profiles in wide open channel flows two further concepts need to be addressed: secondary flows and coherent flows. Secondary flows are flows in directions other than the longitudinal, they are in general low velocity (with a magnitude only a few percent of the longitudinal velocity). The term coherent flows is used to describe structures in the flow that are irregular, in time and space, but are seen to be repetitive and have a definable life cycle. Both phenomena will be described below.

Secondary flows can be split into two groups according to their cause: longitudinal non-uniformity of the flow such as bends and meanders give rise to secondary flows know either as strong secondary flows (French 1985) or secondary currents of Prandtl's first kind (Nezu & Nakagawa 1993). Anisotropy of turbulence causes the secondary flows known as either weak secondary currents (French 1985) or secondary currents of Prandtl's second kind (Nezu & Nakagawa 1993). The laboratory flume was straight and therefore secondary flows induced by anisotropy of turbulence will be concentrated on here.

In narrow open channel flows the velocity field is complex. Figure 4.1 shows the resultant of the vertical and transverse velocity vectors in a channel with a width equal to twice the flow depth. The maximum cross sectional velocity is about two percent of the maximum longitudinal velocity. It will be seen that each half of the channel contains two contra-rotating flows and that there is an up flow at the side walls and a down flow at the centreline. The maximum longitudinal velocity does not occur at the free surface but some distance (approximately 40% of the depth) below it.

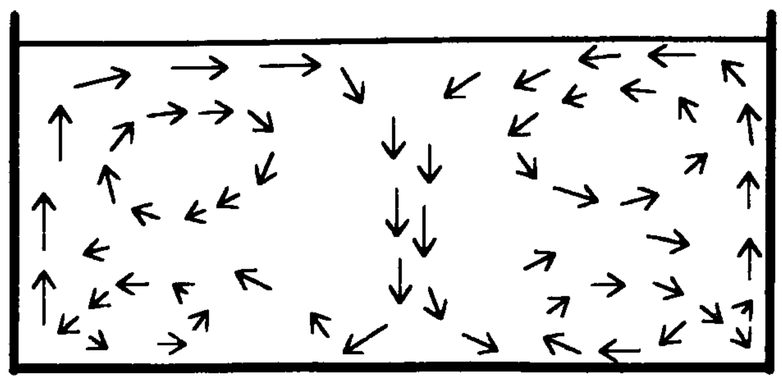

Figure 4.1 Flow in a narrow open channel (after Nezu & Nakagawa 1994)

It is (Nezu & Nakagawa 1994) the anisotropy of the turbulence caused by the presence of the side wall and free surface that drives the secondary flows.

It is found in wide open channel flow (where the width to depth ratio is greater than five) that the time averaged velocity field in the central section of the channel is two dimensional. However close to the side walls anisotropy of the turbulence field leads to secondary flows as in narrow channels. Nezu & Nakagawa describe how in natural straight open channels contra-rotating cells which scale with the flow depth are observed. It is known that changes in bed roughness and depth can promote secondary flow cells; where a ridge or rough area exists there is an up flow and a corresponding down flow occurs between the ridges/rough zones. It has also been observed in the laboratory that the corner flows in a sand bedded wide open channel are able to produce longitudinal ridges and that longitudinal ridges whose lateral spacing scales with the flow depth are developed. The inference is that these ridges stabilise and strengthen the secondary flows and that a feedback occurs where the secondary flow close to the wall produces a ridge, the presence of the ridge in turn strengthens the secondary flow and allows the development of ridges across the width of the channel. In a natural channel Nezu & Nakagawa suggest that vortices shed by boulders or other bed features can give rise or enhance secondary flow cells.

Coherent flow structures differ from secondary flows in that they are temporally and spatially irregular. Coherent flows were first seen during flow visualisation studies of

the near wall zone of a turbulent boundary layer (Smith 1996). Low speed streaks were seen to exist in the wall layer. Although the streaks were not fixed in time or space it was found that they had a fairly well defined span wise spacing. The low speed streaks are probably caused by the interaction of the wall layer with hairpin or horse shoe shaped vortices passing over the top of the wall layer (Smith 1996). Whatever the cause of the low speed streaks they are observed to undergo brief periods of vigorous interaction with the main flow. These periods of interaction are divided into bursts and sweeps. During bursting the low speed streak is seen to erupt into the outer layer. This is followed by a sweep where high speed outer layer fluid moves towards the wall an penetrates the wall layer. The ejection of low momentum fluid during the bursting process can result in the development of a hairpin/horseshoe vortex. The strong interaction between the wall layer and outer layer that coherent flows provide mean that they are very important to the transfer of vorticity from close to the bed where shear is greatest to the outer layer where the turbulent energy is dissipated. Although low speed streaks have been observed in the flow over rough beds (Defina 1996) Smith suggests that they may not be necessary because eddies shed by local irregularities in the bed would be sufficient to cause the cycle of bursts and sweeps. Defina working with a bed covered with spherical roughness elements observed near wall low speed streaks whose widthways spacing was about four times the equivalent sand grain roughness for the bed. As the vertical size of the streak grew the inter streak spacing also grew. Both Defina and Nezu & Nakagawa (1994) suggest that there is a relationship between the streaks and secondary flow cells. Defina noted that when the streaks had grow over the full depth they were very persistent and he suggested that this was because they coincided with secondary current cells.

4.3 Experimental techniques

The time averaged velocities in the flume were measured using a pitot tube and a hot film anemometer was used to investigate the instantaneous velocities. The methods adopted with these two measuring instruments are described in the following two sections.

4.3.1 Pitot static tube

An Airflow Developments pitot static tube with a dynamic port diameter of 1mm was used with an inclined manometer. The pitot tube was not supplied with a calibration certificate but the manufacturer stated that the isentropic efficiency would be unity to within 2%. The overall uncertainty in a velocity measurement was calculated using the equation given in BS 1042 (1983). As BS 1042 was written as a guide to discharge measurements in closed conduits some of the uncertainties given in the Standard are not relevant to open channel flow; using those that were relevant to open channel flow the overall uncertainty was estimated as ±1.6% of a measured value. The minimum velocity for which the pitot measurements were reliable was 0.2m/s according to BS 1042.

4.3.2 Hot film anemometer

A Dantec 55M constant temperature anemometer incorporating a 55M10 standard bridge and a 55R42 conical probe was used to measure the longitudinal component of the instantaneous velocity field.

Hot film probes have been used to measure velocities in liquid flows since the 1960's. A description of the technique can be found in Lomas (1986), McQuivey (1973) and Nezu & Nakagawa (1993). The frequency response is such that they can be used to

measure turbulent quantities. The hot film probe is sensitive to the temperature of the fluid in which it is used and it can become contaminated; to obtain meaningful data care must be taken in its use. As an example of the problems that can be encountered, it was found that the hot film probe could not be used close to the channel inlet because tiny transient air bubbles that existed in the water there rapidly coated the hot film element.

It was found that the best method of calibrating the hot film probe was to measure a velocity profile with a pitot for the flow rate under investigation, and to bring the time averaged hot film data into agreement with the pitot measurements. This insitu calibration technique was also used by McQuivey (1973) and Kironoto & Graf (1994).

The output from the 55M10 bridge was recorded using a CED 1401 intelligent interface and Spike2 logging software at a sampling frequency of 200Hz for one minute. The sampling frequency was chosen after referring to Nakagawa & Nezu (1993) and was selected to ensure that all the turbulent frequencies were recorded. The records were checked for stationarity by splitting the record into four 15 second sections; the mean voltage of these sections was calculated and compared to the mean of the whole record. The length of record used for the stationarity check was an order of magnitude longer than the time required for an eddy of the size of the flow depth to pass the probe at the cross-sectional average velocity. If the mean of the whole record and each section differed by (an arbitrary) 2% or more the record was assumed to be non stationary and the data discarded. If the data was stationary the data was calibrated using:

$$u \equiv \left(\frac{\varepsilon^2 - B}{A} \right)^2 \tag{4.4}$$

where ε is the output voltage of the probe, and A and B are constants obtained by bringing the velocity profile measured with the hot film into agreement with that of the pitot. This equation is known as King's law (McQuivey 1973, Perry 1982).

The instantaneous velocity was calculated using the usual linear approximation, see Perry (1982) and McQuivey (1973). It is known that the linear approximation leads to errors in the value of the instantaneous velocity. For example, Perry (1982) measured the error for a hot wire and found that using the linear assumption lead to errors in the rms. velocity of about 1% for a ratio of 20%. between the fluctuating and mean velocity. For a fluctuating velocity to mean ratio of 30% the error was 2% rising to 5% for a ratio of 40%. The author's calibration software incorporated a check on the number of conversions performed for which the velocity fluctuations were greater than 30% of the mean. This information was only noted as Perry's work suggested that the errors arising from the use of the linear approximation to King's law were small.

4.4 Results

The time averaged and instantaneous velocity measurements are described in turn below.

4.4.1 Time averaged velocity

A main group of nine traverses of the flume using the Pitot static tube were made at distances from the flume inlet of 9m, 15.5m and 22m; these longitudinal positions are referred to below as L9, L15.5 and L22 respectively. The traverses were performed at three flow rates of nominally 7l/s, 13l/s and 26l/s (equivalent to a depth at 6m from the inlet of approximately 50mm, 70mm and 100mm, respectively) as these spanned the range of flows used in the longitudinal dispersion experiments. The longitudinal velocity was measured at approximately ten equispaced locations over the depth. The transverse positions used were the same at all longitudinal sections namely 125mm, 225mm, 325mm, 375mm, 425mm, 525mm & 625mm measured from the left hand side wall of the

flume when looking in the direction of flow. The prefix TP (e.g. TP125) is used to refer to these transverse positions.

Figure 4.2 shows typical velocity profiles measured during the main group of traverses of the flume. These show the complexity of the flow field: the maximum velocities occurred at TP125 and TP325 and the minimum velocity occurring at the mid span position (TP375). It had been expected that the velocity field in the flume would have been two-dimensional because the aspect ratios of the flows were large, however the data does not support this. Similarly, the velocity data in Figure 4.3 (an additional traverse undertaken at 11.5m from the flume inlet) also shows that the velocity field was three-dimensional. Here, the velocities recorded closest to the wall of the flume show a retardation of the flow close to the free surface, this phenomenon is known as a velocity dip and is taken to be evidence of secondary flows set up by the wall (Nezu & Nakagawa 1993). As a check on the accuracy of the pitot velocity measurements the data collected at L9, L15.5 and L22 from the inlet were integrated over the channel cross section and compared to the flow implied by the stage discharge curve. The variation of the velocity between the walls and the nearest measurement point was treated in two ways: firstly, (Method 1), it was assumed to be zero at the wall and to vary linearly up to the measuring position, this method tended to under predict the flow rates. Secondly (Method 2) it was assumed that the velocity was constant up to the walls, this over predicted the flow. These flows are given in Table 4.1 along with their average and the percentage difference between the actual flow rate (equation 3.1) and mean integrated flows. The measurements taken at L15.5 for a flow of 13.3l/s are anomalous in that Method 1 gave a flow rate greater than that from the stage discharge curve. The velocity measurements for this case were performed in the same manner as all the others and no explanation for this difference can be given. The average of Method 1 & 2, for the

13.3l/s experiments at L22, differs from the flow rate by 9.8%. For all the other measurements the agreement is better than 3%.

In order to quantitatively compare the transverse velocity profiles recorded at each of the different flow and longitudinal position combinations the transverse velocity variation, u' , was calculated for each of the measured flow fields using the following equation:

$$u' = \sum (u - \bar{u})^2 \frac{\Delta W}{W} \tag{4.5}$$

in which the width W is divided into a number of transverse slices of width ΔW each with a depth averaged velocity u ; the cross sectional average velocity is $\bar{u}$. The log-law fits to the measured vertical velocity profiles were used to calculate the depth average velocity at each of the seven transverse measurement positions. The transverse velocity variation calculated in this way are given in Table 4.2 and show that the transverse non-uniformity of the flow at all three locations increased with increasing flow rate. At the lowest flow rate the transverse non-uniformity is approximately constant down the flume. At a flow of about 13l/s the transverse non-uniformity is 10% higher at L15.5 and L22 than at L9. At 26l/s the transverse non-uniformity increases down the flume. This probably was due to the increasing influence of the draw down as the flow rate increased which caused the flow to accelerate along the flume. It is shown in chapter seven that the longitudinal increase in transverse non-uniformity of the flow effected the longitudinal dispersion in the flume.

Right angle bends have been known to introduce swirl into a flow. Whilst the pipework leading from the header tank to the flume included a number of bends, it is unlikely that the transverse velocity profiles measured downstream are due to large scale eddies entering the flume from the feeder pipework. This is because the vertical velocity profile was measured at three transverse locations at the flume entrance and it was found

that the velocity was constant over the cross-section. It is more likely that the transverse profiles were generated by the irregularities in the bed profile. Laying a half metre long level across the channel at one metre intervals showed that at the majority of sections a slope existed up from the left to right hand wall. Using a 100mm diameter disc as a local average at TP125, TP375 & TP625 showed the right hand side to be lower than the centre line for three out of eight cases; while the left hand side was lower than the centre for seven of the eight cases. On average the left hand side was 2.3mm lower than the centre and the right 0.5mm higher. The method used to form the bed is probably the reason for this slope because of the difficulty of applying even pressure to the pattern used to impress the dead zones into the sand.

The shear velocity is commonly used to nondimensionalise velocity, longitudinal dispersion and transverse mixing measurements. It can be obtained in a number of ways but two methods were possible with the equipment available: the velocity profiles in the inner region could be fitted to a log-law; and the bed or energy slope could be used with the assumption of uniform flow. Kabir & Torfs (1992) found that with the former method the calculation of shear velocity over a rough bed was sensitive to the definition of the origin of the velocity profile and suggested that the bed slope be used to calculate the shear velocity. The flow in the author's flume was gradually varying and the water surface slope was more appropriate than the bed slope in the calculation of the shear stress. A second order polynomial was fitted to the water surface profiles and differentiated to obtain the slope at the longitudinal position of interest. The walls of the flume used for this work were smooth and a correction, due to Vanoni & Brooks (French 1985) was applied. The correction was less than 10% of the value obtained from assuming the flow to be two dimensional. An alternative side wall correction due to Knight et al (1994) was also applied to the bulk flow data at 15.5m from the flume inlet.

The difference between the two side wall corrections was less than 5%; Vanoni & Brooks' correction giving slightly lower values of bed shear stress. As the average of the bed shear velocities calculated by fitting a log-law to the pitot measurements was lower than those of either correction method; Vanoni & Brooks' correction was used to calculate all the average bed shear velocities reported in this thesis.

A log-wake law (equation 4.3) was regressed to the data from L15.5, the parameter Π took values between -0.006 and -0.1 for a range of Reynolds number $\left(du_*/\nu\right)$ between 878 and 4272. There was no dependence of Π with Reynolds number. In contradiction to these results Nezu & Nakagawa (1993) plotted data from three workers for which Π was positive and increased with increasing Reynolds number from a minimum of 0 for a Reynolds number of about 400 to a maximum value of 0.2 for a Reynolds number greater than 2000. Cardoso et al (1989) fitted a log-wake law to velocity profiles collected in a smooth bedded flume; the wake term was weak and secondary flows were considered to have been the cause of the weak wake. Kirgotz (1990) found that a log-law fitted velocity profiles measured over both a smooth and a rough bed better than a log-wake law. The majority of Kirgotzs' results were obtained in low aspect ratio flows so that secondary flows may have existed. Cardoso et al and Kirgotzs' results suggest that the transverse non-uniformity of the velocity found in the author's flume was the reason for the smallness of the wake correction required in equation 4.3 and why a log-law was a good fit to the entire velocity profile.

It was decided to plot the velocity data in the form of a velocity defect law:

$$\frac{u_{max} = u}{u_*} = -\frac{1}{k} \cdot \ln\left(\left(\frac{y = y_0}{d}\right)\right) - C \qquad (4.6)$$

in which u_{max} is the maximum velocity in the flow, u the local longitudinal velocity at a height y above the bed, y_0 is the velocity offset and C is a constant (see Figure 4.4). It

will be realised that equation 4.6 is equation 4.3 with the wake correction term replaced by a constant. In order to obtain the velocity offset and bed shear velocity a log-law was regressed to each velocity profile:

$$u = \frac{\ln(y)}{b_1} = \frac{b_0}{b_1} \tag{4.7}$$

assuming that von Karman's constant takes a value of 0.41 the bed shear velocity can be calculated by analogy with a log-law.

$$\frac{u}{u_*} = \frac{1}{k}\ln(y) + A \tag{4.8}$$

The height, or velocity offset, at which the velocity profile has its origin, y_0, can also be calculated by rearranging equation 4.8. The velocity offset increased with increasing flow rate having an average value of 0.37mm, 0.47mm, and 0.51mm for the 7l/s, 13l/s and 26l/s flows respectively. The bed shear velocities implied by fitting equation 4.7 to the velocity profiles measured at the seven transverse locations are given in Table 4.3 along with their mean value and the side wall corrected bed shear velocity (the regression coefficients for all but two of the fits were greater than 0.9). The mean of the bed shear velocities evaluated from the log-law fits was lower than the side wall corrected bed shear velocity at all longitudinal locations and flow rates. In general the difference between the two values decreased with increasing flow rate.

The bulk hydraulics of the flow in the flume were investigated by comparing the measured flow to a rough law resistance equation (ASCE 1963):

$$\frac{1}{\sqrt{f}} = a\log\left[\frac{12\mathbf{R}}{k_s}\right] \tag{4.9}$$

where k_s is a roughness parameter (the size of equivalent densely packed sand grains that would give the same head drop as the actual roughness and known as the equivalent

sand grain roughness), **R** the hydraulic radius and when von Karman's constant is 0.4 a takes a value of 2.04. Equation 4.8 can be derived from a log-law if the flow is assumed to be two-dimensional, for such a flow it can be argued that the flow depth is the correct parameter rather than the hydraulic radius. Plotting the side wall corrected friction factor and depth in the form of equation 4.9 implied an equivalent sand grain roughness height of 27mm. The equivalent sand grain height is known (Goldstein 1938, Kay & Nedderman 1979) to be difficult to relate to a physical dimension of the roughness elements and it was not therefore surprising that it was greater than the depth of the dimples. An equivalent sand grain roughness of 20mm would be expected for flow over rubble masonary (French 1985).

Manning's equation is often used to predict flow rates in open channel flows. The equation takes the following form:

$$u = \frac{1}{n}\mathbf{R}^{2/3}\sqrt{\alpha} \qquad (4.10)$$

in which u is the average velocity, **R** is the hydraulic radius, n is a coefficient and α is the bed slope. The value of n for the flume was evaluated by rearanging equation 4.10 and equating it to equation 4.9, this gave a value of $0.028\,s/m^{1/3}$. This is the figure expected (French 1985) for a straight channel excavated in coarse gravel and at the lower end of the range expected for natural streams without pools or riffles.

Unfortunately the velocity measurements were not detailed enough to allow an investigation into the structure or magnitude of any secondary flow cells that may have existed in the channel. Ideally measurements of the transverse and vertical velocity are required in order to quantify secondary flows although some understanding of the flow can be gained by plotting isovels.

4.4.2 Instantaneous velocities

All hot film measurements were made at TP50, TP125, TP225, TP325, TP375 and TP425 from the left hand wall of the flume and at L15.5.

Plotting the turbulence intensity, defined as the rms of the fluctuations divided by the time average (u'/u), against depth showed the turbulence intensity to be a function of position and flow rate. For a given flow rate the turbulence intensity was highest at those transverse positions that had the lowest time averaged velocity and highest local bed shear stress (see for example Figure 4.5 which shows the data for 26l/s) and the spread of the turbulence intensity profiles increased with reducing flow rate. While for a given transverse position the highest turbulence intensity occurred at the lowest flows (see for example Figure 4.6 which shows the data for TP375). This dependence of the turbulence intensity on flow rate can be explained by the work of Nezu & Nakagawa (1993) who showed that an increase in relative roughness led to an increase in turbulence intensity. The equivalent sand grain roughness was 27mm and the relative roughness was greater for the lower flow rates because the the flow depth was lower.

In section 4.1 it was stated that the similarity hypothesis (Raupach et al 1991, Kogstad et al 1992) states that away from the bed the turbulence intensities non-dimensionalised by the bed shear velocity should be independent of the form of the bed roughness. Nezu & Nakagawa (1993) gave a semi-empirical equation for the variation of this definition of turbulence intensity with depth:

$$\frac{u'}{u_*} \equiv A \exp(-By / d) \qquad (4.10)$$

The scatter of the data was reduced if the local bed shear velocity was used rather than the bed average obtained from the surface slope. A regression of equation 4.10 to the author's data is shown as a solid line in Figure 4.7. The degree of scatter of the data

plotted as Figure 4.7 is comparable to that of previous workers. Figure 4.7 also shows (as a dashed line) equation 4.10 with the coefficients found by Nezu & Nakagawa. Table 4.4 gives the coefficients, of equation 4.10, obtained by the author along with those values found by previous workers. There is good agreement between different workers' correlations of turbulence which lends further supports to the similarity hypothesis.

4.5 Conclusions

Manning's n (0.028) for the flume was within the ranges reported for straight natural open channels with no pools or riffles and straight channels excavated in coarse gravels.

The time averaged longitudinal velocity profiles showed that the flow was three-dimensional, the three-dimensionality being ascribed to irregularities in the bed of the flume. Because the flow was three-dimensional a log-law fitted the measured velocity profiles, except close to the side walls, without the need for a wake correction term.

The transverse non-uniformity of the flow, which was a measure of the velocity shear, increased with flow rate. As the flow rate increased from 7l/s to 26l/s the transverse non-uniformity began to increase with longitudinal position in the flume.

The turbulence intensity defined as the rms of the instantaneous longitudinal velocity non-dimensionalised with the local time averaged longitudinal velocity was a function of depth and transverse position. However the turbulence intensity defined as the rms of the instantaneous longitudinal velocity non-dimensionalised by the local bed shear velocity was a function of depth only. The data was well fitted by an exponential law and was similar to that collected by previous workers over a variety of different bed roughnesses. This similarity of the turbulence structure over different roughnesses demonstrates that away from the bed the flow is unaware of the form that the roughness takes.

Distance from inlet (m)	Flow rate (l/s)	Method 1 (l/s)	Method 2 (l/s)	Average (l/s)	Percentage difference
9	7.1	6.4	7.7	7.1	0.7
9	13.4	11.2	15.9	13.6	1.5
9	25.7	23	27.7	25.4	1.2
15.5	7.1	6.4	7.7	7.05	0.7
15.5	13.3	13.7	16.5	15.1	-16.0
15.5	26	23	27.7	25.4	2.3
22	7	6.5	7.8	7.2	-2.9
22	13.3	13.2	15.9	14.6	-9.8
22	26.0	24.2	28.9	26.6	-2.3

Table 4.1 Discharge calculated from velocity profiles.

Section (m)	Flow rate (l/s)	Variance $((m/s)^2)$
9	7.1	0.0031
9	13.4	0.0049
9	25.7	0.0082
15.5	7.0	0.0032
15.5	13.5	0.0055
15.5	26.0	0.0095
22	7.0	0.0032
22	13.3	0.0055
22	26.0	0.0152

Table 4.2 Variance of transverse velocity profiles.

Flow (l/s) Position	u_* (m/s) (TP125)	u_* (m/s) (TP225)	u_* (m/s) (TP325)	u_* (m/s) (TP375)	u_* (m/s) (TP425)	u_* (m/s) (TP525)	u_* (m/s) (TP625)	Mean u_* (m/s)	Side wall corr'ed (m/s)
7.1 L9	0.015	0.023	0.008	0.018	0.013	0.018	0.012	0.015	0.025
7.1 L15.5	0.026	0.023	0.011	0.020	0.019	0.026	0.021	0.021	0.026
7.0 L22	0.017	0.019	0.023	0.021	0.020	0.027	0.030	0.022	0.029
13.4 L9	0.019	0.021	0.011	0.015	0.018	0.016	0.014	0.016	0.031
13.3 L15.5	0.027	0.025	0.023	0.035	0.033	0.037	0.033	0.030	0.034
13.3 L22	0.027	0.014	0.028	0.030	0.031	0.030	0.040	0.029	0.037
25.7 L9	0.029	0.040	0.031	0.043	0.036	0.044	0.036	0.037	0.043
26.0 L15.5	0.034	0.036	0.031	0.042	0.044	0.045	0.042	0.039	0.044
26.0 L22	0.026	0.043	0.043	0.045	0.041	0.044	0.043	0.041	0.049

Table 4.3 Bed shear velocities.

Reference	A	B	Bed
Present work	2.27	0.87	Rough
Nezu & Nakagawa (1993)	2.3	1.00	Rough & smooth
Kirono & Graf (1995)	2.04	0.97	Rough
Nezu & Rodi (1986)	2.26	0.88	Smooth
Cardoso et al (1989)	2.28	1.08	Smooth
Salazar (1993)	2.17	1.23	Rough
Wang et al (1995)	2.14	0.80	Rough

Table 4.4 Comparison of turbulence intensities measured by different workers.

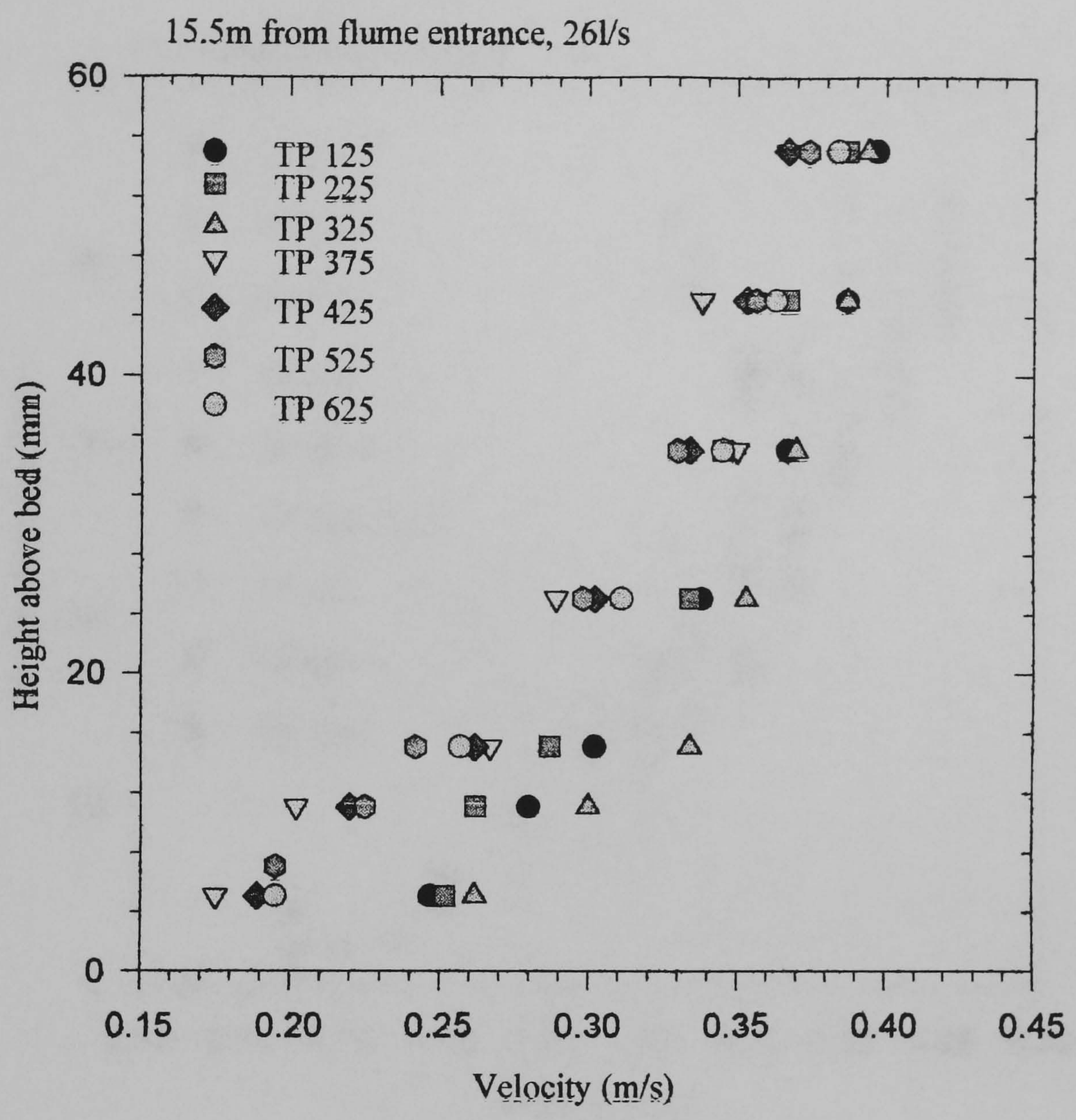

Figure 4.2 Typical velocity profiles (measured for a flow of 26l/s)

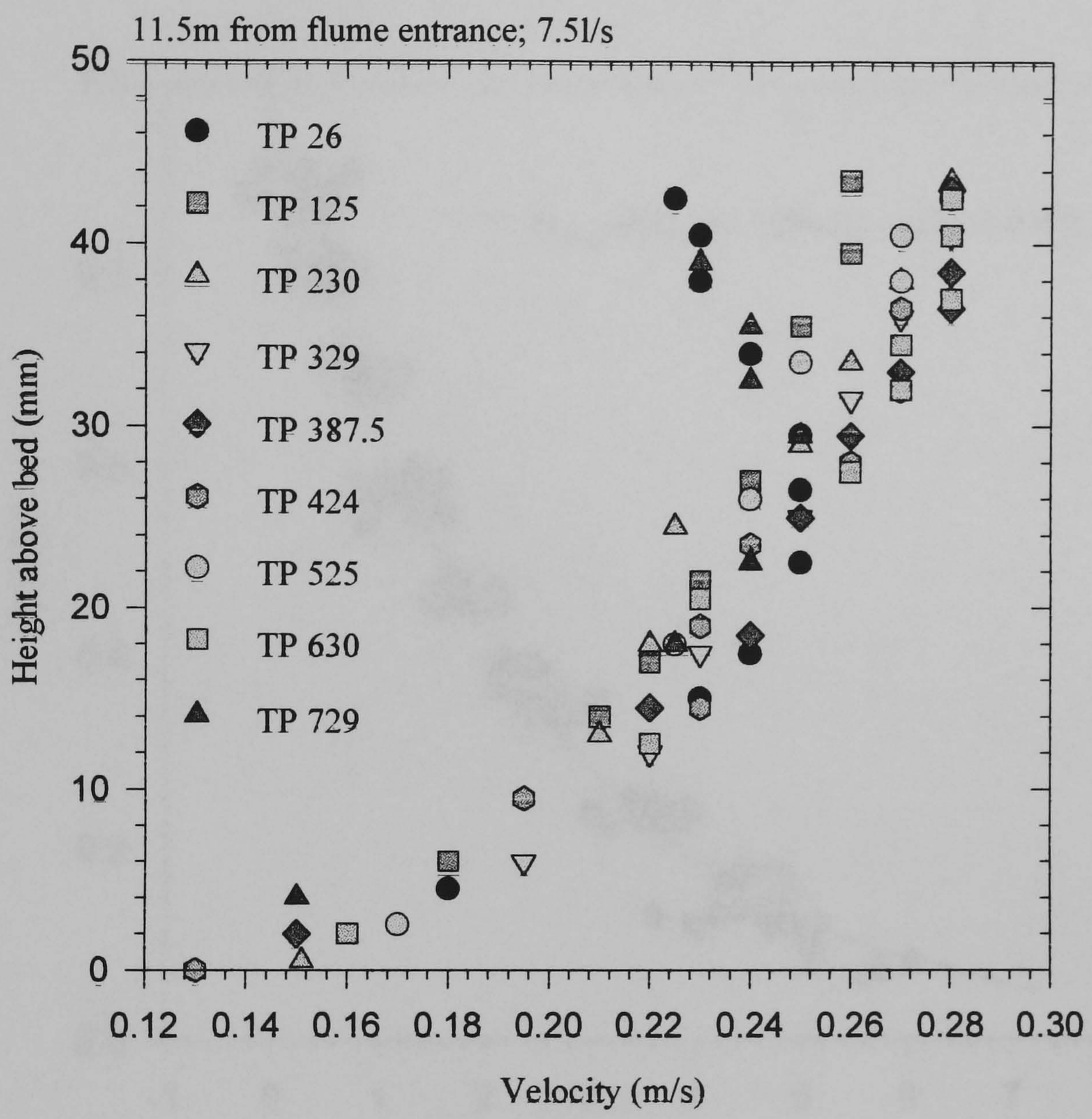

Figure 4.3 Velocity profiles for a flow of 7.5l/s

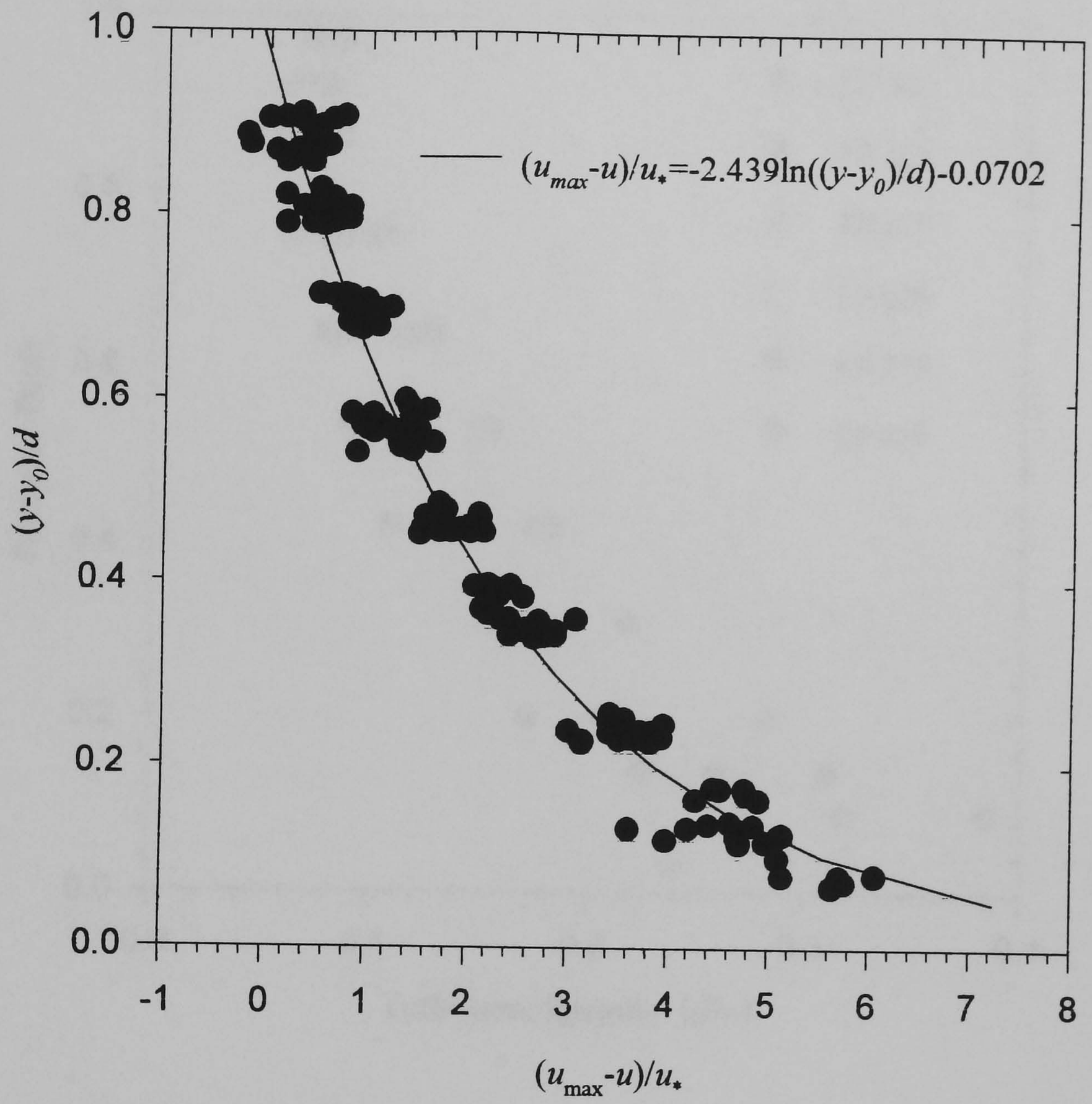

Figure 4.4 Velocity defect plot of pitot data from L15.5

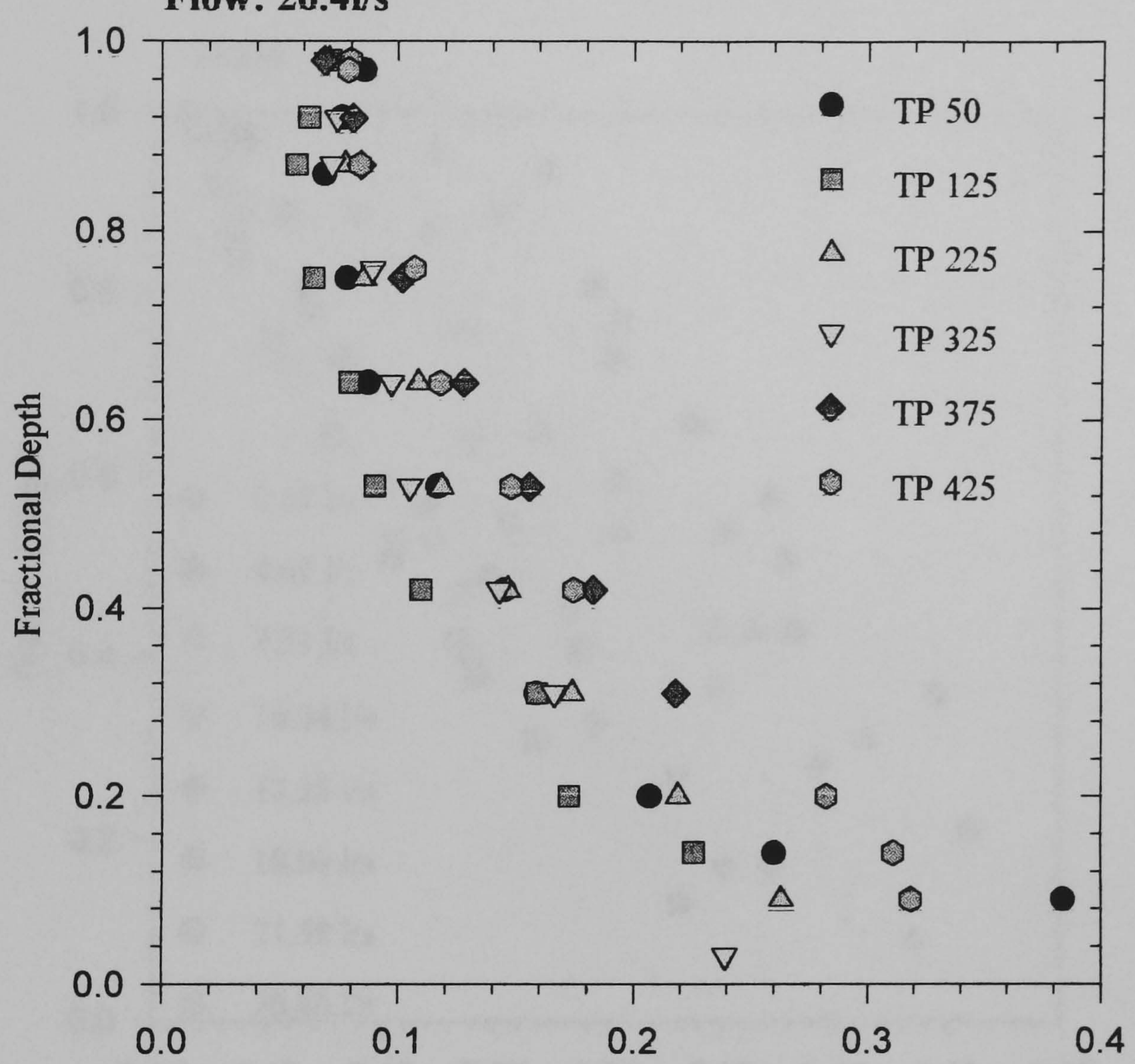

Figure 4.5 Turbulence intensity as a function of depth for a flow of 26l/s

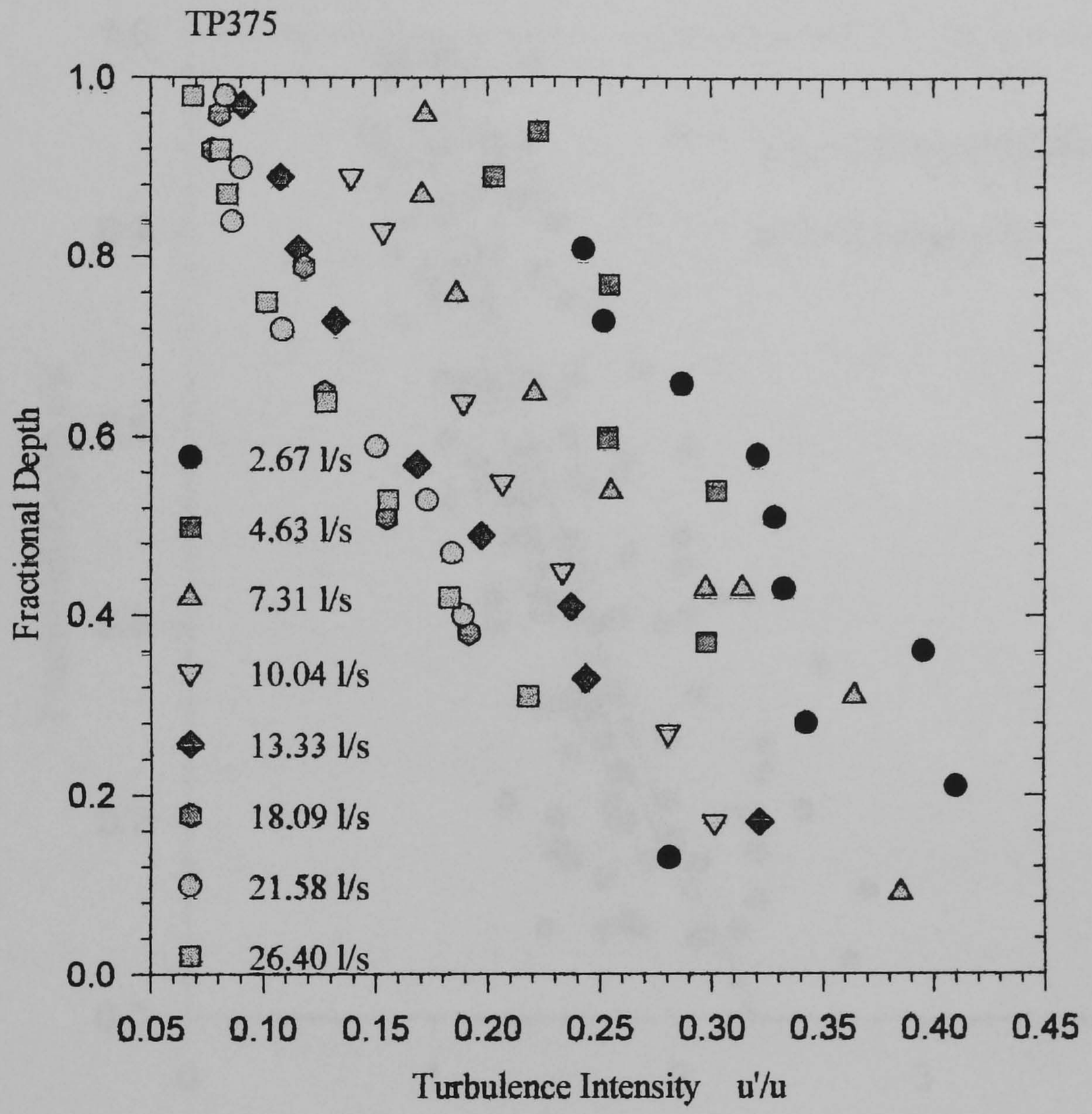

Figure 4.6 Turbulence intensity as a function of depth at TP375

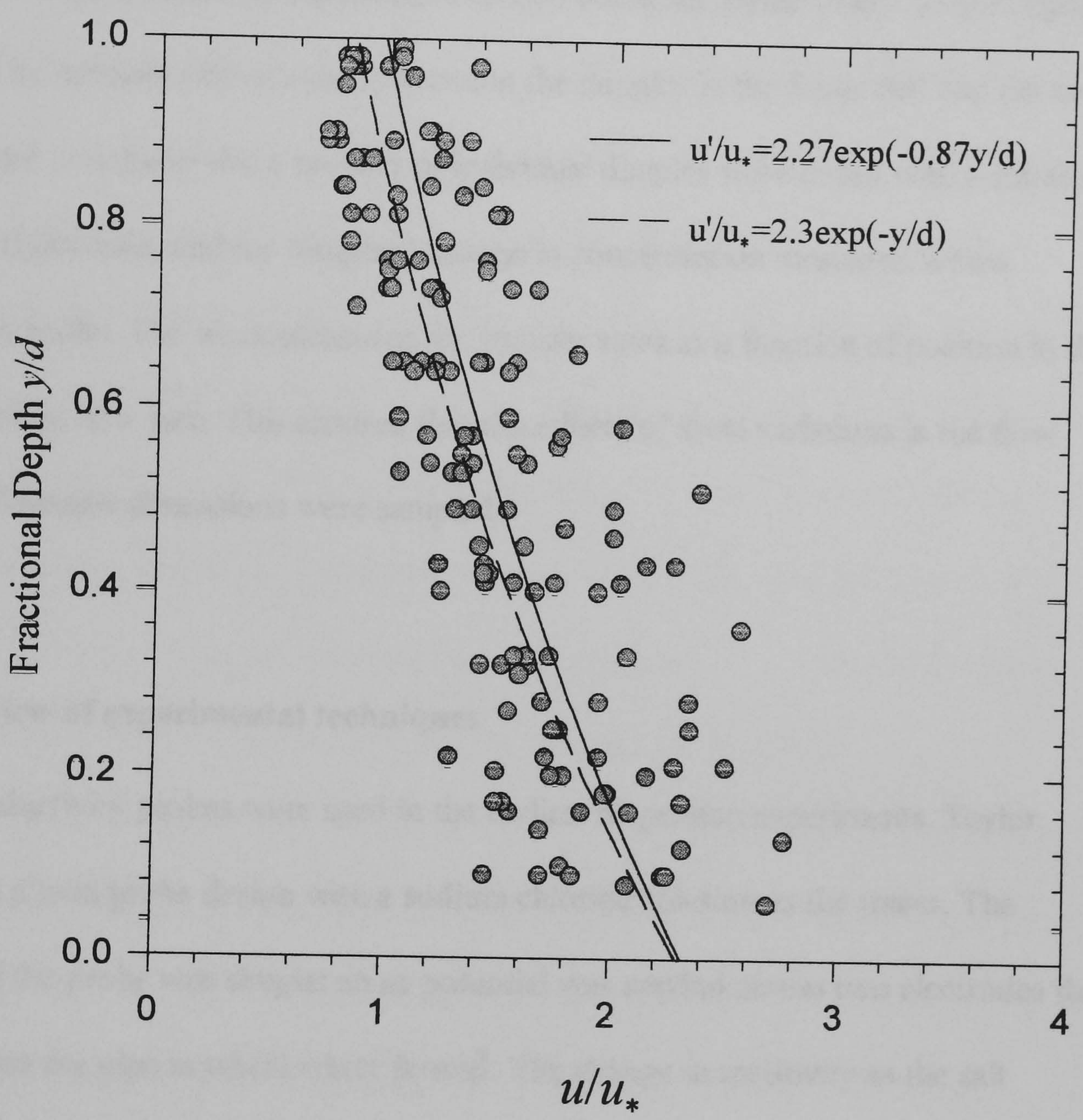

Figure 4.7 Regression of u'/u_* against y/d

Chapter Five Measurement of dead zone transfer rates

5.1 Introduction

This chapter describes experiments carried out in the flume which were designed to quantify the transfer rate of solutes between the dimples in the flume bed and the main flow. In order to achieve this a number of individual dimples were dosed with a solution of Sodium Hydroxide, and the temporal change in concentration measured with a conductivity probe. The work measured the transfer rates as a function of position in the flume as well as flow rate. This ensured that the effects of local variations in the flow velocity and dimple dimensions were sampled.

5.2 Review of experimental techniques

Conductivity probes were used in the earliest dispersion experiments. Taylor (1954) used a twin probe design with a sodium chloride solution as the tracer. The operation of the probe was simple: an ac potential was applied across two electrodes that protruded into the pipe in which water flowed. The change in resistivity as the salt dispersed in the flowing water was taken as a measure of the salt concentration.

Gibson and Schwarz (1963) used a conductivity probe and hot film anemometer to measure the spectra and decay of a random homogeneous field of concentration and temperature behind a grid. Their probe consisted of a fine platinum wire that was encased in epoxy resin apart from one end which formed part of an electrode pair with a much larger plate. The platinum wire/plate pair had an ac potential applied across it and concentration fluctuations were registered as a change in impedance. McQuivey &

Keefer (1972) used a Gibson & Schwarz type conductivity probe (with a salt solution as the tracer) in conjunction with a hot film probe to examine velocity-concentration covariance in a rough open channel flow. Fischer (1967a) also used a salt solution as the tracer in his experiments. The probe he used consisted of three small platinum plates which were arranged such that the electrostatic field was concentrated between the two outer plates and the inner plate. Alonso (1970) described a twin probe design in which the electrodes are formed by 1.5 mm long lengths of 0.05 mm diameter platinum wire; the wires being separated by 0.6 mm. An experimental investigation by Ncube et al (1991) suggested that better spatial resolution and drift characteristics were obtained by cleaning the probe electrode with Aquia Regis. Platinum black was used by earlier workers (Gibson & Schwartz, Fischer 1966) to reduce the effects of polarisation at the electrode surfaces. Ncube et al found that the response of a Gibson & Schwatz type conductivity probe to a change in concentration of a solute was a complex function of supply frequency, water temperature and probe design and materials.

The use of a fluorescence technique to measure concentration was reported by Patterson (1986), Barrett & Van Atta (1991) and Hannoun & List (1988). All of these workers used LDA systems to measure velocity, with a laser also providing the light necessary for the fluorescence measurements. The main problem with the use of fluorescence as a method of measuring concentration is that the intensity of the light at a given point needs to be known so that it can be compared to the intensity of fluoresced light. A method of accounting for the attenuation of the light as it passes through the flow field therefore needs to be developed. Similar problems could be expected with the approach taken by Hishida et al (1992) who used the intensity of the light scattered by particles in the flow as a measure of their size (larger particles scatter more light). Two particle sizes were used, small particles to measure velocity as in a conventional LDA

system and a larger size that acted as a tracer and were used to measure the rate of mixing.

Bousgarbies et al (1982) studied mixing in a shear layer, the velocity being measured with a LDA system and concentration with a conductivity probe. The conductivity probe design was similar to a hot wire anemometer.

It was concluded that for the current project the relative simplicity of the conductivity probe outweighed the advantages of the non instrusive optical methods of concentration measurement. The development of a fluorescent concentration probe would have required a great deal of development time, as would the use of particle size differentiation in a LDA system. The fluorometers used for the longitudinal dispersion measurements could not be used to measure the dead zone transfer rates, or indeed the transverse mixing coefficients described in chapter six, because they required water to be extracted from the flume and had too low a frequency response.

5.3 Development of the conductivity probes

A single wire probe, after Gibson & Schwarz (1963) was built. This consisted of a length of platinum wire coated in epoxy to provide insulation and mechanical strength (see Plate 3). As described above, the second electrode in this design takes the form of a relatively large plate some distance away from the single wire probe. Assuming that the probe formed a spherical electrode an infinite distance away from an infinitely large electrode, Gibson & Schwarz produced an analytical expression for the spatial resolution of the probe. This analysis suggested that the prototype probe would have a measurement volume of the order of 250 μm, and the application of Kolmogorovs' length scale equation to a flow of 25 l/s in the laboratory channel suggested a smallest

turbulence length scale of around 150 μm. Turbulence is known to be produced over a wide range of length scales so this conductivity probe could be expected to average the scales between 250 and 150μm, but should have had an ablity to distinguish motions with a larger scale.

Sodium chloride had been used as a tracer by all the previous workers. However its use was not permitted in the present work because of potential corrosion problems with the valves and pumps that form the return path for the recirculating flume. It was known that alkaline solutions can have an inhibitive effect on corrosion, so sodium hydroxide was considered for the tracer. Experiments showed that the probe was more sensitive to equal mass additions of sodium hydroxide than NaCl, and that sodium hydroxide did not cause any signs of corrosion apart from a slight discolouration of the test piece involved. Araldite epoxy resin was used to encase the platinum wire of the conductivity probes, it was found that the rapid curing epoxy resins tended to swell in sodium hydroxide solutions and use of the standard epoxy resins was necessary.

A common method of using conductivity probes has been to arrange for the probe to form one arm of a four arm bridge network. Assuming the bridge is balanced at the zero concentration point any change in concentration will cause the bridge network to go out of balance. The potential difference across the centre of the bridge is then a measure of the solute concentration. It was found that a commercial signal generator had a sufficiently stable output voltage to allow its use as the oscillator in such a bridge network. Trials showed that the circuit could be simplified and an operational amplifier circuit was designed by the Electronics Workshop. In this design the ac voltage over the probe was amplified and converted to a dc level (see Figure 5.1 below).

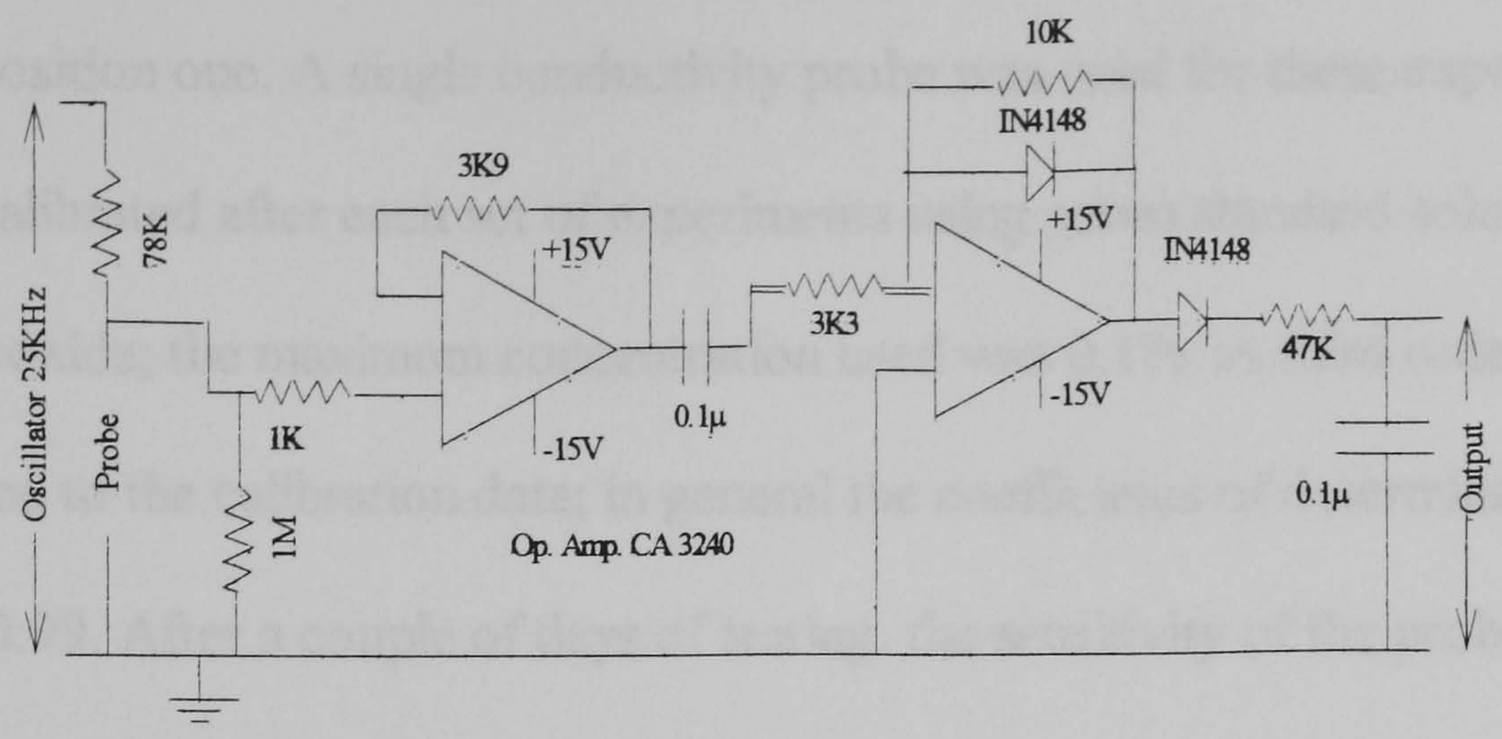

Figure 5.1 Circuit diagram of probe electronics

The electronic circuits were cheap enough to allow each probe to have its own circuit. This avoided the problems that multiplexing can cause. Tests showed that an oscillator frequency of 25Khz and a peak to peak voltage of 1.5V across the probe/plate combination avoided probe output drift, which can occur (Nube et al 1991) when a probe is placed in a salt solution and polarisation occurs at the probe tip.

5.4 Experiments

Dimples at three longitudinal and up to four transverse positions were used to investigate the variability of the dead zone transfer rates. It has been shown (chapter four) that the velocity in the flume varied with transverse and longitudinal position and it was believed that this variability would effect the dead zone transfer. Table 5.1 gives the distance from the left hand wall of the flume, looking downstream, of the centre of each dimple together with the depth and diameter. The depth recorded in the table is the difference between the deepest part of the dimple and an average height of the bed

around the dimple. In Table 5.1 LP15.5_TP1 means: longitudinal position 15.5m, transverse position one. A single conductivity probe was used for these experiments. The probe was calibrated after each set of experiments using seven standard solutions of sodium hydroxide; the maximum concentration used was 0.1%. A third order polynomial was regressed to the calibration data; in general the coefficients of determination were better than 0.99. After a couple of days of testing, the sensitivity of the probe became noticably reduced. Examination under an optical microscope showed the normally shiny surface of the exposed platinum wire to have become dulled. The surface was cleaned, and the original response to the calibration standards regained by using the platinum tip as the anode in a 5V cell of dilute (15%) sulphuric acid.

As stated previously an application of Gibson & Schwarzs' analysis suggested that 98% of the electric field was concentrated within a sphere of radius 250μm; taking this as the effective measurement volume of the probe the frequency implied by a step change in concentration moving across the measurement volume at the mean flow velocity was calculated. This of course depended upon the flow rate in the flume and took values between 20 and 60Hz. The output from the conductivity probe was input to a CED 1401 datalogger the sampling rate used was between 50 and 100 Hz to ensure enough points were recorded to fully describe the probe output.

The sodium hydroxide solution used as a tracer was injected using a syringe with a tube attached. The tube allowed the syringe body to remain out of the water and reduced the disturbance to the flow in the flume. Whilst a 1.5mm diameter tube was tried, it was found to be impossible to inject tracer rapidly enough into a dimple, tracer solution being removed more rapidly than it was injected. Hence a 4mm diameter tube was used for these experiments, care being taken to avoid disturbing the flow in the dimple with a high velocity jet of sodium hydroxide.

An initial set of experiments was undertaken to examine the variation of the transfer coefficient measured at different positions in a dimple. Three positions were studied, the probe on the bottom of the dimple, and 4 and 10mm above the bottom. No appreciable difference was noticed between the rates measured at these three positions so for the remainder of the work the probe was held as close to the bottom of the dimple as possible. The transfer rates were measured between five and seven times for each dimple at every flow rate.

5.5 Data analysis

Examining the traces captured following an injection of Sodium Hydroxide tracer solution showed the output from the probe to be 'noisy'. The noise appeared to be of two sorts: one with relatively high frequency and low amplitude; the other of lower frequency but higher amplitude and of short duration. The low frequency disturbance to the trace was believed to result from the injection process upsetting the normal flow in the dimple. Some traces were not analysed because they did not exhibit a definite trend, again, this was believed to be due to disturbances during the injection process.

Sections of the data record where the initial disturbance of the tracer injection had died away were cut from the whole using a facility of the Spike2 data logging software. After calibration and the addition of a time base the Minitab software package was used to fit a linear regression equation to the natural logarithm of the concentration measurements. This was consistent with the assumption (in equation 2.18) that the rate of change of concentration in the dead zone, c_d , was equal to the product of a constant, k_a , and the difference in concentration between the dead zone, c_d, and main flow, c_a i.e.:

$$\frac{dc_d}{dt} = -k_a(c_d - c_a) \tag{5.1}$$

which is the dead zone transfer equation used in the ADE+DZ model described in chapter two. The data from those curve fits that had a regression coefficient of over 90% is given as Table A.1 in appendix A; files C721, C742, C261 and C262 gave regression coefficients of over 83% and were included because it was felt that a linear regression was a good fit to the trace but that noise had reduced the regression coefficient. As the concentration reached the background levels high frequency low amplitude oscillations produced scatter around the fitted line. A ten point moving average filter was found to improve the regression coefficient but not to alter the fitted curve; because of the limited improvement none of the data was filtered.

The resolution of the transfer measurements were estimated as follows. A typical change in voltage for these experiments was about 0.2 V for which the data logger resolution was 0.15% The shortest time duration of a trace was around two seconds; the data logger resolution was +/- 0.012s which implies a resolution of +/- 0.6% of full scale.

5.6 Results

The transfer coefficients derived from the experiments are plotted in Figures 5.2 to 5.5. At the 11.5m station (Figure 5.2) a general trend was evident, from 0 to 7l/s the transfer coefficient rose for both dimples it was then fairly steady at about $0.9s^{-1}$ for flows up to about 20l/s; it rose again at 24.5l/s.

The data for the 13.5m section (Figure 5.3) showed a similar trend, it was however more complicated as both dimples exhibited low transfer rates at particular flow rates. L13.5_TP2 had low transfer rates at flows of 1 and 16 l/s; whilst L13.5_TP1 had a low transfer rate for flows between for 7 and 8 l/s. The low transfer rate data was

repeatable, it was thought that the flow structure local to a dimple was changing with flow rate in the flume and that this gave rise to the low dead zone transfer rates. There were small differences in the dimensions of the dimples and in the bed geometry around each dimple, these differences probably accounted for the variety of flow rates at which the low dead zone transfer rates were observed.

The data collected at the 15.5m section (Figure 5.4) again showed an initial rise in transfer coefficient between 0 and 7l/s, falling slightly between 7l/s and 9l/s and then slightly rising with increasing flow rate for the remaining flows used. The data from L15.5_TP2 for a flow of around 13l/s fell out side this trend, the transfer coefficient being around half that of the other dimples.

The plot of all the experimental data (Figure 5.5) shows a good deal of scatter. The scatter being increased by the existence for some of the dimples of flows for which the transfer rate was much reduced. In order to obtain a value that could be used in the modelling work (see chapter seven) it was decided to average the transfer coefficient over all eight dimples at a particular flow rate. As the flow rate, for each of the dimples, varied around a nominal value a bin was used. The width of the bin (0.2 to 0.8l/s) was a compromise between the desire to include all eight dimples in an average and the need to have a narrow bin to resolve the flow rate. The overall average transfer rate, for a given bin, was calculated from the average of the mean transfer rates for each dimple. The results of the averaging are shown in Table 5.2 and plotted as Figure 5.6 (which includes error bars that represent the average percentage range of the transfer rates). Figure 5.6 shows that the average transfer coefficient increased with increasing flow between 0 and 7 l/s. The transfer rate then appears to drop slightly before remaining fairly steady at about 1.0 s^{-1}

The transfer rates measured during the present work were two to three times greater than Valentine & Woods' (1977) data for a rectangular slot and two to ten times greater than Seo & Maxells' (1992) values for a recirculation zone. Of the transfer rates obtained by fitting an ADE+DZ model to tracer data obtained in the field those of Legrand Marcq & Laudelot (1985) lay within the range measured for the dimples. All of the other transfer rates (with the notable exception of Bear Creek: Nordin & Troutman 1980) were lower by at least four orders of magnitude.

Assuming that all the dimple volume acted as a dead zone, the dead zone fraction (the dead zone volume divided by the volume of flowing water) in these experiments increased from 5 to 11% as the flow rate decreased from 26 to 1l/s. These values are similar to those reported by Nordin & Troutman (1980) and Yu & Wenzhi (1989) for large U.S. rivers, based on fitting the ADE+DZ model to longitudinal dispersion data.

As the dimples were designed to represent the interstitial volumes on a gravel bed river the difference between the transfer rates measured in the flume and those obtained by previous workers suggests that the dimples did not represent the dead zones in a natural stream. The measurements showed that the transfer rates differed between dimples and it was suggested that this was due to differences in the flow local to the dimple. It is possible that in a natural gravel bed river larger interstitial dead zones occur because of the existence of a range of gravel sizes. Also the flow close to the bed in a natural river would be expected to be more complicated than in the author's flume. For example, Bergeron (1994) measured longitudinal velocity profiles in a number of U.S. and Canadian gravel bed rivers and found that the flow separated from large cobbles or boulders and became reattached at a position further along the channel. These recirculation zones could act as dead zones. Seo & Maxell (1992) measured the transfer rates from interstitial volumes for gravel and for recirculation zones and concluded that

the trapping within the interstitial volumes was insignificant compared to that in the recirculation zones. Another possible way in which the trapping in a river may differ from that in the flume is that in a river the bed can be porous, water may flow through the bed as well as over it. Wallis, Young & Beven (1989) fitted an ADZ model to tracer data and suggested that there was some evidence for bed flow effecting the solute transport. Jackman et al (1984) also considered bed flow as a possible dead zone storage mechanism. It is therefore possible that in natural gravel or cobble bed rivers the dead zone mechanism is due to large scale recirculation zones and/or bed flow. The bed in the author's flume was designed to be impervious and further experiments would be necessary to investigate bed flow as a storage mechanism.

5.7 Conclusions

The transfer rates for eight dimples were averaged to obtain the information that would be needed for a numeric model of the mixing in the flume. The general trend was for a increase in dead zone transfer rate with flow rate. The average transfer rate from a dimple to the main flow ranged from around 0.4 s^{-1} to 1.0s^{-1} for flows between 1l/s & 26l/s.

The transfer rates measured for the dimples are in general higher than those obtained by previous workers regressing ADE+DZ models to field tracer data. The dead zone fraction in the present flume was similar to that reported in large U.S. rivers. The high rates of transfer from the dead zones, in comparison to those of Valentine & Wood, suggest that they will make a relatively small contribution towards the longitudinal dispersion in the flume.

Label	Distance from wall (mm)	Depth (mm)	Diameter (mm)
LP15.5_TP1	225	13	34
LP15.5_TP2	376	13	34
LP15.5_TP3	528	13	34
LP15.5_TP4	686	13	35
LP13.5_TP1	225	13	36
LP13.5_TP2	356	15	33
LP11.5_TP1	230	15	36
LP11.5_TP2	383	14	36

Table 5.1 Details of the dimples used in the dead zone transfer experiments.

Range of flows in the bin (l/s)	Central flow rate (l/s)	Average Transfer Coeff (1/s)	Number of Dimples in the Bin
0.92 to 1.11	1.11	.38	8
2.28 to 2.44	2.44	.69	7
4.37 to 4.59	4.48	.87	2
6.34 to 6.36	6.36	1.18	3
7.00 to 7.88	7.44	.723	5
9.05 to 9.45	9.25	.81	5
12.78 to 13.58	13.18	.91	8
15.95 to 16.67	16.31	.88	8
20.07 to 20.6	20.35	1.0	7
24.45 to 24.79	24.47	.99	4
26.23 to 26.23	26.23	1.42	4

Table 5.2 Averaged dead zone transfer rates.

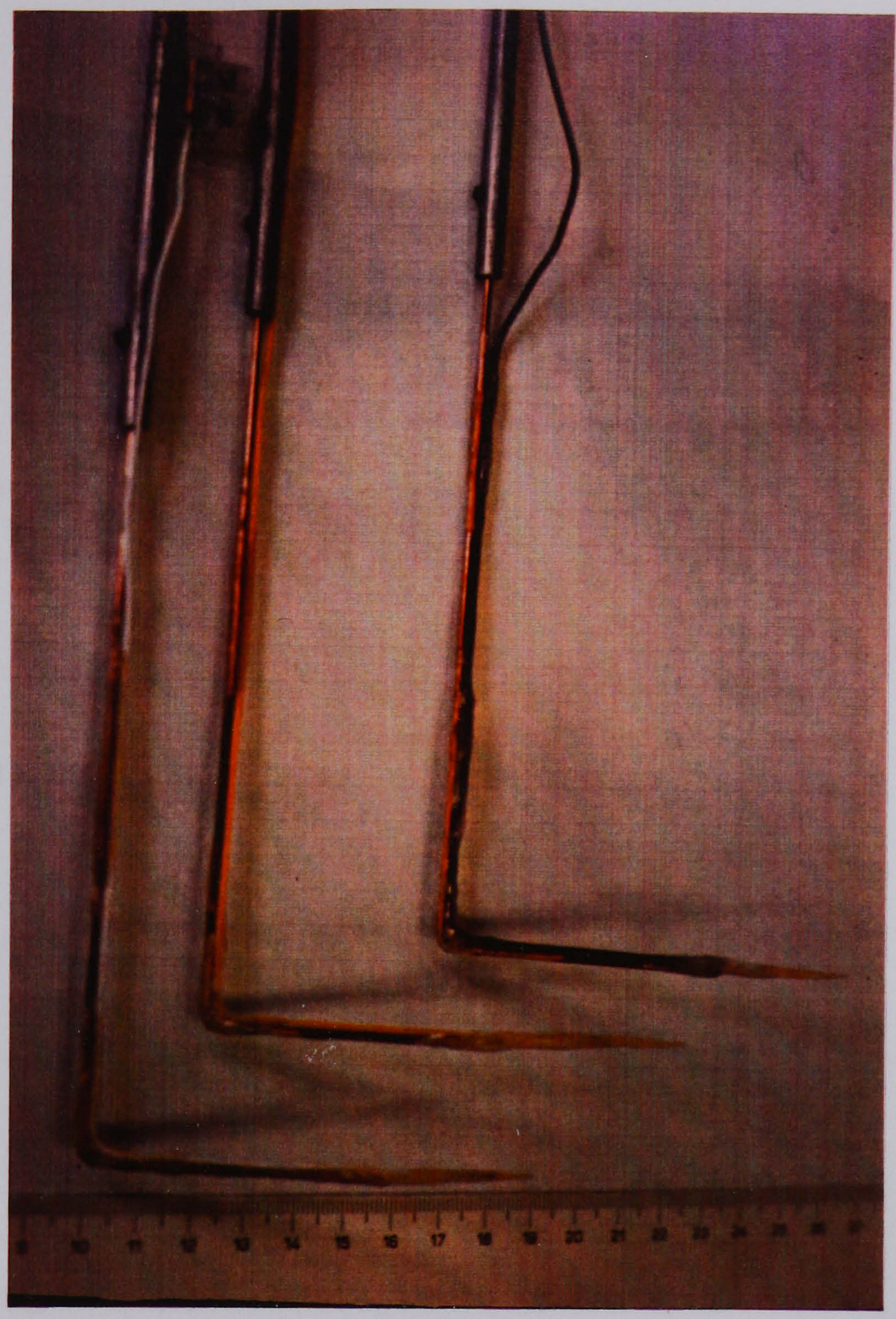

Plate 3 **Conductivity probes**

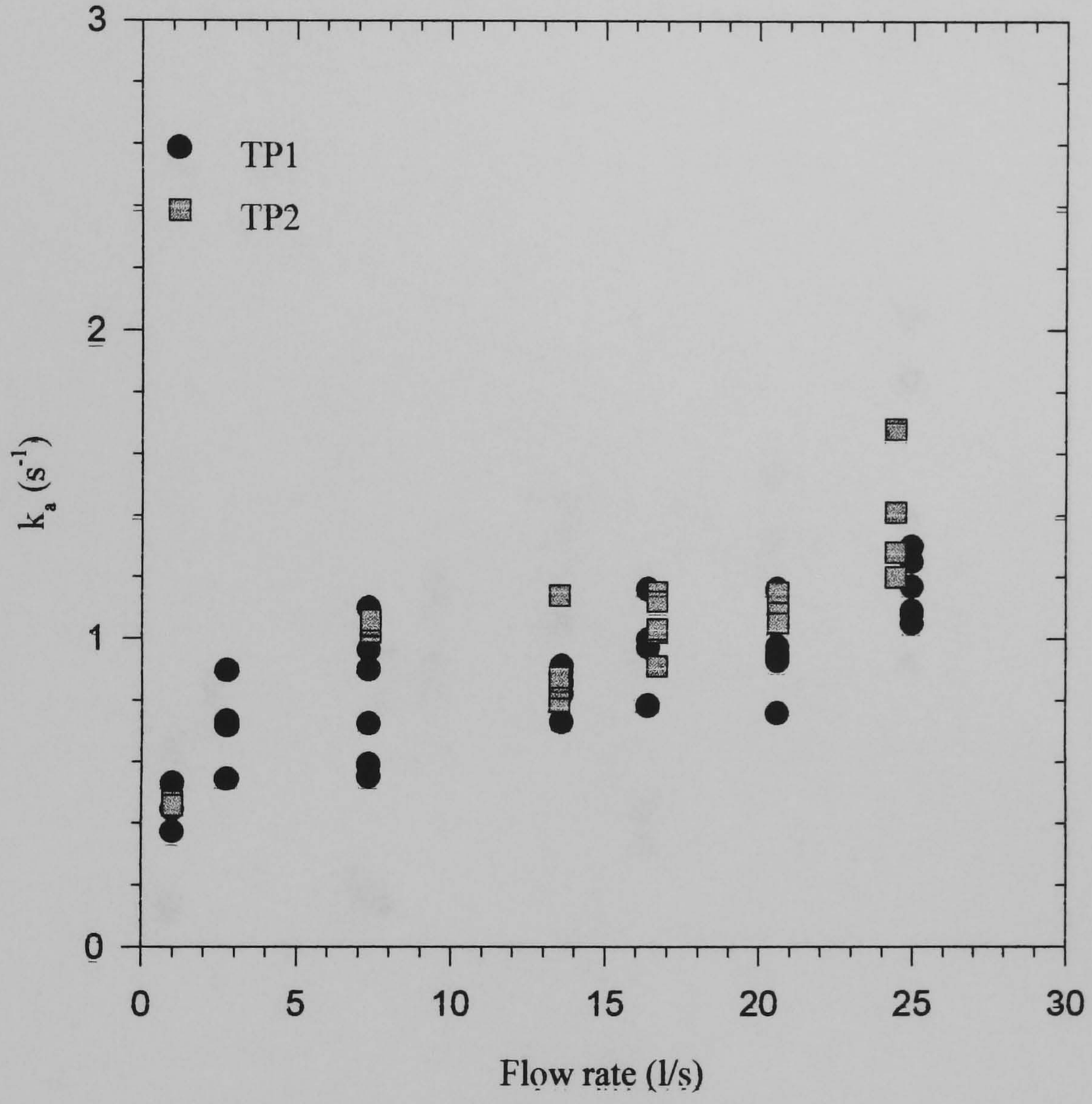

Figure 5.2 Transfer coefficients measured at L11.5

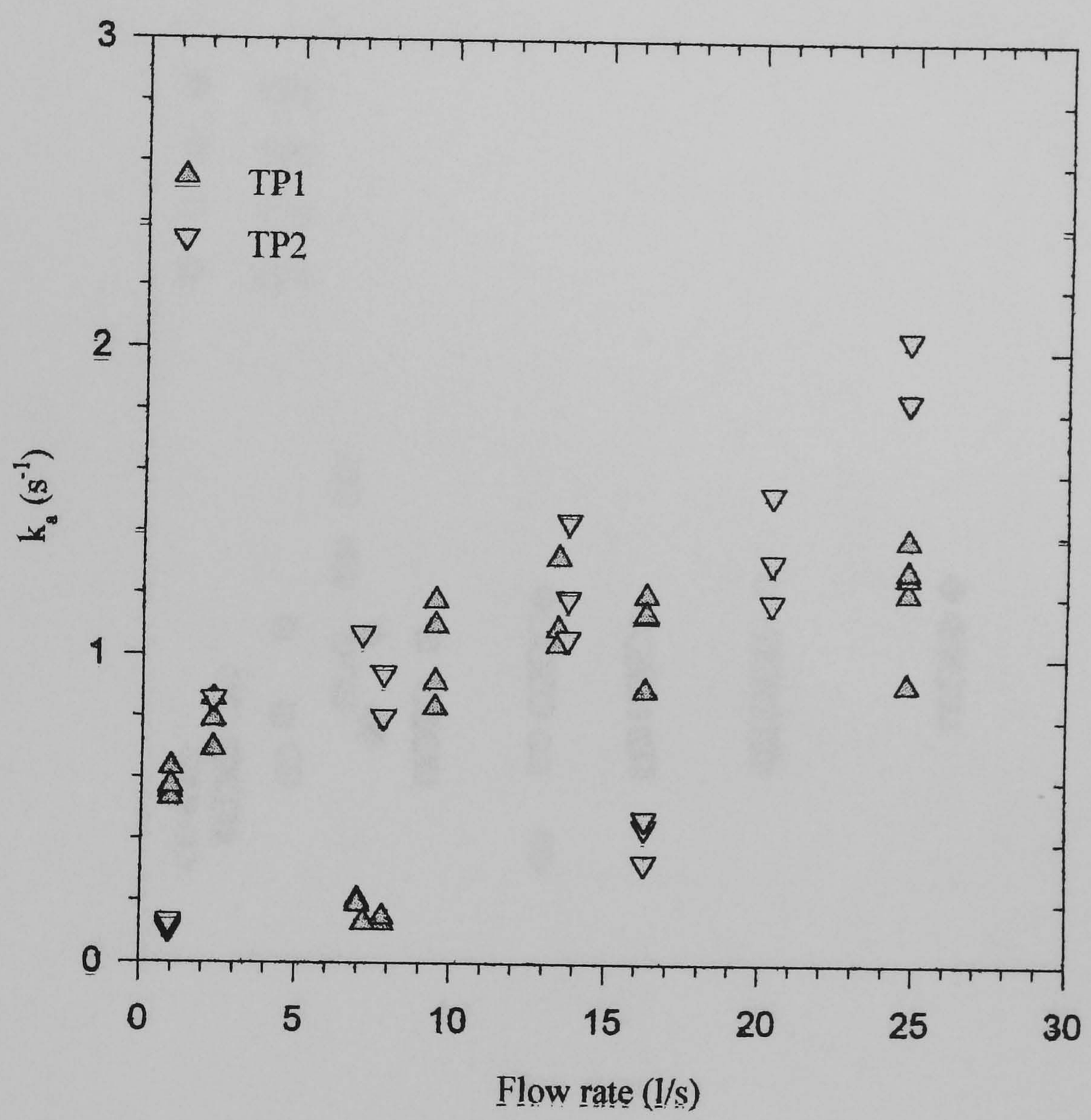

Figure 5.3 Transfer coefficients measured at L13.5

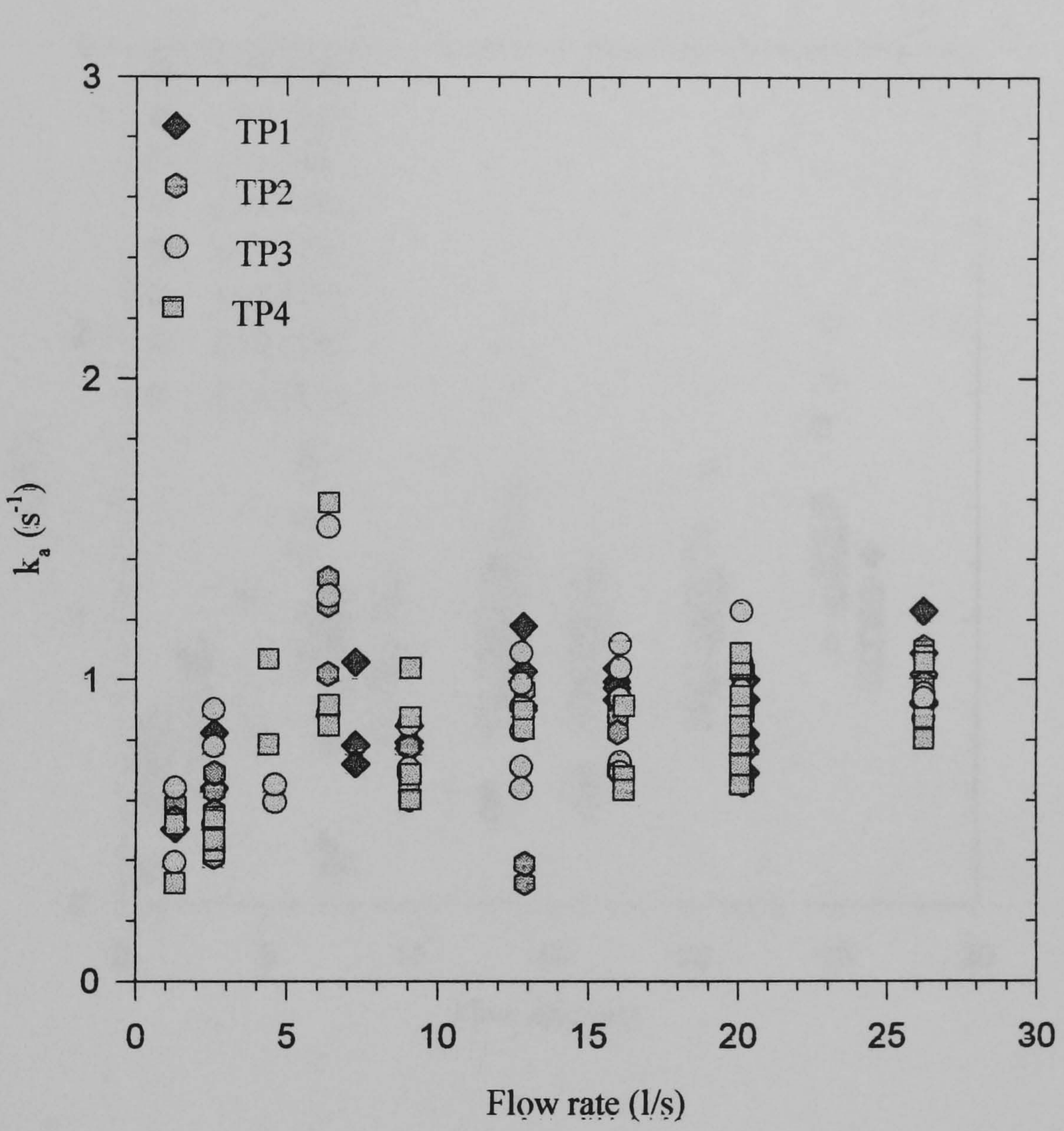

Figure 5.4 Transfer coefficients measured at L15.5

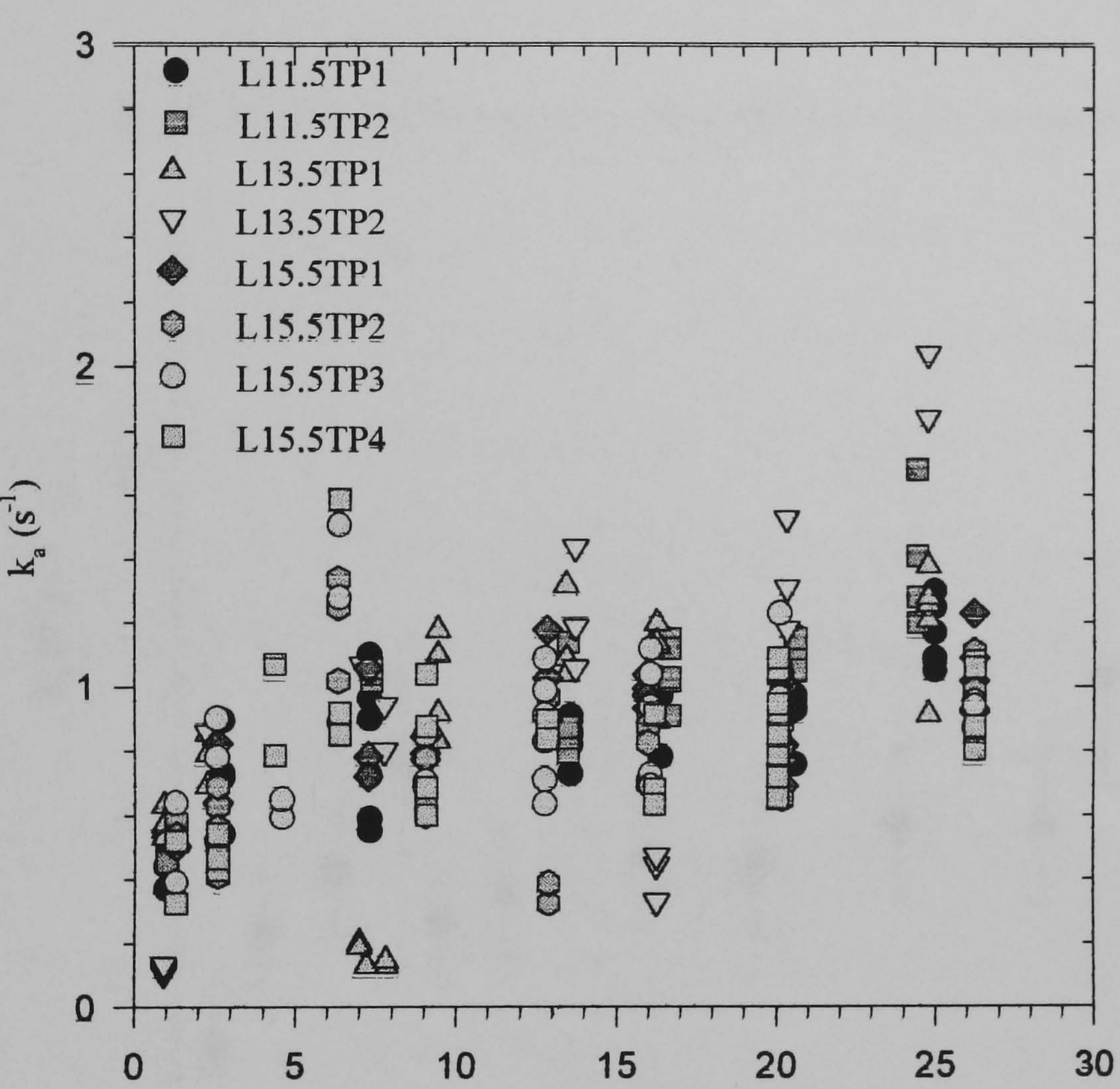

Figure 5.5 Transfer coefficients measured in the flume

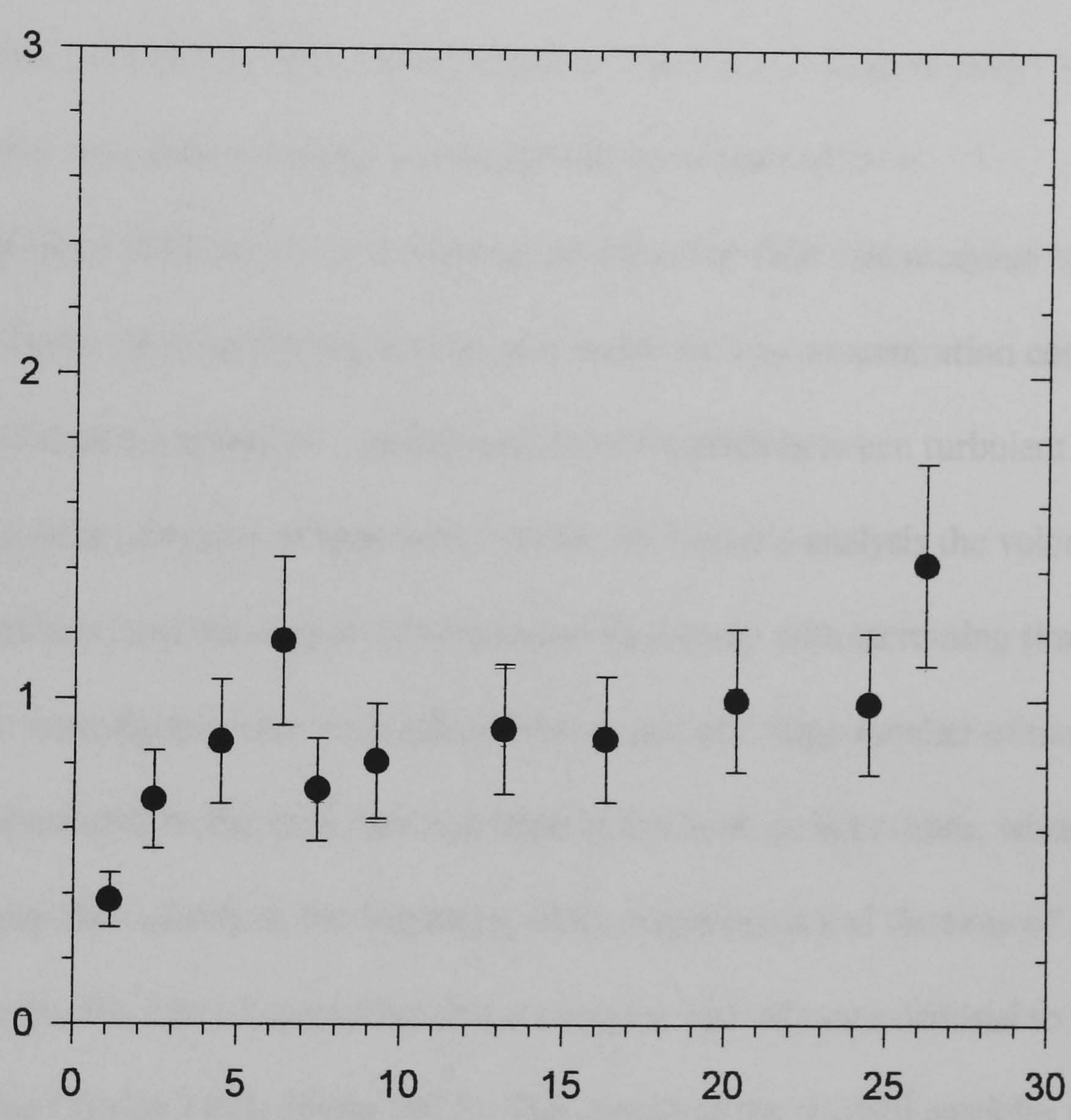

Figure 5.6 Averaged transfer coefficients

Chapter six Measurement of mixing coefficients

6.1 Introduction

The transverse and vertical rates of mixing for solutes are important to an understanding of longitudinal dispersion in a flow. Measurements of the vertical and transverse rates of mixing were undertaken in the laboratory flume to provide information needed to model the longitudinal dispersion process in chapter seven. The work also provided new data on mixing coefficients in open channel flow.

The problem of diffusion in a homogeneous turbulence field was analysed by Taylor in 1921. Taylor showed that the spread of a scalar such as concentration could be calculated if the rms of the turbulent velocity and the correlation between turbulent velocities at successive moments of time were known. In Taylor's analysis the velocities were initially correlated and the degree of correlation died away with increasing time. This implied that: immediately after their release the spread of a large number of marked particles was proportional to the time they had been in the flow; at later times, when the correlation between the velocity at the beginning of the experiment and the time of interest became zero, the rate of spread became a constant and was proportional to the square root of time (Taylor 1921, Hinze 1975). The spread of the marked particles was therefore analogous to a diffusion process. A coefficient of eddy diffusion (or a turbulent diffusivity) can be defined as half the rate of change of the variance of the particle positions with time. For example the eddy diffusivity in the y-direction, ε_y , is defined as:

$$\varepsilon_y = \frac{1}{2}\frac{d\sigma_{ys}^{\,2}}{dt} \tag{6.1}$$

where σ_{ys}^2 is the variance, of a diffusing solute cloud, in the *y*-direction. Equation 6.1 relates the eddy diffusivity to the rate of change of the second spatial moment of the solute cloud. If the solute is diffusing perpendicular to a uniform velocity, *u*, and the rate of change of the temporal moments, σ_{yt}^2, of the solute cloud are measured equation 6.1 becomes:

$$\varepsilon_y = \frac{1}{2} \cdot u \cdot \frac{d\sigma_{yt}^2}{dx} \tag{6.2}$$

Equations 6.1 and 6.2 can be used to measure and, assuming the diffusivity is known, predict the spreading of a solute. Taylor's analysis concerned mixing in homogeneous turbulence. Analyses of mixing in non-homogeneous turbulence are available for several special cases (Hinze 1974, Okoye 1970, Holley et al 1972), wide (two-dimensional) open channel flow being one, but in general equations 6.1 and 6.2 can not be used to measure eddy diffusivities in open channel flows. The methods that can be used to calculate or measure the rates of vertical and transverse mixing in open channel flows will be discussed in the following two sections, but it is instructive to consider the mixing of a solute discharged into a wide open channel flow. First imagine a transverse line source of tracer; because there is no transverse mixing (the line source precludes a transverse concentration gradient) the only mixing will occur in the vertical direction and it should be possible to use an equation such as 6.1 or 6.2 to obtain an averaged measure of the diffusivity over the height of the tracer plume. Now imagine that the dye issues from an outfall at the mid-depth of such a flow, it will spread in the vertical and horizontal directions and we map the concentration of the dye over a plane perpendicular to the direction of flow at a given distance downstream of the outfall. We will assume that the dye has not spread over the full width or depth so as to avoid the additional complexity of a boundary condition. The flow is slower close to the bed than at the free

surface, so that the dye measured at the base of our mapped plane will have been in the flow longer than that at the top. Now if in our imaginary flow the transverse diffusivity is constant over the depth then we might assume that the dye plume would be wider close to the bed than at the free surface because of the difference in the time that it takes for dye at these two depthwise positions to reach our measurement plane. Whilst this may be plausible we have ignored the effect of the vertical diffusivity which would be to reduce any vertical concentration gradient that was set up. Therefore the rate of change of the variance of the transverse concentration profiles that we see at two, or more, of our measurement planes can not be used in equation 6.2 to calculate the transverse diffusivity because it does not incorporate the effect of the vertical mixing. It will be appreciated that in a natural river a transverse velocity is likely to exist and that this will further complicate the problem of measuring and predicting mixing processes. In this thesis the term eddy diffusivity will be used to describe the mixing characteristics of turbulence in situations where equations 6.1 and 6.2 are valid. Often the rate of change of the variance of the concentration is used to quantify the mixing rates in cases where the non-homogeneity of the velocity field invalidates the use of equations 6.1 and 6.2. Mixing rates determined from such measurements are termed mixing coefficients in this thesis.

A distinction can be draw between a diffusion and a mixing coefficient because while diffusivity is a fundamental feature of turbulence; a transverse (or vertical) mixing coefficient incorporates all the processes that transport material in the transverse (or vertical) direction. Thus a mixing coefficient will represent the mixing due to secondary flows as well as diffusivity.

6.2 Methods of calculating and measuring the mixing coefficients in open channel flows

In the following two sections the methods that previous workers have used to determine the vertical and transverse rates of mixing in open channel flows are described.

6.2.1 The vertical mixing coefficient in open channel flows

Reynolds' analogy (which assumes equivalence between the transport of momentum and a scalar which in turn implies that the eddy viscosity is equal to the eddy diffusivity) has been used in the past to calculate the rate of scalar transport (Taylor 1954, Elder 1959). The eddy viscosity/diffusivity for the log-law region of a wide open channel flow is given by (Nezu & Nakagawa 1993 , Rutherford 1994):

$$\varepsilon_y = \kappa d u_* (1 - y/d)\, y/d \qquad (6.3)$$

If equation 6.3 is depth averaged it yields a depth averaged vertical diffusivity, $\overline{\varepsilon}_y$, of $0.068 d u_*$ if von Karman's constant (κ) is taken to be 0.41.

Kalinske & Pien (1944) measured the vertical mixing coefficient in an open channel flow. The rate of change of variance, $d\sigma_{yt}^2/dx$, of a spreading plume of hydrochloric acid and alcohol was measured, the diffusion coefficient being given by equation 6.2. Kalinske & Pien state that the measured diffusion coefficients compared well with calculated values of the eddy viscosity; which is probably explained by the fact that their experiments were carried out around the mid depth where the velocity field was probably fairly homogeneous.

Rutherford (1994) presented a simplified model of mixing in open channel flows from which the vertical mixing coefficient can be inferred from the degree of mixing, over the depth, of a solute from a continuous source.

6.2.2 The transverse mixing coefficient in open channel flows

Elder (1959) used a photographic technique to evaluate transverse and longitudinal mixing in a two-dimensional (wide) open channel flow. Photographs of a spreading drop of dye were taken and the concentration inferred from the darkness of the image (which gave a measure of the average concentration over the depth). Elder's transverse diffusivity, given by $\varepsilon_z = 0.23du_*$, was about three times his longitudinal diffusivity. This transverse diffusivity is somewhat higher than the value recommended by later workers, for example Nokes & Wood (1987) and Rutherford (1994) suggest $\varepsilon_z = 0.13du_*$. It is possible that this was because of the rather shallow flows used by Elder (10 to 15mm). Webel & Schatzman (1984) suggested that a depth of greater than 30mm was necessary to avoid surface tension being unduly influential although they did not state what the effect of surface tension would be. Also Okoye (1970) stated that Elder made an error in the analysis of his data and that the diffusivity should have been $0.16du_*$, which is closer to the value suggested by Nokes & Wood and Rutherford. If Okoye is correct and Elder's method of calculating the transverse diffusivity was in error then the implication is that his measured longitudinal dispersion coefficient should also be reduced (to $D = 5.3du_*$).

Okoye (1970), beginning from a three-dimensional mass conservation equation for a wide open channel flow showed, using Aris' method of moments, that if both the concentration and the rate of growth of the second moment of the transverse concentration profile of a tracer plume was uniform over the depth, then the depth averaged transverse diffusion coefficient could be evaluated from equation 6.2, if the depth averaged velocity was used instead of u. The assumption that the second moment does not vary over the depth, which was demonstrated experimentally to be valid once the plume was well mixed over the depth, was also shown to imply that the transverse

diffusivity varied over the depth in the same way as the longitudinal velocity. Okoye also showed how the vertical distribution of the transverse diffusivity could be measured for a wide open channel flow if the two-dimensional concentration profile were mapped at a number of planes, perpendicular to the direction of flow, along the channel. For Okoye's experiments in a smooth bedded flume the depth averaged transverse diffusivity was: $\bar{\varepsilon}_z = 0.16 d u_*$. Nokes & Wood (1987) also inferred that the transverse diffusivity has the same vertical variation as the longitudinal velocity for a two-dimensional flow. They obtained an analytical solution for the three-dimensional mass conservation equation and compared the results of three different assumptions for the variation of transverse diffusivity over the depth. This comparison suggested that if, as found experimentally, the transverse diffusivity was insensitive to the depth at which it was measured, then the transverse diffusivity varied with depth in the same way as the longitudinal velocity did. In Nokes & Wood's smooth bedded flume the depth averaged transverse diffusivity was found to be: $\bar{\varepsilon}_z = 0.13 d u_*$. The work of Okoye and Nokes & Wood is important because it shows how, for the special case of a wide open channel flow, the transverse eddy diffusivity can be measured.

Miller & Richardson (1974) performed mixing and velocity measurements in a rectangular flume, whose bed was roughened with rectangular blocks. The aspect ratio used for Miller & Richardson's experiments was less than five which is held by Nokes & Wood (1987) to have influenced their results by setting up secondary flows that would have increased the transverse mixing rate. Miller & Richardson evaluated the transverse mixing coefficient from the rate of change of the transverse variance of a Rhodamine WT tracer cloud using:

$$k_z = \frac{1}{2} \cdot u_q \cdot \frac{d\sigma_{zs}^{\,2}}{dx} \tag{6.4}$$

in which k_z is the transverse mixing coefficient, σ_{zs}^2 the spatial variance in the transverse direction and u_q the cross-sectional averaged velocity. A regression to their data gave a transverse mixing coefficient $k_z = 0.23Ru_*$ in which R is the hydraulic radius. The mixing coefficient was found to increase with cross-sectional average velocity, slope and turbulence intensity.

Lau & Krishnappan (1977) analysed the results of their own and other workers transverse mixing experiments (they mistakenly include Kalinske & Pien's (1944) vertical mixing experiments among their transverse mixing data). Lau & Krishnappan concluded that secondary currents are the dominant mechanisms causing transverse transport in open channel flows with the width being the dominant length scale. For two-dimensional flows, where secondary currents do not exist, other workers, notably Nokes & Wood (1987), have found that the depth averaged lateral diffusivity was best non-dimensionalised using the product of the depth and bed shear velocity as a parameter which suggests that the depth is the dominant length scale.

Webel and Schatzmann (1984) conducted transverse mixing measurements in a straight flume of rectangular cross-section, for plumes of solute that did not cover the full width. Dimensional analysis was used to suggest suitable parameters with which to correlate the experimental data. It was found that the effective roughness could be used to describe the effect of the shape, distribution and height of the roughness elements. Away from the walls the mixing coefficient was independent of the aspect ratio of the channel. For fully rough flow (Darcy-Weisbach friction factor greater than 0.08) the mixing coefficient non-dimensionalised with the product of the depth and bed shear velocity was considered to be a constant with a value: $k_z = 0.13du_*$. Although Webel & Schatzmann use the term mixing coefficient it is clear (because the flow was two-dimensional) that they measured the depth averaged eddy diffusivity. They contradict

Lau & Krishnappan's assertion that secondary flows are the most important driving force behind transverse mixing and criticise their experimental techniques suggesting that the shallow flows used by Lau & Krishnappan would have been unduly influenced by surface tension. Webel & Schatzmann found that turbulence generated secondary flows increased the mixing coefficient close to the wall but the effect was considered small for channels with an aspect ratio greater than five. When the aspect ratio was less than five a large part of the channel was affected by secondary flows and the transverse mixing was a function of aspect ratio.

Rutherford (1994) tabulated a large amount of transverse mixing data from laboratory flumes. Rutherford stated that a lower bound estimate for the transverse eddy diffusivity was $\varepsilon_z = 0.13du_*$ but does not say how the estimate was obtained (He also includes the vertical mixing data of Kalinske & Pien 1944). In order to ensure that only data collected in wide fully rough flumes for which the depth averaged transverse eddy diffusivity, $\bar{\varepsilon}_z$, could be measured (Okoye 1970, Nokes & Wood 1987) and in which it was not a function of friction factor (Webel & Schatzmann 1984) the author examined the data referred to by Rutherford. That data which met these criteria are given in Table 6.1. A regression to the data, Figure 6.1, suggested $\bar{\varepsilon}_z = 0.16du_*$. It can be seen that the data of Sayre & Chang had a strong influence on the regression. The data of Engelund was not plotted because it was measured using floats (other workers used a solute as a tracer) and Sayre & Chang state that the spread of surface floats was greater than that of neutrally buoyant tracer by an amount equal to the ratio of the surface to the mean velocity.

There are several conclusions that we can draw from the work reviewed in this section. For a two-dimensional open channel flow Okoye's (1970) and Nokes & Wood's (1987) studies showed how the transverse diffusivity can be measured either as a depth

average or as a function of the position in the depth. Again for a two-dimensional flow the vertical diffusivity can be calculated, for the log-law region of the flow, from equation 6.3 or measured using a line source and equation 6.2. The depth averaged transverse eddy diffusivity obtained from an analysis of the data of four previous workers showed: $\overline{\varepsilon}_z = 0.16du_*$. In the work reviewed above the transverse eddy diffusivity was non-dimensionalised by the product of the flow depth and bed shear velocity (du_*). This is sensible for plain shear flows where the turbulence is generated by velocity shear at the bed and the depth is the only length scale. For three-dimensional flows it is not obvious that du_* is the be the correct scaling for the mixing processes because of the influence of secondary currents. However du_* has been commonly used to non-dimensionalise transverse mixing coefficients (see, for example, the treatment by Rutherford 1994). It will also be noted that secondary flows in straight open channels have been found to scale with the flow depth (see Chapter 4, section 4.2).

In three-dimensional flows it is not possible to obtain the depth averaged transverse eddy diffusivity from equation 6.2, however an equation of a similar form (equation 6.4) has been used to quantify the rate of transverse mixing.

6.3 Vertical mixing measurements in the laboratory flume

6.3.1 Experimental technique

Two sets of experiments were performed to measure the rate of vertical mixing in the experimental flume. The first group of vertical mixing experiments were carried out to determine how far down stream from a source it was necessary to go before a tracer became vertically well mixed. This information being required for the transverse mixing experiments of section 6.3. The second set of experiments were designed to measure the rate of vertical spreading of a tracer as it issued from an outfall, from which the vertical

mixing coefficient could be inferred. Both sets of experiments were performed using a peristaltic pump to supply a constant flow of tracer via a small outfall pipe to the laboratory flume. The tracer used was an aqueous (flumewater) solution of sodium hydroxide, the maximum concentration for these experiments being 3%. The peristaltic pump fed the outfall pipe via an accumulator which removed the pulsations inherent in the flow. The accumulator consisted of an air tight vessel with a volume of 600ml. The inlet and outlet were in the bottom half of the vessel, vertically separated by 25mm and at right angles to each other. Flow visualisation using Rhodamine dye showed that the accumulator removed the flow pulsations created by the peristaltic pump. The outfall consisted of a stainless steel tube of 3mm outside and 2.5mm inside diameter held in a simple traverse. The tube was formed into a right angle with a horizontal length of 150mm between the vertical stem and the open end and oriented so that the tracer discharge was in the flow direction.

The concentration of the sodium hydroxide tracer in the flume was measured using the conductivity probe described earlier (Chapter five). The probe was operated with a 25kHz signal of less than 1Volt rms. The output of the probe was sampled at 100Hz for one minute at each measurement position using either the SPIKE or CHART data logging package for the CED 1401 data logger; trials showed this to be long enough to collect a stationary record.

Before each run the probe was calibrated using eight to ten standards. The concentration of the standards, for the first set of experiments, ranged between zero and 0.04%; for the second set the maximum was 0.018% The wider range of standards reflects the greater range of longitudinal positions used for the first set of experiments and the consequently greater dilution of the tracer. The range of concentrations used for the first set of experiments was such that a third order curve was regressed to the

calibration data; for the second set a first order curve was used. The coefficient of determination was generally between 0.96 and 0.99. The accuracy with which the concentrations of the standards were known was estimated to be ±0.00005% on a given value, i.e. 0.018% lay between 0.01795% and 0.01805%. The high level of accuracy reflects the method used to create the standards: a relatively large volume of flume water (2l) was dosed with sodium hydroxide weighed using a high quality balance. Software was written to apply the calibration to the sampled voltage data and to calculate the mean and rms concentrations. During the experiments the background concentration was monitored and when the calibration was applied the background was removed from the concentration profiles.

The highest time averaged solute concentration recorded in the experiments was less than 0.012% which indicates that the buoyancy of the solute had a negligible effect on its transport. The influence of buoyancy upon measured rates of mixing is referred to again in section 6.3.1

The peristaltic pump was set to deliver tracer at the local longitudinal velocity for the chosen injection position in order to reduce the outfall's disturbance of the normal flow field in the channel. Having set up the required flow in the flume a pitot tube, latterly a total head tube, was used to measure the local velocity without the outfall present; the outfall was then placed about 5 to 10mm upstream of the pitot tube and the pump flow rate adjusted until the previously recorded velocity was repeated.

The conductivity probe was held in a traverse system comprising screw driven saddles moving in the vertical (Y) and transverse (Z) directions. One revolution of the vertical screw moved the probe 1mm and one revolution of the Z traverse screw moved the probe 2mm in the transverse direction. The YZ traverse ran on rails along the top of the flume. The rails had scales attached that in conjunction with indicators on the

traverse allowed the longitudinal position of the probe to the set. As both rails had a scale it was possible to ensure that the traverse remained perpendicular to the flume's longitudinal axis at all times. It was estimated that the uncertainty of positioning in the vertical was less than 0.25mm. For the transverse and longitudinal positions the uncertainty was +/-0.5 and +/-1.0mm respectively.

6.3.2 Results

The first set of experiments consisted of a series of six measurements designed to determine the distance from the outfall at which the tracer became well mixed over the depth. Three flow rates and two outfall positions were used. All the experiments were carried out on the centre line of the flume, with the outfall being at either a quarter of the distance from bed to free surface or at mid depth. The outfall was set at 14m from the inlet to the flume, a position close to where velocity measurements were previously performed.

Figure 6.2 shows a typical plot of the vertical time averaged concentration profiles recorded (symbols). This particular run had a flow rate of 26l/s and the outfall was at the mid depth position. The legend shows the distance downstream from the outfall at which each profile was taken. Cubic spline fits (lines) to the data are also shown. Figure 6.3 shows the time averaged profiles recorded at a similar flow rate but with the outfall at the quarter depth position. Both plots show that the peak concentration fell and the vertical concentration profile became more uniform with distance downstream of the outfall. It was also found, see Figure 6.4 which shows the intensity of the concentration fluctuations for the data of Figure 6.2, that the intensity of the concentration fluctuations reduced as the downstream distance increased and that the fluctuations also became more uniform over the depth. Close to the outfall (3.3 times the

flow depth) the rms of the fluctuations were 70% of the mean value. Further downstream at 900mm (9.9 times the flow depth) this ratio reduced to about 16%. The statistics of the concentration fluctuations are important (Rutherford 1994). For example it could be possible to have a case where the mean concentration levels of a pollutant were safe but the fluctuations about the mean were fatal to aquatic life. Only the time averaged concentration profiles were required to calculate the mixing coefficients that were the aim of this part of the work. Detailed analysis of the intensity and duration of the fluctuations about the mean is left for the future.

In order to obtain an estimate of the rate of vertical mixing in the laboratory flume the concentration data was compared to the predictions of a constant coefficient model of vertical diffusion, which assumes that both the eddy diffusivity (ε_y) and velocity (u_q) are constant over the depth (d), given by Rutherford (1994). Rutherford's model was developed to predict absolute concentration downstream of a transverse line source. However, as demonstrated by Rutherford, if the ratio of the minimum to maximum concentration over the depth is calculated then the model can be used to analyse data measured downstream of a point source. Data collected in the laboratory flume has been analysed in accordance with the model and the results recorded in Table 6.2. The non dimensional distance, x^*, is given by:

$$x^* = \frac{x\varepsilon_y}{u_q d^2} \tag{6.5}$$

and the degree of mixing by the ratio of the minimum to maximum concentrations in the depth,

$$P_m = \frac{c_{\min}}{c_{\max}} \tag{6.6}$$

In equation 6.5 ε_y was given by the depth average of equation 6.3 in which the centreline depth and the side wall corrected bed shear velocity was used. The data of Table 6.2 is

plotted, as symbols, in Figure 6.5 which also shows, as lines, the degree of mixing predicted by the constant coefficient model. The dashed line is the predicted mixing for the mid depth outfall while the solid line is that for an outfall at the quarter depth position.

The constant coefficient model predicts that the degree of vertical mixing in a flow will only depend on the location of the outfall. The change in slope of the constant coefficient model predictions show an initially rapid rate of mixing with distance that reduces as the vertical concentration profile becomes more uniform further downstream from the outfall. The reason for this reduction in the rate of change of P_m with distance is that as P_m becomes closer to unity the reduced concentration gradients over the depth lead to reduced mass transfer. The measured data agrees with the predicted reduction in the degree of mixing with distance from the outfall. However, contrary to the constant coefficient model predictions, the degree of mixing in the flume appears to be a function of flow rate; as the flow rate is increased so the non dimensional distance at which a particular value of P_m is achieved is reduced. At the highest flow of about 26l/s the position of the outfall does not seem to affect the degree of mixing. For a flow of about 7l/s the tracer from a mid depth outfall mixes more rapidly than that from a quarter depth outfall; while for the lowest flows (2.5l/s to 2.7l/s) the opposite is true.

Figure 6.5 was used during the transverse mixing experiments to predict the degree of mixing at a given downstream of the outfall. For flows of 26l/s approximately 9 flow depths were needed to achieve 95% mixing (ie a value of P_m=0.95), for flows of 2.5l/s and 7l/s the same degree of mixing was achieved approximately 16 flow depths downstream of the outfall.

A possible cause of the scatter of the data in Figure 6.5 may be the transverse variation in the bed shear velocity that was discussed in Chapter four. In Table 6.3 the

bed shear velocities obtained by fitting a log law to the pitot measurements at the centreline are compared to the side wall corrected bed shear velocity, u_{*_b}, calculated from the surface slope at the position where the velocity measurements were performed. The change in the magnitude of the centreline shear velocity relative to the bed average value as the flow reduces is evidence of a change in the structure of the flow field. Whether a change in flow structure altered the vertical mixing or not, a consideration of equations 6.3 and 6.5 shows that a rise in the local bed shear velocity above the average value would cause a x^* based upon the local conditions to be higher than the bed averaged value. Therefore a value of x^* based on the bed shear velocity obtained from the velocity profiles would be lower than that implied by the surface slope at 7l/s and higher for 13l/s and 26l/s, which would reduce the scatter of the data plotted in Figure 6.5. This idea was not tested because the aim of the first set of experiments was primarily to determine the distance downstream of a source that it was necessary to go before a tracer became acceptably well mixed over the depth. It was also felt that to allow for the transverse variation of the bed shear velocity went against the spirit of an approximate model such as Rutherford's constant coefficient model.

Figures 6.6 and 6.7 show the concentration profiles, for outfalls at mid and quarter (measured from the bed) depths respectively, from the low flow experiments. The concentration for both outfall positions was at a maximum close to the bed. This is in contrast to the concentration profiles developed for the high flow/mid-depth experiments shown in Figure 6.2 where it will be noted that the maximum concentration seemed to remain at the mid-depth (the data measured at 280/300mm for the low flow experiments and at 900mm for the high flow experiments were an equal number of flow depths downstream of the outfall). There was evidence of the local flow around the tracer outfall being directed towards the bed for the low flow experiments. It was noted

during some flow visualisation experiments that the plume issuing from the outfall was deflected vertically and transversely towards the centre of a dimple. Obviously if the dimples caused the local flow upstream of a dimple to be into a dimple there must have been a corresponding outflow towards the free surface from the downstream edge of the dimple. This could not be seen during the flow visualisations because the tracer plume was very rapidly mixed over the depth and the vertical concentration profile could not been seen by eye.

There were therefore three factors that caused the vertical data collected in the author's flume to be poorly represented by the constant coefficient model, firstly the constant coefficient model is only an approximation to the mixing processes even in a two-dimensional flow, secondly the data plotted in Figure 6.5 was calculated using an average bed shear velocity and thirdly there was some evidence of the dimples deflecting the flow towards the bed at the lower flow rates.

The depth averaged eddy diffusivity required by the constant coefficient model to give the degree of mixing actually measured can be calculated using equation 6.5. This was done for the experimental flows referred to above and the results are given in Table 6.5. The average of the eddy diffusivities (in Table 6.4) implied by the constant coefficient model was $\overline{\varepsilon}_y = 0.102 du_{*_b}$ which is larger than the depth average diffusivity implied by integrating equation 6.3 over the flow depth ($\overline{\varepsilon}_y = 0.068 du_{*_b}$). The increased vertical mixing is consistent with enhanced mixing due to the dimples effecting the velocity field. There is a large amount of scatter of the data in Table 6.3; the individual values laying within -39% and +54% of the average. There is no evidence of the depth averaged eddy diffusivity being a function of flow rate.

The second set of vertical mixing experiments measured the rate of change of variance of the tracer plume at two transverse positions and for three flow rates. A

vertical mixing coefficient was then inferred from the rate of spreading. The range of flows that could be used was limited by the necessity to avoid the plume impinging on the free surface or bed. Flows of approximately 11l/s, 17l/s and 22l/s were used. The transverse positions were 215mm and 375mm from the left hand wall of the flume. These positions were chosen because the pitot velocity profile work described in chapter four had shown them to be areas where the local longitudinal velocity was faster (215mm) and slower (375mm) than the cross-sectional average velocity.

The analysis of the data took the following form. The time averaged concentration profiles were plotted and a Gaussian fitted to them, the variance for each curve fit was then plotted as a function of distance from the outfall. A linear regression of this data gave the rate of change of the variance, which was used to calculate a vertical mixing coefficient from:

$$k_y = \frac{1}{2} \cdot u_q \cdot \frac{d\sigma_y^{\,2}}{dx} \tag{6.7}$$

where u_q is the cross-sectional average flow velocity and $d\sigma_y^{\,2}/dx$ is the rate of change of the variance of the vertical concentration profiles. As was previously stated the term mixing coefficient is used to reflect the fact that an equation like equation 6.2 cannot be used to obtain eddy diffusivities in a three-dimensional flow. A typical data set is shown in Figures 6.8 & 6.9.

When the tracer reaches the free surface and bed, equation 6.2 is no longer valid even for homogeneous turbulence. Any concentration profiles which showed evidence of the plume having reached the boundaries were rejected. The vertical mixing coefficients calculated using equation 6.7 are given in Table 6.5 which includes the height of the outfall above the bed, y, non-dimensionalised with the flow depth. In Table 6.5 the side wall corrected bed shear velocity, u_{*_b}, is used. The average of the vertical mixing

coefficients was $k_y = 0.109du_{*_b}$ which is 7% greater than that inferred from the constant coefficient model and nearly 63% greater than the depth averaged eddy diffusivity calculated from equation 6.3 ($\overline{\varepsilon}_y = 0.068du_{*_b}$). The individual vertical mixing coefficients were within -17% and +11% of the average; the scatter was less than with the constant coefficient model.

The parabolic eddy viscosity distribution (equation 6.3) has a value at mid depth of $\overline{\varepsilon}_y = 0.1025du_{*_b}$. This seeming agreement between the mid depth eddy viscosity and the measured mixing coefficient was coincidental as the mixing coefficient tabulated above was an average value over the depth of the tracer plume. The high vertical mixing coefficients, compared to the depth averaged eddy diffusivity, reflects the increased, compared to a two-dimensional flow, vertical mixing that exists in the laboratory flume. The flow visualisation work, although limited, suggested that the time averaged longitudinal velocity can have a vertical component which would be expected to enhance vertical mixing.

Rutherford (1994) tabulates the results of a number of experimental measures of the vertical eddy diffusivity in laboratory flumes for which: $0.042 < \frac{\overline{\varepsilon}_y}{du_*} < 0.067$. Rutherford's own measurements in a New Zealand river gave: $0.055 < \frac{\overline{\varepsilon}_y}{du_*} < 0.099$ which implies that vertical mixing is greater in natural open channel flows than in laboratory channels. It would be expected that the flow in Rutherford's river was three-dimensional and that this is the reason for the vertical mixing to be greater in natural open channel flows than in laboratory flumes.

6.3.3 Conclusions

To conclude, these mixing experiments showed the vertical mixing to be greater (by 63%) than that expected for a two-dimensional flow of equal volumetric flow rate. The average vertical mixing coefficient calculated from a constant coefficient model interpretation of measured concentration profiles and that calculated from the change of variance of profiles agreed to within 7%. The scatter of the mixing coefficients obtained from the constant coefficient model was much greater (three times) than that found from the rate of change of variance of measured concentration profiles. The better estimate of the mixing coefficient from the change of moments method compared to the constant coefficient model would reduce the number of experiments needed to obtain a reliable value. Therefore the use of the change of moments method would lead to a time saving.

The distance downstream from the outfall at which tracer became well mixed over the depth was a function of flow rate and the height of the outfall above the bed whereas Rutherford's constant coefficient model predicted that the non-dimensional distance required for a desired degree of mixing would be a function of outfall position only. The difference between the model predictions and experiments reflects the simplifications in the constant coefficient model. From the experimental data it can be seen that at 26l/s a distance of nine times the flow depth was required to achieve a ratio of the minimum to maximum concentration of 0.93. A distance of approximately sixteen flow depths was required to achieve an equal degree of mixing when the flow rate was 2.7l/s.

6.4 Transverse mixing experiments in the laboratory flume

6.4.1 Experimental technique

The conductivity probe used for the vertical transfer work was used to measure the change of transverse variance of a plume of sodium hydroxide solution 14m from the entrance to the laboratory flume. The experimental procedure was similar to that used for the vertical mixing work. The outfall was set up at either half or a quarter of the distance from the bed to the free surface. The spread of the plumes was measured over a distance of between 0.5m and 0.8m at 4 to 6 longitudinal positions.

More than one probe was used in order to speed up the experiments. Although an array of six probes was used for the first experiment in general only two probes were used. Using two probes had two practical advantages over the array of six probes used initially: two probes could be calibrated at the same time but six could not, and with only two traces on the data logger display during an experiment the concentration fluctuations could be seen more clearly. The visual indication of the concentration from the data logger display was very helpful in deciding how far in the transverse direction it was necessary to go in order to survey the plume adequately.

The concentration of the injected tracer was much stronger than that used previously (5% to 15%, depending on the flow rate in the flume) because it was desirable to allow the tracer to become vertically well mixed before measuring the rate of change of transverse variance. The tracer was buoyant at the injection site but it will be appreciated that the concentration at the measurement stations, which were nine to twenty-seven times the depth downstream of the outfall, were much lower than this and any momentum or buoyancy effects were negligible (Bruno et al 1990). It would have been possible to have injected a solution with the same density as the flume water by adding a low density liquid such as alcohol, but then a greater volume of fluid would

have needed to have been pumped with perhaps a need for a larger nozzle that would have caused more disturbance to the flow.

The concentration profiles were plotted and a Gaussian curve fitted through the data. The variance of the concentration curves was then plotted against longitudinal distance and a linear regression applied. As was discussed previously, only for two-dimensional flow can the rate of change of variance of a tracer plume be related to the eddy diffusivity; as the flow in the flume was not two-dimensional the eddy diffusivity could not be measured. However the rate of change of variance does give a measure of the transverse mixing that includes the effects of the turbulent eddy diffusivity and secondary flows. Accordingly the transverse mixing coefficient was calculated from equation 6.8.

$$k_z = \frac{1}{2} \cdot u_q \cdot \frac{d\sigma_z^2}{dx} \tag{6.8}$$

where u_q is the cross-sectional average flow velocity and $d\sigma_z^2/dx$ is the rate of change of the variance of the vertical concentration profiles.

Typical plots of the concentration profiles and the rate of change of variance are shown in Figures 6.10 and 6.11 respectively. Ten to fourteen points were used to define the concentration profile and five to six points used to define the longitudinal rate of change.

6.4.2 Results

The transverse mixing coefficients measured in the flume are shown in Table 6.6; the position of the outfall as a fraction of depth is given, as is the relative depth of the conductivity probe, the flow depth and the side wall corrected bed shear velocity at the location of the outfall. Although the flow in the flume was gradually varying, it was found that the product of the centreline depth and the side wall corrected shear velocity

varied by less than 4% over the measurement reach. As it was known that much larger, of the order of 20%, transverse variations in the local bed shear velocity would occur because of the three-dimensional flow it was not felt necessary to allow for minor longitudinal variations in the flow conditions.

The coefficients of determination for the least squares fit used to find the rate of change of the variance of the transverse concentration profiles were generally better than 0.94; data set Res53b had a coefficient of 0.79, while data set Res49b had a coefficient of 0.90.

When the concentration profiles were analysed some of the tails of the profiles were not well fitted by a Gaussian. Because confidence was lower in the low concentration measurements the tails were removed. This resulted in reduced scatter in the rate of change of variance plots but did not significantly alter the transverse mixing coefficients implied by the rate of change of variance. The relative insensitivity of the Gaussian curve fit to the tails is a point in favour of this technique. In contrast, the estimation of variance from the moments of a measured concentration profile is very sensitive to the noise and the accurate determination of background levels (see Chapter three and Sayre & Chang 1968). It is important to note that the curve fit technique worked because a Gaussian was a good model of the measured data.

The mixing coefficients in Table 6.6 represent a measure of the mixing over the tracer plume. The influence of the plume width and the height above the bed at which concentration profiles were measured on the mixing coefficients was investigated. The plumes typically covered up to about 50% of the flume width. There was no evidence for a plume width effect: e.g. Res37 used a plume grid half that of Res56 which had a similar flow rate but the non-dimensional mixing coefficients agree within 8%. For six of the flow rates used experiments were performed at two or more depths in the flow. Of

these four have a lower rate of mixing at the lower depth; however when the degree of scatter, for nominally similar flow rates and positions, is considered it seems unlikely that this is significant.

Experiment Res56 was undertaken in order to investigate the transverse variation of the transverse mixing coefficient. For this run the outfall was moved to 200mm from the left hand side of the flume (looking downstream), the longitudinal position being still 14m from the flume inlet. The plume in this case was measured for a transverse distance of 120mm either side of the outfall. Previous longitudinal velocity measurements suggested that the presence of the side wall would not have influenced the longitudinal velocity field. The non-dimensional mixing coefficient for Res56 was within the range of values measured for similar flows over the central section of the channel, which implies that there was no detectable transverse variation in mixing. The method used to evaluate the mixing coefficient, fitting a Gaussian, was only valid in the absence of reflections of the plume from the boundary. If experiments were to have been made closer to the side wall a technique such as the generalised method of moments (Holley et al 1972) could have been used to cope with reflections. However, the problems experienced with defining tails of distributions when applying the method of moments to the longitudinal dispersion measurements suggested that it was better to ensure the plume did not reach the walls of the flume. Therefore transverse variation of the transverse mixing coefficient was not investigated further.

Supplementary experiments were carried out to investigate the sensitivity of the transverse mixing coefficients to a 25% change in the tracer injection rate and the use of a larger outfall pipe (4mm OD, 3.5mm ID). The results for both of the investigations fell within the scatter of the original data indicating that these features were relatively unimportant.

The transverse mixing coefficients measured by the author are plotted in Figure 6.12. A linear regression gave: $k_z = -1.4e^{-4} + 0.40du_{*_b}$ (with a coefficient of determination, r^2, of 0.76). These coefficients are greater than those obtained by previous workers for laboratory flumes ($0.16du_*$ see section 6.1). It will be recalled from Chapter four that the flow in the author's flume was three-dimensional and it is likely that this increased the rate of transverse mixing over that found in two-dimensional flows. It will be noted from Figure 6.12 that the scatter increases with increasing flow rate, this was probably because the concentrations of tracer in the flume were lower at the higher flow rates making the task of measurement more difficult. Also, at the higher flows the concentrations reduced more rapidly with downstream position. The dependence of the transverse mixing coefficients on the flow rate was investigated because the aspect ratio of the flow depended upon the flow rate. If the transverse mixing coefficient were found to be a function of flow rate it would imply that the mixing coefficients may have depended upon the aspect ratio. Figure 6.13 shows the non-dimensional mixing coefficient measured in the flume plotted against flow rate; at the 95% confidence limit there was no relationship between the flow rate and the transverse mixing coefficient. Previously it has been suggested, Lau & Krishnappan (1981), that the width is the dominate length scale in transverse mixing. It would appear, because the aspect ratio did not affect the measured mixing coefficients, that the flow depth is the correct length scale for the mixing processes in the laboratory flume. For a two dimensional flow the depth is the obvious length scale but the question arises why it should be the correct length scale for a three dimensional flow. Unfortunately the velocity measurements reported in Chapter four did not allow allow any secondary flows to be quantified. It is, however, interesting to note that the secondary flow cells described in Chapter four scale with the flow depth.

Rutherford (1994) and West & Cotton (1980) tabulate the results of transverse mixing experiments undertaken in natural channels. A regression to the straight channel data of both West & Cotton and Rutherford gave: $k_z = 0.39du_{*b}$ (with a coefficient of determination, r^2, of 0.65). Adding the data for meandering channels gave: $k_z = -0.02 + 0.61du_{*b}$ (with a coefficient of determination, r^2, of 0.87). That data from meandering channels dominates this last regression can be seen by comparing the regression for data from straight and meandering natural channels with that for meandering channels alone: $k_z = -0.03 + 0.59du_{*b}$ (with a coefficient of determination, r^2, of 0.86). This is because there are 27 values from meandering channels compared to 14 from straight channels.

It has been stated that the transverse mixing coefficients measured during the present work were greater than previously measured in laboratory flumes and that this was due to the three-dimensional flow in the author's flume. It will also now be noted that the relationship between the mixing coefficients and product of the depth and bed shear velocity measured in the flume were very similar to that for straight natural open channel flows. Figure 6.14 shows the author's data along with the straight channel data of Rutherford and West & Cotton. A regression gave: $k_z = 0.38du_{*b}$ (with a coefficient of determination, r^2, of 0.73). The author's data were obtained at lower values of du_* than existed in the natural open channel flows.

West & Cotton (1980) analysed transverse mixing data obtained for laboratory flumes and from field measurements in straight channels and obtained the following best fit to the data: $k_z = 0.399(du_*)^{1.12}$. West & Cotton used data (twenty points) from wide smooth bedded laboratory flumes, given by Lau & Krishnappen (1977) for which we might have expected to have measured the transverse eddy diffusivity, and seven from

field work. It is not correct to mix eddy diffusivities and mixing coefficients because they are different phenomena.

6.4.3 Conclusions

The three-dimensional flow field in the author's flume led to enhanced transverse mixing ($k_z = 0.40du_*$) compared to that previously measured in two-dimensional flows ($k_z = 0.16du_*$).

The transverse mixing coefficients were not a function of flow rate, which for the fixed width used in this work implies that the mixing was not a function of the aspect ratio. The transverse mixing coefficients did not vary over the depth or the width of the flume.

The relationship between the transverse mixing coefficient and product of the flow depth and bed shear velocity is similar to that obtained by a regression to transverse mixing data obtained in straight natural open channel flows ($k_z = 0.39du_*$).

Author	du_* (*e^{-4}) m^2/s	ε_z (*e^{-4}) m^2/s	ε_z/du_*
Webel & Schatzmann (1984)	16.911	2.215	0.131
	9.204	1.206	0.131
	5.012	0.652	0.130
	16.911	2.249	0.133
	9.204	1.215	0.132
	5.012	0.657	0.131
	13.374	1.779	0.133
	7.278	0.961	0.132
	3.964	0.519	0.131
	10.359	1.378	0.133
	5.640	0.744	0.132
Lau & Krishnappen (1977)	6.740	0.878	0.130
	4.159	0.592	0.142
	4.004	0.601	0.150
	6.780	1.162	0.173
	4.302	0.850	0.197
	3.416	0.883	0.259
	2.926	0.335	0.114
	5.242	0.915	0.175
	3.705	0.740	0.199
Prych (1970)	14.547	1.98	0.136
Sayre & Chang (1968)	56.4	9.57	0.170
	122.3	21.4	0.175
	223.7	35.8	0.160
Engelund (1969)	19.8	4.0	0.202

Table 6.1 Previously measured transverse mixing coefficients.

Q (l/s)	y/d	x (mm)	x^*	P_m
2.15	0.26	400	0.027	0.65
		450	0.031	0.71
		500	0.034	0.76
		600	0.04	0.80
		700	0.048	0.87
		800	0.054	0.88
		900	0.06	0.88
2.69	0.49	300	0.104	0.41
		340	0.118	0.52
		400	0.139	0.62
		440	0.153	0.70
		480	0.167	0.76
		520	0.183	0.73
		560	0.194	0.76
		600	0.208	0.81
		700	0.241	0.93
		800	0.278	0.94
6.84	0.50	300	0.051	0.74
		350	0.059	0.77
		450	0.076	0.84
		550	0.093	0.85
		650	0.110	0.93
		750	0.130	0.95
		850	0.140	0.93
2.51	0.25	200	0.073	0.45
		240	0.087	0.57
		280	0.102	0.73
		320	0.117	0.75
		360	0.131	0.83
		420	0.153	0.94
		360	0.131	0.85
		500	0.182	0.98
7.05	0.27	300	0.058	0.13
		350	0.068	0.22
		400	0.078	0.26
		450	0.087	0.42
		500	0.097	0.52
		550	0.107	0.65
		600	0.116	0.64
		650	0.126	0.77
		750	0.146	0.76
25.78	0.51	300	0.022	0.66
		400	0.031	0.81
		500	0.038	0.68
		600	0.046	0.86
		700	0.054	0.90
		800	0.061	0.91
		900	0.069	0.93

Table 6.2 Ratio of maximum to minimum concentration measured over the flume depth.

Q (l/s)	u_{*_b} (m/s)	u_* TP375 (m/s)	%
7.1	0.0226	0.0202	-10.6
13.3	0.0295	0.0349	18.3
25.7	0.0349	0.0421	20.6

Table 6.3 Comparison of bed averaged shear velocities.

Q (l/s)	y/d	ε_y / du_{*_b}
2.51	0.25	0.157
2.69	0.49	0.030
7.05	0.27	0.137
6.84	0.5	0.062
27.15	0.26	0.107
25.78	0.51	0.121

Table 6.4 Depth averaged eddy diffusivity implied by the constant coefficient model.

Q (l/s)	y/d	TP	$k_y/(du_{*_b})$
21.56	0.52	375	0.107
16.67	0.52	375	0.115
10.95	0.57	375	0.091
21.93	0.44	215	0.121
17.12	0.46	215	0.105
10.77	0.48	215	0.114

Table 6.5 Vertical mixing coefficient.

Res. No.	Outfall y/d	Probe y/d	Flow l/s	du_{*b} ($*10^{-6}$) m^2/s	k_Z ($*10^{-6}$) m^2/s	k_Z/du_{*b}
37	0.5	0.68	2.81	574.9	109.4	0.19
37b	0.5	0.5	2.81	574.9	110.06	0.19
39	0.52	0.52	7.54	1309	810.38	0.62
41	0.5	0.07	7.49	1305	444.17	0.34
42	0.5	0.53	13.59	2201	592.0	0.27
43b	0.45	0.33	13.7	2220	791.1	0.36
44	0.52	0.52	17.2	2410	742.27	0.31
44b	0.52	0.25	17.2	2410	570.87	0.24
45	0.5	0.5	17.95	2449	817.7	0.33
46	0.47	0.47	4.95	792.5	108.99	0.14
47	0.46	0.46	4.65	757	148.4	0.20
47b	0.46	0.19	4.65	757	117.99	0.16
48	0.46	0.46	4.82	776	168.88	0.22
50	0.53	0.53	21.06	2305	1041.93	0.45
51	0.51	0.51	20.94	2806	1512.75	0.54
52	0.5	0.5	20.34	2734	850.01	0.31
53	0.51	0.51	10.43	1515	692.64	0.46
53b	0.51	0.33	10.43	1515	313.17	0.21
54	0.52	0.52	5.74	897.3	238.22	0.27
54b	0.52	0.15	5.74	897.3	153.16	0.17
56	0.52	0.52	2.86	497.7	130.64	0.26

Table 6.6 Transverse mixing coefficients.

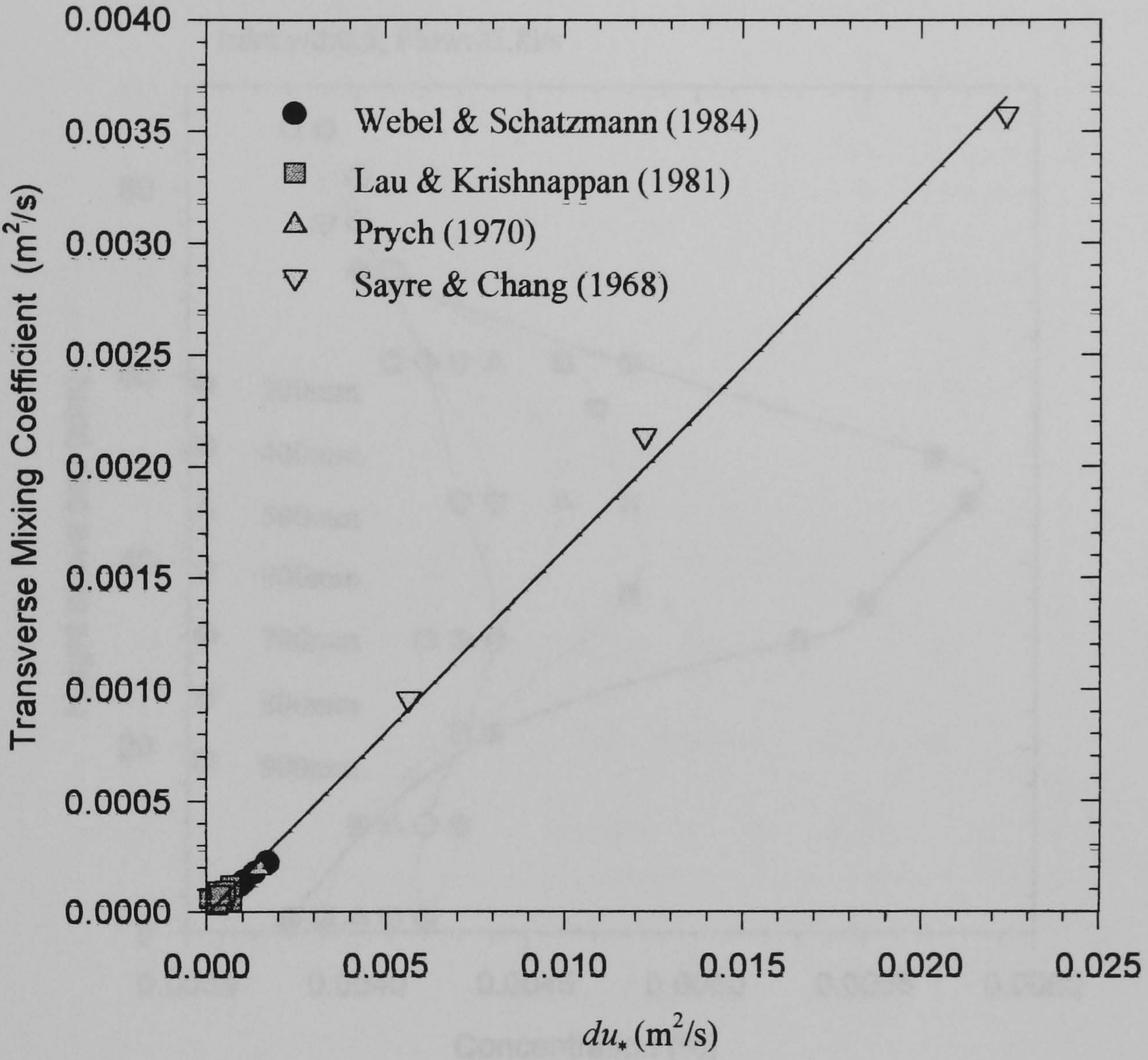

Figure 6.1 Transverse diffusivities measured in flumes as function of the product of flow depth and the bed shear stress

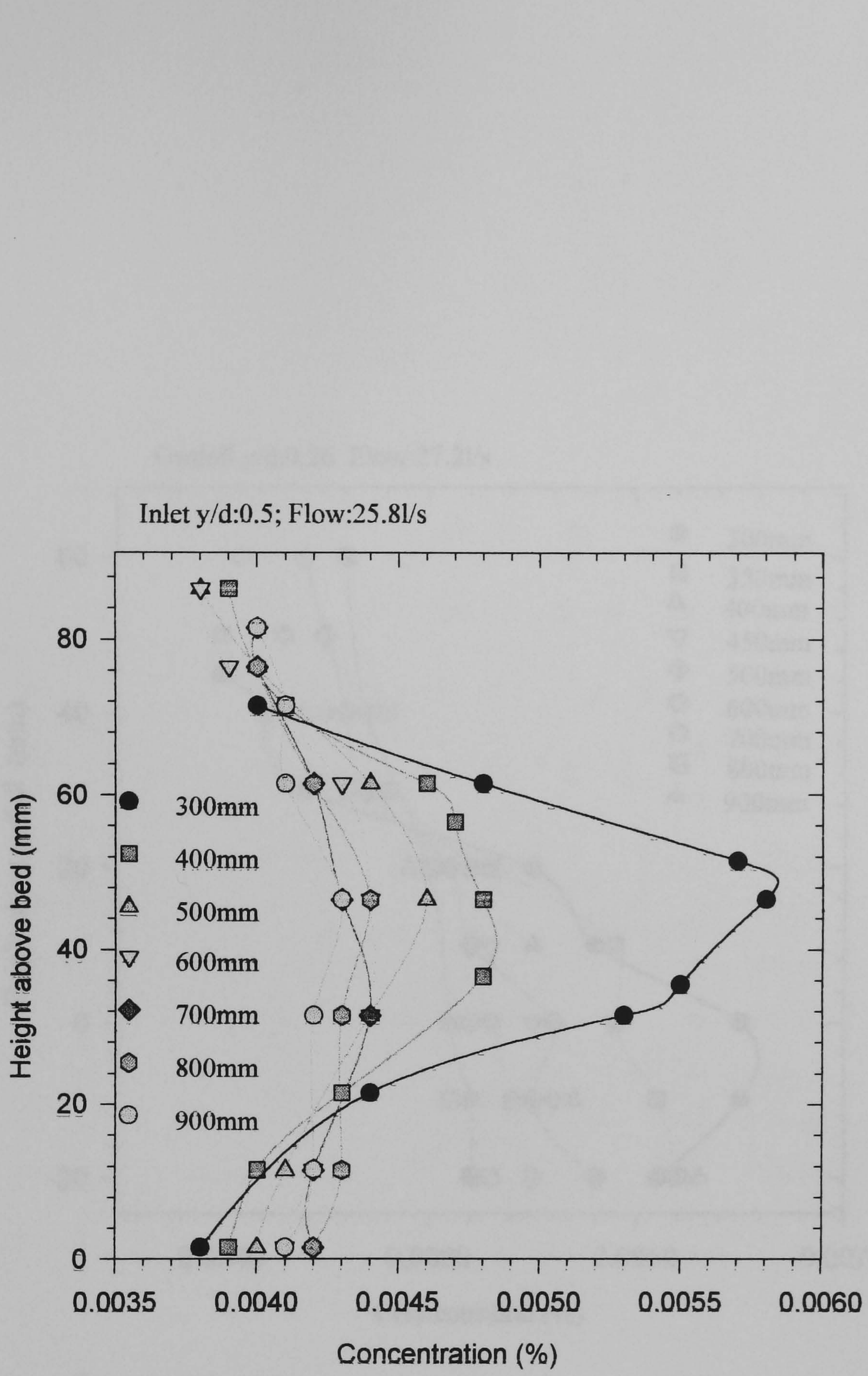

Figure 6.2 Concentration profiles for a source at mid depth in a flow of 25.8l/s

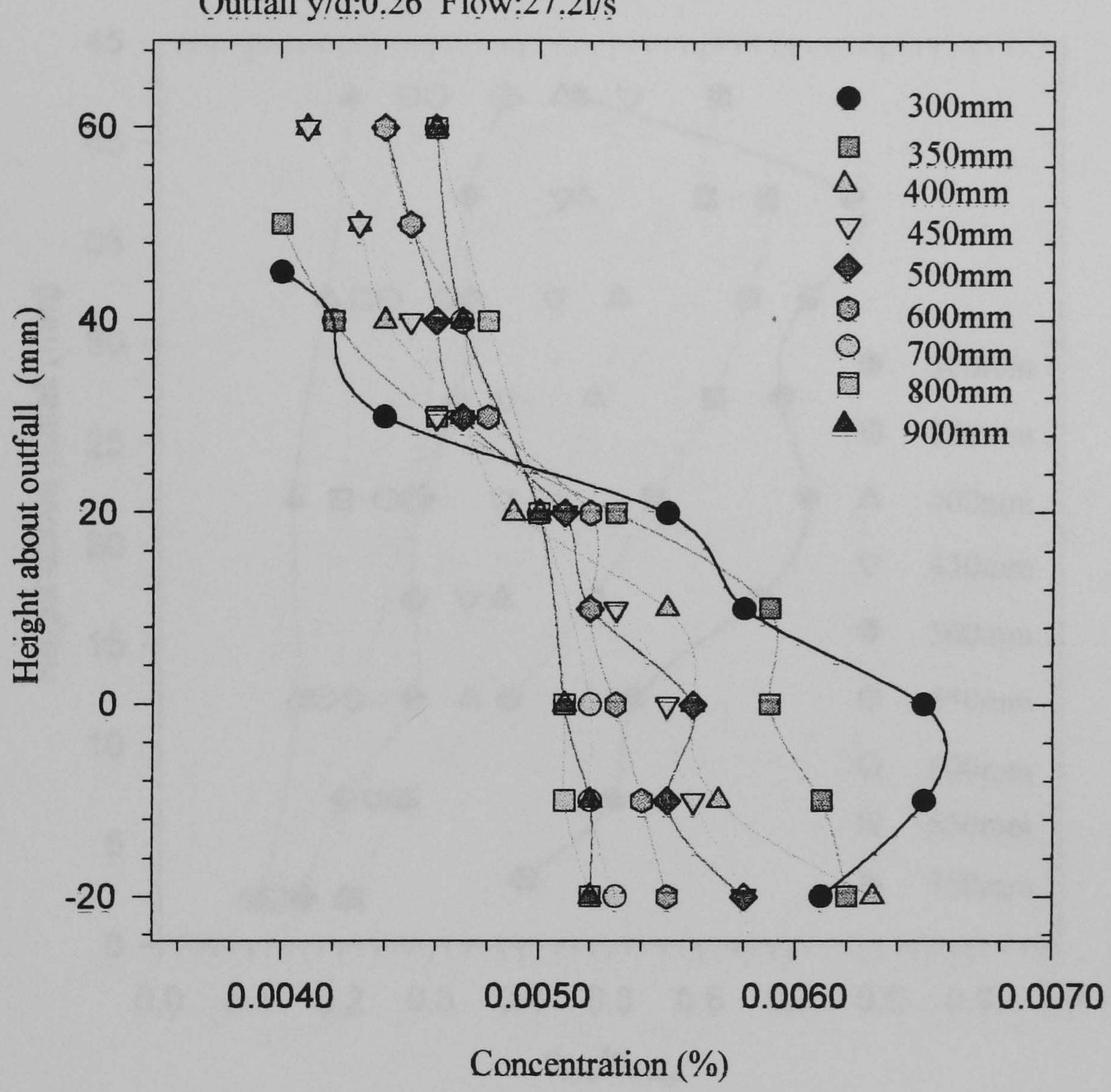

Figure 6.3 Concentration profiles for a quarter depth source in a flow of 27.2l/s

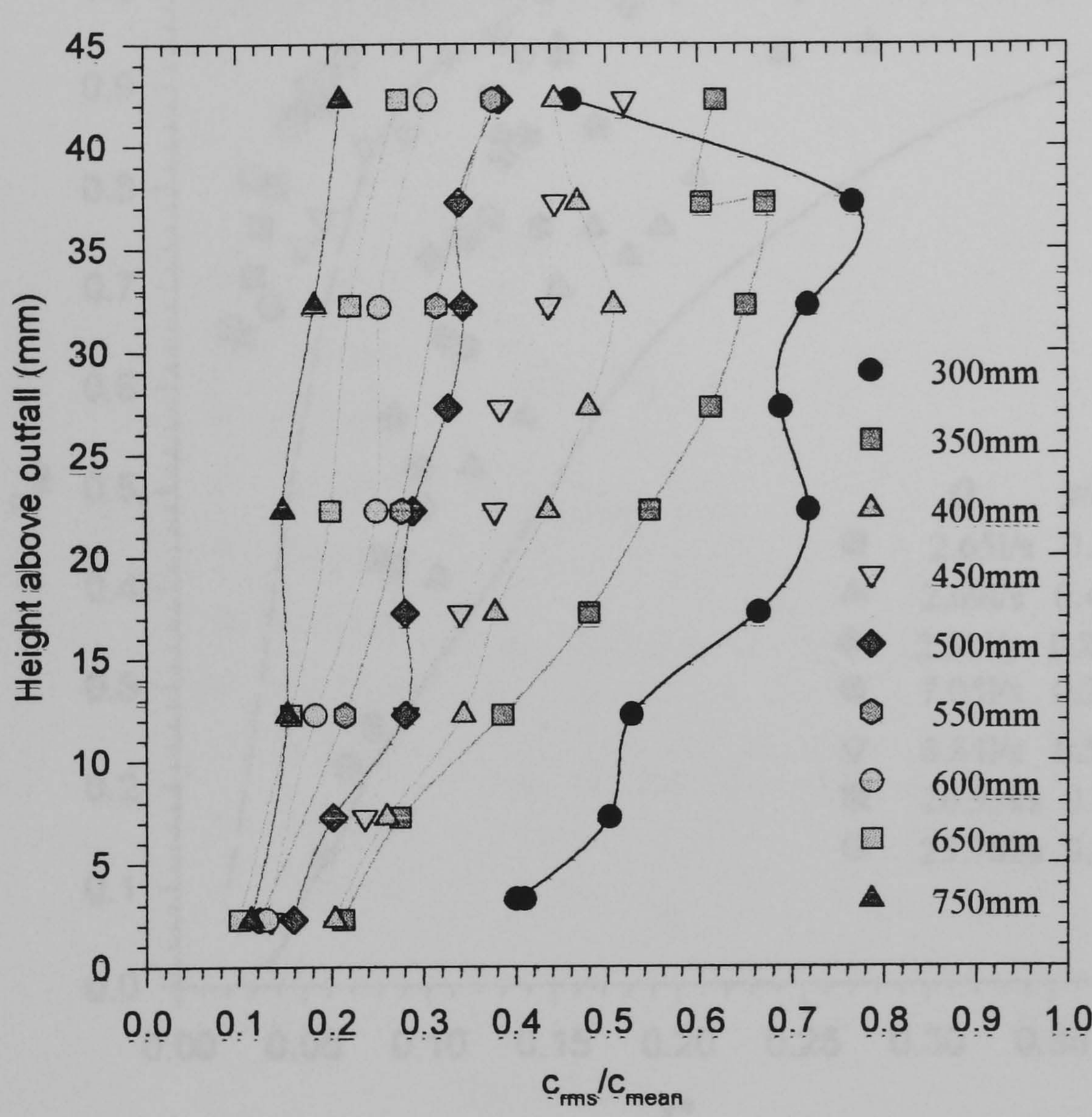

Figure 6.4 Concentration fluctuations for a flow of 26.8l/s

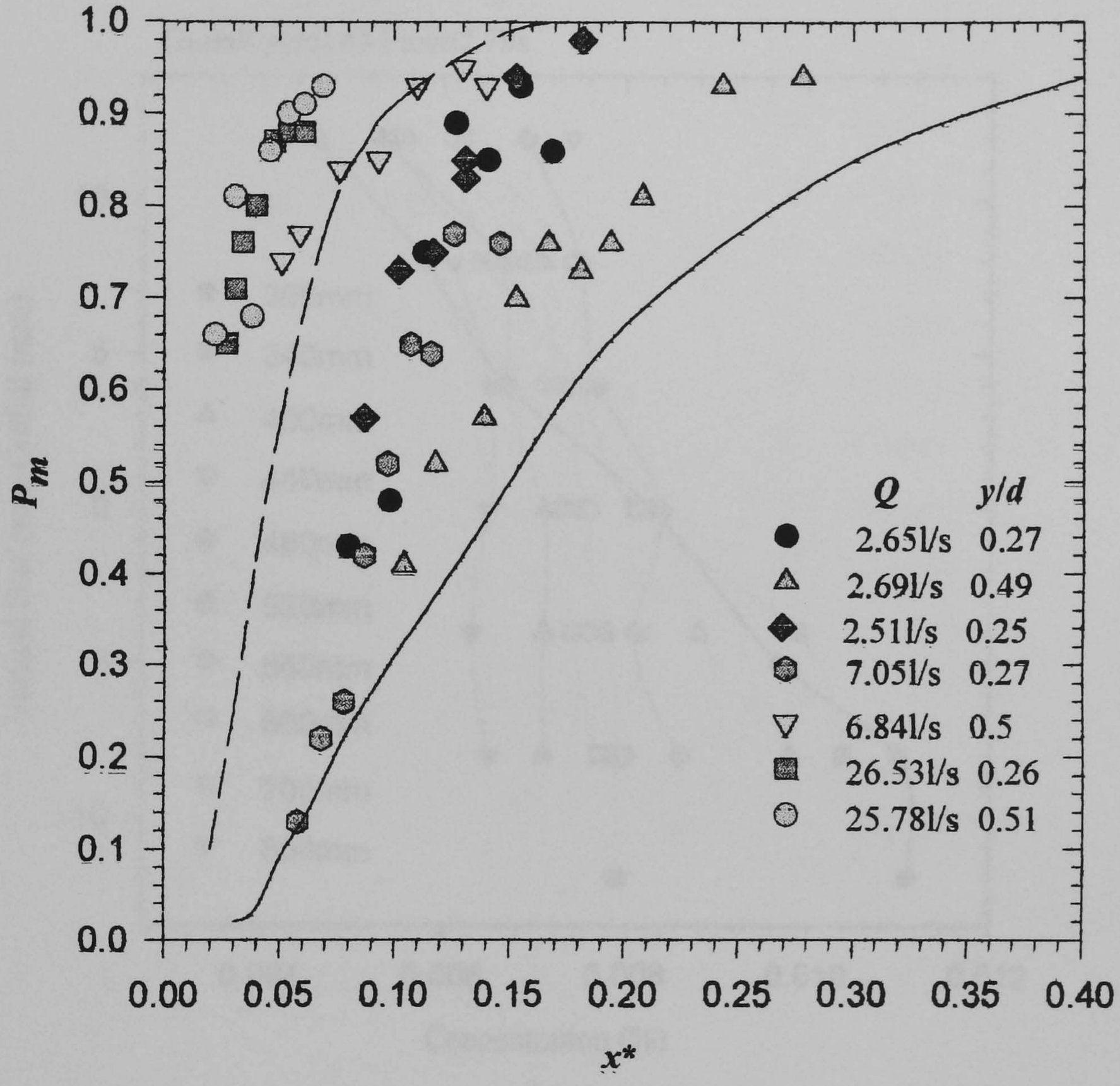

Figure 6.5 Comparison of measured data with constant coefficient model predictions

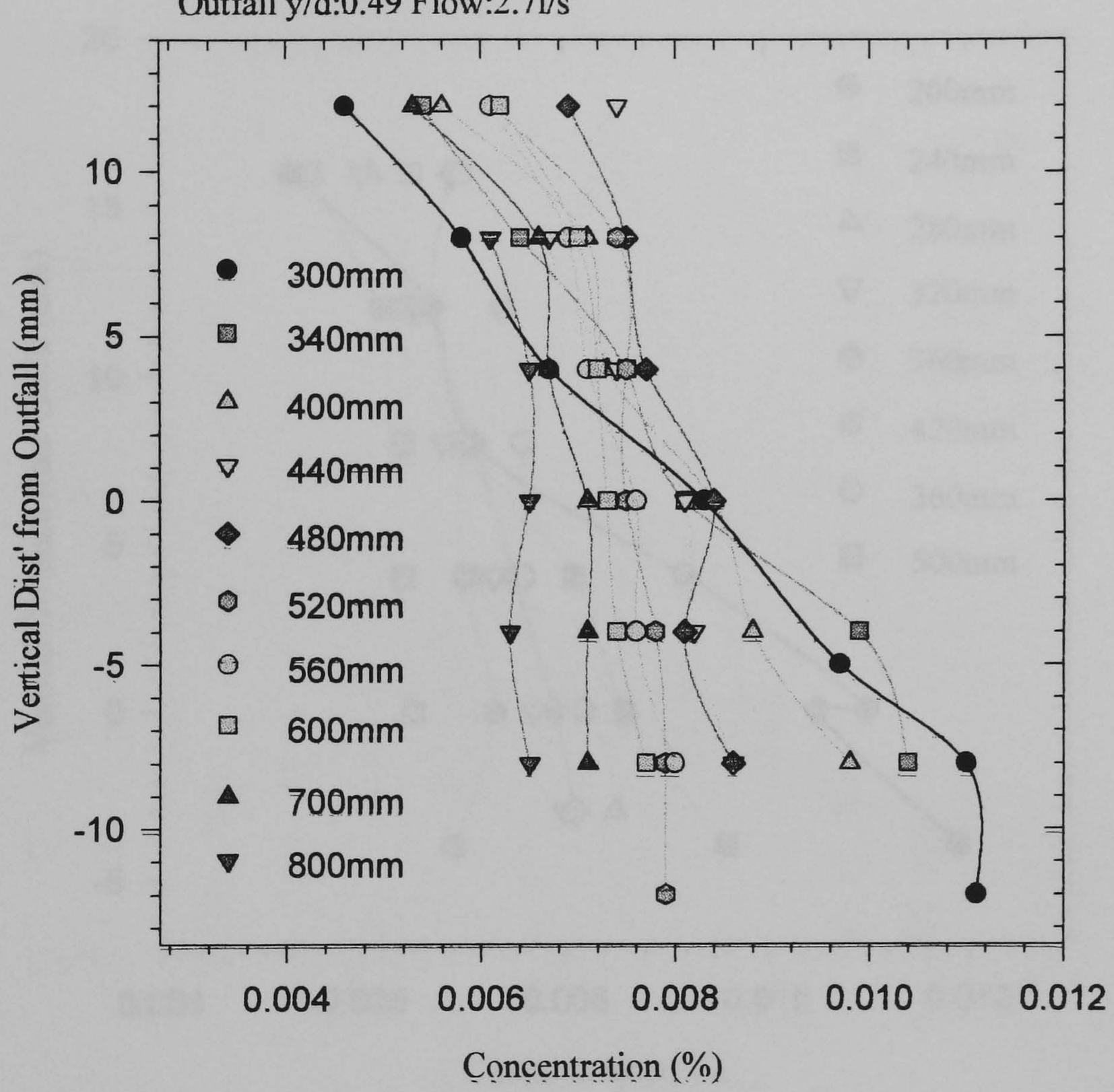

Figure 6.6 Concentration profiles for a quarter depth source in a flow of 2.7l/s

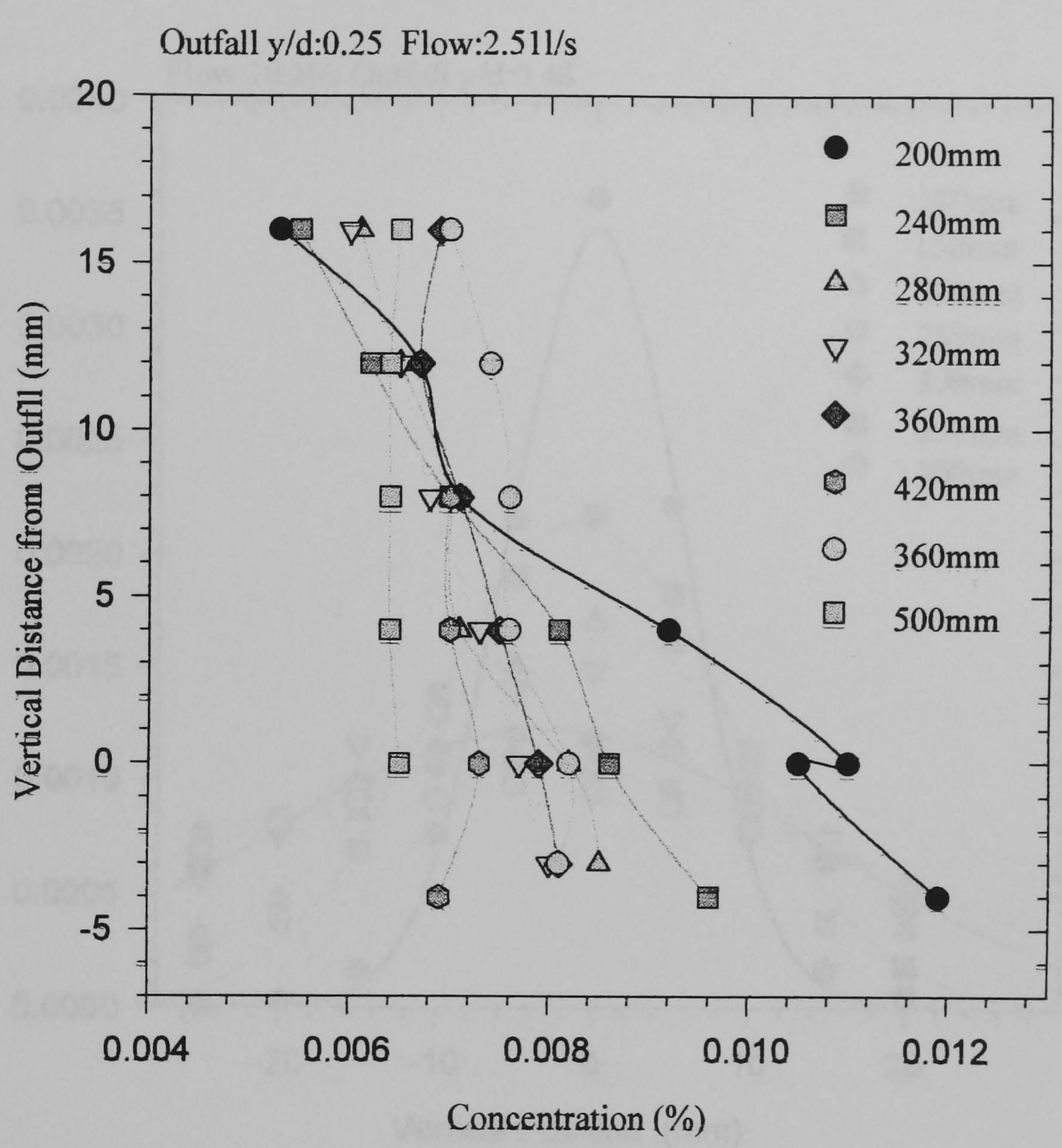

Figure 6.7 Concentration profiles for a mid depth source in a flow of 2.5l/s

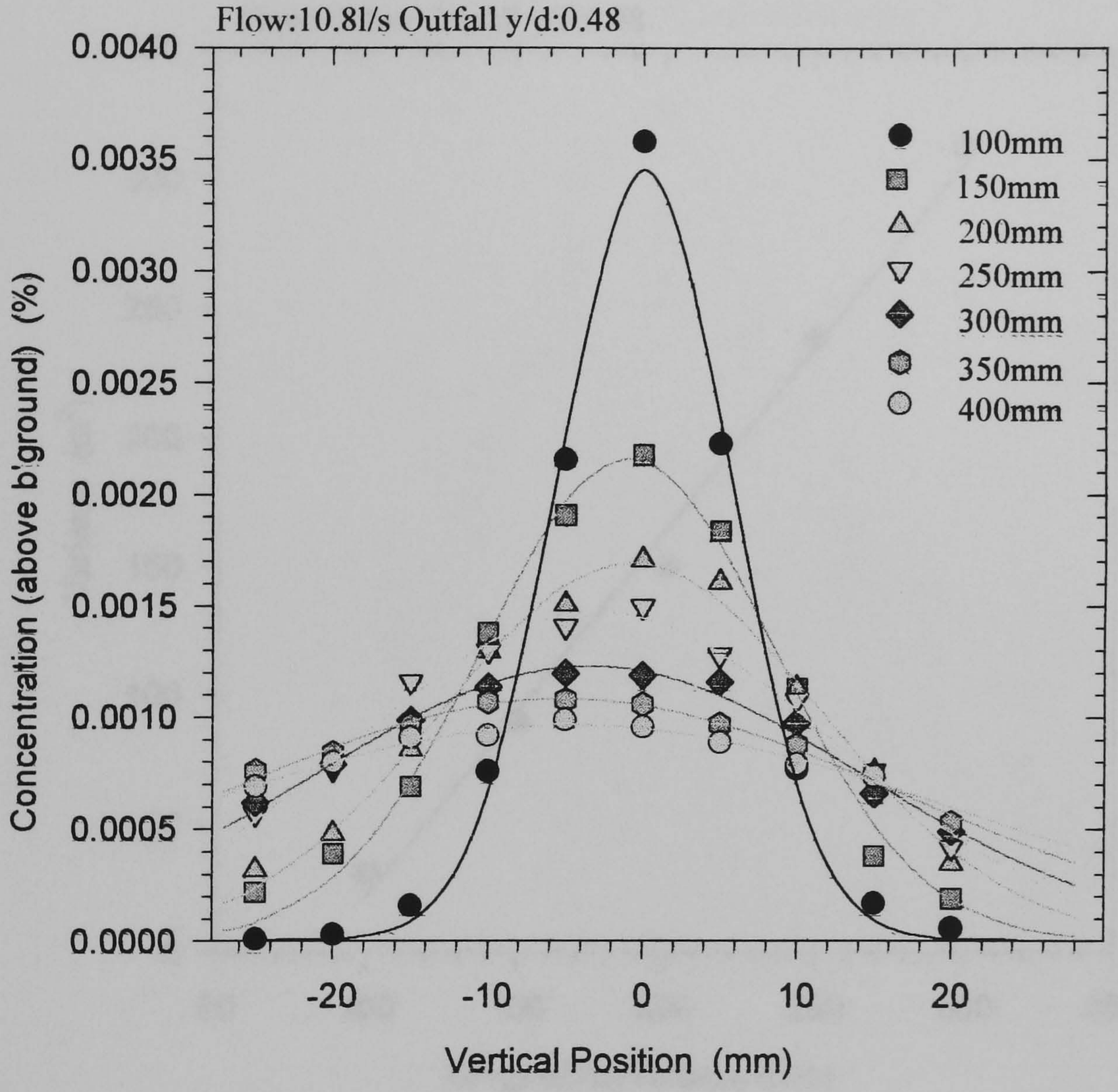

Figure 6.8 Typical vertical concentration profiles

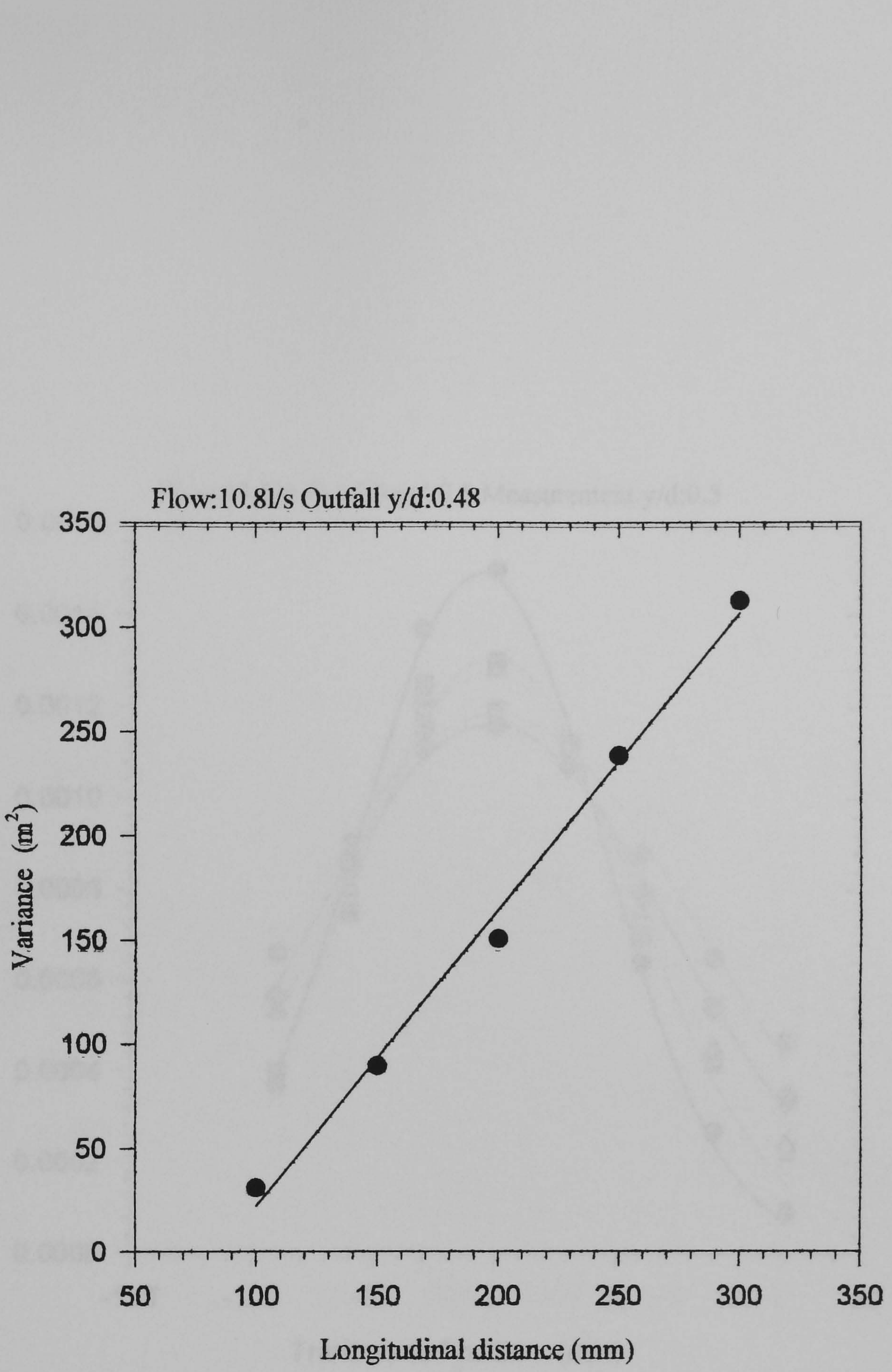

Figure 6.9 Typical change of vertical variance with distance from outfall

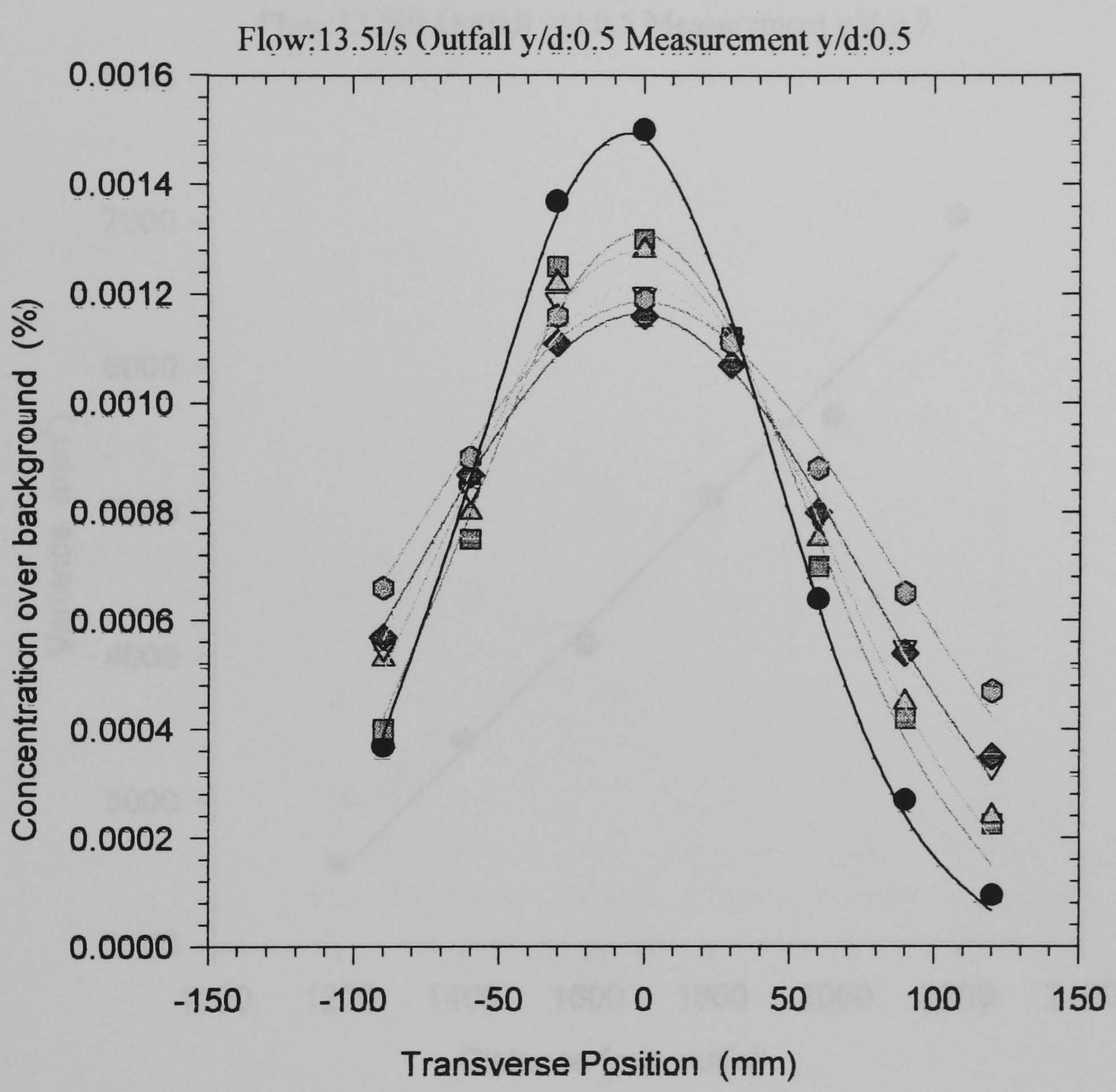

Figure 6.10 Typical transverse concentration profiles

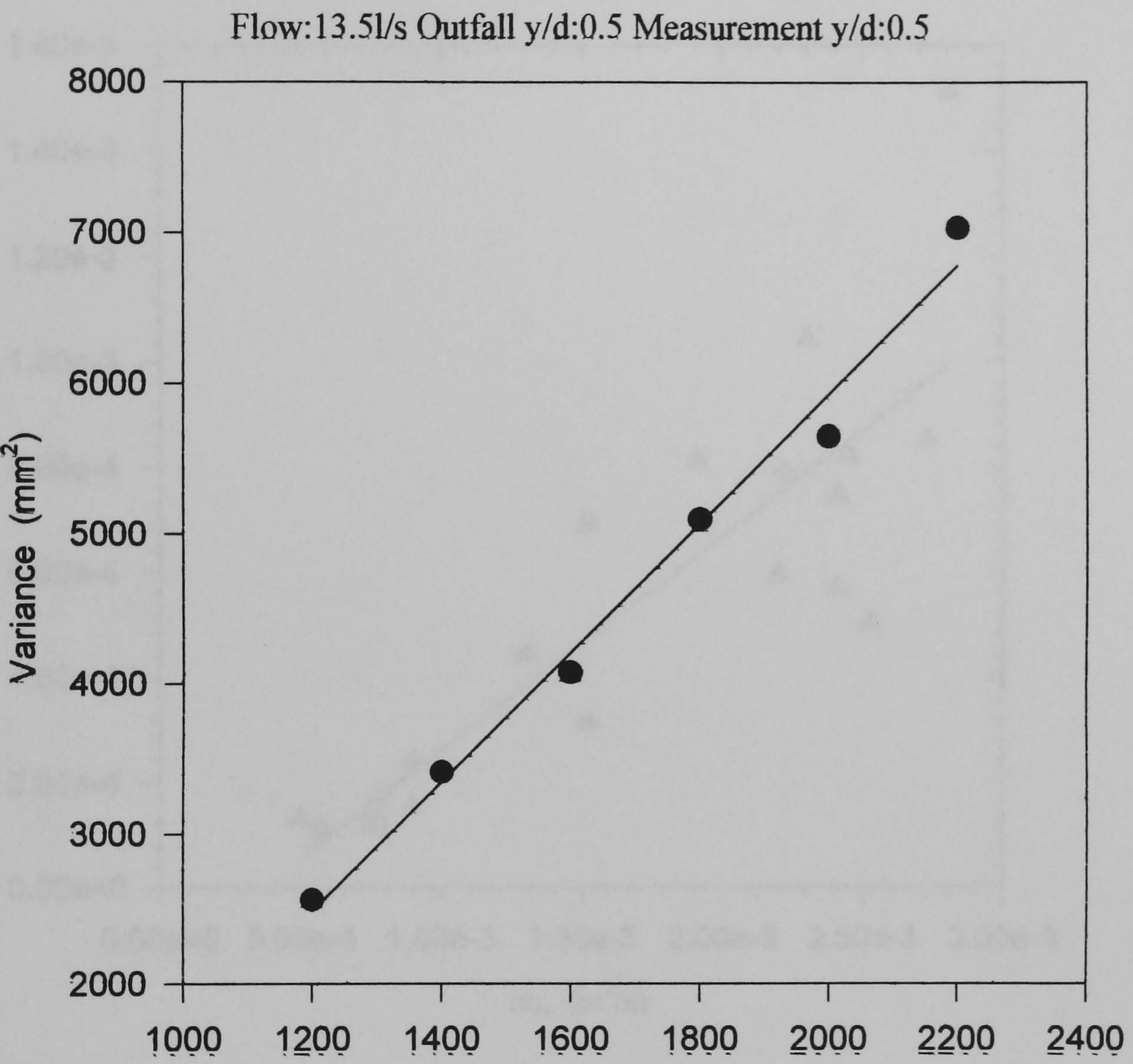

Figure 6.11 Typical change of transverse variance with distance from outfall

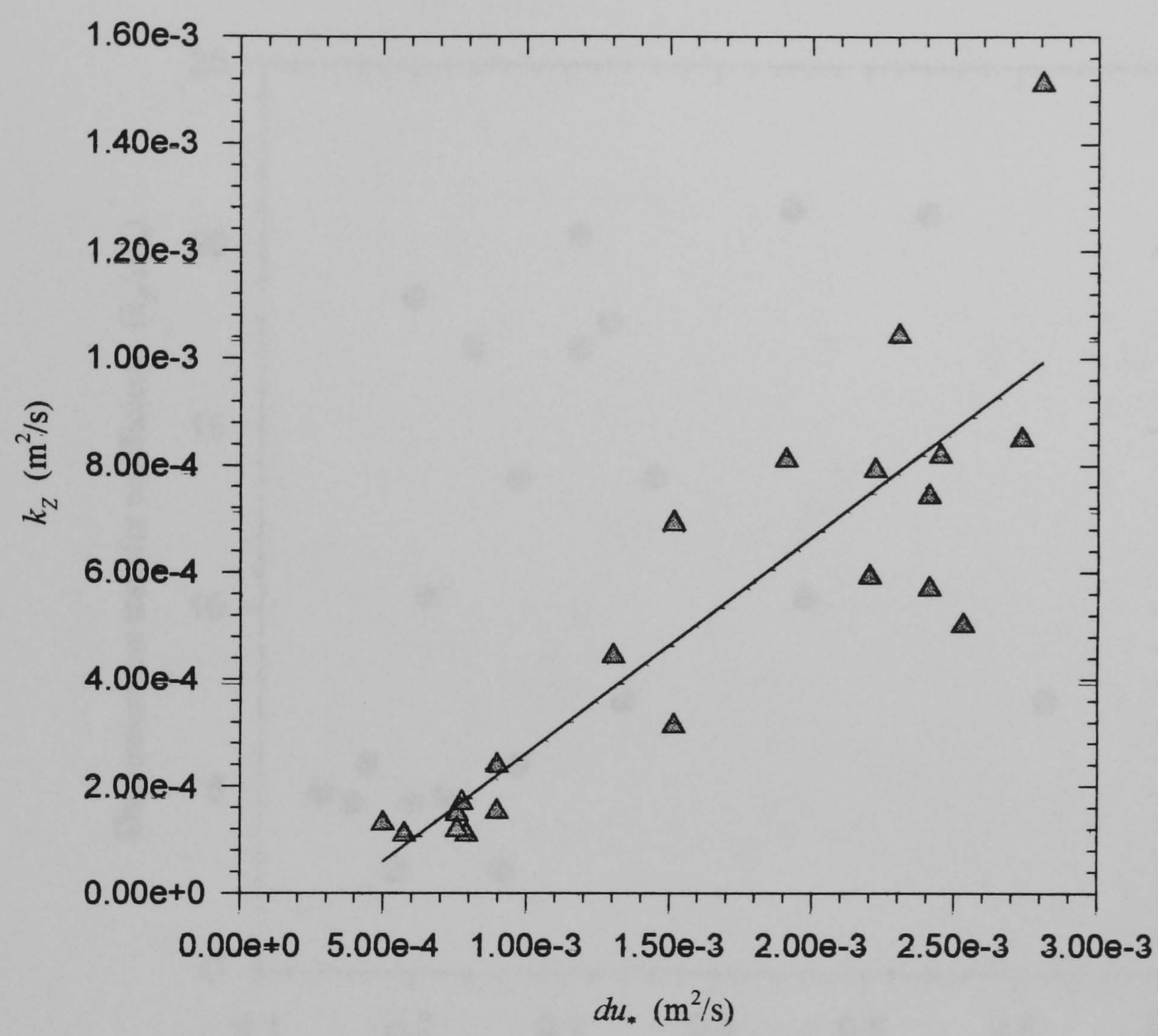

Figure 6.12 Transverse mixing coefficients from present work

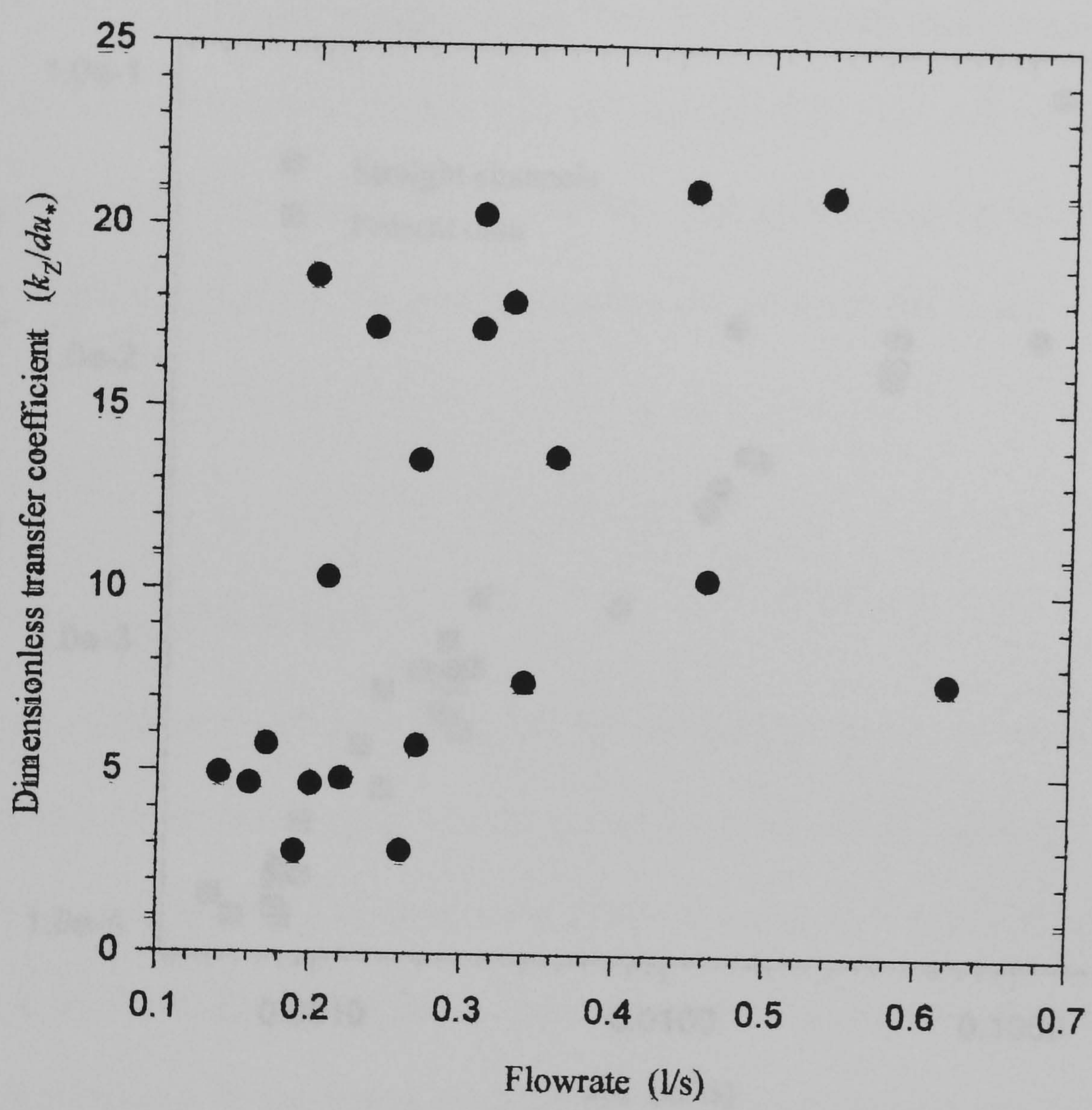

Figure 6.13 Transverse mixing coefficient against flow rate

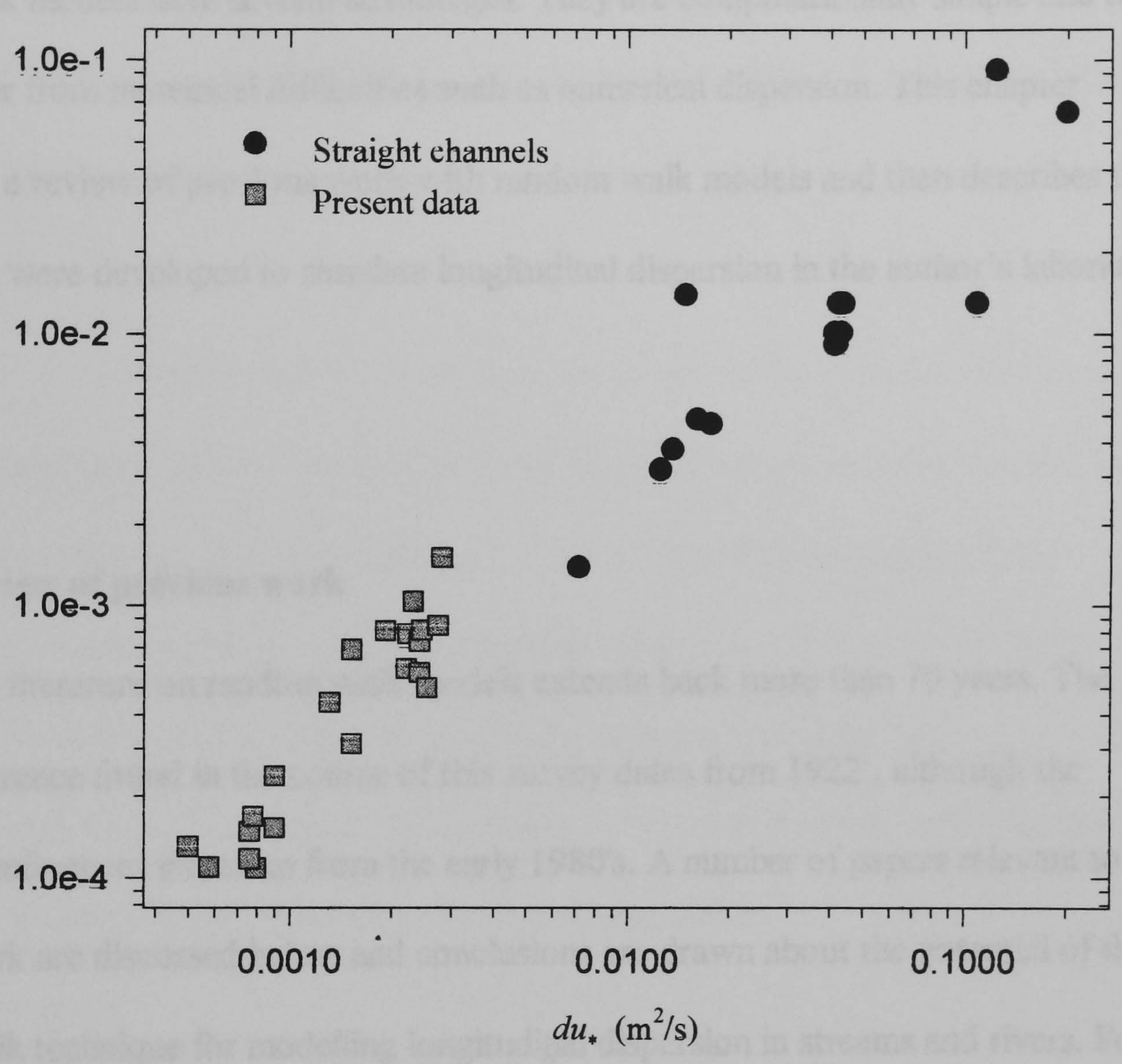

Figure 6.14 Mixing data from Rutherford (1994) West & Cotton (1980) & present work

Chapter 7 Random Walk Modelling

7.1 Introduction

Random walk models for longitudinal dispersion were introduced in chapter two. Compared to other numerical solutions for longitudinal dispersion in open channel flow random walk models have several advantages. They are computationally simple and they do not suffer from numerical difficulties such as numerical dispersion. This chapter begins with a review of previous work with random walk models and then describes the models that were developed to simulate longitudinal dispersion in the author's laboratory flume.

7.2 Review of previous work

The literature on random walk models extends back more than 70 years. The earliest reference found in the course of this survey dates from 1922 , although the number of references increases from the early 1980's. A number of papers relevant to the present work are discussed below and conclusions are drawn about the potential of the random walk technique for modelling longitudinal dispersion in streams and rivers. Four main types of random walk models are evident in the literature. Each type of model is described in a sub-section below.

7.2.1 Simple random walk models

These models track the progress of a large number of particles as they move through a representation of a flow field. Let us consider a model for the vertical mixing in a plane shear flow (where the longitudinal time averaged velocity, u, is a function of

the distance, y, measured in the direction, Y, perpendicular to the bed only). In a simple random walk model a particle is moved longitudinally for each time step, Δt, a distance, x, given by $u \cdot \Delta t$, and the vertical mixing is simulated by giving the particle a step, Δy, in the Y direction, and it is the direction of the step, either towards or away from the bed, which is the random element in such a model.

For a homogeneous turbulence field it is possible (Goldstein 1938) to derive a relationship between the step length, Δy, and the mixture length, l', of mixing length theory (Goldstein 1938, Kay & Nedderman 1979):

$$\overline{Y}^2 = 2 \cdot l' \cdot v' \cdot T = \Delta y \cdot v \cdot T \qquad (7.1)$$

in which $\overline{Y}^2$ is the mean square distance, from the origin, of the particles after a time T, v' is the rms of the turbulent fluctuations in the flow and v is the velocity at which the particles make their random step. Equation 7.1 shows that if there is equivalence between the velocity at which a particle is considered to make its random step (the random step velocity) and the rms velocity of the turbulence then the random step length should be twice the mixture length. The product $l' \cdot v'$ is the kinematic eddy viscosity (Kay & Nedderman 1979). Using equation 7.1 we can write:

$$\varepsilon_v = l' \cdot v' = \frac{\Delta y \cdot v}{2} \qquad (7.2)$$

in which ε_v is the eddy viscosity. The velocity at which a particle makes each step is $\frac{\Delta y}{\Delta t}$ so that $\varepsilon_v = \frac{(\Delta y)^2}{2 \cdot \Delta t}$. If Reynolds' analogy between momentum and mass transfer is invoked it is now possible to calculate the step length necessary to simulate a desired eddy diffusivity, ε_y, assuming that the step velocity and time step are given:

$$\Delta y = \sqrt{2 \cdot \varepsilon_y \cdot \Delta t} \qquad (7.3)$$

We choose to refer to this random walk model as Taylor's random walk because Goldstein's treatment of dispersion in homogeneous turbulence built upon the work of Taylor (1921).

It is possible to derive the relationship between the mixture length, l', and Prandtl's mixing length, l, by writing the equation for the turbulent shear stress, τ, in a plane shear flow using both mixing length approaches:

$$\tau = \rho \cdot l' \cdot v' \cdot \frac{du}{dy} \tag{7.4}$$

taking the mixture length approach in which ρ is the fluid density; and

$$\tau = \rho \cdot l^2 \cdot \left(\frac{du}{dy}\right)^2 \tag{7.5}$$

using Prandtl's mixing length. Equations 7.4 and 7.5 show that:

$$l' \cdot v' = l^2 \cdot \frac{du}{dy} \tag{7.6}$$

If the velocity and shear stress profile in the flow is known the right hand side of this equation can be evaluated, and knowledge of the rms turbulent velocity allows the mixture length to be obtained. This method of calculating the step velocity and step length for a random walk model of mixing in a flow is attractive because experimental data for turbulent and time averaged velocities are more widely available than measurements of eddy diffusivity.

A different approach to the problem of simulating the mixing in a flow was taken by Sullivan (1971). Sullivan reported an extensive series of experiments concerned with dispersion in a two-dimensional shear flow. One part of the work was a simulation of the dispersion using a simple random walk model. Sullivan's algorithm tracked the position of up to 5000 particles as they moved in a numerical representation of the flow field. The vertical profile of the time averaged longitudinal velocity was described by a log-law. At

each time step the particles were advected longitudinally at the local time averaged velocity and given a vertical movement which modelled the effect of the turbulence. The vertical motion had a randomly positive or negative direction and a step length size which depended on the position in the flow. For positions lower than the bottom 20% of the depth the step length was equal to the distance from the bed. For the rest of the depth, d, the step was fixed at $0.21d$. Sullivan noted that his step length distribution was a simplification of the actual motion in turbulent flow but his intention was to produce an approximate simulation. The model results were considered by Sullivan to agree qualitatively with his experimental data. Sullivan's model at first sight was very similar to the Taylor model but it has a very different basis. The step length in Sullivan's random walk model was chosen to represent a length scale of the turbulent motion rather than being based on the desired turbulent eddy diffusivity via equation 7.3. Sullivan's model is therefore closer in concept to the Langevin equation which attempts to model the motion of particles as they are affected by a turbulent flow. The Langevin equation is discussed in section 7.2.2 below.

Sullivan (1974) later published the results of particle tracking experiments in open channel flow that were performed in order to obtain data for use in his random walk models. Sullivan filmed the motion, in three dimensions, of 150 0.5mm diameter neutrally buoyant spheres in a 0.46m wide laboratory flume. The depth of flow was about 0.09m. Approximately 200 instantaneous positions were recorded at intervals of 0.07 seconds for each particle track. Sullivan observed that the particles followed radial paths through the water as they were being advected downstream and tried to measure the radius and angular velocity of the radial motion as functions of depth. The probability distribution of the radius of the particle tracks was found to be a Gamma function whose coefficients varied with the height above the bed. The angular velocity was a function of

the track radius but not of height. The average track radius was $0.097d$ which implied an average angular velocity of $11.2\frac{u_*}{d}$ (u_* being the bed shear velocity).

Allen (1982) developed a random walk model based upon Sullivan's ideas for modelling dispersion in estuaries. Allen's first formulations of the model used a random step length and step velocity that were functions of the height above the bed. Both the step length and step velocity reduced as a particle approached the bed. Allen stated that the reduced vertical mixing close to the bed that this implied caused two problems. Firstly the simulations did not give a uniform probability distribution of particles positions across the depth even when run for times such that the equilibrium zone should had been reached. Allen, referencing Batchelor et al (1956), stated that in a steady (two-dimensional) flow, once the particles have become mixed across the depth, a particle should have an equal probability of being at any position in the depth. This is equivalent to saying that the number of particles at a given depth should be constant along the flume. For a given longitudinal position a depth-wise concentration profile can exist but when averaged along the whole flume the concentrations should be equal. Clearly, such a particle concentration distribution can be used as a check on the validity of a given random walk model. Secondly the program spent a long time tracking those particles that were close to the bed because of the small step lengths and step velocities that the particles were subjected to. Allen overcame these problems by using a model with a fixed vertical step length and fixed step velocity derived from Sullivan's (1974) measurements. The vertical step velocity was $1.1u_*$ and the vertical step length was $0.1d$. Allen considered that her model gave qualitative agreement with other analyses of dispersion in estuaries.

Brockie, Allen & Guymer (1991) extended Allen's model to three dimensions in order to simulate mixing experiments in a large laboratory channel. Initially the

transverse step velocity was set to 1.2 times the vertical step velocity; this ratio being suggested by the LDA experiments of Knight & Shiono (1990). It was found that the particles rapidly reached the transverse limits of the channel and the transverse step velocity was reduced. Brockie et al do not give details of their model but for a fixed transverse step length and time step this would have had the effect of reducing the transverse mixing. With the reduced transverse step velocity the model under predicted lateral spreading compared to their experimental data. It was, however, considered to provide good qualitative agreement with the experimental data sets. This work is interesting because it attempted to make use of Sullivan's Lagrangian length scales (which it will be recalled were originally the radii of particle paths) and Knight & Shiono's Eulerian velocity measurements which were linear velocities. Unfortunately Brockie et al's paper was only a preliminary report and the implications of the reduction in transverse mixing implied by their lowering of the transverse turbulent velocity from the initial estimate was not addressed.

Heslop & Allen (1993) used a two-dimensional (longitudinal and vertical) random walk model to simulate dispersion in a reach of the river Severn. The model included a viscous sub layer at the bed into which the particles were not allowed to penetrate. The vertical step length was $0.1d$ and the vertical step velocity was $0.4u_*$ which was derived from measurements of the turbulent velocity perpendicular to the bed of the river. The agreement with concentration measurements was not good. Heslop & Allen believed this to be due to the three dimensional nature of the flow in the river and the effect of dead zones. They reported better agreement when dead zones were included in the model, particles being trapped and released from these zones caused the tails of the distributions to become longer. Heslop & Allen do not comment upon the effect of their choice of the vertical time step and step length. It is clear from equation

7.2 that a reduction in the step velocity while the mixture length is held constant leads to a reduction in the vertical mixing. It was shown in chapter six that the vertical mixing in natural open channels is often greater than in two dimensional flows (for which the Sullivan's step lengths and step velocities were derived). It would, therefore, have been useful if Heslop & Allen had compared the vertical mixing implied by their choice of length and velocity scales with the eddy viscosity implied by the velocity profile in their test reach.

7.2.2 The Langevin Equation

van Dop et al (1985), Etling et al (1986), Sawford (1986) and Pope (1987), when discussing turbulent dispersion in the atmosphere, made use of the Langevin equation:

$$du = -\frac{u}{T_L}dt + a^{1/2}dW \qquad (7.7)$$

which models the change, du, in velocity, u, of a particle for a time interval, dt. In the Langevin equation T_L is the Lagrangian integral time scale which describes how long turbulent velocities remain correlated, a is a flow dependant parameter which, for the special case of homogeneous turbulence takes the form: $a = 2\frac{\sigma_u^{\,2}}{T_L}$ ($\sigma_u^{\,2}$ being the turbulence intensity of the flow), while dW is, again for homogeneous turbulence, a random number with zero mean and a variance equal to dt. Etling et al reported difficulties in obtaining the parameters required by the Langevin equation. van Dop et al, Sawford and Pope discuss the modifications necessary to the Langevin equation in order to apply it to non-homogeneous turbulence. The Sullivan/Allen random walk model can be thought of as a simplification to the Langevin equation in which there is an absence of any correlation between turbulent velocities at successive time steps. This implies that

the time step chosen is so long that any correlation has decayed. The Langevin equation should therefore be able to model the dispersion of a solute closer to a source than the Sullivan/Allen random walk model.

7.2.3 Random walk with spatially varying diffusivity

Hunter et al (1993) discuss problems with the simple random walk models if the diffusivity were allowed to vary in space in that particles drifted to zones of low diffusivity. They suggested a transformation of the problem to a co-ordinate system where the diffusivity was constant. Kitanidis (1994) addressed the problem of variable diffusivity in a random walk solution of a one-dimensional advection dispersion equation and showed how the drift velocity due to the variable diffusivity could be evaluated.

Heemink (1990) and Heemink & Blockland (1995) also discuss random walk models with spatially varying diffusivity and introduce the use of stochastic differential equations in solving the depth averaged dispersion in a model of a Dutch estuary. These models have an advantage over the simple random walk in that they can correctly incorporate the spatial variation of the mixing coefficients.

7.2.4 Fractal Brownian motion

Fractal Brownian motion has been recently (Addison 1995) proposed as a method for modelling dispersion. Fractal Brownian motion differs from Brownian motion in that the standard deviation of a cloud of particles undergoing Brownian motion increases as the square root of time whereas this is not necessarily the case for particles undergoing fractal Brownian motion.

A dispersion coefficient, D_f, can be defined for particles undergoing fractal Brownian motion as

$$D_f = \frac{\sigma^{\frac{1}{H}}}{2t} \tag{7.8}$$

in which σ is the standard deviation of the particle positions and H is the Hurst exponent. A Hurst exponent of 0.5 is equivalent to regular Brownian motion. A particle in a fractal Brownian motion with a Hurst exponent less than or equal to 0.5 will tend to wander over all the plane in which it moves (assuming the motion is two-dimensional), this property being known as antipersistence. A Hurst exponent of greater than 0.5 leads to the behaviour known as persistence in which a particle would have a tendency to persist in the direction in which it was already moving. The motion of surface drifters in the ocean has been suggested as an example of persistent fractal Brownian motion (Addison 1995).

7.2.5 Previous work with random walk models: conclusions

Random walk models can be thought of as falling into three groups. The Langevin equation and the Sullivan/Allen model attempt to model the motion of particles as they are affected by turbulence. The Heemink & Blockland and Taylor models do not model the motion of particles as they are affected by turbulence but rather simulate the diffusion or mixing processes (that could include advection as well as turbulent diffusion). The fractal Brownian motion models offer an alternative method of describing dispersion data.

Of the various models the simple random walk models of Taylor and Sullivan/Allen were easiest to apply to the mixing measurements collected in the author's laboratory flume. The Langevin equation required Lagrangian velocity data which was

not available. The transverse and vertical mixing coefficients were measured as averages rather than as a function of the depth, transverse or longitudinal positions so that Heemink's stochastic models were unnecessarily complicated. Fractal Brownian motion models have not been widely reported in the literature and their creation would have involved a good deal of risky development. Also, the data from which the transverse mixing coefficients were derived did not exhibit any fractal Brownian motion characteristics, i.e. the assumption of a Hurst exponent of 0.5 was consistent with the data. Hence the fractal Brownian motion model was not needed to simulate the observed mixing. It is interesting to speculate that had a well defined secondary current structure been exhibited in the flume, its effects could have been simulated using a fractal Brownian motion approach. However, the question would then have arisen as to whether the secondary current should have been modelled as part of the bulk flow or as a persistent fractal Brownian motion.

7.3 The random walk model

In the following two sections the random walk models that were used to simulate the mixing in the laboratory flume are described along with the tests cases that were run to validate the models.

7.3.1 Two-dimensional random walk model

The two dimensional models used a fixed magnitude vertical step, Δy, whose length was related to the depth averaged eddy diffusivity, $\bar{\varepsilon}_d$, and the time step Δt using an equation similar to equation 7.3 The vertical step length was calculated from:

$$\Delta y = \sqrt{2 \cdot \bar{\varepsilon}_d \cdot \Delta t} \tag{7.9}$$

The algorithm used in the random walk was simple, and used 5000 particles all of which were initially located at the mid depth of a logarithmic velocity profile. At each time step the particles were advected longitudinally at the local time averaged velocity and given a vertical step (evaluated from equation 7.9) whose direction was random. Particles reaching the free surface or bed were reflected. During a run of the model the first two moments of the spatial particle distribution were calculated at a predetermined number of time intervals. At the end of a model run the data was imported into a graph plotting package and plots of the change of centroid and variance produced. These plots were used to define the times when the rate of change of the centroid and variance were linear, and to calculate the cloud velocity and longitudinal dispersion coefficient. It was found that 5000 particles were sufficient to ensure that the longitudinal dispersion coefficient differed by less than 4% between repetitions of a simulation. Because the particles had a constant vertical step they could only take up a limited number of positions in the depth which caused plots of the particle positions to have a banded appearance and, more importantly, meant that particles did not sample the entire velocity field. It was found that this banding of the particle positions could be overcome if instead of a single step length the step was chosen from a uniform distribution of lengths chosen such that the ensemble average step length was the same as that given by equation 7.9. The uniform distribution comprised 200 values equally spaced between $\pm 1.72\Delta y$. In the work described later a step length chosen in this way from a uniform distribution, is called a fuzzy step. For a simulation of dispersion in a plane shear flow with a logarithmic velocity profile a bed slope of 0.001 and a flow depth of 0.1m the use of a fuzzy step did not alter the longitudinal dispersion coefficient. The time step used for all the random walk model simulations reported in this thesis was set at 0.5s because preliminary testing suggested that it was a good compromise between the desire for a

very short, ideally zero (van Dam, 1994), time step and a long time step which reduced the number of iterations that the model required.

Hunter et al (1993) discussed the importance of the random number generator to a successful random walk model and stated that a poor random number generator can lead to non-linear growth of the variance of the particle positions even for the case of a homogeneous turbulence field where the growth should be linear. In order to test the performance of the random number generator being used a test programme was written that calculated the moments of 5000 particles undergoing a one dimensional random walk. It was found that the variance growth given by the model was linear and the diffusion coefficient was correct.

Prior to the use of a fixed step in the random walk model, the use of a step length related to the local mixing length was considered because: (a) it was possible to calculate the mixing length from a velocity profile and; (b) the vertical turbulent velocity could be estimated from other worker's measurements. This approach offered the prospect of developing (using equations 7.5 and 7.6 with a linear shear stress distribution) a random walk model without the necessity to measure the mixing coefficients. Initially, empirical mixing length and turbulence data were used to test such a model and the vertical step lengths and step velocities that resulted varied over the depth. When the model was run rather than becoming well mixed over the depth it was found that particles tended to drift towards the bed and free surface.

This tendency for a particle to walk down a gradient of decreasing step lengths is easy to understand. Particles that move from a given depth in the flow to a lower depth, where there is a smaller step length, have to make several successive upwards steps to regain their original position in the flow, but with the direction being random this cannot happen. Hence particles get trapped near to the bed and free surface. Incorporating a

variable step length into the random walk is equivalent to specifying a variable diffusivity and, as discussed in section 7.2.3, using a variable diffusivity is known to cause problems with simple random walk models.

The effect of a variable step length can also be seen in figure 4 of Sullivan's 1971 paper, in which a plot is given of particle concentrations that resulted from a random walk simulation of the spread of a plume of solute. Examining the plot shows a greater concentration of particles near the bed, although the dimensionless time (see chapter two) for which the particle cloud had been evolving was long enough for the particles to have become well mixed. It is now clear, of course, that this would be expected because the step length in Sullivan's model decreased linearly from a constant in the upper part of the depth to zero at the bed. Sullivan did not appear to have appreciated that his random walk model gave non-physical results. It will be recalled (section 7.2.1) that Allen originally developed random walk models that had a varying step length and step velocity. The diffusivity, implied by the product of the random step length and step velocity, varied over the depth. Allen abandoned the models because they had some problems, it is probable that these were due to the varying diffusivity. In retrospect it might have been obvious that the use of an equation similar to equation 7.3 with a non constant eddy diffusivity would be invalid because, as was indicated in section 7.2.1 the derivation of equation 7.3 relies on an implicit assumption of a homogeneous turbulence field.

There is evidence to suggest that the water industry is unaware of the unsatisfactory behaviour of the simple random walk models which employ spatially varying step lengths. For example: Danish Hydraulic Institute's commercial software PARTICLE employs such a technique (DHI,1991) and the sediment transport work of

Hoyal et al (1995) is contaminated by a vertical drift velocity (see Wallis & Moores, 1996).

The author has compared the eddy diffusivity, in a plane shear flow, implied by a Sullivan/Allen random walk model using Sullivan's recommended values of step length and velocity, a Taylor random walk model using the depth averaged eddy viscosity and a Sullivan /Allen model in which empirical equations were used to obtain the vertical turbulent velocity and the mixture length. The first Sullivan/Allen model implied a diffusivity of $0.051du_*$, the Taylor model had a diffusivity of $0.068du_*$, while the second Sullivan/Allen model had a diffusivity of $0.071du_*$. These results demonstrate why previous workers have been able to use different formulations of a simple random walk model to obtain good simulations of mixing in open channel flow (assuming they used a constant step length and step velocity). It does not matter how the step length and step velocity are arrived at as long as their product gives the correct degree of mixing.

7.3.2 Validation of the two-dimensional model

The two dimensional random walk model was tested against the longitudinal dispersion work of Elder (1959). The random motion in the model simulated the mixing in the vertical direction. From a limited number of runs, the rate of change of the longitudinal variance implied that the longitudinal dispersion was $6.49du_*$ which was 11% greater than Elder's theoretical value. Since the random walk model did not have exactly the same longitudinal time averaged velocity profile as Elder used in his analysis (because it was not possible to write Elder's profile explicitly) some difference between the analytical and simulated longitudinal dispersion coefficients may be expected. The random walk simulations also differed from Elder's analysis in the assumptions used for the vertical variation of the eddy diffusivity. In Elder's analysis the eddy diffusivity

distribution was parabolic; in the random walk it was assumed to be constant. In order to calculate a theoretical value of the longitudinal dispersion coefficient for the velocity profile and eddy diffusivity used in the random walk model the numerical integration technique given by Fischer et al (1979) (French 1985) was applied. The method solves the triple integral (equation 2.15) as a series of summations. This gave a longitudinal dispersion coefficient of $6.2du_*$ which is 6.5% greater than Elder's value and 4% less than the random walk model predicted.

7.3.3 Three-dimensional random walk model

The first three-dimensional random walk model was similar to the two-dimensional model except that the step lengths were related to the mixing coefficients rather than the eddy diffusivity. The vertical step was calculated from:

$$\Delta y = \sqrt{2 \cdot k_y \cdot \Delta t} \tag{7.10}$$

in which k_y was the vertical mixing coefficient measured in the flume.

The transverse step length, Δz, was chosen to give the desired transverse mixing using:

$$\Delta z = \sqrt{2 \cdot k_z \cdot \Delta t} \tag{7.11}$$

in which k_z was the transverse mixing coefficient measured in the flume. As with the two-dimensional model 5000 particles were used for each simulation, starting in the middle of the cross-section. As with the two-dimensional random walk model it was the direction of the particle motions that was the random element in this model and the effect of longitudinal turbulence was not simulated.

7.3.4 Validation of the three dimensional model

As a first test of the three-dimensional model a simulation was performed of the dispersion in an open channel flow with no transverse velocity profile. It was found that

the three-dimensional model gave, as expected, the same longitudinal dispersion coefficient as a two-dimensional simulation.

The vertical velocity profiles recorded in the laboratory flume showed a good deal of transverse variability. Hence in order to model the mixing in the laboratory flume it was necessary to incorporate the effects of this transverse shear. The vertical velocity profiles had been measured at seven transverse positions (125mm, 225mm, 325mm, 375mm, 425mm, 525mm and 625mm from the sidewall of the flume) and it was necessary to include the measured velocity field in the simulations. Before the mixing in the laboratory flume was simulated a preliminary series of model runs were undertaken to ensure that the basic features of mixing in open channel flows were correctly reproduced by the model. To do this a simplified version of the measured velocity field was created using a rough bed vertical velocity profile scaled at nine nodes (the seven used for the measurements and the two sidewalls), linear interpolation being used to calculate a particle's longitudinal velocity at intermediate locations. The scaling at each node was choosen to give a transverse velocity profile that took the form, in plan view, of a saw tooth pattern. The degree of transverse shear was varied between runs but the cross-sectional average velocity was held constant.

The rate of transverse mixing simulated by the preliminary model was not affected by the imposition of a transverse velocity profile but the longitudinal dispersion increased with increasing transverse velocity shear while the longitudinal dispersion was seen to be inversely proportional to the transverse diffusivity which was in accordance with the results of Fischer's (1966a) analysis. The influence of the vertical mixing coefficient in the three-dimensional model was also investigated and it was found that the longitudinal dispersion was due predominantly to the balance between the transverse velocity shear and transverse mixing and that the vertical mixing contributed little to the

overall longitudinal dispersion. However, increasing the vertical mixing tended, as expected, to reduce the longitudinal dispersion.

Following the identification of these trends, a quantitative test of the transverse component of the three-dimensional model was undertaken. In this the longitudinal dispersion coefficient obtained from the particle positions was compared to that given by Fischer's integral (equation 2.15) for the case of a depth-wise constant parabolic transverse velocity profile and a cross-sectionally constant transverse mixing coefficient. Clearly in these runs all the longitudinal dispersion was generated by the transverse shear and transverse mixing. The analytical solution of equation 2.15 for this case is:

$$D = \frac{u_q{}^2 dW^3}{210 A \varepsilon_t} \tag{7.12}$$

where u_q is the cross-sectional average flow velocity, d is the depth, W the width A the area of the flow and ε_t the depth averaged transverse diffusivity. The three-dimensional random walk model was therefore implemented with a uniform vertical velocity profile, a parabolic variation of the longitudinal velocity in the transverse direction, no vertical mixing and a constant transverse mixing coefficient. Three cases were run with different flow depths and the longitudinal dispersion from the simulation compared to the theoretical values. Agreement between the theoretical values of longitudinal dispersion and the results from the random walk model was better than 8%. The random walk simulations tended to over predict the longitudinal dispersion compared to the theoretical value.

7.3.5 The addition of dead zones to the random walk model

In order to simulate the trapping effect of dead zones, particles that reached the bed, and were considered to have entered a dead zone, were held for a number of time steps. The dimples in the bed of the laboratory flume covered 51% of the bed. For ease

of computation the particles in the random walk model that reached the bed were given a 50% chance of entering a dead zone. It was believed that the 2% difference between the average area of the dimples in the laboratory flume and the area of dead zones in the simulated flume was not significant when compared to the uncertainties in the mixing coefficients and dead zone transfer rates. The incorporation of an array into the program which was used to store flags identifying those particles that were in dead zones reduced the maximum number of particles that could be used to 4500. It will be appreciated that the random walk model differed from an ADE+DZ model, which uses a transfer rate to control the solute mass in a dead zone, because in the random walk model particles could only be trapped for an interval of time.

The time that the particles remained trapped in a dead zone was taken to be the inverse of the dead zone transfer rate measured in chapter 4. There is a theoretical justification for this choice; the dead zone transfer rate equation (equation 2.18) gives the dead zone concentration as a function of time as:

$$c_d(t) = c_i e^{(-k_d t)} \tag{7.13}$$

in which c_i is the initial concentration in the dead zone. The dead zone model (implied by equation 2.18) assumes that there is no concentration profile within the dead zone, which is equivalent to a continuously stirred cell. For a discrete input the concentration in such a cell is given by (Rutherford 1994):

$$c(t) = \frac{M}{V} e^{(-t/T)} \tag{7.14}$$

in which M is the mass of tracer added to the cell, V is the cell volume and T is the residence time in the cell (which is the cell volume divided by the flow rate through the cell). A comparison of equations 7.13 & 7.14 shows that the dead zone residence time is the reciprocal of the transfer rate. In order to distinguish between the random walk

model and the continuously stirred cell the time for which a particle is held once it has entered a dead zone is called the dead zone trapping time.

7.3.6 Validation of the dead zone model

Because the inclusion of dead zones into random walk models that simulated measured longitudinal dispersion had not been reported before (although Allen 1991 began to investigate the effects of including dead zones) it was felt to be particularly important to validate these dead zone random walk models.

The incorporation of dead zones into the two-dimensional random walk was validated by comparison with the data of Valentine & Wood (1977). The flow depths and bed slope used were those given by Valentine & Wood. A rough wall velocity profile was used in which the equivalent sand grain roughness was adjusted so that the cross-sectional averaged velocity equalled Valentine & Wood's discharge velocity. Three flow depths were used and the model run with four values of trapping time ranging between 0 and 4 seconds. The effect of the trapping time was to reduce the cloud velocity (obtained from the rate of change of the centroid of the particle positions) and to increase the longitudinal dispersion coefficient as Valentine & Wood's and Denton's (1990) analytical work predicted. The cloud velocity and dispersion coefficients were linearly regressed against the trapping time and the results are given in Table 7.1 (the coefficients of determination, r^2, were better than or equal to 0.98). The cloud velocity for the no dead zone case was within 2% of the discharge velocity. The random walk simulation with no dead zones gave a dispersion coefficient within 22% of that predicted by Elder's analysis for the highest flow simulated and better than 8% for the other two flows. The relatively large difference between the analytical result and the random walk model at the highest flow rate was inexplicable. The trapping time required by the random walk model to reproduce the non-dimensional longitudinal dispersion coefficients measured by

Valentine & Wood is compared to the dead zone transfer coefficient, k_a, that they measured for their dead zones in Table 7.2. Clearly the trapping time required by the random walk model was approximately the inverse of the dead zone transfer rate as was predicted in section 7.3.3.

A comparison was made of the behaviour of a random walk models of two flows: one with dead zones, a uniform depth wise and a parabolic width wise velocity profile and a flow with dead zones, a logarithmic depth wise and a sawtooth transverse velocity profile. It was found that for the simulation of the parabolic transverse velocity profile that the longitudinal dispersion fell with increasing dead zone trapping time, while for the simulations with a transverse and a vertical variation of longitudinal velocity the change of longitudinal dispersion with dead zone trapping time was found to be a function of the degree of the transverse non-uniformity. For a flow with a relatively weak transverse variation in longitudinal velocity the rate of change of longitudinal dispersion increased with increasing dead zone trapping. The rate of change reduced as the transverse variation of the flow was increased and eventually the longitudinal dispersion began to decrease with any further increase in the dead zone trapping time. The results of these simulations suggested that the longitudinal dispersion in the presence of dead zones depended upon the relative strength of the transverse and vertical velocity shear. With little or no transverse velocity shear an increase in trapping led to an increase in longitudinal dispersion, a flow with strong transverse shear and little or no vertical shear, however, showed a decrease in longitudinal dispersion for a similar increase in dead zone trapping.

7.4 Application of the random walk model to the flume

The random walk model was used to simulate the solute transport in the laboratory flume firstly with the assumption that the flow was longitudinally uniform and then with the longitudinal non-uniformity of the flow incorporated.

Three flow rates were used in the simulations 7l/s, 13l/s and 26l/s because full surveys of the velocity field were performed for these flow rates. The simulations used dead zone trapping times of 1.5s for the 7l/s flow and 1.0s for the flows of 13l/s and 26l/s, these trapping times being suggested by the dead zone transfer measurements of chapter five.

7.4.1 Uniform flow

The three-dimensional random walk model was used to simulate the longitudinal dispersion previously measured in the laboratory flume. The (cross-sectionally constant) vertical and transverse step lengths were calculated from equations 7.10 and 7.11, using the mixing coefficients measured in the flume. After substituting for the vertical and transverse mixing coefficients equations 7.10 and 7.11 became:

$$\Delta y = \sqrt{2 \cdot 0.1 \cdot d \cdot u_{*_b} \cdot \Delta t} \tag{7.15}$$

$$\Delta z = \sqrt{2 \cdot 0.4 \cdot d \cdot u_{*_b} \cdot \Delta t} \tag{7.16}$$

The side wall corrected bed shear velocity was used in these equations, and the random walk model was run with the flow fields that had been measured at 9m, 15.5m and 22m from the flume inlet. Each run simulated the dispersion in a uniform open channel flow with one of the measured velocity fields. As in the earlier tests of a three-dimensional random walk the velocity profiles were specified at nine transverse positions and linear

interpolation was used to evaluate the velocity if a particle took up an intermediate location.

After the particles become well mixed over the depth and width of the computational representation of the flume the average particle velocity, in the absence of dead zones, should equal the cross-sectional average velocity (Batchelor et al 1956); this gives a method of checking the random walk model. The cloud velocity (the mean particle velocity) was compared to both the cross-sectional average flow velocity, u_q, in the flume (calculated from the stage discharge equation) and the average integration of the measured velocity profiles, u_{av} (calculated from the average integrated discharge, see column 5 Table 4.1, and the relevant flow area). The results are given in Table 7.3. In general the cloud velocity, u_c, was lower than the cross-sectional average velocity, u_q, and both were lower than the average of the integrated velocity profiles, u_{av}. The cloud velocity was within -13% to +7.9% of the cross-sectional average and within -22% to 4% of the average of the integrated profiles. The approximations made when integrating the measured velocity profiles mean that u_{av} is in general a poorer measure of the cross-sectional average velocity than the cloud velocity is.

The incorporation of a dead zone trapping time caused the centroid velocity of the particle cloud to lag the no dead zone velocity by about 10% for each 1s of trapping. Typical plots of the centroid and variance of the particle position distributions are shown in Figures 7.1 & 7.2 respectively, these are from simulations using the velocity field at 15.5m in the flume for a flow rate of 26l/s. The moments of the particle distributions were calculated every two seconds for all the runs of the random walk model. The centroid and the variance of the particle positions increase with time. Both exhibit an initial non-linear rate of change (of shorter duration and less obvious for the centroid position compared to the variance) before a linear rate of change with time. It is seen

(Figure 7.1) that the centroid cloud velocity is reduced as the trapping time in a dead zone is increased and that the variance (Figure 7.2) is increased with increasing dead zone trapping time. Both of these effects are consistent with the theoretical analyses of Denton (1990) and Valentine & Wood (1977).

The results from simulations using the velocity fields measured for a flow of 7l/s are shown in Figure 7.3; for all three flow fields (9m, 15.5m & 22m) the longitudinal dispersion decreases with an increase in dead zone trapping time. The results from similar random walk simulations for a discharge of about 13l/s are shown in Figure 7.4; the longitudinal dispersion exhibits first a reduction then an increase with increasing dead zone trapping time but there is no definite trend. Finally results from random walk simulations for a discharge of about 26 l/s are shown in Figure 7.5; the longitudinal dispersion increases with increasing dead zone trapping time. Although the relationship between dispersion and trapping time depended on the flow rate the results were consistent between velocity fields at a particular flow rate.

The behaviour of the flume simulations was compared to the results of the investigation of the three-dimensional random walk (section 7.3.6), in which the relationship between longitudinal dispersion and dead zone trapping time was found to be dependent on the relative strength of the transverse and vertical velocity shear. This comparison suggested that the vertical velocity shear, relative to the transverse velocity shear, was strong at the highest flow rate and that the relative strength of the vertical shear reduced with decreasing flow rate.

In chapter four it was described how the transverse velocity variation, u', was quantified for each of the measured flow fields and the results (given in Table 4.2) showed that the transverse velocity shear of the flow increased with increasing flow rate. The values of u' were then used to calculate longitudinal dispersion coefficients using a

numerical integration of equation 2.15 (French 1985, Fischer et al 1979). The average (for the three velocity fields at a particular flow rate) of the longitudinal dispersion coefficients obtained from the numerical integration of equation 2.15 are compared to the average of the longitudinal dispersion coefficients from the random walk model in Table 7.4. The random walk results are from those simulations with the dead zone trapping time implied by the dead zone transfer experiments. The transverse mixing coefficient used for the random walk model and numerical integration technique was the same; namely that implied by the mixing experiments. Agreement between the two techniques and the measured longitudinal dispersion was best at the lowest flow rate. For the higher flow rates the integral method, which ignored the contribution of the vertical velocity shear and dead zones, predicted less dispersion than the random walk model which included the vertical velocity profile and the dead zone trapping effect. The longitudinal dispersion coefficients from the random walk simulations and the integral method are shown along with the measured longitudinal dispersion coefficients in Figure 7.6, it will be noted that the integral method was not able to predict the measured increase in longitudinal dispersion with increasing flow rate. Whilst the uniform flow random walk simulations under predicted the measured longitudinal dispersion they were able to reproduce qualitatively the increase in longitudinal dispersion with increasing flow rate. The improvement in the predicted dispersion coefficients of the random walk simulations over the integral method increased with increasing flow rate. This also suggested that the vertical velocity shear and dead zones made an increasing contribution to the longitudinal dispersion in the laboratory flume as the flow rate was increased.

The influence that the inclusion of dead zones into the random walk model had on the predicted concentration profiles was investigated. A three-dimensional random walk model run at a flow rate of 26l/s and using the 22m velocity field was used to

produce concentration profiles by summing the number of particles at each of a number of longitudinal positions. Figure 7.7 shows the predicted spatial concentration distribution (in arbitrary units) 200 seconds after an initial point release of tracer for a case with no dead zones and for a case where the dead zones had a 1 second trapping time. Two methods were used to obtain the standard deviation of the simulated concentration profiles. Firstly, the equation for a Gaussian distribution was regressed to both profiles using the non-linear regression facility of the Sigma Plot graphing package. The Gaussian fitted by Sigma Plot is shown on Figure 7.7 and it will be noted that the fit to the data is good. Secondly, the variance was also obtained from a calculation of the moments of the concentration profiles. The difference in the standard deviation found using the two techniques was about 1% which was taken to validate the use of a Gaussian as a curve fit to the data. That the concentration profiles given by the random walk with dead zones were Gaussian was in agreement with the work of Valentine & Wood (1977) and Denton (1990) who stated that the effect of dead zones was to increase the initial skewness of the concentrations and reduce the rate at which the skewness decays, but that spatial concentration profiles eventually become Gaussian. Some workers (e.g. Graf 1995) have taken the presence of long tails on measured concentration profiles to indicate the presence of dead zone trapping. In fact long tails, or skewness, can only really be taken to indicate that the tracer material has not been in the flow long enough for the skewness to decay.

In chapter two the various stages that a discrete dose of a tracer material evolves through as it disperses in an uniform flow were introduced (see Figure 2.1). The time required for the change of variance in the uniform flow random walk model results to become linear was noted for all the runs. This time was taken to be the end of the advective period in the dispersion process. Equation 2.16 was used to calculate the non-

dimensional length, α, using the measured values of k_z and u_q and putting L_t equal to the half width.

The average values and range of α for the three flow rates and three dead zone trapping times are given in Table 7.5. Rutherford (1994) gives values of the constant α between 0.3 and 2.8 for laboratory flumes with larger values of the constant being for flumes with a higher percentage of dead zones. The author's data fit in the lower end of the range. However, an increase in dead zone trapping in the random walk model did not lead to an increase in α as expected from Rutherford and the work of Valentine & Wood (1977), although the skewness predicted by the random walk model did reduce more slowly when dead zones were present than when they were not. It is probable that the limited range of dead zone trapping times used and the difficulty of estimating the onset of the linear change of variance are the reasons the expected increase in α with increasing dead zone trapping is not evident in these results.

7.4.2 Non-uniform flow

The three-dimensional random walk model was then modified to include the longitudinal variation in the velocity and depth in the flume. The depth of the flow in the flume varied between the three positions used for the velocity surveys because of changes in the bed slope and the draw down of the water surface due to the free overfall at the end of the flume. The depth between 15.5m and 22m from the inlet fell, rose and fell again; whereas between 9m and 15.5m the depth fell at an approximately constant rate. It would have been possible to input the depth at 2m sections along the channel as a detailed survey of the depth was available. However, as velocity profiles were only available at three locations a linear interpolation for both the depth and velocity was used to obtain conditions at longitudinal positions between the 9m and 15.5m and the 15.5m

and 22m velocity fields. The dead zone trapping times used in the non-uniform flow simulations were the same as those used in the uniform flow simulations.

Both the uniform flow and non-uniform flow random walk simulations used a point source of particles; in order to calculate the longitudinal dispersion from the change of variance it was necessary for the particles to be well mixed and the mixing to be occurring within the equilibrium zone. For the uniform flow simulations it was possible to allow the simulations to continue until the rate of change of the centroid and variance of the particle positions was linear and take this as evidence that the mixing processes were occurring within the equilibrium zone. The uniform flow simulations indicated that over 10m of flume was required to reach the equilibrium zone. It was, therefore, decided to provide 26m of uniform flow for the particles to mix in before they reached the beginning of the non-uniform flow field. The 9m, 15.5m and 22m profiles from the laboratory were therefore located at 35m, 41.5m and 48m in the computational flume. A uniform flow was used as a run out section from the 48m point of the computational flume (the 22m section of the laboratory flume).

The results of the simulations are plotted in Figures 7.8 to 7.13; these show a reduction in cloud velocity with increasing dead zone trapping time as was seen in the constant flow field simulations. Whilst the change of centroid was smooth it was not linear, which reflected the acceleration that the water experienced as it approached the overfall of the flume. The plots of the longitudinal variance also differ from those obtained during the uniform flow simulations, they have a less linear change in variance. For the lowest flow rate (Figure 7.9) the variance of the particle positions towards the end of the simulation was lower for increasing dead zone trapping time, whereas for the other two flows the variance was increased by an increase in dead zone trapping time.

In order to obtain the rate of change of longitudinal variance the centroid position was used to determine the times when the centroid of the cloud was between 35m and 48m in the computational flume, these limits are shown as dashed lines in Figures 7.9, 7.11 & 7.13. These times were used to determine the limits of the variance data used in the regression for the rate of change of the variance, which ensured that the longitudinal dispersion coefficients were calculated for a cloud travelling along a simulation of the laboratory flume. Because of the non-linear change of variance that can be seen in Figures 7.9, 7.11 & 7.13 the calculated longitudinal dispersion coefficient depended upon the locations chosen to evaluate the rate of change. If 20m and 50m in the computational flume were chosen the longitudinal dispersion coefficients obtained from a linear regression to all the variance data between those two points differed by ±3% from the value obtained if a regression were taken to the data between the dashed lines. Using the individual variances at 35m and 48m to calculate the rate of change of variance, rather than regressing a line to all the data, gave results within 8% of the linear regression.

The dispersion coefficients from the non-uniform flow field simulations are plotted with those from the uniform flow simulations in Figures 7.14 to 7.16. For the 26l/s flow case shown as Figure 7.16 the non-uniform flow simulations implied an increase in dispersion of about 50% compared to the uniform flow field simulations. The 13l/s case, Figure 7.15, gave slightly less dispersion from the non-uniform flow simulation than from the uniform flow simulation; the dispersion was approximately constant with dead zone trapping time for the uniform flow case and it reduced with increasing trapping time for the non-uniform flow simulation. The dispersion reduced with increasing dead zone trapping time for both the uniform and non-uniform simulations of the 7l/s flow shown in Figure 7.14 but the non-uniform flow simulation predicted slightly lower values of longitudinal dispersion. Repeating the 26l/s run four

times for a one second dead zone trapping time suggested an uncertainty of about 6% in the value of the longitudinal dispersion if a single run were used to simulate the measurements in the laboratory flume. It will be recalled that in chapter four a measure of the transverse variability of the depth averaged longitudinal velocity was calculated and that this showed that only for the highest flow rate (26l/s) did the transverse variability significantly increase with longitudinal position in the flume. It is likely that the non-uniform flow simulations only differ from the uniform flow simulations at the highest flow rate because it is only at this flow that there was a significant longitudinal change in the transverse variability of the velocity field.

As the time step used for all the simulations was 0.5s, increasing the flow rate led via a rise in du_* to an increase in step length. The transverse step length for the highest flow rate (40mm) was possibly too large to enable particles to sample the full extent of the velocity shear that occurred between measured velocity profiles (a minimum distance of 50mm apart) and close to the boundaries. The non-uniform flow random walk was therefore run with a fuzzy step (see section 7.3.1). The results of the fuzzy step simulations are plotted with the fixed step runs on Figures 7.14 to 7.16. Little or no difference was noted for the lower two flows, but for the highest flow rate the fuzzy step simulations gave higher levels of longitudinal dispersion than the fixed step runs. This greater longitudinal dispersion was consistent with the particles being better able to sample the velocity shear and allowed the results of the fuzzy step simulations to be closer to the measured data than those from the fixed step simulations.

In Figure 7.17 the measured dispersion coefficients are plotted along with the results from the random walk simulations and Fischer's integration method. The random walk data is that implied by a 1s trapping time for the 26l/s and 13l/s flows and 1.5s for the 7l/s flow. It will be noted that all three simulation techniques gave very similar results

at the lowest flow. As the flow rate, and hence du_* increased the integration technique suggested that the longitudinal dispersion did not increase, while the uniform and non-uniform flow random walk models both showed an increase in dispersion. The rate of increase of the longitudinal dispersion implied by both the fixed and fuzzy step non uniform flow random walk models was greater than that of the uniform flow simulations and was closer to that of the measured data. All the random walk models under predicted the longitudinal dispersion at flows of 13l/s and 26l/s. The simulated longitudinal dispersion is compared to the regression ($D = 0.02 + 65.39du_*$) to the measured data in Table 7.6. For the integral equation, the uniform flow and the non-uniform flow random walk models the difference between the simulations and the predictions from the regression increases with increasing flow rate. For the fuzzy step random walk the difference between the simulated and measured longitudinal dispersion coefficients are fairly independent of flow rate. The relative performance of the models can be understood as follows; at the lowest flows the transverse velocity shear dominated the dispersion processes, which meant that the depth averaged integration technique predicted the same longitudinal dispersion coefficient as the three-dimensional random walk models did. As the flow rate increased the longitudinal variation in the flow, the vertical velocity shear (and possibly the dead zone trapping) became increasingly influential. The random walk model was able to include these effects while the integral technique was not. It would appear that only for the highest flow did the longitudinal non-uniformity in the velocity field affect the longitudinal dispersion process as it was only for this flow rate that there was a notable difference between the results of the uniform and non-uniform simulations. This latter point may be expected if it is recalled that the flume was operated with a fixed tailgate which meant that the draw down caused

by the overfall became more influential and the flow less uniform as the flow rate was increased.

7.5 Conclusions

The work described in this chapter has demonstrated that a simple random walk model can be used to predict longitudinal dispersion in open channels that include dead zones. The work is significant because while previous workers have added dead zone trapping to random walk models the present work is the first time that measured dead zone transfer rates, mixing coefficients and velocity profiles have been used in a random walk model to predict longitudinal dispersion and the predictions compared to measured longitudinal dispersion data. Use of the random walk model to simulate the longitudinal dispersion experiments allowed valuable insights into the mixing processes in the laboratory flume, conclusions arising from the modelling work are given in the following paragraphs.

The random walk model can give better predictions of the longitudinal dispersion coefficients in the flume than Fischer's numerical integration technique. Whilst Fischer's integral technique predicted that the longitudinal dispersion coefficient was not a function of flow rate, the random walk model correctly predicted a rise in dispersion coefficients with flow rate.

The random walk simulations showed that, for the laboratory flume at least, the vertical velocity shear and longitudinal non-uniformity made important contributions to the longitudinal dispersion. Previously it had been assumed that for three-dimensional flows, such as in the laboratory flume, that transverse velocity shear was the dominant dispersion mechanism. For the laboratory flume the influence of the vertical velocity

shear and longitudinal non-uniformity varied with flow rate. At low flows the transverse velocity shear was the dominant dispersion mechanism, as the flow rate increased the vertical velocity shear and longitudinal non-uniformity made an increasing contribution.

The random walk simulations showed that the high transfer rates between the dimple dead zones and the main flow meant that the dead zone had little effect on the longitudinal dispersion coefficients. The random walk simulations were consistent with experiments such as those of Valentine & Wood (1977) which showed that for flows with significant dead zone trapping times that the dead zone effect can come to dominate the dispersion.

The random walk simulations were in agreement with analytical work (Valentine & Wood 1977 and Denton 1990) that predicts that Gaussian spatial concentration profiles eventually develop in flows that have dead zones. This implies that the existence of skewness in spatial concentration profiles is not evidence of the existence of dead zones but rather can only be taken as evidence (in a uniform flow) of insufficient time having elapsed for the skewness to have decayed.

Depth (m)	Volumetric Flow Velocity (m/s)	Centroid Velocity as a function of trapping time (DT) (m/s)	D/du_* as a function of trapping time (DT)
0.010	0.156	0.155-0.0156DT	6.73+17.45DT
0.024	0.25	0.220-0.0170DT	5.80+12.25DT
0.053	0.373	0.370-0.037DT	6.54+12.66DT

Table 7.1 Output of random walk model as a function of trapping time.

Depth (m)	D/du_* Measured	D/du_* Random Walk	Trapping time (s)	1/ka (s)
0.010	14.6	14.6	2.0	1.7
0.024	18.2	18.2	1	1
0.053	12.2	12.5	0.5	0.7

Table 7.2 Comparison of dead zone trapping time and transfer rate.

Q (Position)	u_q (m/s)	u_c (m/s)	$(u_c-u_q)/u_q$ (%)	Integrated discharge (see Table 4.1) u_{av} (m/s)	Percentage difference $(u_c-u_{av})/u_{av}$
7.1l/s (9m)	0.189	0.204	7.9	0.197	3.6
7.1l/s (15.5m)	0.210	0.190	-9.5	0.210	-9.5
7.0l/s (22m)	0.205	0.195	-4.5	0.210	-7.1
13.4l/s (9m)	0.255	0.26	2.0	0.270	-3.7
13.3l/s (15.5m)	0.271	0.260	-4.1	0.332	-21.8
13.3l/s (22m)	0.290	0.267	-7.9	0.321	-16.8
25.7l/s (9m)	0.347	0.327	-5.8	0.361	-9.4
26.0l/s (15.5m)	0.391	0.340	-13.0	0.381	-10.8
26.0l/s (22m)	0.405	0.372	-8.1	0.412	-9.7

Table 7.3 Cross-sectional averaged velocities from the random walk model.

du_* (m^2/s)	Long' Disp' (m^2/s)	Integral equation (m^2/s)	uniform flow random walk (m^2/s) Average of 9,15.5 & 22m
0.00124	0.101	0.089 (-12%)	0.085 (-16%)
0.00218	0.163	0.080 (-51%)	0.107 (-34%)
0.00395	0.278	0.080 (-71%)	0.122 (-56%)

Table 7.4 Comparison of random walk and Fischer's integral equation for uniform flow.

Q (l/s)	No Trapping time	1s Trapping time	2s Trapping time
7	0.37+/- 0.03	0.43+/- 0.02	0.41+0.07,-0.05
13	0.64+0.12,-0.14	0.58+0.09,-0.05	0.63+/-0.01
26	1.07+0.15,-0.16	0.82+0.21,-0.23	0.90+0.4,-0.5

Table 7.5 Non-dimensional length of the advective zone from the random walk model.

du_* (m^2/s)	Long' Disp' (m^2/s)	Integral equation (m^2/s)	uniform flow random walk (m^2/s) Average of 9,15.5 & 22m	non-uniform flow random walk (m^2/s)	fuzzy step non-uniform flow random walk (m^2/s)
0.00124	0.101	0.089 (-12%)	0.085 (-16%)	0.077 (-24%)	0.066 (-35%)
0.00218	0.163	0.080 (-51%)	0.107 (-34%)	0.097 (-40%)	0.102 (-37%)
0.00395	0.278	0.080 (-71%)	0.122 (-56%)	0.158 (-43%)	0.185 (-33%)

Table 7.6 Comparison of the random walk models and Fischer's integral method for uniform and non-uniform flow.

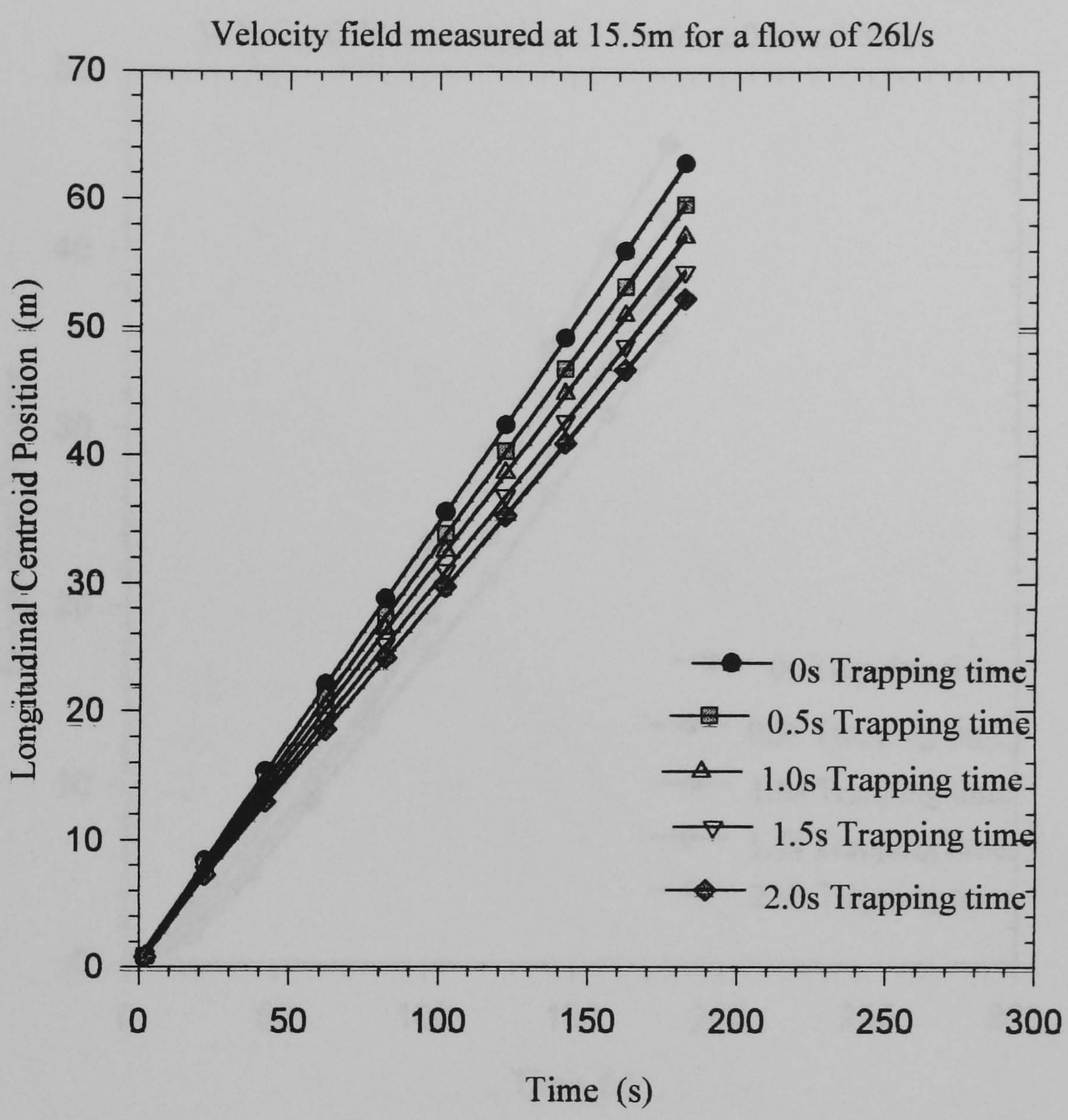

Figure 7.1 Rate of change of longitudinal centroid for a flow of 26l/s

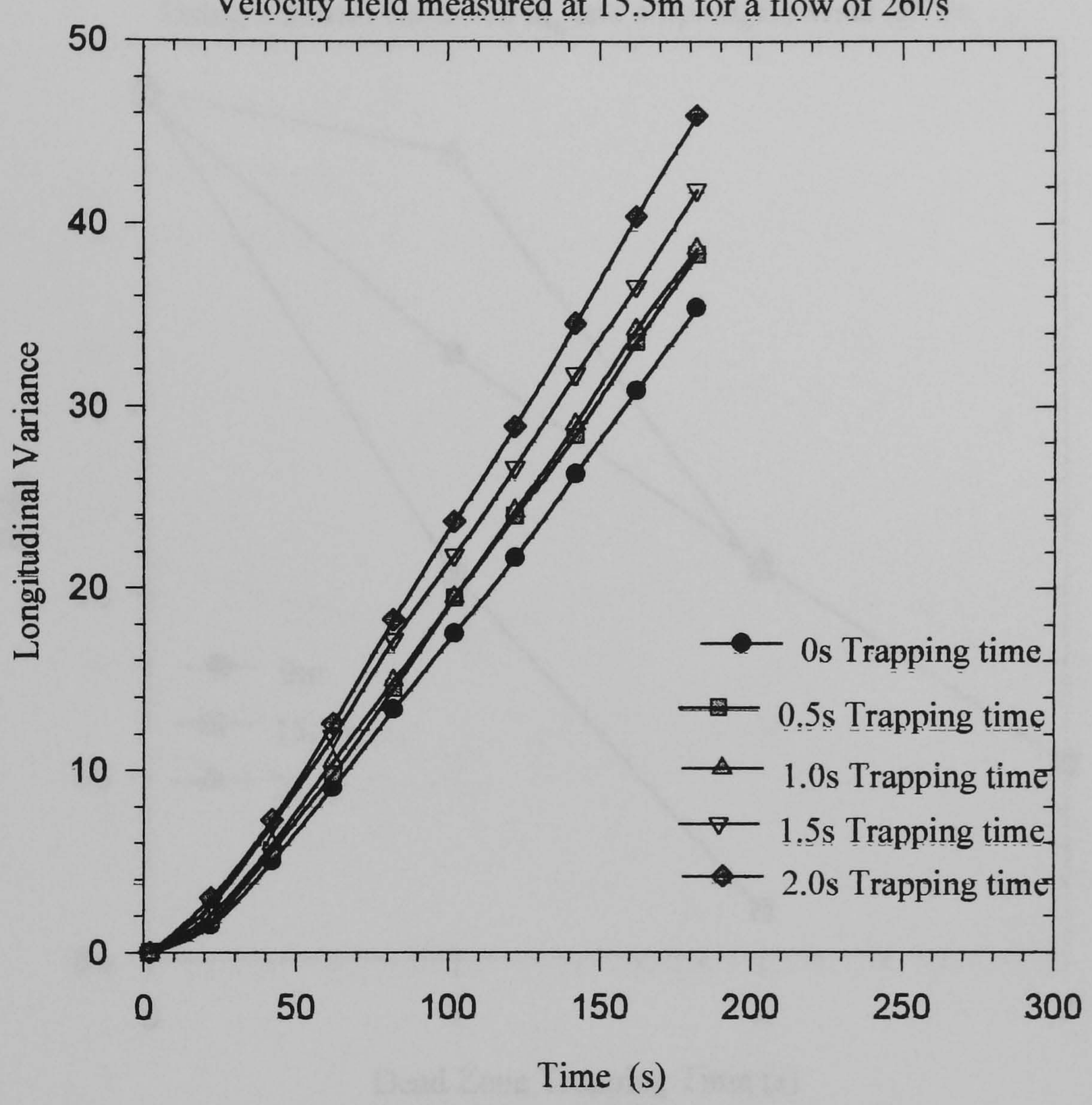

Figure 7.2 Rate of change of longitudinal variance for a flow of 26l/s

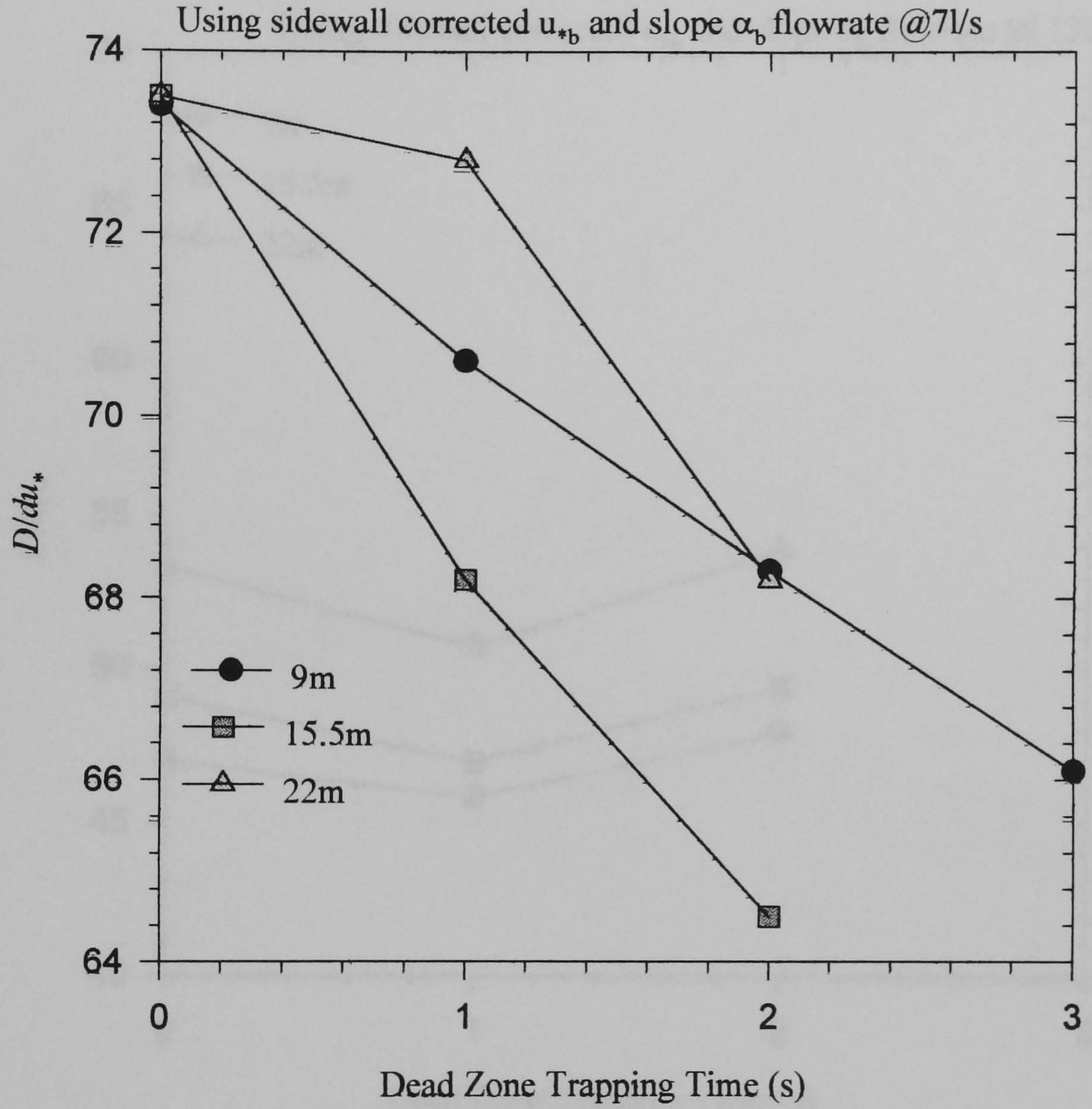

Figure 7.3 Dispersion as a function of trapping time for a flow of 7l/s

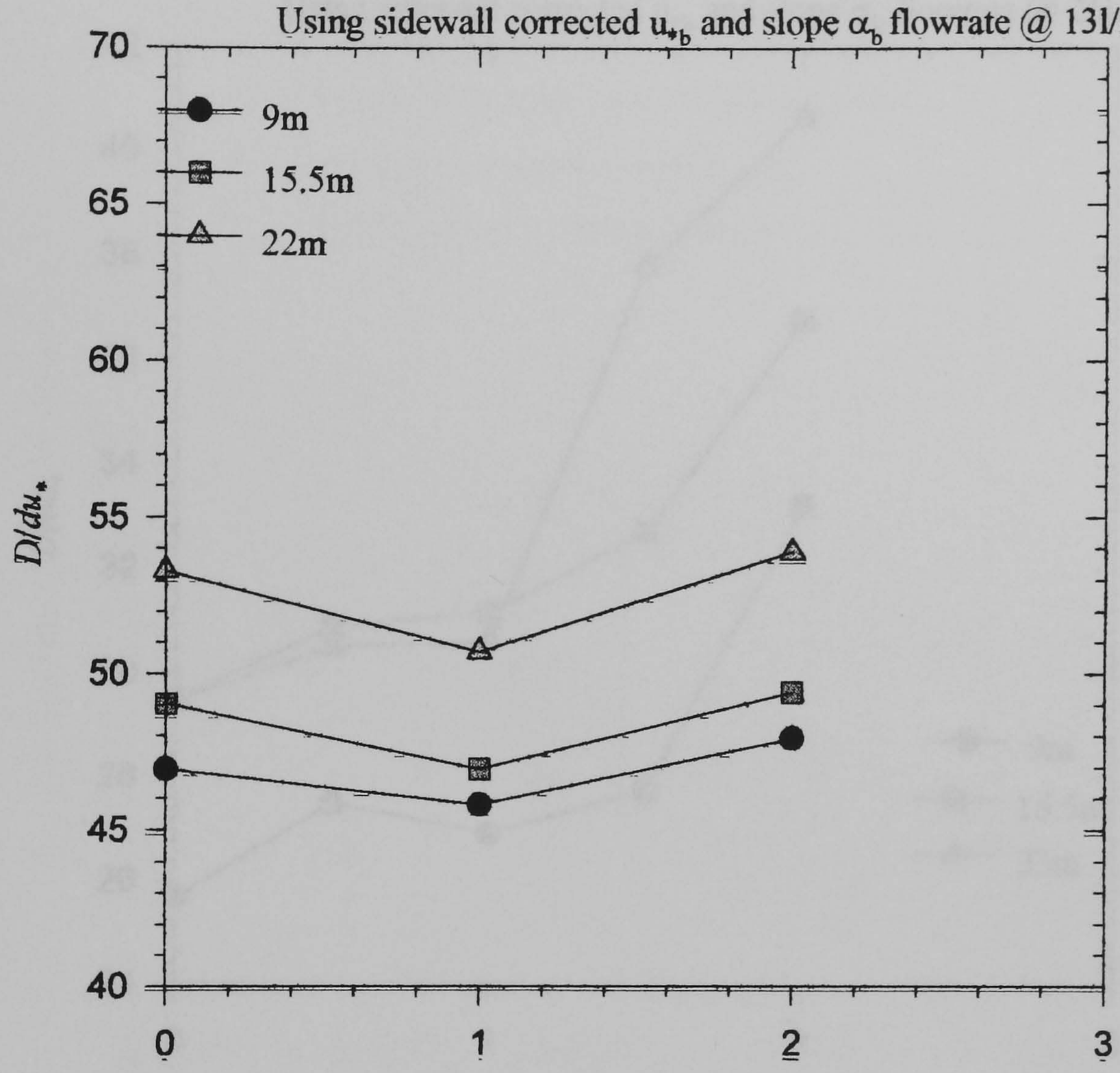

Figure 7.4 Dispersion as a function of trapping time for a flow of 13l/s

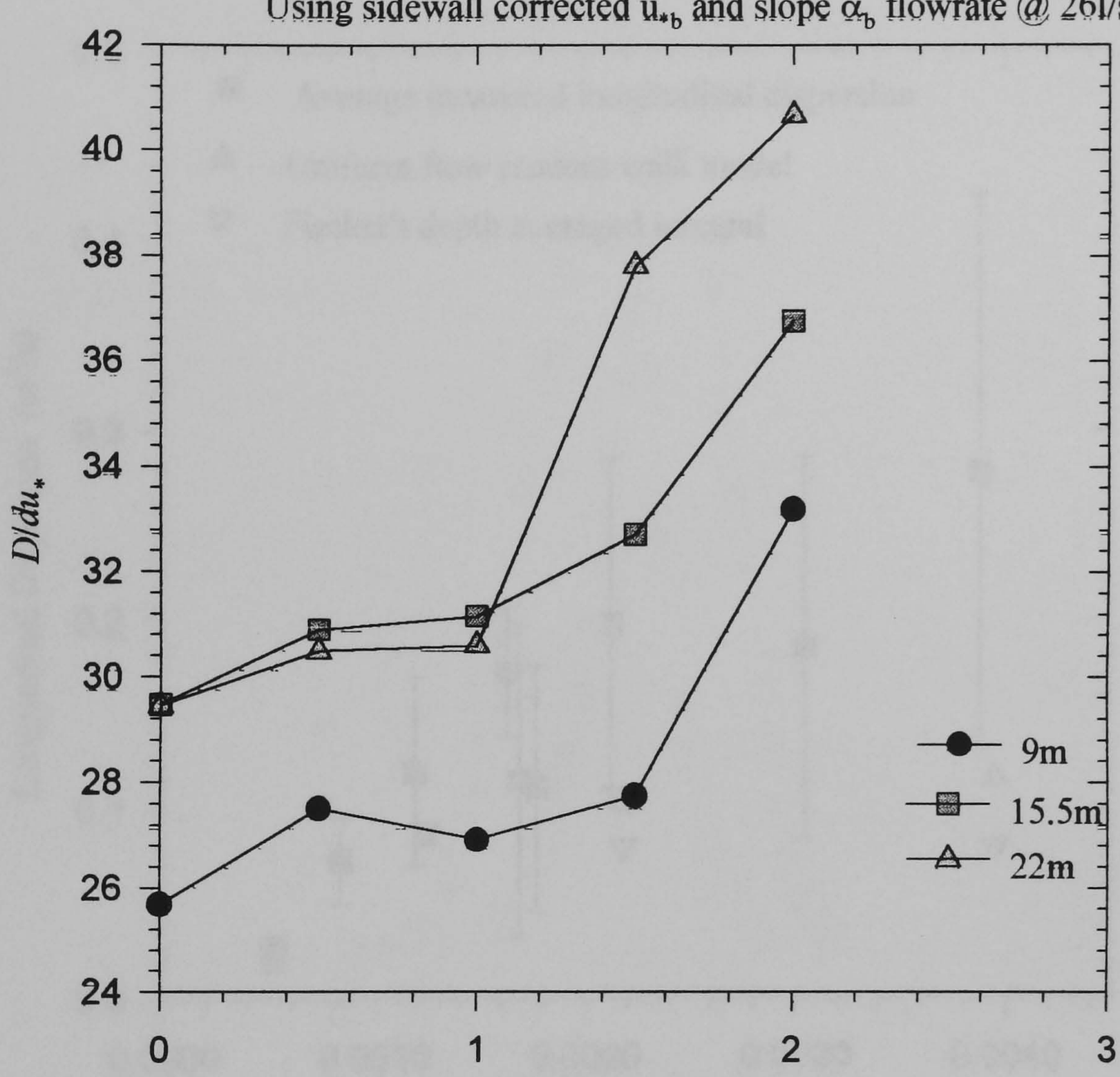

Figure 7.5 Dispersion as a function of trapping time for a flow of 26l/s

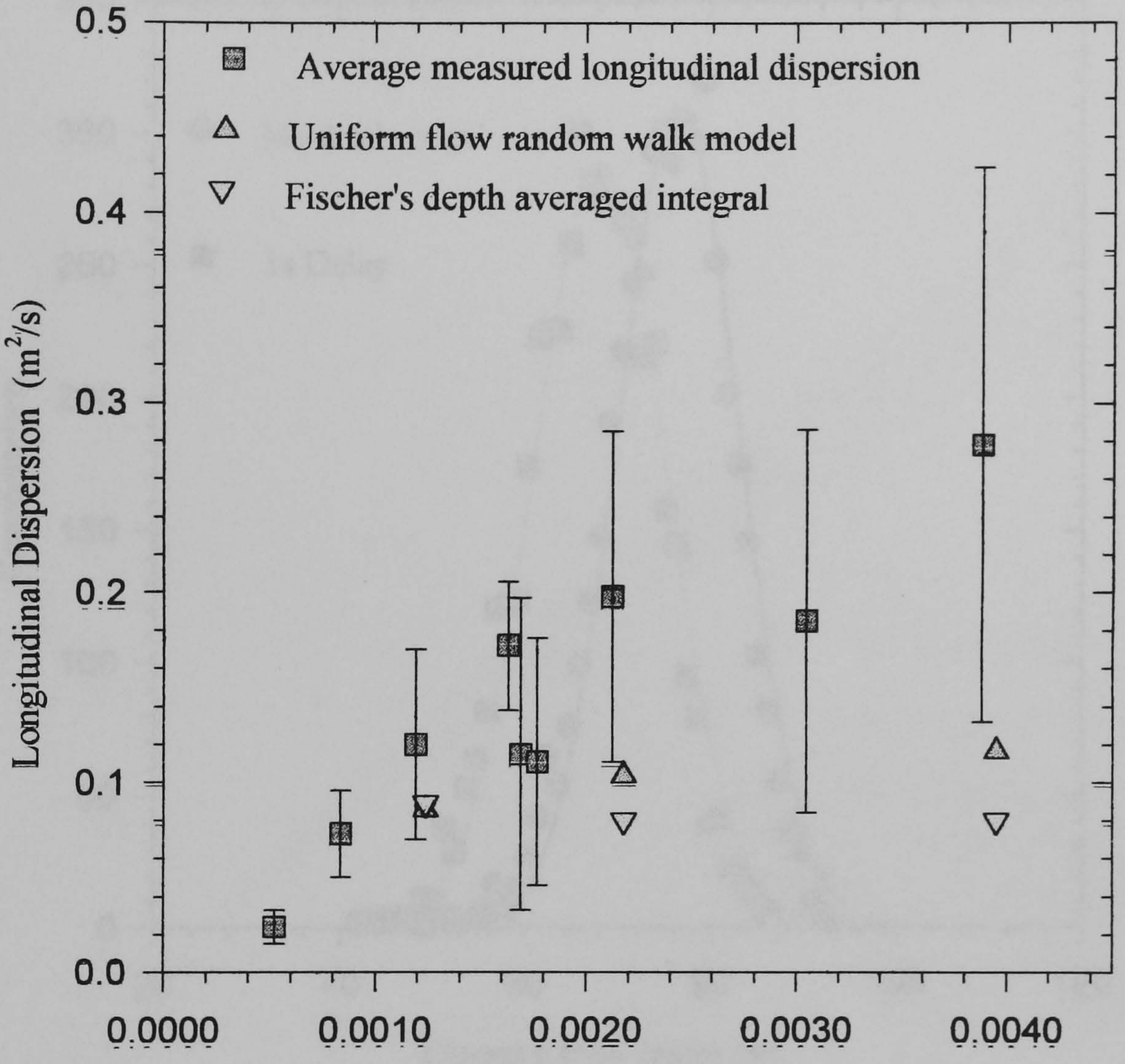

Figure 7.6 Measured & simulated longitudinal dispersion

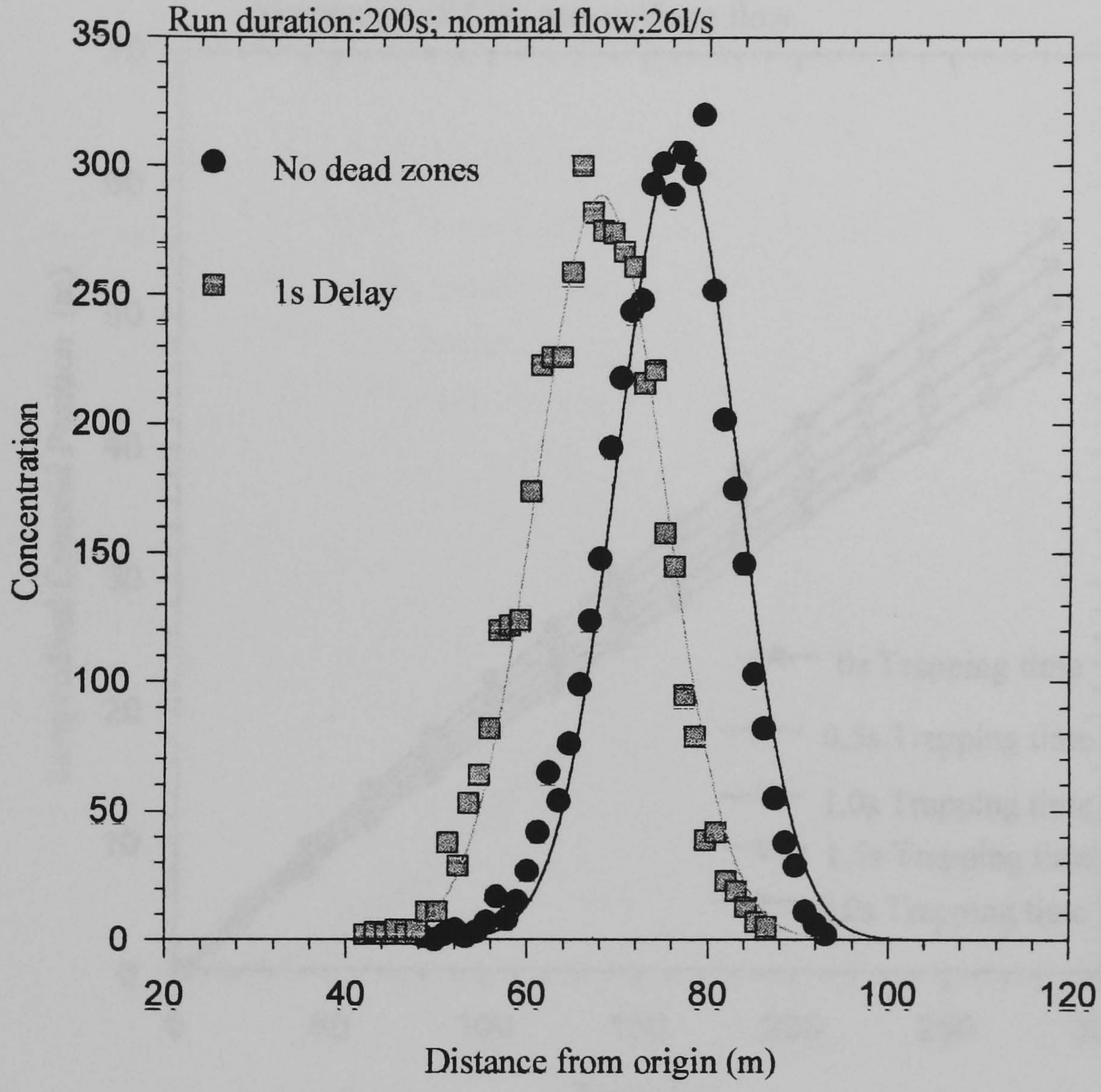

Figure 7.7 Concentration profiles from random walk model

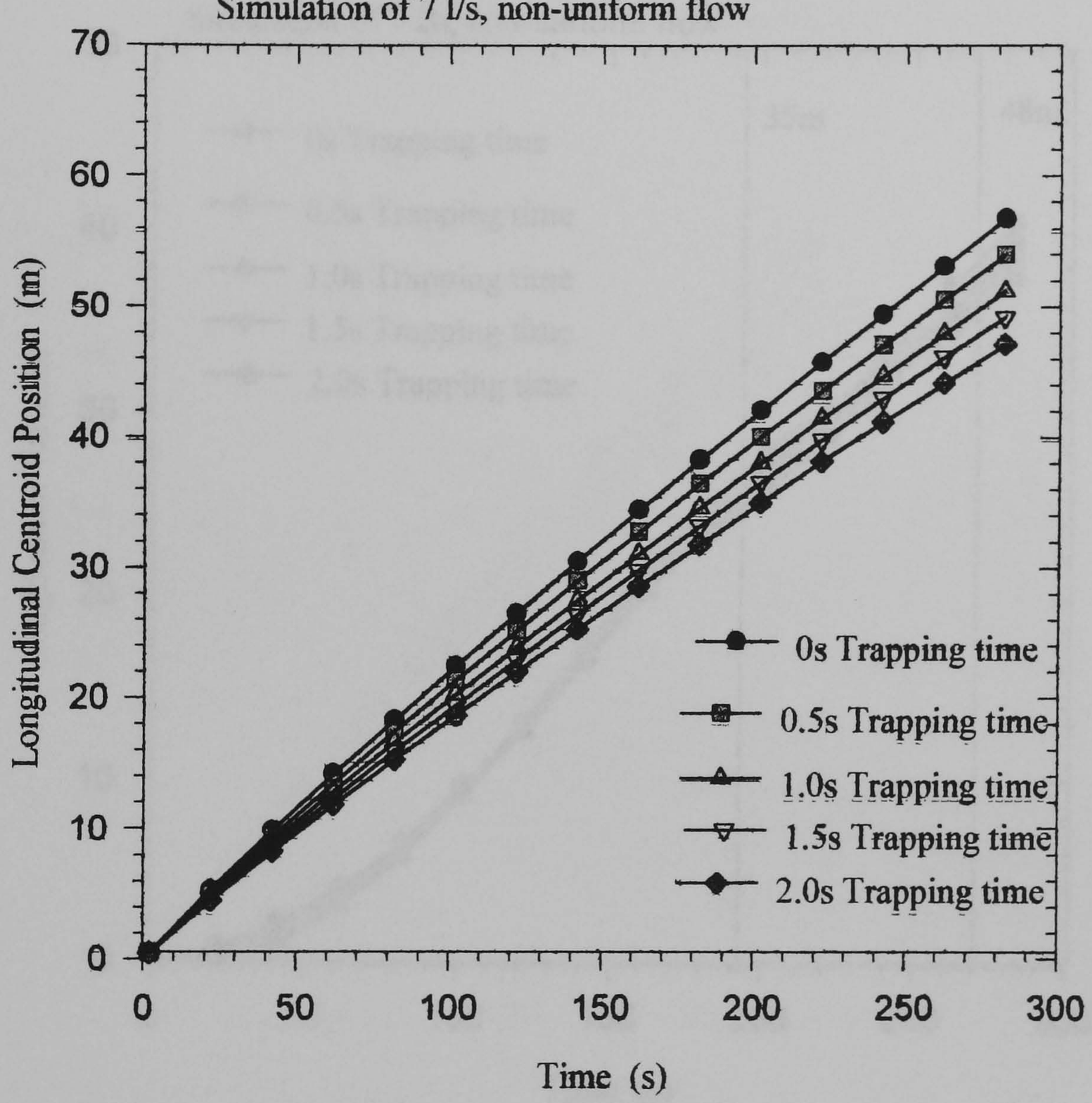

Figure 7.8 Rate of change of longitudinal centroid for a flow of 7l/s

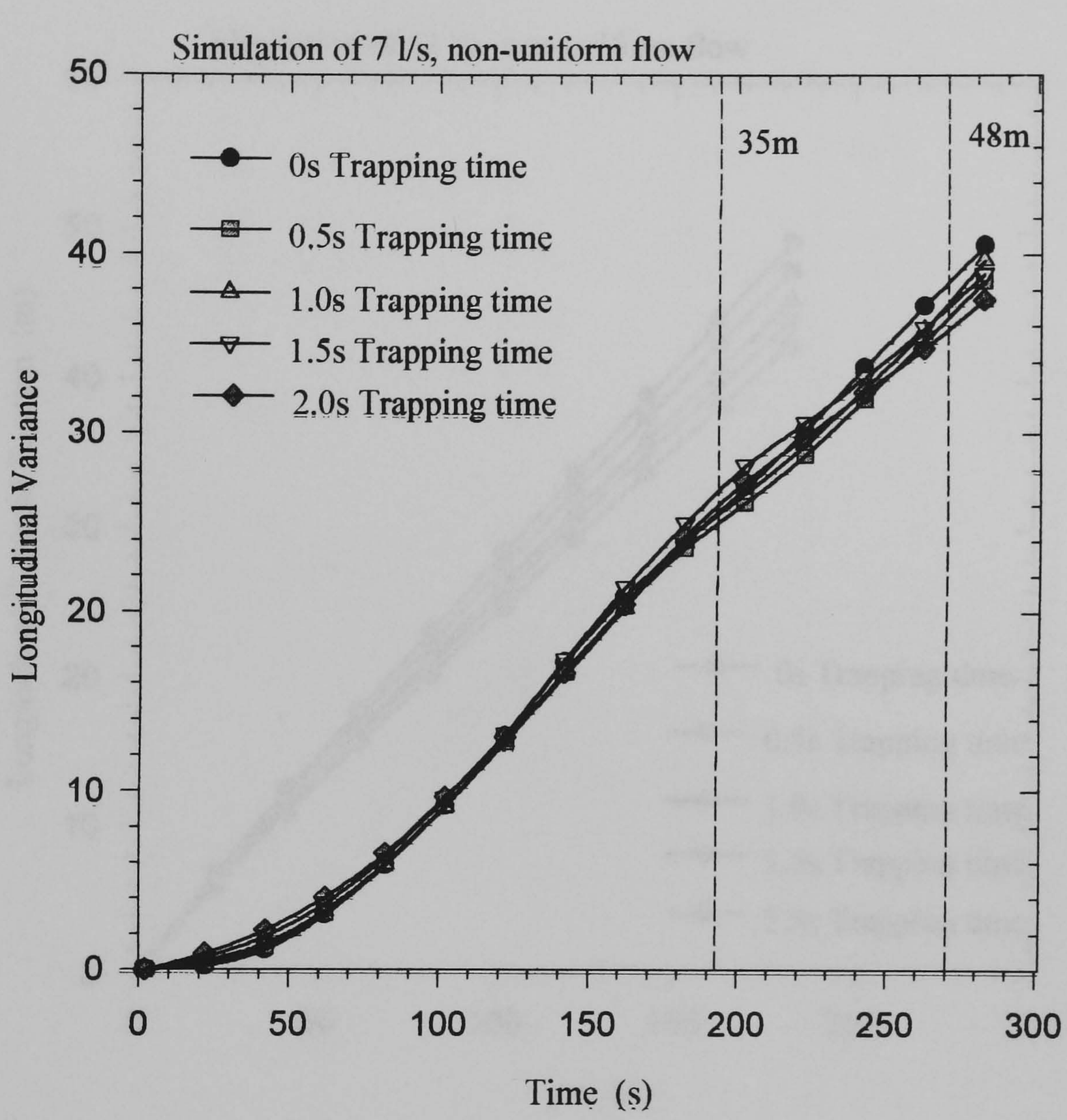

Figure 7.9 Rate of change of longitudinal variance for a flow of 13l/s

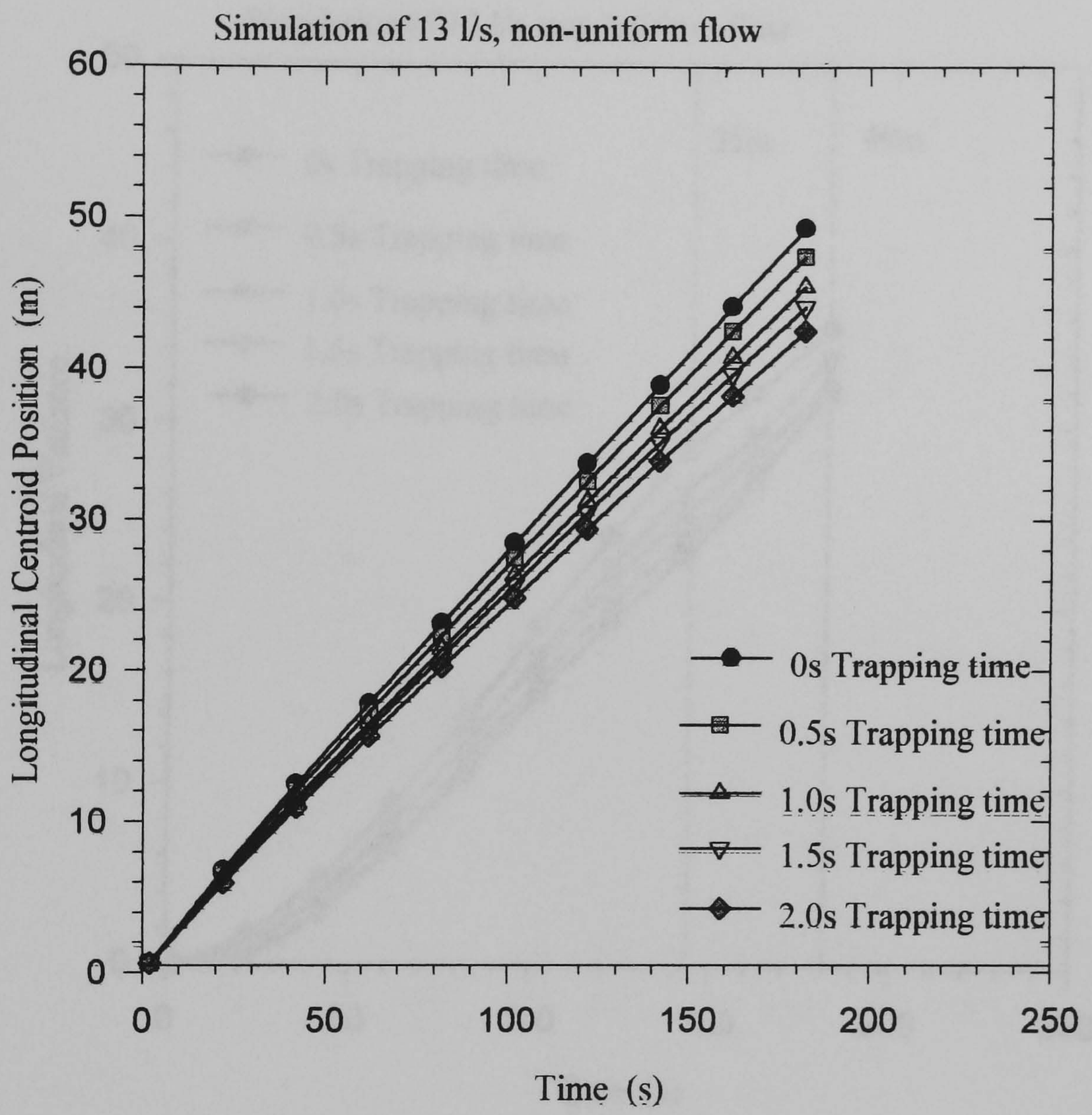

Figure 7.10 Rate of change of longitudinal centroid for a flow of 13l/s

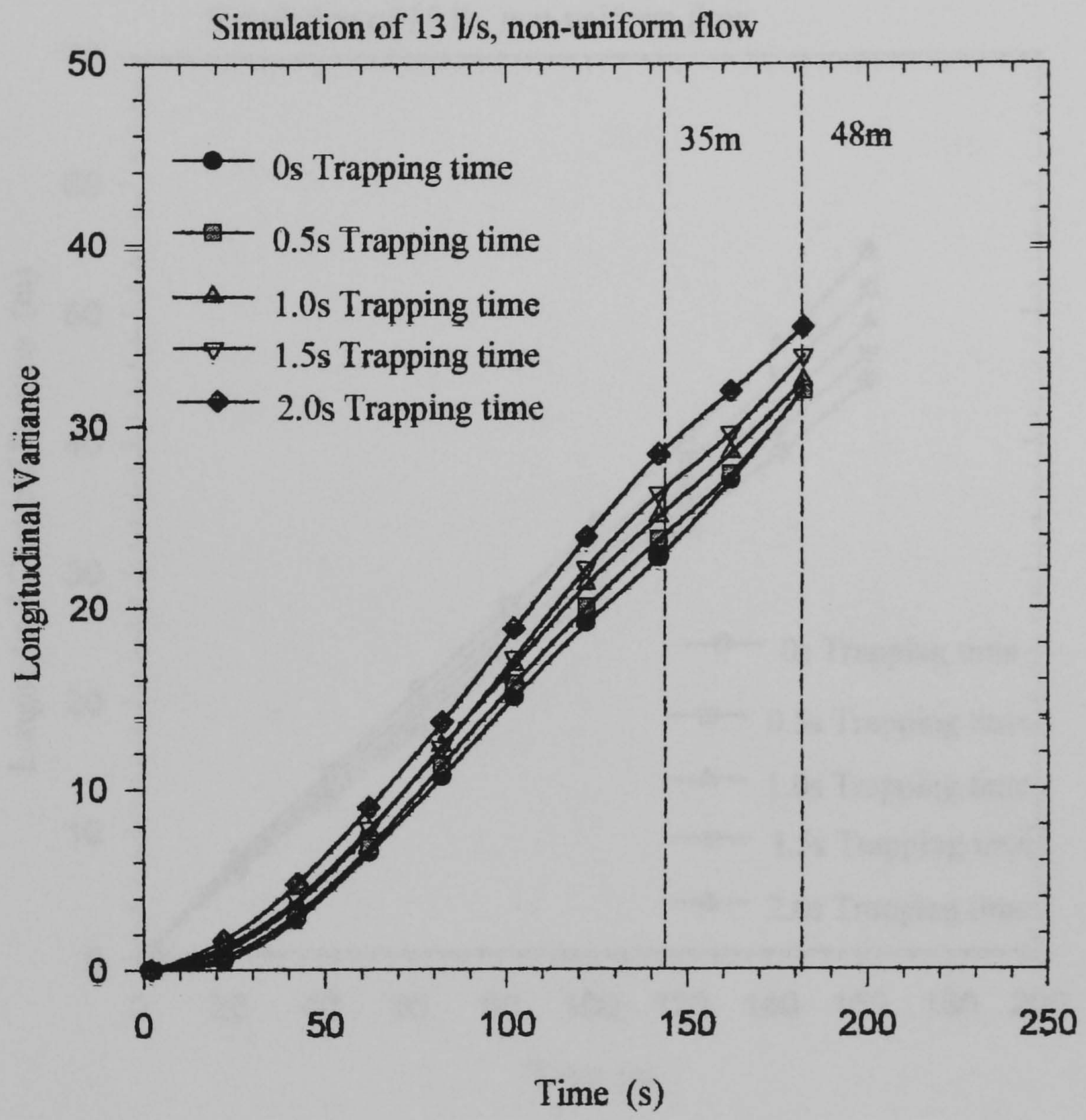

Figure 7.11 Rate of change of longitudinal variance for a flow of 13l/s

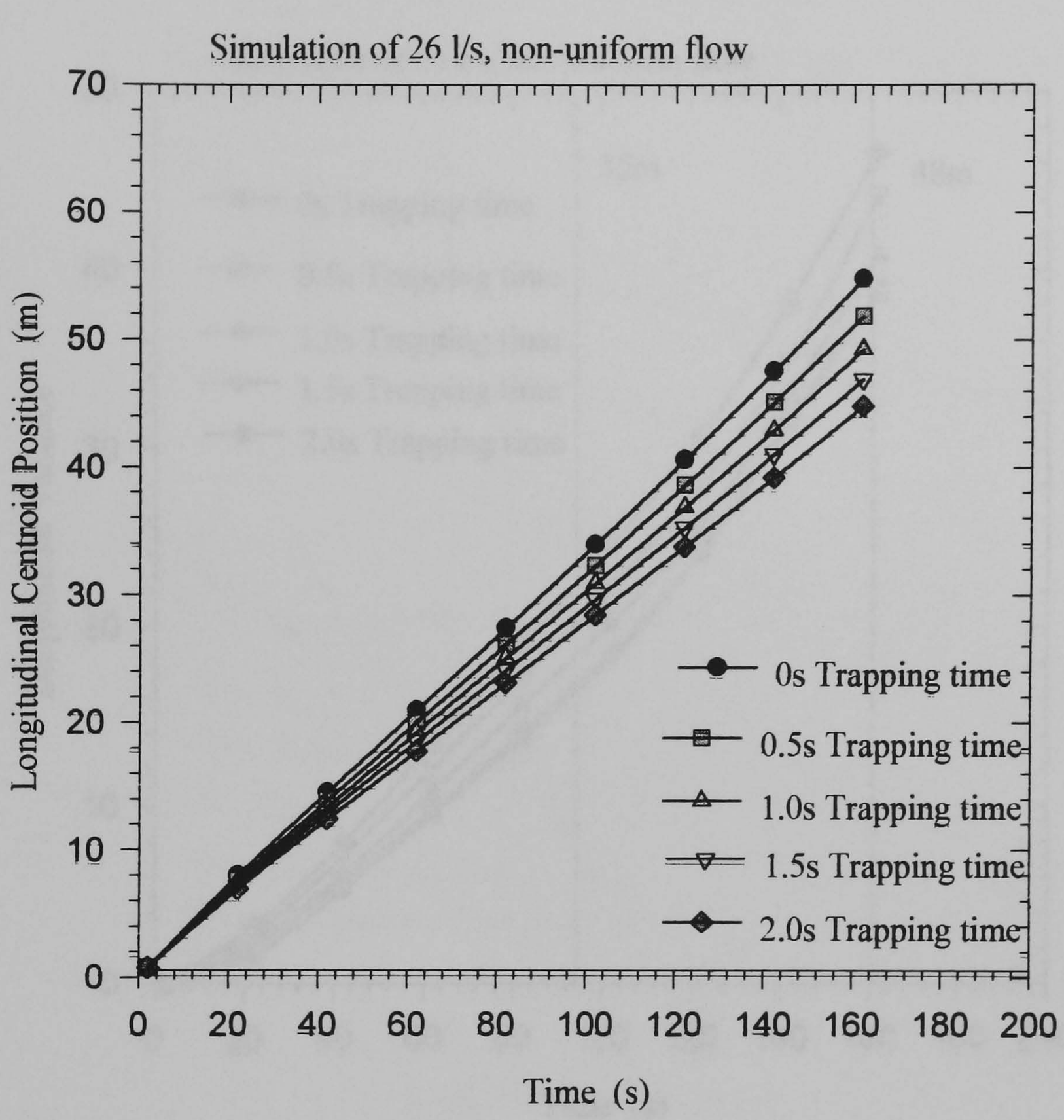

Figure 7.12 Rate of change of longitudinal centroid for a flow of 26l/s

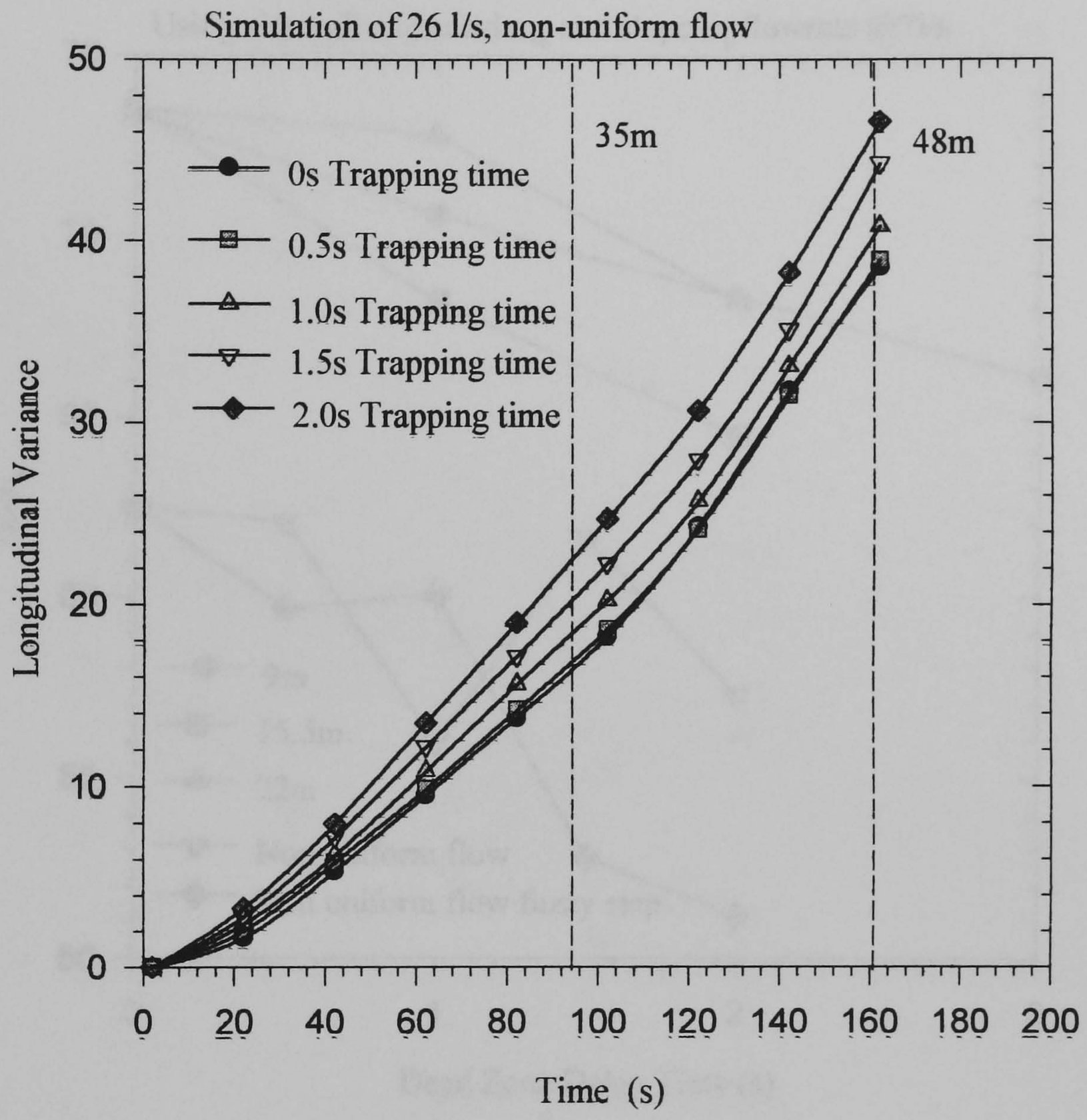

Figure 7.13 Rate of change of longitudinal variance for a flow of 26l/s

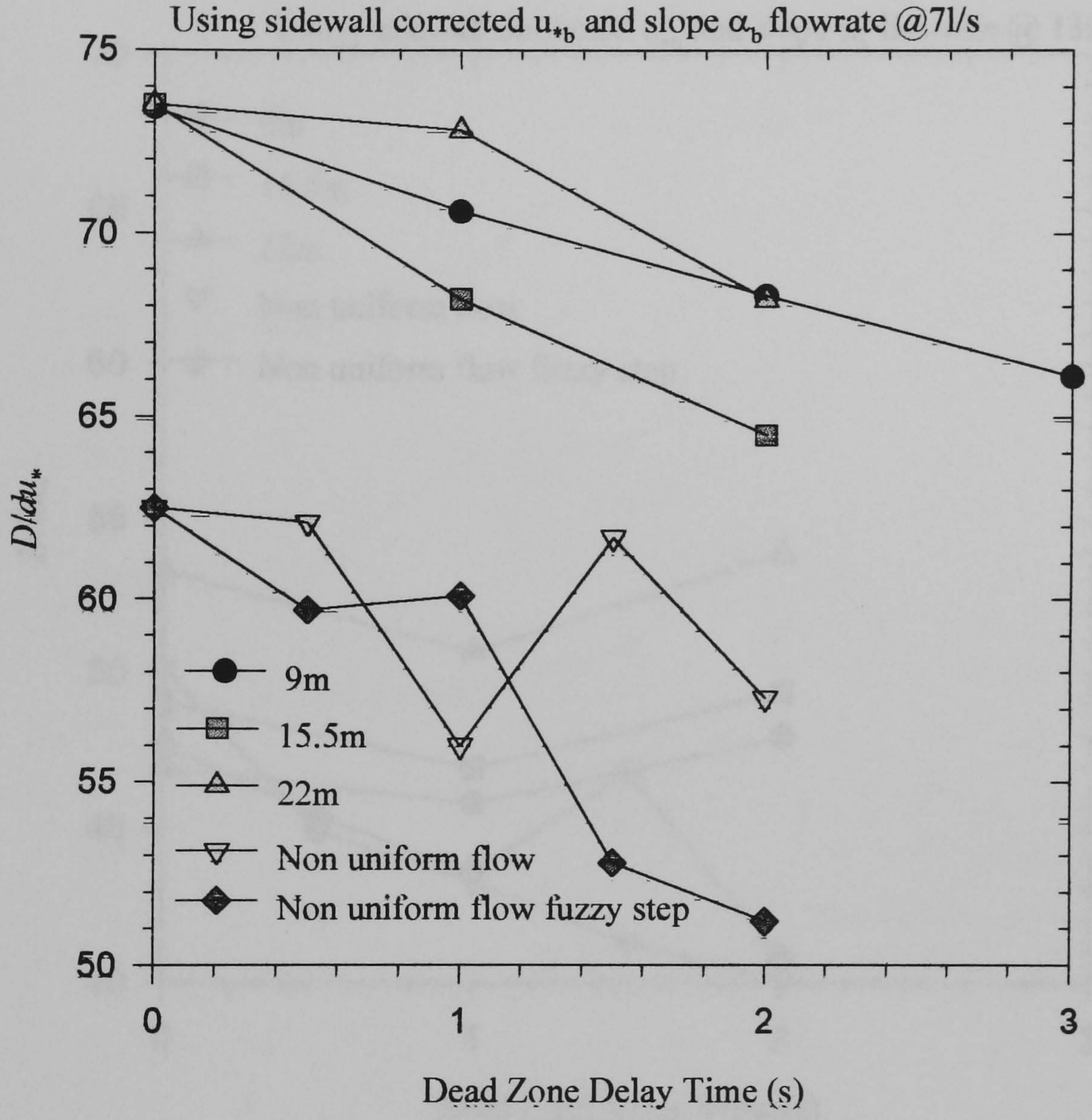

Figure 7.14 Dispersion as a function of trapping time for a flow of 7l/s

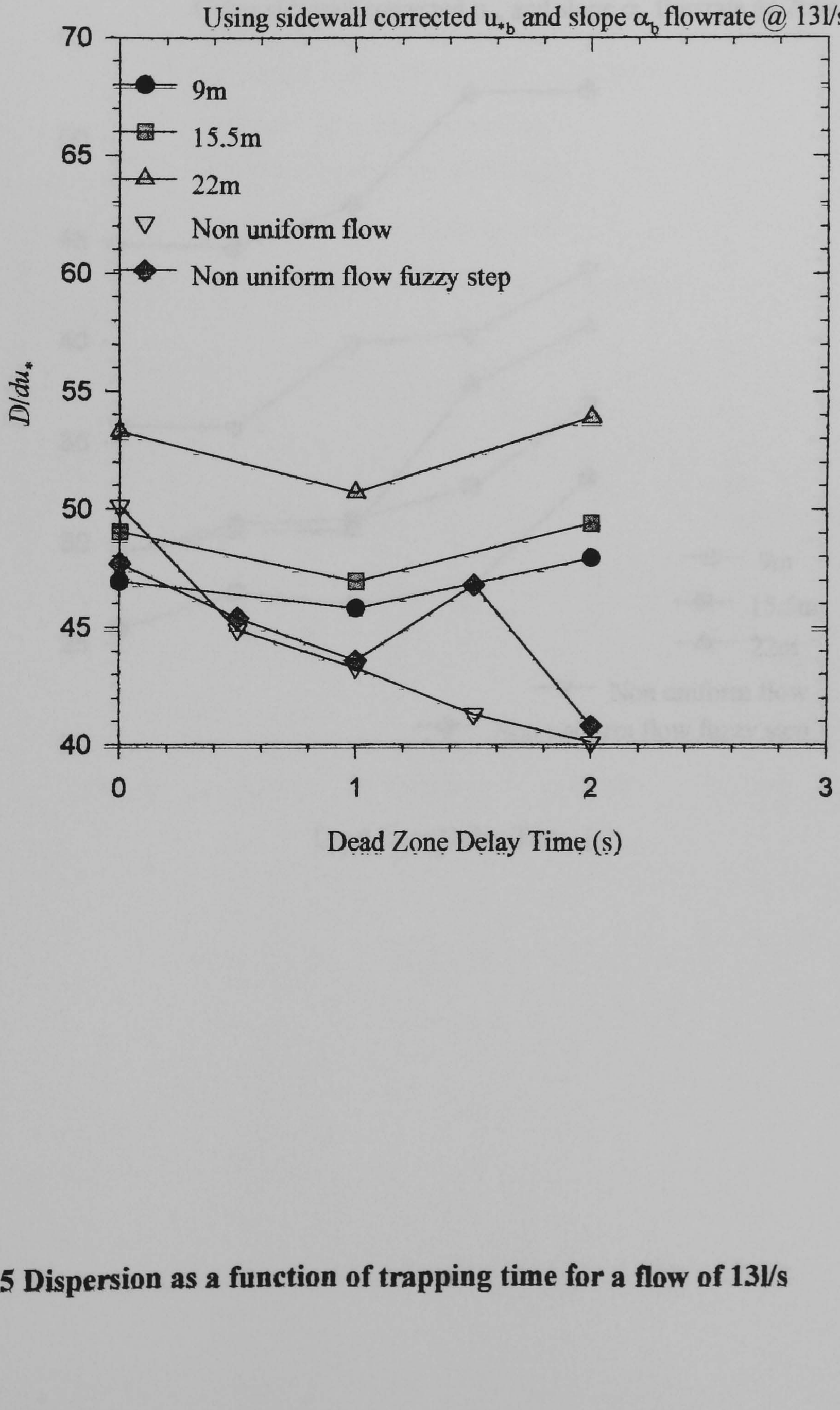

Figure 7.15 Dispersion as a function of trapping time for a flow of 13l/s

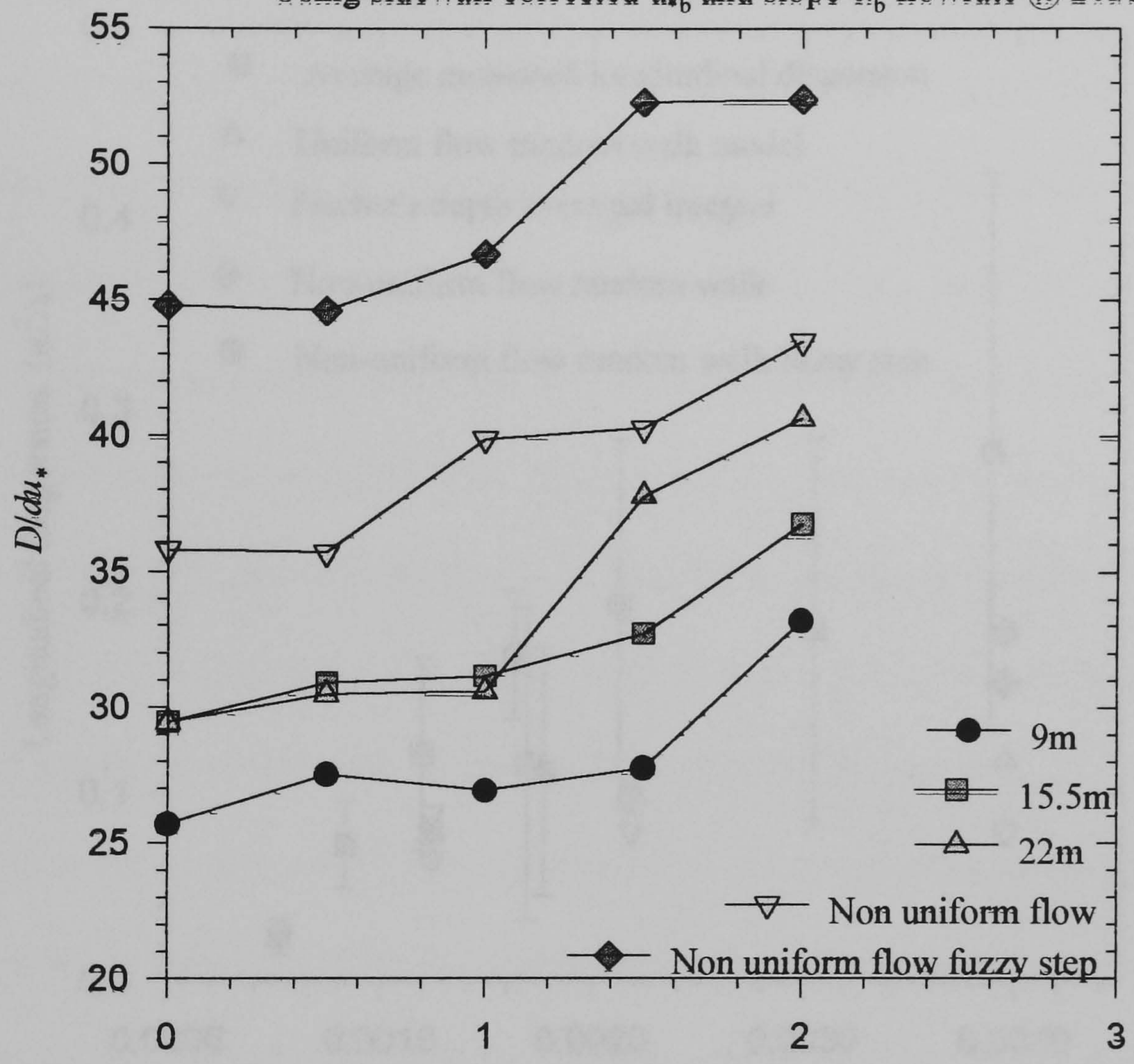

Figure 7.16 Dispersion as a function of trapping time for a flow of 26l/s

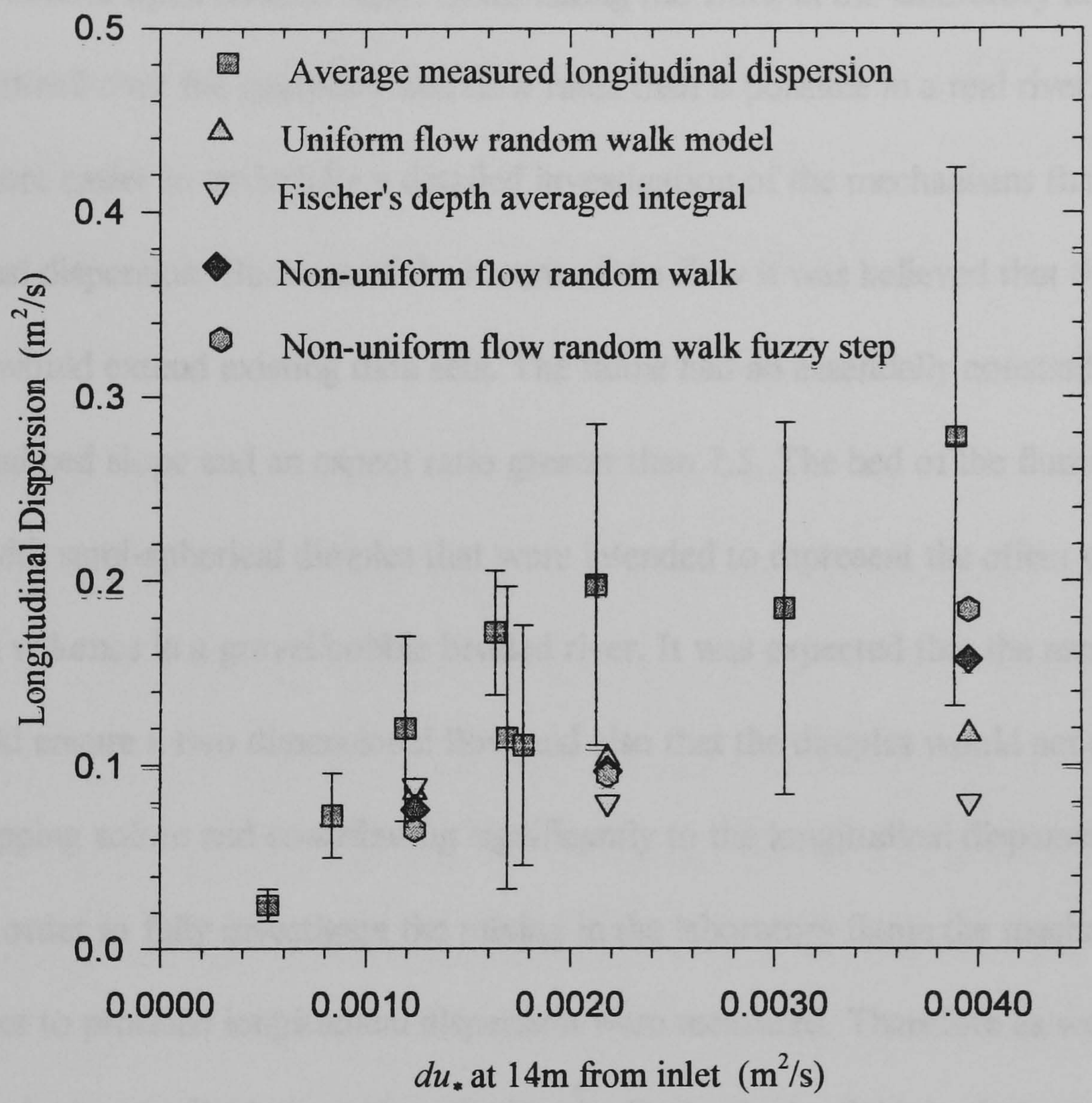

Figure 7.17 Measured & simulated longitudinal dispersion

Chapter eight Summary and discussion of the work

8.1 Introduction

The overall aim of the work contained in this thesis was to investigate longitudinal dispersion in a laboratory flume which had been designed to simulate a simplified natural open channel flow. Undertaking the work in the laboratory allowed greater controll over the geometry and flow rates than is possible in a real river. This made it more easier to undertake a detailed investigation of the mechanisms that led to longitudinal dispersion. Because of the nature of the flow it was believed that the data collected would extend existing data sets. The flume had an essentially constant longitudinal bed slope and an aspect ratio greater than 7.5. The bed of the flume was covered with semi-spherical dimples that were intended to represent the effect of the interstitial volumes in a gravel/cobble bedded river. It was expected that the aspect ratios used would ensure a two dimensional flow and also that the dimples would act as dead zones, trapping solute and contributing significantly to the longitudinal dispersion.

In order to fully investigate the mixing in the laboratory flume the mechanisms that interact to produce longitudinal dispersion were measured. Therefore as well as measuring the longitudinal dispersion, the longitudinal velocity field, both time averaged and instantaneous, was mapped. Also the transverse and vertical rates of mixing were quantified as was the mass transfer between the dimples and the main flow. Because the dimple bed was a type that had not been used by previous workers new data sets for these transport processes were obtained.

An important part of the study was the development of a numeric model of the mixing into which all the measured data could be fed. A simple random walk model was chosen because the effect of including dead zone trapping in such a model had not been

fully investigated before although the technique has advantages over other more traditional models. It does not, for example, suffer from numeric dispersion (see section 2.4) and is relatively simple to translate into software. The current work provided a unique opportunity to validate the incorporation of dead zones in a simple random walk model, and the development of the model helped the understanding of the physical processes that contribute to longitudinal dispersion in the laboratory flume.

The various sets of experiments are described in the preceding chapters. A decision was taken that each chapter would be written to stand alone. This chapter therefore summarises and draws together the work described in chapters two to seven.

8.2 Summary of the contents of the previous chapters

In chapter two the concept of longitudinal dispersion was introduced. It was described how, some time after a solute is introduced as a discrete dose into a uniform flow, that the cross-sectional average solute concentration in the flow can be described by a one-dimensional equation known as the Advection Dispersion Equation (ADE). To use the ADE requires the cross-sectional mean flow velocity to be known along with the longitudinal dispersion coefficient for the flow in question. The longitudinal dispersion coefficient can be calculated if the time averaged transverse velocity profile and the depth averaged transverse mixing coefficient in the flow are known. It was also described how the spatial concentration profiles in the flow are initially highly skewed and how the skewness eventually decays leaving the spatial concentration profile as a Gaussian. Before the spatial concentration becomes Gaussian the rate of change of variance of the concentration profiles becomes linear and the longitudinal dispersion coefficient can be calculated from this rate of change, the so-called change of moments method. The addition of dead zones which trap and slowly release solute back into the flow reduces

the rate at which the skewness of the spatial concentration profile decays and increases the length of time required before the variance grows linearly. Once the variance does grow linearly the rate of change is greater than that before the addition of the dead zones.

In chapter three measurements of the longitudinal dispersion using the method of moments applied to tracer data obtained from the author's laboratory flume were described. It was noted that the flow was longitudinally non-uniform. Strictly this invalidated the method of moments and the concept of a longitudinal dispersion coefficient because the ADE model from which they arise is only valid for uniform flow. However because no alternative was readily available and because the method of moments is commonly used to analyse data collected in natural channels, which cannot be expected to be uniform, the method was used to analyse the data collected in the laboratory flume. While the laboratory tracer experiments were carried out under what might be, when compared to the field, termed ideal conditions the calculation of the longitudinal dispersion coefficient using the method of moments was not straightforward. It was crucial that the correct background was subtracted from the data. The more highly skewed the concentration profile the more difficult it was to analyse. The results of the work showed that the non-dimensional longitudinal dispersion coefficient in the flume was within the range previously reported for straight natural channels but was larger than previously reported for laboratory flumes. The uncertainty in a single measurement of longitudinal dispersion was about ±50%. The longitudinal dispersion coefficients, D, measured by the author were a function of the product of the flow depth, d, and side wall corrected bed shear velocity, u_{*_b}, namely: $D = 56.4du_{*_b}$ and there was no noticeable influence of the aspect ratio of the flow on the longitudinal dispersion.

Three empirical equations were used to predict the longitudinal dispersion in the flume. None of the equations were very successful. One over predicted the longitudinal dispersion coefficients by a factor of six, another predicted a range of values which covered the measured dispersion coefficients (although the predicted range varied by a factor of ten). The third predicted the longitudinal dispersion coefficient to within 24% at a flow rate of 13l/s, however it under predicted by 50% at the highest flow rate tested (26l/s) and over predicted by a factor of three at the lowest.

In chapter four the results of velocity measurements in the flume were given. Whilst it had been expected that the high aspect ratios used for the author's experiments would lead to a two dimensional flow it was found that the time averaged velocity field was three-dimensional. It was concluded that the three-dimensional velocity field was due to the bed of the flume having a slight transverse slope. The three-dimensional nature of the flow was believed to be the reason why a log-law fitted the vertical time averaged longitudinal velocity profiles well (except close to the side walls) and why a wake correction term was not needed. The turbulence intensity, non-dimensionalised by the local bed shear velocity, measured in the flume was similar to that measured by other workers over a range of different bed types and roughnesses which was taken as support for the similarity hypothesis. The equivalent sand grain roughness of the flume was 27mm. Manning's n took a value of 0.028 which is in the range expected for straight natural streams without pools or riffles and for straight channels excavated in coarse gravel.

In chapter five the measurements of the solute transfer rates from semi-spherical dimples formed in the bed of the flume were discussed. This work was valuable because only two previous sets of measurements of the transfer rates from dead zones existed in the literature. All of the data on dead zone transfer rates in natural open channel flows

had been obtained by fitting ADE+DZ models to tracer data. The dimples were intended to represent interstitial volumes on a gravel/cobble bed and it was found that the removal of solute from the dimples could be represented by the first order mass transfer law used in the ADE+DZ model. The dead zone fraction (the ratio of the volume of the dimples relative to the flow volume) was similar to that obtained by previous workers who had fitted ADE+DZ models to tracer data from natural waterways. The transfer rates from the dimple dead zones were, in general, much greater than those obtained by previous workers. Analytical work (Valentine & Wood 1979, Denton 1990) suggested that this high rate of transfer into and out of the dead zones would result in the dead zones having relatively little effect on the longitudinal dispersion. The transfer rate from the dimples was a function of the flow rate and for a given flow varied between dimples. This variability could be explained by differences in the bed geometry local to a dimple leading to differences in the local flow. An average over the eight dimples examined gave an increase in transfer rate from $0.4s^{-1}$ to $1s^{-1}$ as the flow increased between 1l/s and 26l/s. Whilst the dimples were intended to simulate the effect of interstitial volumes in a natural river the measured trapping rates suggested that the dimples either were not a good model of interstitial volumes or that in natural channels other trapping mechanisms contribute to the overall dead zone trapping effect. Possible examples of other trapping mechanisms are recirculation zones, both large scale shed from bends, bank features etc or small scale shed from larger bed material and exchange flows within the stream bed.

In chapter six measurements of the transverse and vertical rates of mixing were described. It was stated that for a two dimensional open channel flow a theoretical expression for the vertical eddy diffusivity could be obtained. It was also shown that (again for the special case of a two-dimensional flow) that the depth averaged transverse eddy diffusivity could be obtained by measuring the rate of spread of a tracer plume. For

flows that were not two-dimensional it was stated that measuring the rate of spread of a tracer could provide a useful measure of the mixing processes in the flow. Such a measure was termed a mixing coefficient. In the literature the terms eddy diffusivity and mixing coefficient have sometimes been used interchangeably, however it is important to be aware of the difference. While a transverse eddy diffusivity can be though of as model of the mass transfer due to transverse turbulence the mixing coefficient represents all the processes (turbulence , secondary flows and velocity shear) that lead to a transfer of mass.

For two dimensional open channel flows an analysis of previous worker's data suggested that the transverse depth averaged eddy diffusivity was a function of the flow depth and the bed shear velocity: $\overline{\varepsilon}_z = 0.16du_*$. In the author's flume the transverse mixing coefficient was again a function of the flow depth and (side wall corrected) bed shear velocity but indicated a greater rate of mixing: $k_z = 0.4du_{*_b}$. The vertical mixing in the author's flume was also found to be greater than that for a two-dimensional flow. The enhanced transverse and vertical mixing, compared to a two dimensional flow, was due to the three dimensional nature of the flow in the author's flume. The non-dimensional transverse mixing coefficients were similar to those measured by previous workers in straight natural open channel flows but lower than those in meandering channels. It had been suggested that the width was the correct length scale for transverse mixing in open channel flows this was not the case in the author's flume in which the mixing scaled with the flow depth.

In chapter seven it was shown that a simple random walk model was able to simulate longitudinal dispersion in a flow that included dead zones. Previous workers had begun to modify random walk models to include the effect of dead zone effects but the present work was the first attempt to compare simulations using a modified random walk

model with experimental data. It was found that simulating the longitudinal dispersion in the author's flume gave valuable insights into the physical processes of the dispersion mechanisms. The influence of the dead zones in the flume bed on the longitudinal dispersion was seen to be relatively small compared to that of the transverse and vertical velocity shear. However it was seen that the longitudinal non-uniformity of the flow in the laboratory flume could have a significant influence on the dispersion if the non uniformity led to an increase in the degree of transverse velocity shear along the flume. It was also found to be important for the step length in the random walk simulation to be small enough to enable the particles to sample all the velocity gradients in the flow field.

The random walk model was compared to Fischer's method of predicting the longitudinal dispersion coefficient from a knowledge of the transverse mixing coefficient and the transverse variation of the depth averaged velocity. It was found that Fischer's integral equation worked well at the lowest flow rate examined but was unable to predict the measured increase in longitudinal dispersion with increasing flow rate.

8.3 Discussion

One common theme of the work has been the sensitivity of the mixing processes: the sensitivity of the calculations of the variance of the tracer profiles to the correct handling of the background data; the sensitivity of the flow in the flume to the small transverse bed slope that existed and the sensitivity of the transfer rates from the dimples to the local flow field were all noted.

Originally it had been expected that the use of a relatively wide flume with smooth walls would result in an essentially two dimensional flow. However during the construction of the bed of the flume a slight transverse bed slope was unintentionally introduced. This transverse slope was small and not constant but on average the bed at

the left hand (looking in the direction of flow) wall was 3.5mm lower than that at the centre line while the bed at the right hand wall was 0.75mm higher. The combination of the transverse bed slope and the longitudinal non-uniformity due to the draw down from the fixed tail gate gave a flow in which the longitudinal dispersion coefficients (non-dimensionalised by the product of the depth and bed shear velocity) were larger than those previously measured in straight laboratory flumes but were similar to the lower range of values measured in rivers.

The bulk flow characteristics of the flow suggested that the flume had a value of Manning's n similar to that for straight channels excavated in coarse gravel and at the lower end of the range for straight natural streams without pools or riffles. While the flow therefore had similarities to a natural open channel flow, empirical equations were unable to predict the longitudinal dispersion coefficients. None of the empirical equations include a measure of the bed roughness or a measure of the resistance to flow such as Manning's n. The energy needed to overcome the resistance to flow is dissipated as turbulence and recognising the importance of turbulence and velocity shear in the mixing processes, it might be useful to include a measure of the resistance to flow in future correlations.

The work has demonstrated the sensitivity of the calculation of longitudinal dispersion coefficients to the treatment of the tails when using the change of moments method. The calculated variances and hence dispersion coefficients were sensitive to the value chosen for the background concentration, if the background was set too low the result was to leave a low but finite level of concentration in the tails of the profile which led to the variance of the tracer profile being overestimated. If the background was set too high then the tails were foreshortened and the variance was underestimated. Fischer (1966a) recognised these difficulties and suggested that profiles should be routed in

preference to the change of moments method. Routing involves using a measured concentration profile as an input to a solution of the ADE and observing the predicted downstream concentration. The longitudinal coefficient in the ADE can be adjusted until the downstream predicted concentration matches the measured concentration profile. Fischer stated that a 10% error in the longitudinal dispersion coefficient used in the routing method would cause a visible mismatch between the predicted and measured downstream concentration profile. He compared this to a 100% error in the longitudinal dispersion coefficient that could arise if the change of moments method were used. It is interesting to note that Graf (1995) found better agreement between the two methods, but still up to a 51% difference when applied to data collected on a reach of the Colorado river. The routing method was not used for the present work for two reasons; firstly because while an analytical solution to the ADE is available for routing spatial concentration profiles the concentration data measured in the flume was temporal. Secondly longitudinal non-uniformity and the presence of dead zones in the flow was expected to invalidate the ADE model. The first of these problems could have been overcome because it is possible to convert temporal data to spatial data using the so called frozen cloud assumption (Fischer 1966a, Valentine & Wood 1979). An ADE+DZ model could have been used rather than an ADE, however the use of the ADE+DZ model and the longitudinal non-uniformity of the flow would require a numerical solution. It was noted in chapter two that the numerical solution of the ADE/ADE+DZ model is not a trivial problem and was beyond the scope of the present work.

It was noted in chapter five that two groups of workers had obtained quite different dead zone transfer rates and dead zone fractions by applying their ADE+DZ model to the same river. There is, therefore, a danger with routing using an ADE+DZ

model that coefficients may lose their physical significance and become simply coefficients that allow an equation to be fitted to data.

The sensitivity of longitudinal dispersion coefficients to the handling of the background and tails of tracer data suggests that one problem that would arise if an empirical equation for longitudinal dispersion was being developed would be that of finding values that had been obtained in from tracer data in a consistent way.

Fischer also suggested another alternative to the method of moments for the calculation of longitudinal dispersion coefficients, the diffusive transport method (Fischer, 1966a). In this method the longitudinal dispersion coefficient is expressed as the product of the local deviations of the velocity and concentration from the cross-sectional mean. Fischer stated that the technique has the disadvantage of requiring the accurate measurement of the small deviations of concentration that occur in a cross-section of a uniform channel when the ADE is valid. Because the method involves a detailed mapping of the concentration over a cross-section when a known longitudinal concentration profile prevails in the flume it is time consuming and requires a number of concentration measurements to be made simultaneously. For these reasons it was not used during the present work.

Chatwin's method of plotting data from longitudinal dispersion measurements could also be considered as an alternative to the method of moments. It was found that the method had a serious draw back in that it is only valid for data collected in the Gaussian zone. If data is collected in the equilibrium zone, for which the method of moments is applicable, Chatwin's transformation results in a skewed plot from which it is difficult to infer a dispersion coefficient. If data has been collected in the Gaussian zone then the method may be a better method of calculating the longitudinal dispersion

coefficients than the change of moments method because it avoids the difficulties associated with handling the tails of a concentration profile.

The transverse and vertical mixing coefficients measured in the flume were a function of the depth and bed shear velocity. The non-dimensionalised (by the product of the depth and bed shear velocity) transverse mixing coefficients were greater than previously measured in a laboratory flume because of the three dimensional longitudinal velocity field that was itself due to the unevenness of the bed. The non-dimensional vertical mixing coefficients were also greater than would be expected for a two-dimensional flow. It was noted that there was a good deal of scatter in the transverse mixing data obtained in natural channels by other workers. Regressing the transverse mixing coefficient data against the product of the depth and bed shear velocity suggested that the non-dimensional transverse mixing coefficient for straight natural channels and the author's flume were very similar. The transverse mixing in meandering natural channels is greater than that in the straight channels which reflects the enhanced mixing due to secondary currents. As with the longitudinal dispersion data it may be possible to reduce the scatter in the regressions of the natural channels data if a measure of the energy requirements of the flow were included. However there is only a limited amount of transverse mixing data available and a lengthy research program would be needed to collect enough data to test this hypothesis.

The high transfer rate between the dimples and the main flow measured in the flume needs to be considered. The flume was intended to be a simplified version of a natural open channel flow and the dimples were supposed to mimic the effect of the interstitial volumes of a gravel bedded river. Whilst Manning's n and the transverse mixing coefficients suggest that the flow in the flume had similarities with that in a natural open channel flow the dead zone transfer rates were in general higher than

previously reported. The reason for this is that the dimples did not represent the dead zones found in a natural flow. It was suggested that in a natural open channel flow solute is also trapped in larger recirculation zones. The transfer rates in these zones have been found by previous workers to be lower than the transfer rates for the dimples. It is also possible that the dead zone effect in some natural channels is due to solute entering a bed flow; a bed flow being as its name suggests a flow that takes place within the bed material. Unfortunately it is not possible to draw any conclusions as to how the dead zone transfer rates could be estimated in a practical case. Several previous workers (Thackston & Schnelle 1970, Bencala & Walters 1983, Legrand-Marcq & Laudelout 1985) have attempted to correlate the dead zone fraction and transfer rate against the friction factor for their flows. They found it possible to obtain correlations for the dead zone fraction but not the transfer rates. There was no agreement between the different workers' correlations. Knowing that previous workers have found dead zone trapping to be an important part of the longitudinal dispersion process and that it would therefore be necessary to include the effect in any modelling perhaps the best that can be done is to ensure that the modeller is aware of the possibility of dead zone trapping and to incorporate a sensible range of values for the dead zone fraction and transfer rate in order to examine the sensitivity of the model. The present work has shown that a simple random walk model can be modified to incorporate just such a dead zone trapping effect.

The random walk model allowed the contributions of the vertical and transverse velocity shear, the dead zones and the non-uniformity of the flow to be examined. It is often assumed that for three dimensional flows transverse velocity shear is the dominant mechanism for longitudinal dispersion. In the authors' flume vertical velocity shear and longitudinal non-uniformity of the flow made important contributions to the longitudinal dispersion. The relative importance of the longitudinal non-uniformity and vertical

velocity shear compared to the transverse velocity shear depended on the flow rate. The dead zones were found to contribute little to the longitudinal dispersion. In a practical modelling exercise it may be possible to use an estimate of the transverse mixing coefficient and measurements of the velocity field in a random walk model to predict longitudinal dispersion coefficients.

The simple random walk model used for the present work had to use spatially constant transverse and vertical mixing coefficients. While this was acceptable in the author's flume where experiments showed that the mixing coefficients were constant it might be a limitation in other channels. Methods exist that can allow spatially varying mixing coefficients to be incorporated into random walk models.

It was noted during the random walk simulations of longitudinal dispersion that the longitudinal non-uniformity of the flow was reflected in a non-uniform rate of change of cloud variance, even after a period of time when the uniform flow simulations had reached a uniform change of variance. It had been expected that the non-linear rate of change of variance would make the calculations of dispersion coefficients sensitive to the locations at which the variance was evaluated and some effort was taken to ensure that the positions used for the simulations were those used during the tracer experiments. However it was found that the longitudinal dispersion coefficients were not very sensitive to the particular positions used. This is an interesting point and has similarities to the work of Graf (1995), who investigated longitudinal dispersion in a reach of the Colorado river. Graf performed tracer experiments and divided the reach into sub-reaches on the basis of channel slope, width and the flow depth. Graf's concentration profile variances at the beginning and end of a 245km length of the river (sub-reaches 4 to 7 in her paper) implies a longitudinal dispersion coefficient of $128m^2/s$. Similarly the data implies the following longitudinal dispersion coefficients in the sub-reaches: $108m^2/s$

for sub-reach number 4 (25km); 68m^2/s for sub-reach 5 (68km); 102m^2/s for sub-reach 6 (79km) and 202m^2/s for sub-reach 7 (76km). While the longitudinal dispersion coefficient for the individual sub-reaches differs by up to 56% from that calculated over the entire 245km length the difference is surprising small when one considers the striking differences in the hydraulic characteristics of the sub-reaches; for example the bed slope of sub-reach 4 was twice that of sub-reach 7 whilst its width was twice that of subreach 5. The explanation for this apparent lack of sensitivity of the longitudinal dispersion coefficient to the hydraulic characteristics of the subreaches probably lies in the tracer cloud; it had a duration of over 10 hours, which implies that its length was about 40km, half that of the subreachs. The cloud may have been so long that it averaged the local flow conditions.

Returning to the random walk simulations it was found that they too used long clouds of tracer particles. For a flow rate of 7l/s, 95% of the particles where within ±9.8m of the mean at the first measurement position and ±11.8m at the second; for a flow of 13l/s the figures were 9.8m and 11.3m and at 26l/s 95% were within ±6.2m and ±12.4m of the mean respectively. The length of the particle clouds were therefore similar to the length of the flume over which the longitudinal dispersion coefficients were evaluated. It is difficult to draw definite conclusions from the random walk experiments and the work of Graf, but it does seem that providing the non-uniformity of the flow is of a similar or smaller scale than the tracer cloud then the non-uniformity of the flow may not significantly affect the longitudinal dispersion coefficients calculated from the experiments. It is the case that small scale local non-uniformities do not invalidate the ADE. For example the irregularities introduced by dead zones do not prevent the spatial longitudinal concentration profiles from eventually becoming Gaussian.

Chapter nine Conclusions

9.1 Introduction

The work on which this thesis is based has involved an experimental and numerical investigation of solute mixing in a laboratory flume. The transverse and vertical rates of mixing, the rate of solute transfer into dead zones, the longitudinal velocity field and the longitudinal dispersion coefficient were all measured as a function of flow rate. The bed roughness in the flume had not been used in any previous work and therefore the data sets that were generated during the investigation were unique. The numerical work involved the development of a random walk model. This work was the first time that detailed knowledge of mixing coefficients, dead zone transfer rates and the velocity field had been fed into a random walk model and the predicted longitudinal dispersion coefficients compared to measurements. The following paragraphs give the main conclusions of the work and recommend areas where more work is needed.

9.2 Conclusions

The hydraulic characteristics of the author's flume suggested that it had similarities to straight channels excavated in coarse gravel or to a straight natural stream without pools or riffles. The longitudinal time averaged vertical velocity profiles were well fitted by a log law and the three dimensional nature of the flow meant that a wake correction term was not required. The vertical variation of the longitudinal turbulence intensity in the flume was similar to that measured by previous workers over beds of different roughness. This is confirmation of the similarity hypothesis which implies that away from the bed the flow is not aware of the particular type of the bed roughness.

The longitudinal dispersion coefficients in the author's flume were a function of the product of the flow depth and side wall corrected bed shear velocity: $D = 56.3du_{*_b}$. The longitudinal dispersion coefficients non-dimensionalised by the product of the depth and bed shear velocity were greater than the values previously recorded in straight laboratory flumes and were similar to the lower range of values obtained in natural open channel flows. The longitudinal dispersion was largely caused by the velocity field, but the dimples in the flume bed, that were supposed to simulate dead zones in a natural channel contributed little to the longitudinal dispersion. Calculation of the longitudinal dispersion coefficient was sensitive to the treatment of the background concentration and data in the tails of the tracer concentration profiles. It was found that symmetrical profiles were less sensitive, compared to skewed profiles, to the treatment of the background.

The transverse and vertical mixing coefficients in the author's flume were a function of the product of the flow depth and side wall corrected bed shear velocity. The vertical mixing coefficient was: $k_y = 0.1du_{*_b}$ and in the transverse direction the mixing coefficient was: $k_z = 0.4du_{*_b}$. The relationship between the transverse mixing coefficient and the product of depth and bed shear velocity was similar to that suggested by a regression to transverse mixing data obtained in straight natural open channel flows. The vertical mixing coefficient implies that the rate of vertical mixing was greater than in a two-dimensional flow, for which a theoretical value of the depth averaged vertical eddy diffusivity is: $\overline{\varepsilon}_y = 0.068du_*$. It is important to draw a distinction between the depth averaged eddy diffusivity and the mixing coefficients. While both can be evaluated from the rate of change of variance of concentration profiles downstream of a tracer source, the depth averaged eddy diffusivity can only be measured for wide (two-dimensional) open channel flows. An analysis of previous workers' data gave the following regression

for the depth averaged transverse eddy diffusivity: $\bar{\varepsilon}_z = 0.16du_*$. The rate of transverse mixing in the author's flume, and that in natural open channel flows, is greater than in a wide open channel.

The rate of transfer of solute between semi-spherical dimples formed in the bed of the flume and the main flow had the same form as the dead zone transfer rate of the ADE+DZ model. The general trend, of an average of the transfer rates from eight dimples, was for an increase with flow rate. The average transfer rate ranged between $0.4s^{-1}$ to $1.0\ s^{-1}$ for flows between 1l/s and 26l/s. Because of these relatively high transfer rates, which equated to a short dead zone trapping time, compared to those inferred from field tracer data, the dimples were found have to have little influence on the longitudinal dispersion.

The work has shown that a simple random walk model can be modified to include the effect of dead zones and longitudinal non-uniformity. The trapping time used in the random walk model was equal to the reciprocal of the dead zone transfer rate. As a model the simple random walk model has certain advantages over other techniques. It is better able to predict longitudinal dispersion than existing empirical equations and is not prone to the numerical dispersion that is possible with some finite difference based models. It can also aid in the understanding of the mixing processes. In the author's flume the random walk model suggested that the influence of the vertical velocity shear and the longitudinal non-uniformity became more important as the flow rate increased. Because of the difficulties with obtaining reliable measurements of longitudinal dispersion coefficients it was suggested that a random walk model could be used to predict longitudinal dispersion coefficients needed for other models. However the random walk model requires detailed information about the velocity field, mixing coefficients and dead zone trapping in the flow, information that may be lacking or

difficult to obtain. The random walk model implemented during the present work was unable to accommodate spatially varying mixing coefficients. A varying mixing coefficient was not required for the simulations of the author's flume where experiments suggested that the mixing coefficients were constant over the cross-section but may be needed for other applications.

Longitudinal non-uniformity invalidates the ADE/ADE+DZ models. There is some evidence (from the random walk modelling and the work of Graf 1995) that the longitudinal dispersion coefficients obtained from the change of moments method may not be strongly influenced if the scale of the non-uniformity is similar or smaller than the length of the tracer cloud. It is known that the small scale non-uniformities caused by dead zones do not prevent a Gaussian concentration profile from developing but merely delay it.

9.3 Future work

In this section several useful pieces of work that could have been done with the existing data and equipment, but which time did not allow, and several new items that would usefully extend the work already carried out are described.

It was mentioned in chapter six that the intensity of the concentration fluctuations recorded during the transverse and vertical mixing experiments had not been investigated thoroughly and that Rutherford (1994) suggested that the concentration fluctuations about the mean were important. Measurements of the time varying concentration profiles were taken during the transverse and vertical mixing experiments. It would be possible to obtain useful concentration fluctuation data if the records were reanalysed.

There are several useful pieces of work that could be done with the existing and new random walk models. A better comparison between the flume measurements and

random walk simulations would be obtained if the existing random walk model was used to route the concentration profiles measured at the upstream sampling station. The random walk model could also be used to investigate how much non-uniformity in a flow can be tolerated before the longitudinal dispersion coefficient is affected and what the effects of different scales, of the order of the depth upwards, of non-uniformity are.The reason why, for certain combinations of vertical and transverse velocity profiles, the random walk model predicts a reduction of longitudinal dispersion when dead zones are included in the flow needs to be investigated further.

A random walk model with spatially varying mixing coefficients would allow the sensitivity of the longitudinal mixing coefficient to variations in the mixing coefficients to be investigated. Such a model could also be used to investigate the mechanisms that led to the enhanced vertical and transverse mixing coefficients. Running a model which uses the transverse and vertical eddy diffusivities for two dimensional flow along with the measured three dimensional velocity field may enable the mixing coefficients to be recovered. If so, and recognising the relative ease of velocity measurements compared to tracer work, the technique would have great practical use in predicting transverse and vertical mixing coefficients.

Because of the importance of secondary flows in solute transport future investigations should measure all three components of the velocity field.

Considering the uncertainty over the cause of the dead zone effect noted in natural open channel flows. It would be useful to lay a gravel bed in the flume and measure the bed flow of tracer as well as the transfer rates to and from the interstitial volumes. This could help quantify the dead zone storage mechanisms in a more realistic model of a natural channel.

It may also be useful to attempt to use Manning's n or the equivalent sand grain roughness to correlate measured longitudinal dispersion coefficients in natural open channel flows. Although it must be borne in mind that all longitudinal dispersion data should be treated with caution because of the difficulty of evaluating coefficients from tracer data. Indeed the present work would suggest that if the longitudinal dispersion coefficient is to be obtained from tracer data using the method of moments then it is important that a number of experiments should be under taken for the same flow conditions and an average taken. This is because the coefficient implied from a single experiment may be as much as 50% larger or smaller than the mean of a number of experiments.

References

Abbott,M.B. & Basco,D.R. (1989) Computational fluid dynamics
Longman, Harlow

Addison,P.S. (1995) On the fractal nature of particle paths in fluids
Paper presented at the Eighth Scottish Fluid Mechanics Meeting, 26th May, Napier University

ASCE (1963) Friction factors in open channels
J. Hydraulics Division, ASCE, 89,HY2, pp97-143

Alonso,C.V. (1970) Electrical conductivity probes for the measurement of turbulent fluctuations
J. Physics E. Vol. 3, pp 658-452

Allen,C.M. (1982) Numerical simulation of contaminant dispersion in estuary flows.
Proc. R. Soc. London Ser. A 3:1 pp 179-194

Allen,C.M. (1991) Particle tracking models for pollutant dispersion
In: Computer modelling in the environmental sciences, OUP. ed. Farmer

BS 1042 Sect. 2.1 (1983) Measurement of fluid flow in closed conduits

Barrett, T.K. & Van Atta,C.W. (1991) Experiments on the inhibition of mixing in stably stratified decaying turbulnce using laser Doppler anemometry and laser-induced fluorescence.
Phys. Fluids A 3 (5) May pp1321-1331

Batchelor,G.K., Binnie,A.M. & Phillips,O.M. The mean velocity of discrete particles in turbulent flow in a pipe
Proc. Phys. Soc., B68, pp1095-1104

Beer, T. & Young, P.C. (1984) Longitudinal dispersion in natural streams
J. Environ. Engin., 109 pp1049-1067

Bencala, K.E.; McKnight,D.M. &Zellweger, G.W. (1990) Characterisation of transport in an acidic & metal rich mountain stream based on a lithium tracer injection and simulations of transient storage
*Water Resources Research,*Vol 26, No 5, 1990, pp989-1000

Bergeron,N.E. (1994) An analysis of flow velocity profiles, stream bed roughness and resistance to flow in natural gravel bed rivers
Hydraulic Engineering 94, pp692-696

Bousgarbies,J.L.; Nerault,J. & Gatard,J.M. (1982) Experimental study of chemically reacting turbulent mixing zones.
Physico Chemical Hydrodynamics Vol. 3, No. 2, pp113-118

Bray, D.I. (1979) Estimating average velocity in gravel-bed rivers
J. Hydraulics Div. Proceedings ASCE ,Vol.105, No. HY9 ,Sep. 1979, pp1103-1122

Brockie,N.J.W., Allen,C.M. & Guymer,I. (1991) An initial comparison between 3D random walk simulations and tracer studies in a large experimental facility
Proc. 24th Congress of IAHR, Madrid

Bruno,M.S., Muntisov,M. & Fischer,H.B. (1990) Effect of bouyancy on transverse mixing in streams
J. Hydr. Eng. Vol. 116, No. 12, Dec.

Cardoso,A.H.,Gust,G. & Graf,W.H. (1989) Uniform flow in a smooth open channel
J. Hydraulic Research, Vol. 27, No. 5

Chatwin,P.C. (1971) On the interpretation of some longitudinal dispersion experiments
J. Fluid Mech., 48, pp689-702

Chatwin,P.C. & Allen,C.M. (1985) Mathematical models of dispersion in rivers and estuaries
Ann. Rev. Fluid Mech., 17, pp 119-149

Chikwenou,S.C. & Ojiakor,G.U. (1985) Slow zone model for longitudinal dispersion in two dimensional shear flows
J. Fluid Mech. Vol. 152, 1985, pp 15-38

van Dam,G. C. (1994) Study of shear dispersion in tidal waters by appying discrete particle techniques
Mixing and transport in the environment, Ed. Bevin,K., Chatwin,P. & Millbank,J.
John Wiley & Sons, Chichester, ISBN 0-471-94142-5

Defina, A (1996) Transverse spacing of low speed streaks in a channel flow over a rough bed
Coherent flow structures in open channels, Ed, Ashworth, P.J., Bennett, S.L., Best, J.L. and McLelland, S.J.
John Wiley & Sons Chichester

Denton,R.A. (1990) Analytical asymptotic solutions for longitudinal dispersion with dead zones
J. Hydraulic Research,Vol. 28, No. 3, 1990

Dong,Z., Li,X., Chen,C. & Mao,Z. (1995) Some turbulence characteristics of open-channel flow over rough bed with different slopes
Proc. 26th Congress of IAHR, London, 11-15 September,
Thomas Telford ISBN:0727720562

van Dop,M. Nieuwstadt,F.T.M. & Hunt,J.C.R (1985) Random walk models for the particle displacements in in homogeneous unsteady turbulent flows
Phys. Fluids 28. (6) June

Elder, J.W. (1959) The dispersion of marked fluid in turbulent shear flow
J. Fluid Mech, 5, pp544-560

Engelund,F. (1969) Dispersion of floating particles in uniform flow
Am. Soc. Civ. Engin., 95, pp1149-1162

Etling,G. Preuss,J. & Wamser,M. (1986) Application of a random walk model to turbulent diffusion in complex terrian
Atmospheric Envronment Vol. 20, No. 4, pp 741-747

Fischer,H.B. (1966a) Longitudinal dispersion in laboratory and natural streams
Phd Thesis, Californian Institute of Technology, Pasadena, California

Fischer,H.B. (1966b) A note on the one dimensional dispersion equation model
Air & Wat. Pollut. Int. J. Vol. 10, pp 443-452.

Fischer,H.B. (1967), The mechanics of dispersion in natural streams
J. Hydraulics Division ASCE, Vol. 93, No. HY6, Nov. 1967

Fischer,H.B. List,E.J. Koh,R.C.Y. Imberger,J. Brooks,N. (1979) Mixing in Inland Rivers and Streams
Academic Press

French,R.H. (1985) Open-channel hydraulics
McGraw-Hill Inc. New York

Gibson,C.H. & Schwarz,W.H. (1963) Detection of conductivity fluctuations in a turbulent flow field.
J. Fluid Mechanics, Vol. 16, pp365-384

Goldstein,S. (1938) Modern developments in fluid mechanics
Clarendon Press

Graasvoll (1992) An experimental investigation of longitudinal dispersion in a natural stream
Final Year Project Report, Dept. Civil & Offshore Eng. Heriot Watt University

Graf,J.B. (1995) Measured and predicted velocity and longitudinal dispersion at steady and unsteady flow, Colorado River, Glen Canyon dam to Lake Mead
Water Resources Bulletin, Vol. 31, No. 2

Guymer,I. Brockie,N.J.W. & Allen,C.M. (1990) Towards random walk models in a large scale laboratory facility.
Int. Conf. on Physical Modelling of Transport & Dispersion. M.I.T. Boston, August 1990

Hannoun,I.A. & List,E.J. Turbulent mixing at a shear free density interface.
J. Fluid Mechanics 1988, Vol. 189, pp211-234

Heemink,A.W. (1990) Stochastic modelling of dispersion in shallow water
Stochatic Hydrol. Hydraulic., 4, pp161-174

Heemink,A.W. & Blockland,P.A. On random walk models with space varying diffusivity
Journal of Computational Physics 119. pp388-389

Hinze (1975) Turbulence
Mc Graw Hill, New York

Hishida,K.; Ando,A. & Maeda,M. (1992) Experiments on particle dispersion in a turbulent mixing layer
Int. J. Multiphase Flow Vol. 18, No. 2, pp 181-194

Holly,F.M. (1985) Dispersion in rivers and coastal waters
in Developments in hydraulic engineering, Ed P. Novak, Elsevier Applied Science Publishers, London, 1985

Holley,E.R., Siemons,J. & Abraham,G. (1972) Some aspects of analysing transverse dispersion in rivers
J. Hydr. Res. 10, No. 1

Hotiges,J.,Wallis,S. & Guymer,I. (1992) The ADZ model for the prediction of pollutant transport in rivers
Wasserwirtschaft, 82, 10, pp494-497

Hou, Ho-Shong & Christensen, B.A. (1976) Influence of equivilant sand roughness on the dispersion coefficient in laboratory and natural streams
Vol. 2. *Rivers '76; Proceedings of third Annual Symposium of the Waterways, Harbors and Coastal Engineering Division ASCE*

Hoyal,D.C.J.D., Depinto,J.V., Atkinson,A.F. & Taylor,S.W. (1995) The effect of turbulence on sediment deposition
J. of Hydraulic Research, vol 33, no 3, pp 349-360

Hunter,J,R., Craig,P.O. & Phillips,H.E. (1993) On the use of random walk models with spacially variable diffusivity
J. of Computational Physics, 106, pp366-376

Jain,S.C. (1976) Longitudinal dispersion coefficients for streams
Am. Soc. Civ. Engin., 102 (EE2), pp465-474

Kabir,M.R. & Torfs,H. (1992) Comparison of different of different methods to calculate bed shear stress
Wat. Sci. Tech. Vol. 25, No. 8 pp 131-140

Kalinske,A.A. & Pien,C.I. (1944) Eddy diffusion
Industrial & Engineering Chemistry, March

Kay,J.M. & Nedderman,R.M. (1978) An introduction to fluid mechanics and heat transfer
Cambridge University Press 1978

Kitanidis,P.K. (1994) Particle tracking equations for the solution of the advection-dispersion equation with variance of coefficients
Water Resources Research, Vol. 30, No. 11, pp3225-3227, Nov.

Kironoto,B.A. & Graf,W.H. (1994) Turbulence characteristics in rough uniform open-channel flow
Proc. Instn. Civ. Engrs. Wat. Marit. & Energy 106 Dec. pp33-344

Kirkgoz,M.S. (1989) Turbulent velocity profiles for smooth and rough open channel flow
J. Hydraulic Engineering ASCE Vol. 115, No. 11, Nov. 1989 pp1543-1561

Khalil,M.B. (1972) On preserving the sand patterns in river models
J. Hydr. Res. 10, No.3

Koussis, A.D.; Saenz,M.A. & Tollis,I.G. (1983) Pollution routing in streams
J. Hydr. Eng. Vol. 109, No. 12 Dec.

Knight,D.W; Yuen,K.W.H. & Alhamid,A.A.I. (1994) Boundary shear stress in open channel flow
In 'Physical Mechanisms of mixing and transport in the environment' ed. Bevin, Chatwin & Millbank; J. Wiley

Knight,D.W. & Shiono,K.S. (1990) Turbulence measurements in a shear layer of a compound channel
J. Hydr. Res. IAHR

Krogstad,P.A., Antonia,R.A. & Browne,L.W.B. (1992) Comparison between rough- and smooth-wall turbulent boundary layers
J. Fluid Mech. vol. 245, pp599-617

Lau, Y. Lam & Krishnappan, B.G. (1977) Transverse dispersion in rectangular channels
J. Hydraulics Division, ASCE, Vol. 103, No. HY10, October.

Leonard,B.P., MacVean,M.K. & Lock,A.P. (1995a) The flux integral method for multidimensional convection and diffusion.
Appl. Math. Modelling 19,333-343

Leonard,B.P., Lock,A.P. & MacVean,M.K. (1995b) The Nirvana scheme applied to one-dimensional advection.
Int. J. Num. Meth. Heat and Fluid Flow 5(4),341-377

Legrand-Marq,C. & Laudelout, H.(1985) Longitudinal dispersion in a forest stream
J. of Hydrology, 78, 1985, pp 317-324

Lo,K.S.L. & Chen,H.H. (1991) Numerical errors of river quality models
Environmental hydraulics, eds Lee & Cheung, Balkema, Rotterdam

Lomas,C.G. (1986) Fundamentals of hot-wire anemometry
Cambridge University Press

Liu,H. (1977) Predicting dispersion coefficients of streams
Am. Soc. Civ. Engin., 103, (EE1), pp59-69

Manson,J.R. & Wallis,S.G. (1995) An accurate numerical algorithm for advective transport.
Comm. Num. Meth. Eng. 11,1039-1045

McBride,G.B. & Rutherford,J.C. (1984) Accurate modelling of river pollutant transport.
J. Env. Eng. Vol 110, 4, August

McQuivey,R.S. (1973) Principles and measuring techniques of turbulence characteristics in open channel flows
U.S.G.S. Professional Paper 802-A

McQuivey,R.S. & Keefer,T.N. (1972) Measurement of velocity-concentration covariance
Proc. ASCE vol. 98, HY9, Sept. pp1625-1646

Miller,A.C. & Richardson,E.V. Diffusion & dispersionin open channel flow
J. Hydraulics Div. ASCE Jan. HY1 pp159-171

Ncube, Kastrinakis (1991) Drifting behaviour of a conductivity probe
J. Hydr. Res. Vol. 25, No. 5. pp 643-654

Nezu,I. & Nakagawa,H. (1993) Turbulence in open channel flows
Pub. A.A. Balkema, Rotterdam

Nezu,I. & Rodi,W. Discussion of Uniform flow in a smooth open channel
J. Hydraulic Research, Vol. 29, 1991, No. 2

Nezu,I. & Rodi,W. (1986) Open channel flow measurements with a laser doppler anemometer
J. Hydraulic Engineering ASCE, Vol. 112, No. 5, May

Nordin,R.I & Wood,I.R. (1988) Vertical and lateral turbulent dispersion: some experimental results
J. Fluid Mech. Vol. 187, pp373-394

Nordin,C.F. & Troutman,B.M. (1980) Longitudinal dispersion in rivers: The persistance of skewness in observed data
Water Resources Research, Vol. 16, No 1, 1980, pp 123-128, Feb.

Okoye,J.K. (1970) Characteristics of transverse mixing in open-channel flow
Report No. KH-R-23 W.M Keck Laboratory of Hydraulics and Water Resources, Californian Istitute of Technology, Pasadena, California

Patterson,G.K. (1986) Development of a fluorescence method for reaction conversion measurement in a turbulent mixing tank.
PhysicoChemical Hydrodynamics Vol. 7, No. 1, pp33-44

Perry,A.E. (1982) Hot-wire anememometry
Clarendon Press, Oxford

Pope,S.B. (1987) Consistancy conditions for random walk models of turbulent dispersion
Phs. Fluids 30 (8) August pp 2374-3379

Prych,E.A. (1970) Effects of density differences on lateral mixing in open channel flows
Rep. No.KH-R-21 W.M Keck Laboratory of Hydraulics and Water Resources, Californian Istitute of Technology, Pasadena, California

Purnama,A. (1988) The effect of dead zones on longitudinal dispersion in streams
J. Fluid Mech. Vol. 186, 1988, pp 351-177

Raupach,M.R., Antonia,R.A. & Rajagopalan,S. (1991)
Rough-wall turbulent boundary layers
Appl. Mech. Rev. vol 44, no 1, January

Reichart,P. & Wanner,O. (1991) Enhanced one dimensional modelling of transport in rivers
J. Hyd. Eng. Vol 117, No 9, 1991

Rutherford,J.C. (1994) River mixing
John Wiley & Sons, Chichester

Sabol,G.V. & Nordin,C.F. (1978) Dispersion in rivers as related to storage zones
J.Hydraulics Div. Proceedings ASCE, Vol.104, No HY5, May, 1978

de Salazar,K.H. (1993) Characteristics of the flow field over rough surfaces
Proc. 25th Congress of IAHR, Vol. 6, S-5, pp33-40

Sawford,B.L. (1986) Generalised random forcing in random walk turbulent dispersion models.
Phys. Fluids, 29, (11), Nov. 1986, pp2582-2585.

Sayre,W.W. & Chang,F.M. (1968) A laboratory investigation of open channel dispersion processes for dissolved, suspended and floating dispersants.
US Geol. Surv. Prof. Pap. 433-E

Schoellhamer,D.H. (1988) Lagrangian transport modelling with Qual 2 kinetics.
J. Env. Eng. Vol 114, No. 2, April

Seo,I.W. & Maxell,W.H.C. (1992) Modeling low flow mixing through pools and riffles.
J. Hydraulic Eng. 118 (10) pp1406-1423

Shiono,K.& Knight,D.W. (1991) Turbulent open channel flows with variable depth across the channel.
J. Fluid Mech. Vol.222, pp 617-646

Smart,P.L. & Laidlaw,I.M.S. (1977) An evaluation of some fluorescent dyes for water tracing.
Water Resources Research, Vol. 13, No. 1, Febuary, pp 15-33

Smith,R. (1987) Diffusion in shear flows made easy: The Taylor limit.
J. Fluid Mech. Vol. 175 pp 201-214

Smith,C. R. Coherent flow structures in smooth-wall turbulent boundary layers: facts, mechanisms and speculation
Coherent flow structures in open channels, Ed, Ashworth, P.J., Bennett, S.L., Best, J.L. and McLelland, S.J.
John Wiley & Sons Chichester

Sullivan,P.J. (1971) Longitudinal dispersion within a two dimensional turbulent shear flow
J. Fluid Mech. Vol. 49, Prt. 3, pp 551-576

Sullivan,P.J. (1974) Instantaneous velocity and length scales in a turbulent shear flow
Adv. Geophys. Vol. 18, Prt. A, pp213-223

Taylor,G.I. (1921) Diffusion in continuous movements
Proc. London Math. Soc. (2), 20 (1922) pp 196-212

Taylor,G.I (1954) The dispersion of matter in turbulent flow through a pipe
Proc. Royal Soc. of London Series A, Vol. 223

Thackston,E.L. & Schnelle,K.B.(1970) Predicting effects of dead zones on stream mixing
J. Sanitary Eng. Proceedings ASCE, Vol. 96, No SA2, April 1970

Tjomsland,T.(1983) Longitudinal dispersion in a stream calculated by one dimensional numerical model
Nordic Hydrology, 14, 1983 pp41-46

Valentine,E.M. &Wood, I.R. (1977) Longitudinal dispersion with dead zones
J. Hydraulics Div. Proceedings ASCE, Vol. 103, No HY9, Sept. 1977

Valentine,E.M. & Wood,I.R. (1979a) Experiments in longitudinal dispersion with dead zones
J. Hydraulics Div. Proceedings ASCE, Vol. 105, No. HY8, Aug. 1979

Valentine,E.M. & Wood,I.R. (1979b) Dispersion in rough rectangular channels
J. Hydraulics Div. Proceedings ASCE ,Vol.105, No. HY12 ,Dec. 1979

Wallis,S.G.(1993) The simulation of solute transport in open channel flow
Environmental flows and pollution transport (ed) Beven, Chatwin & Millbank

Wallis,S.G.(1993b) Aggregated mixing zone modelling of solute transport in rivers
Fourth National Hydrology Symposium, University of Wales College of Cardiff, 13-16 September, pp5.9-5.14, ISBN 0948540524

Wallis.S.G. & Clarke.R. (1995) Hydrological modelling of solute transport in the river Rhine
Proc. of 5$^{5th.}$ National BHS Hydrology Symposiuom, Edinburgh 4-7 Sept. pp9.32-9.36

Wallis,S.G.; Guymer,I. & Bilgi,A. (1989) A practical engineering approach to modelling longitudinal dispersion
Hydraulic & Environmental modelling of Coastal , Esturine & River waters: Proceedings of the International Conference held at the University of Bradford 19-21 September 1989

Wallis,S.G. & Manson,J.R. Accurate simulation of advection using large time steps
Int. J. Num. Meth. Fluids, Accepted for publication 1996

Wallis,S.G. & Moores,A. Velocity measurements in open channel flow over a rough bed
Proc. 26th Congress of IAHR, London, 11-15 September,
Thomas Telford ISBN:0727720562

Wallis,S.G.; Young,P.C. & Bevin,P.C. (1987) Experimental investigation of the Aggegated Dead Zone model for longitudinal solute transport in stream channels
Proc. Instn. Civ. Eng. Prt 2 , 87, 1987 pp 1-22

Wallis,S.G. & Manson,J.R. (1993) Numerical techniques for the advection dispersion equation
Proceedings *UKSS '93 First conference of the UK simulation society*, Keswick Sept 13-15

Wallis S.G. & Moores A. (1996) discussion of Hoyal et al (1995) The effect of turbulence on sediment deposition

Wallis,S.G; Guymer,I. & Bilgi,A. (1989) A practical engineering guide to modelling longitudinal dispersion
Hydraulic & Environmental modelling of coastal, esturine & river waters: Proceedings of Int. Conf. Uni. Bradford 19-21 Sept. 1989 Pub. Gower Technical

Wang,J., Dong,Z., Chen,C. & Xia,Z. (1993) The effects of bed roughness on the distribution of turbulence intensities in open-channel flow
J. Hydr. Res. Vol.31 No.1

Webel,G. & Schatzmann,M. Transverse mixing in open channel flow
J. Hydraulic Engineering, Vol. 110, No. 4, April, 1984

West,J.R. & Cotton,A.P. (1980) Transverse diffusion for unidirection flow in wide open channels
Proc. Instn. Civ. Engrs., Prt 2, 69, June, pp491-498

Young.P.C. & Wallis,S.G. (1993) Solute Transport and dispersion in channels
Channel network function, K. Beven & M. Kirkby (eds), Wiley,

Yun-Sheng Yu & Liu Wenzhi (1989) Longitudinal dispersion in rivers: A dead zone model
Water Resources Bulletin, April ,Vol 25, No 2, 1989

Appendix A Measured dead zone transfer rates

Label	Flow rate (l/s)	File (.txt)	k_a (1/s)
L15.5_TP1	1.3	C143	.506
	2.59	C211	.642
	2.59	C213	.643
	2.59	C214	.826
	7.27	C222	1.06
	7.27	C224	.785
	7.27	C225	.722
	9.05	C301	.796
	9.05	C302	.775
	9.05	C303	.849
	12.85	C341	.915
	12.85	C342	1.18
	12.85	C344	1.03
	12.85	C345	.902
	15.95	C422	1.04
	15.95	C423	.937
	15.95	C424	.995
	15.95	C425	.974
	20.25	C431	.767
	20.25	C432	.821
	20.25	C433	1.0
	20.25	C434	.692
	20.25	C435	.936
	26.23	C501	1.09
	26.23	C502	1.23
	26.23	C504	1.02
	26.23	C503	.921
	26.23	C507	.929

Label	Flow rate (l/s)	File (.txt)	K_A
L15.5_TP2	1.3	C153	.589
	1.3	C154	.541
	2.59	C201	.631
	2.59	C202	.494
	2.59	C203	.564
	2.59	C204	.412
	2.59	C205	.45
	2.59	C206	.693
	6.34	C282	1.34
	6.34	C284	1.02
	6.34	C285	1.25
	9.05	C311	.781
	9.05	C312	.602
	9.05	C314	.65
	12.89	C353	.97
	12.89	C354	.327
	12.89	C355	.39
	15.99	C411	.927
	15.99	C412	.88
	15.99	C414	.828

	15.99	C415	.703
	15.99	C416	.942
	20.2	C442	.886
	20.2	C443	.652
	20.2	C444	.814
	20.2	C446	.912
	20.2	C447	1.03
	26.23	C491	1.11
	26.23	C493	.988

Label	Flow rate (l/s)	File (.txt)	K_A
L15.5_TP3	1.29	C161	.394
	1.29	C163	.641
	2.57	C192	.522
	2.57	C196	.903
	2.57	C193	.781
	4.59	C242	.595
	4.59	C245	.652
	6.37	C272	.891
	6.37	C273	1.28
	6.37	C274	1.51
	9.05	C321	.852
	9.05	C322	.69
	9.05	C323	.708
	12.78	C361	.832
	12.78	C363	.712
	12.78	C364	.914
	12.78	C371	1.09
	12.78	C372	.99
	12.78	C374	.638
	16.07	C401	.691
	16.07	C402	.728
	16.07	C403	.694
	16.07	C404	.938
	16.07	C405	1.12
	16.07	C406	1.04
	20.11	C451	.9
	20.11	C452	1.23
	20.11	C453	.922
	20.11	C454	.836
	20.11	C455	.966
	20.11	C456	1.04
	20.11	C457	1.06
	26.23	C481	.873
	26.23	C483	.954
	26.23	C485	.94

Label	Flow rate (l/s)	File (.txt)	K_A
LP15.5 TP4	1.29	C172	.325
	1.29	C174	.52
	2.59	C183	.43
	2.59	C184	.468
	2.59	C185	.544
	4.37	C255	1.07
	4.37	C254	.787
	6.37	C261	.919
	6.37	C262	.85
	6.37	C266	1.59
	9.08	C331	1.04
	9.08	C334	.603
	9.08	C335	.877
	9.08	C332	.688
	12.85	C381	.838
	12.85	C384	.896
	12.85	C385	.838
	16.19	C391	.914
	16.19	C392	.68
	16.19	C393	.635
	20.07	C461	1.04
	20.07	C462	1.05
	20.07	C463	.905
	20.07	C464	.788
	20.07	C465	1.09
	20.07	C466	.848
	20.07	C467	.947
	20.07	C468	.716
	20.07	C469	.652
	26.23	C471	1.08
	26.23	C472	.804
	26.23	C473	1.06
	26.23	C474	.874
	26.23	C475	.874

Label	Flow rate (l/s)	File (.txt)	K_A
L13.5 TP1	2.28	C514	.791
	2.28	C515	.694
	2.28	C516	.857
	7.0	C541	.203
	7.0	C543	.191
	7.82	C551	.13
	7.82	C552	.132
	7.82	C554	.148
	9.45	C571	.834
	9.45	C572	.919
	9.45	C574	1.18
	9.45	C575	1.1
	13.43	C591	1.32

	13.43	C592	1.04
	13.43	C593	1.09
	0.92	C832	.572
	0.92	C833	.632
	0.92	C834	.555
	0.92	C835	.533
	0.92	C831	.572
	16.27	C791	1.2
	16.27	C792	1.13
	16.27	C793	.893
	16.27	C796	1.14
	24.79	C781	.914
	24.79	C782	1.38
	24.79	C783	1.21
	24.79	C784	1.26
	24.79	C785	1.28
L11.5 TP1	2.74	C631	.732
	2.74	C632	.719
	2.74	C634	.544
	2.74	C635	.897
	7.32	C661	.592
	7.32	C662	1.1
	7.32	C663	.726
	7.32	C664	.553
	7.32	C665	.901
	7.32	C666	.964
	13.58	C671	.853
	13.58	C672	.864
	13.58	C673	.823
	13.58	C674	.732
	13.58	C675	.897
	13.58	C676	.911
	20.6	C701	.953
	20.6	C702	1.16
	20.6	C703	.929
	20.6	C704	.759
	20.6	C705	.975
	20.6	C708	.949
	1.0	C713	.531
	1.0	C714	.373
	1.0	C715	.445
	16.39	C741	.973
	16.39	C742	.999
	16.39	C743	.784
	16.39	C745	1.16
	24.98	C751	1.3
	24.98	C753	1.08
	24.98	C754	1.25
	24.98	C755	1.09
	24.98	C756	1.05
	24.98	C757	1.17

Label	Flow rate (l/s)	File (.txt)	K_A
LP13.5_TP2	2.28	C525	.857
	7.08	C534	1.07
	7.77	C562	.802
	7.77	C565	.945
	13.73	C601	1.19
	13.73	C602	1.06
	13.73	C604	1.44
	20.34	C611	1.18
	20.34	C613	1.53
	20.34	C615	1.31
	0.92	C811	.124
	0.92	C812	.106
	0.92	C813	.109
	0.92	C821	.117
	0.92	C822	.128
	0.92	C823	.133
	16.27	C801	.447
	16.27	C803	.475
	16.27	C806	.331
	24.79	C774	1.84
	24.79	C775	2.04
L11.5_TP2	7.38	C654	1.02
	7.38	C655	1.04
	7.38	C656	1.06
	13.5	C681	.797
	13.5	C682	.841
	13.5	C683	1.14
	13.5	C685	.875
	20.6	C692	1.1
	20.6	C693	1.09
	20.6	C694	1.05
	20.6	C695	1.15
	0.99	C721	.469
	0.99	C724	.457
	16.67	C731	.912
	16.67	C732	1.15
	16.67	C734	1.02
	16.67	C735	1.12
	16.67	C736	1.03
	24.45	C762	1.2
	24.45	C763	1.28
	24.45	C764	1.68
	24.45	C767	1.41

Table A.1 Measured dead zone transfer rates.

Appendix B Ratio of maximum to minimum concentration measured over the flume depth

Q (l/s)	y/d	x (mm)	x^*	P_m
2.15	0.26	400	0.027	0.65
		450	0.031	0.71
		500	0.034	0.76
		600	0.04	0.80
		700	0.048	0.87
		800	0.054	0.88
		900	0.06	0.88
2.69	0.49	300	0.104	0.41
		340	0.118	0.52
		400	0.139	0.62
		440	0.153	0.70
		480	0.167	0.76
		520	0.183	0.73
		560	0.194	0.76
		600	0.208	0.81
		700	0.241	0.93
		800	0.278	0.94
6.84	0.50	300	0.051	0.74
		350	0.059	0.77
		450	0.076	0.84
		550	0.093	0.85
		650	0.110	0.93
		750	0.130	0.95
		850	0.140	0.93
2.51	0.25	200	0.073	0.45
		240	0.087	0.57
		280	0.102	0.73
		320	0.117	0.75
		360	0.131	0.83
		420	0.153	0.94
		360	0.131	0.85
		500	0.182	0.98
7.05	0.27	300	0.058	0.13
		350	0.068	0.22
		400	0.078	0.26
		450	0.087	0.42
		500	0.097	0.52
		550	0.107	0.65
		600	0.116	0.64
		650	0.126	0.77
		750	0.146	0.76
25.78	0.51	300	0.022	0.66
		400	0.031	0.81
		500	0.038	0.68
		600	0.046	0.86
		700	0.054	0.90
		800	0.061	0.91
		900	0.069	0.93

Table B.1 Ratio of maximum to minimum concentration measured over the flume depth.

Appendix C Software used to calculate the moments of the tracer data

```
# include <stdio.h>
# include <math.h>

# define maxval 8000

void main()
{
 FILE *fptr;
 int start_time,end_time,duration,localcount,locavtime,num;
 int loopcount,count,avindex,ans,junk,found;
 float far *valptr,*txtptr;
 static float valarray[maxval];
 static float txtarray[maxval];
 float val,avtime,average,background,mean,loctime,sample_rate,hilim,con,temp;
 float
stan_dev,backvar,locaverage,variance,skewness,sum,sum1,sum2,sum3,time,localavtime,coef
2;
 char filestr[30],backstrg[20];

   puts("\ncalibration coefficients held in c:\\andy\\frcal.txt");
   if ((fptr=fopen("c:\\andy\\frcal.txt","r"))==NULL)
      {
       printf("can't open calfac file for reading\n");
       exit(0);
      }
      else
       puts("reading calfac.txt.....");
       fscanf(fptr,"%f\n",&coef2);   /* get values of calibration coefficients */
       fclose(fptr);

do
 { /* another file loop */
    valptr=valarray;
    txtptr=txtarray;
   puts("\n what data file is to be examined ?\n");
   gets(filestr);
   puts("\n reading text file.....");

      if ((fptr=fopen(filestr,"r"))==NULL)
      {
 printf("can't open file for reading\n");
 exit();
}
else

count=0;
while (fscanf(fptr,"%f\n",&val)!=EOF)   /* get values and store in array */
```

```
{
    count++;
    val=val*100;
    temp=ceil(val);
    if((temp-val)>0.5) temp--;
    val=temp/100;     /* round to two sig fig  */
    *txtptr=val;
    txtptr++;
}
fclose(fptr);
  sample_rate=0.1;    /* 10 Hz sampling frequency */

do
 {
  txtptr=txtarray;
  valptr=valarray;
  for(loopcount=1;loopcount<=count;loopcount++)
  {
     *valptr=*txtptr;
     valptr++;
     txtptr++;
  }            /* get an array with background */

     do
      {
   puts("\nhow much of the time record to average over ?");
   scanf("%f",&avtime);

/* average over avtime seconds of data */

   sum=0;
   sum1=0;
   avtime=avtime/sample_rate;
   avindex=ceil(avtime);
   if ((avindex-avtime)>0.5) avindex--;
   valptr=valarray;
   for (loopcount=1;loopcount<=avindex;loopcount++)
    {
     sum+=*valptr;
     sum1+=*valptr*(*valptr);
     valptr++;
    }
average=sum/avindex;
backvar=(sum1-(sum*sum/avindex))/(avindex-1);
printf("mean value of data is %6.4f,variance is %6.5f\n",average,backvar);
puts("\n analysise another background (y/n) ?");
```

```
        /* ensure the answer is y or n */
         do
           {
           junk=ans=getchar();
           while (junk!=EOF && junk!='\n')
           junk=getchar();
           } while (ans!='y' && ans!='n' && ans!=EOF);

        } while (ans=='y');   /*do average time loop */

/* try to detect rise of curve using backvar(iance) */
/* start at begining of array look for a value n times standard deviation */

 puts("\n how long as a local average ?");
 scanf("%f",&loctime);
 loctime=loctime/sample_rate;
 locavtime=ceil(loctime);
 if((locavtime-loctime)>0.5) locavtime--;
 puts("\n how many standard deviations above background ?");
 scanf("%d",&num);
 if(backvar<0)
 {
    puts("\ntail background has zero or negative variance");
    stan_dev=0;
 }
 else stan_dev=sqrt(backvar);
 hilim=average+num*stan_dev;
 hilim=hilim*100;
 temp=ceil(hilim);
 if((temp-hilim)>0.5) temp--;
 hilim=temp/100;     /* round to  sig fig  */


 valptr=valarray;
 found=0;
 locaverage=average;

 for(loopcount=1;(loopcount<=count & found==0);loopcount++)
    {
     sum=0;
 for(localcount=1;localcount<=locavtime;localcount++)
  {
  sum+=*valptr;
  valptr++;
  loopcount++;
  }
 locaverage=sum/locavtime;
```

```
        if (locaverage>hilim) found=1;
        loopcount--;        /* needed cos of loopcount++ in for loop */
      }
      if(found==0)
       {
       puts("edge not found\n");
       exit(0);
       }
  start_time=loopcount+locavtime;
  printf("start of rise at element %d\n",start_time);
/* do the same for the tail of the record */
  do
      {
      puts("\nhow much of the end of the time record to average over ?");

      scanf("%f",&avtime);

     /* average over avtime seconds of data */
      valptr=valarray+count-1;
      sum=0;
      sum1=0;
      avtime=avtime/sample_rate;
      avindex=ceil(avtime);
      if ((avindex-avtime)>0.5) avindex--;
      for (loopcount=1;loopcount<=avindex;loopcount++)
       {
        sum+=*valptr;
        sum1+=*valptr*(*valptr);
        valptr--;
       }
  average=sum/avindex;
  backvar=(sum1-(sum*sum/avindex))/(avindex-1);
  printf("mean value of tail data is %6.4f,variance is %6.5f\n",average,backvar);
  puts("\n analysise another background (y/n) ?");
  /* ensure the answer is y or n */
  do
   {
    junk=ans=getchar();
    while (junk!=EOF && junk!='\n')
     junk=getchar();
   } while (ans!='y' && ans!='n' && ans!=EOF);

  } while (ans=='y');   /*do average time loop */

/* try to detect rise of curve using backvar(iance) */
/* start at end of array look for a value n times variance */
```

```
puts("\n how many standard deviations above background ?");
 scanf("%d",&num);

 valptr=valarray+count-1;
 if(backvar<0)
 {
    puts("\ntail background has zero or negative variance");
    stan_dev=0;
 }
 else stan_dev=sqrt(backvar);
 hilim=average+num*stan_dev;
 hilim=hilim*100;
 temp=ceil(hilim);
 if((temp-hilim)>0.5) temp--;
 hilim=temp/100;    /* round to  sig fig  */

 found=0;
 locaverage=average;
 for(loopcount=count;(loopcount>=1 & found==0);loopcount--)
    {
     sum=0;
     for(localcount=1;localcount<=locavtime;localcount++)
      {
       sum+=*valptr;
       valptr--;
       loopcount--;
      }
      locaverage=sum/locavtime;
      if (locaverage>hilim) found=1;
      loopcount++;
    }
    if(found==0)
     {
      puts("back edge of curve not found\n");
      exit(0);
     }
 end_time=loopcount-locavtime;

 printf("end of curve at element %d\n",end_time);
/* only use the time record between start and end times */
/* start at vararray+start_time        */
/* end is at vararray+count-end_time    */

 duration=end_time-start_time;

/* now subtract the averaged background of the tail from each point */
 valptr=valarray+start_time;
```

```
for (loopcount=1;loopcount<=duration;loopcount++)
{
    *valptr-=average;
    val=*valptr*100;
    temp=ceil(val);
    if((temp-val)>0.5) temp--;
    val=temp/100;    /* round to  sig fig  */
    *valptr=coef2*val;
    valptr++;
}
```

```
/* calculate mean and variance using trapesium rule */
/* int of f(x) between a and b is h[0.5f(a)+sum of f(a+1 to b-1)+0.5f(b)] */
/* assume delta t is 0.1 seconds */
/* sum, sum1 and sum2 are zeroth, first and second moments respectivly */

 time=sample_rate;
 valptr=valarray+start_time;
 sum=sum1=sum2=sum3=0.0;
 sum+=(*valptr/2);
 sum1+=time*(*valptr/2);
 sum2+=time*time*(*valptr/2);
 valptr++;
 time+=sample_rate;
 for(loopcount=1;loopcount<=duration-2;loopcount++)
 {
     sum=sum+(*valptr);
     sum1=sum1+(*valptr)*time;
     sum2=sum2+(*valptr)*time*time;
     valptr++;
     time+=sample_rate;
 }

 sum+=(*valptr/2);
 sum1+=time*(*valptr/2);
 sum2+=time*time*(*valptr/2);

 sum=sum*sample_rate;        /* h is the sample rate */
 sum1=sum1*sample_rate;
 sum2=sum2*sample_rate;
 mean=sum1/sum;
 variance=(sum2/sum)-mean*mean;
 stan_dev=sqrt(variance);
 /*now calculate the skewness */
 valptr=valarray+start_time;
 for(loopcount=1;loopcount<=duration-2;loopcount++)
```

```
{
    sum3+=(*valptr-mean)*(*valptr-mean)*(*valptr-mean);
    valptr++;
}
skewness=sum3/(duration*stan_dev*stan_dev*stan_dev);
printf("area of the curve is %6.2f units\n",sum);
printf("mean: %6.2f, variance: %6.2f,skewness %6.2f\n",mean,variance,skewness);


puts("\n subtract another background (y/n) ?");
/* ensure the answer is y or n */
do
      {
      junk=ans=getchar();
      while (junk!=EOF && junk!='\n')
      junk=getchar();
      } while (ans!='y' && ans!='n' && ans!=EOF);
}
while (ans=='y');   /* another background loop */

puts("\n analysis another file (y/n) ?");
/* ensure the answer is y or n */
do
      {
      junk=ans=getchar();
      while (junk!=EOF && junk!='\n')
      junk=getchar();
      } while (ans!='y' && ans!='n' && ans!=EOF);

} while (ans=='y');     /* another file loop */
}
```

Appendix D The random walk model

```
# include <stdio.h>
# include <math.h>
# include <stdlib.h>
# include <time.h>

void initpos(float *xposptr,float *yposptr,float *zposptr,float *depth,int *dzptr);
void xmoment(float *xposptr,float *xcentroid,float *xvariance);
void zmoment(float *zposptr,float *zvariance);
float u9(float *ypos,float *zpos);
float u155(float *ypos,float *zpos);
float u22(float *ypos,float *zpos);

# define numpart 4500
# define dynvisc 0.000001
# define width 0.75
# define dustar 0.00395
void main()
{
 FILE *ofp;
 int count,op_int,op_count,dz_flag,dztime;
 static float xposition[numpart];
 static float yposition[numpart];
 static float zposition[numpart];
 static int dz_time[numpart];
 int h1,h2,h3,h4,h5,h6,h7,h8,h9,h10;
 char stroutfile[30];
 char numstrg[10];
 float far *xposptr,*yposptr,*zposptr;
 int far *dzptr;
 float delta_t;

 float ustar, depth,delta_x,up,down,random_num;
 float xpos,ypos,zpos,uloc,umax,delta_y,y_step,delta_z,z_step;
 float timecount,xcentroid,xvariance,zvariance,soltime;

 puts("\n This program outputs variances at set intervals");
 puts("  please give the filename and path... eg c:\\outfile");
 gets(stroutfile);

  if ((ofp=fopen(stroutfile,"w"))==NULL)
 {
  printf("can't open file for writing");
  exit(0);
 }
 else
```

```
delta_t=0.5;
y_step=sqrt(2*0.109*dustar*delta_t);
z_step=sqrt(2*0.39*dustar*delta_t);
depth=0.0972; /* initial depth */

puts("How long to run program ?");
scanf("%f",&soltime);
puts("how many timesteps between outputting variances\n");
scanf("%i",&op_int);
puts("how many timesteps delay in dead zones\n");
scanf("%i",&dztime);

xposptr=xposition;
yposptr=yposition;
zposptr=zposition;
                    /* set pointer to arrays            */
dzptr=dz_time;

initpos(xposptr,yposptr,zposptr,&depth,dzptr);      /* call fuction to initialise positions */

 randomize();
 op_count=0;
 dz_flag=0;
 for (timecount=delta_t; timecount<=(soltime+delta_t); timecount=timecount+delta_t)
 {
/*   printf("\n elapsed time is %.2f",timecount);  */

xposptr=xposition;
yposptr=yposition;
zposptr=zposition;
                    /* reset to the first element of the array */
dzptr=dz_time;
for (count=1;count<=numpart; count++)
 {
 xpos=*xposptr;
 ypos=*yposptr;
 zpos=*zposptr;
                    /* assign values to position variables */

 if(*dzptr!=0)
{
 *dzptr=*dzptr-1;   /* loop to keep track of time steps spent in the dead zone */
 xposptr++;
 yposptr++;
 zposptr++;
 dzptr++;
}
```

```
else   /* if not in dead zone then move */
 {

    if(ypos==0) uloc=0;
    else    /* calculate velocity */
     {    if(xpos<35)
             uloc=u9(&ypos,&zpos);
          if((41.5>xpos)&&(xpos>=35))
          {
             up=u9(&ypos,&zpos);
             down=u155(&ypos,&zpos);
             uloc=up+((down-up)/6.5)*(xpos-35);
          }
          if((48.5>xpos)&&(xpos>=41.5))
          {
           up=u155(&ypos,&zpos);
           down=u22(&ypos,&zpos);
           uloc=up+((down-up)/6.5)*(xpos-41.5);
          }
          if(xpos>=48.5) uloc=u22(&ypos,&zpos);
 } /* end of find veloc' else */
if(xpos<=35) depth=0.0973;
else if((xpos>35)&&(xpos<41.5)) depth=0.0973-0.001308*(xpos-35);
else if((xpos>=41.5)&&(xpos<48)) depth=0.0888-0.000523*(xpos-41.5);
else depth=0.0854;
delta_x=uloc*delta_t;
xpos=xpos+delta_x;
*xposptr=xpos;
xposptr++;

/*  calculate vertical motion    */
random_num=random(201);
random_num=(100-random_num)*0.0171916;
delta_y=random_num*y_step;
if ((ypos+delta_y)<= 0)
 {
  if(dz_flag==1)
   {
    *dzptr=dztime; /* if second hit in dz */
    dz_flag=0;  /* reset the flag  */
  ypos=(-1*(ypos+delta_y)/2);
 }
else
 {
  ypos=(-1*(ypos+delta_y)/2);
  dz_flag++;
 }
```

```
 }  /* particle passes through bed + reflected */
else
 if ((ypos+delta_y)>depth)
  ypos=depth-(((ypos+delta_y)-depth)/2);
  else ypos=ypos+delta_y;


   /* calculate transverse motion  */

random_num=random(201);
random_num=(100-random_num)*0.0171916;
delta_z=random_num*z_step;
      if ((zpos+delta_z)< 0)
zpos=(-1*(zpos+delta_z)/2);
else
     if ((zpos+delta_z)>width)
      zpos=width-(((zpos+delta_z)-width)/2);
      else zpos=zpos+delta_z;

      *yposptr=ypos;
      yposptr++;
      *zposptr=zpos;
      zposptr++;          /* set pointer  next particle */
      dzptr++;

} /* as long as not in a dead zone  */

}     /* end of particle array loop */

op_count++;   /*increment the counter */

if (op_count==op_int)
  {
      op_count=0; /* reset counter  */
      xposptr=xposition;
      zposptr=zposition;
      xcentroid=0.0;
      xvariance=0.0;
      zvariance=0.0;
      xmoment(xposptr,&xcentroid,&xvariance);
      zmoment(zposptr,&zvariance);
      printf("\n at time %.1f,xcentroid is %.3f, xvariance is %.4f, zvariance is
%.4f",timecount,xcentroid,xvariance,zvariance);
      fprintf(ofp,"%4.2f\t%6.4f\t%6.4f\t%6.4f\n",timecount,xcentroid,xvariance,zvariance
);

    }
```

```
} /*end of soltime loop */


 fclose(ofp);

       /* write out number of particles in each depth slice */
h1=h2=h3=h4=h5=h6=h7=h8=h9=h10=0;
 yposptr=yposition;
 for(count=1;count<=numpart;count++)
 {
  ypos=*yposptr;
      if(ypos<depth/10) h1++;
      else if(ypos>depth/10 && ypos<depth*0.2) h2++;
      else if(ypos>depth*0.2 && ypos<depth*0.3) h3++;
      else if(ypos>depth*0.3 && ypos<depth*0.4) h4++;
      else if(ypos>depth*0.4 && ypos<depth*0.5) h5++;
      else if(ypos>depth*0.5 && ypos<depth*0.6) h6++;
      else if(ypos>depth*0.6 && ypos<depth*0.7) h7++;
      else if(ypos>depth*0.7 && ypos<depth*0.8) h8++;
      else if(ypos>depth*0.8 && ypos<depth*0.9) h9++;
      else h10++;
      yposptr++;
     }
      printf("\n %d %d %d %d %d %d %d %d %d
%d",h1,h2,h3,h4,h5,h6,h7,h8,h9,h10);


}     /* end of main function */

void initpos(float *xposptr,float *yposptr,float *zposptr, float *depth,int *dzptr)

{
/* set initial positions of the particles */

 int count;

 for (count=1; count<=numpart; count++)
   {
    *xposptr=0;
    xposptr++;
    *yposptr=*depth*0.5;
    yposptr++;
    *zposptr=width*0.5;
    zposptr++;
    *dzptr=0;
    dzptr++;
```

```
    }

}

/* Calculate the first and second longitudinal moments */
  void xmoment(float *xposptr,float *xcentroid,float *xvariance)
   {
    int count;
    float sum1,sum2;
    sum1=sum2=0.0;
    for (count=1;count<=numpart;count++)
     {
      sum1=sum1+*xposptr;
      sum2=sum2+(*xposptr*(*xposptr));
      xposptr++;      /* move to next x position   */
     }
    *xcentroid=sum1/numpart;
    *xvariance=(sum2-(sum1*sum1/numpart))/(numpart-1);
   }

/* Calculate the first and second transverse moments */

 void zmoment(float *zposptr,float *zvariance)
   {
    int count;
    float sum1,sum2;
    sum1=sum2=0.0;
    for (count=1;count<=numpart;count++)
     {
      sum1=sum1+*zposptr;
      sum2=sum2+(*zposptr*(*zposptr));
      zposptr++;      /* move to next z position   */
     }
    *zvariance=(sum2-(sum1*sum1/numpart))/(numpart-1);
   }

/* The velocity field at 9m from the channel entrance */
float u9(float *ypos,float *zpos)
{
 float uleft,uright,uloc9;

if((0<=*zpos)&&(*zpos<0.125))
{
 uleft=0;
 uright=0.6525+0.0708*log(*ypos);
 uloc9=(uright-uleft)*(*zpos)/0.125;
}
```

```
else if((0.125<=*zpos)&&(*zpos<0.225))
{
 uleft=0.6525+0.0708*log(*ypos);
 uright=0.8065+0.1188*log(*ypos);
 uloc9=uleft+((uright-uleft)*(*zpos-0.125)/0.1);
}

else if((0.225<=*zpos)&&(*zpos<0.325))
{
 uleft=0.8065+0.1188*log(*ypos);
 uright=0.6690+0.0752*log(*ypos);
 uloc9=uleft+((uright-uleft)*(*zpos-0.225)/0.1);
}
else if((0.325<=*zpos)&&(*zpos<0.375))
{
 uleft=0.6690+0.0752*log(*ypos);
 uright=0.7080+0.1059*log(*ypos);
 uloc9=uleft+((uright-uleft)*(*zpos-0.325)/0.05);
}
else if((0.375<=*zpos)&&(*zpos<0.425))
{
 uleft=0.7080+0.1059*log(*ypos);
 uright=0.6927+0.0867*log(*ypos);
 uloc9=uleft+((uright-uleft)*(*zpos-0.375)/0.05);
}
else if((0.425<=*zpos)&&(*zpos<0.525))
{

 uleft=0.6927+0.0867*log(*ypos);
 uright=0.7353+0.1064*log(*ypos);
 uloc9=uleft+((uright-uleft)*(*zpos-0.425)/0.1);
}
else if((0.525<=*zpos)&&(*zpos<0.625))
{
 uleft=0.7353+0.1064*log(*ypos);
 uright=0.7049+0.0884*log(*ypos);
 uloc9=uleft+((uright-uleft)*(*zpos-0.525)/0.1);
}
else if((0.625<=*zpos)&&(*zpos<0.750))
{
                 uleft=0.7049+0.0884*log(*ypos);
                 uright=0.0;
                 uloc9=uleft+((uright-uleft)*(*zpos-0.625)/0.125);
                }
                return uloc9;
} /* end of 19 field */
```

```
/* The velocity field at 15.5m from the channel entrance */
float u155(float *ypos,float *zpos)

  {
   float uleft,uright,uloc155;
                    if((0<=*zpos)&&(*zpos<0.125))
                    {
                     uleft=0;
                     uright=0.7208+0.0817*log(*ypos);
                     uloc155=(uright-uleft)*(*zpos)/0.125;
                    }
                    else if((0.125<=*zpos)&&(*zpos<0.225))
                    {
                     uleft=0.7208+0.0817*log(*ypos);
                     uright=0.7334+0.0881*log(*ypos);
                     uloc155=uleft+((uright-uleft)*(*zpos-0.125)/0.1);
                    }

                    else if((0.225<=*zpos)&&(*zpos<0.325))
                    {
                     uleft=0.7334+0.0881*log(*ypos);
                     uright=0.7000+0.0746*log(*ypos);
                     uloc155=uleft+((uright-uleft)*(*zpos-0.225)/0.1);
                    }
                    else if((0.325<=*zpos)&&(*zpos<0.375))
                    {
                     uleft=0.7000+0.0746*log(*ypos);
                     uright=0.7485+0.1027*log(*ypos);
                     uloc155=uleft+((uright-uleft)*(*zpos-0.325)/0.05);
                    }
                    else if((0.375<=*zpos)&&(*zpos<0.425))
                    {
                     uleft=0.7485+0.1027*log(*ypos);
                     uright=0.7660+0.1069*log(*ypos);
                     uloc155=uleft+((uright-uleft)*(*zpos-0.375)/0.05);
                    }
                    else if((0.425<=*zpos)&&(*zpos<0.525))
                    {

                     uleft=0.7660+0.1069*log(*ypos);
                     uright=0.7727+0.1093*log(*ypos);
                     uloc155=uleft+((uright-uleft)*(*zpos-0.425)/0.1);
                    }
                    else if((0.525<=*zpos)&&(*zpos<0.625))
                    {
                     uleft=0.7727+0.1093*log(*ypos);
                     uright=0.7618+0.1023*log(*ypos);
```

```
                uloc155=uleft+((uright-uleft)*(*zpos-0.525)/0.1);
               }
               else if((0.625<=*zpos)&&(*zpos<0.750))
               {
                uleft=0.7618+0.1023*log(*ypos);
                uright=0.0;
                uloc155=uleft+((uright-uleft)*(*zpos-0.625)/0.125);
               }
               return uloc155;
  }  /* end of1155 field */

/* The velocity field at 22m from the channel entrance */
float u22(float *ypos,float *zpos)
  {
   float uleft,uright,uloc22;
                if((0<=*zpos)&&(*zpos<0.125))
                {
                 uleft=0;
                 uright=0.7091+0.0643*log(*ypos);
                 uloc22=(uright-uleft)*(*zpos)/0.125;
                }
                else if((0.125<=*zpos)&&(*zpos<0.225))
                {
                 uleft=0.7091+0.0643*log(*ypos);
                 uright=0.8141+0.1048*log(*ypos);
                 uloc22=uleft+((uright-uleft)*(*zpos-0.125)/0.1);
                }

                else if((0.225<=*zpos)&&(*zpos<0.325))
                {
                 uleft=0.8141+0.1084*log(*ypos);
                 uright=0.8390+0.1043*log(*ypos);
                 uloc22=uleft+((uright-uleft)*(*zpos-0.225)/0.1);
                }
                else if((0.325<=*zpos)&&(*zpos<0.375))
                {
                 uleft=0.8390+0.1043*log(*ypos);
                 uright=0.8349+0.1096*log(*ypos);
                 uloc22=uleft+((uright-uleft)*(*zpos-0.325)/0.05);
                }
                else if((0.375<=*zpos)&&(*zpos<0.425))
                {
                 uleft=0.8349+0.1096*log(*ypos);
                 uright=0.7774+0.0995*log(*ypos);
                 uloc22=uleft+((uright-uleft)*(*zpos-0.375)/0.05);
                }
                else if((0.425<=*zpos)&&(*zpos<0.525))
```

```
{

 uleft=0.7774+0.0995*log(*ypos);
 uright=0.8195+0.1073*log(*ypos);
 uloc22=uleft+((uright-uleft)*(*zpos-0.425)/0.1);
}
else if((0.525<=*zpos)&&(*zpos<0.625))
{
 uleft=0.8195+0.1073*log(*ypos);
 uright=0.8005+0.1048*log(*ypos);
 uloc22=uleft+((uright-uleft)*(*zpos-0.525)/0.1);
}
                else if((0.625<=*zpos)&&(*zpos<0.750))
                {
                 uleft=0.8005+0.1048*log(*ypos);
                 uright=0.0;
                 uloc22=uleft+((uright-uleft)*(*zpos-0.625)/0.125);
                }
                return uloc22;
} /* end of l22 field */
```